The Design and Manufacture of an Accelerated Fatigue Testing Machine for Coronary Stents

Martin Philip Hereford Hoole

Declaration

The Design and Manufacture of an Accelerated Fatigue Testing Machine for Coronary Stents

I, Martin Philip Hereford Hoole, hereby declare:

(i) This thesis of the above title is of my own unaided work and that apart from the normal guidance from my supervisor, I have received no assistance except as stated;

(ii) Where indicated to the contrary, neither the substance nor any part of this thesis of the above title has been submitted in the past, or is to be submitted for a degree in this university or any other university.

This thesis has been submitted by the author for examination in partial fulfilment of the requirements for the degree of Master of Science in Medicine in Biomedical Engineering at the University of Cape Town.

Signed by candidate

Signature Removed

Signature of Author

01/02/07
Date

Acknowledgements

I would like to thank the following people and organizations for their support and committed help throughout this project:

My supervisor, Christopher Vaughan for continued advice and support;

To all the people at DISA Vascular for their unfailing support and encouragement, and muscle power when that too was needed;

To my family; Philip, Elsa, Caryn and Kevin, thank you for your continuous words of motivation and encouragement;

To my uncles; Manfred and Otto without whom my design would still be a drawing on a few pieces of paper;

Jacques Hugo from Denel Landsystems, for very kindly offering the use of their high speed camera and measurement software.

Synopsis

International standards governing the design, manufacture and testing of implanted medical devices are constantly calling for better quality products. Failure of coronary stents can present in various ways, but most times result in repeated occlusion of the artery segment and this almost inevitably requires a further operation. With operations of this type carrying a definite underlying risk, one cannot ignore the importance of conforming to relevant international governing standards. One such improvement, which forms the focus of this project, is the increased importance and flexibility of the coronary stent fatigue testing procedure. Thorough *in vitro* (biological phenomena made to occur outside the human body) testing of this kind should reduce the risk of *in vivo* (biological phenomena occurring inside the human body) stent failure and thus lead to increased survivability for patients suffering with cardiovascular disease.

One of the factors which led to the selection and approval of this subject as a suitable thesis topic was a recommendation to the University of Cape Town from a locally based cardiovascular stent manufacturer, DISA Vascular (Pty) Ltd, for an academic study into the design and manufacture of a device capable of testing the extent to which their stents comply with the applicable international standards. DISA Vascular undertook to render support and assistance to the University, including access to their premises and facilities.

With the latest European and American standards used as a point of design reference, the machine would have to comply with certain essential requirements. Examples of such requirements include the simulation of appropriate physiological parameters (axial and radial deformation, bending and temperature) and operation at accelerated frequencies of above 60 Hz.

The machine produced and documented in this report is capable of subjecting a stent to appropriate physiological loading by deploying it in a simulated vessel and subjecting it to cyclic bending and pressurization. Loading of this kind can be performed at frequencies up to 60 Hz and, as such, simulates 380 million cycles of coronary artery pulsation, equivalent to 10 years in the human, in approximately 3 months.

Testing of the final machine yielded satisfactory results with high speed measurement of the vessel's motion identified as one of the main areas of project improvement. Investigation into alternative test vessels and their compliance characteristics was also considered advisable.

Table of Contents

List of Figures

List of Tables

List of Abbreviations

Abbreviation	Description
UCT	University of Cape Town
FDA	American Food and Drug Administration
BS EN	British Standard (European)
LMCA	Left Main Coronary Artery
RCA	Right Coronary Artery
LCX	Left Circumflex Coronary Artery
LAD	Left Anterior Descending Corollary Artery

Chapter One

Introduction

The heart requires a constant supply of oxygenated, nutrient-rich blood to provide for its high-energy functionality. Blood is supplied to the heart via the left and right coronary arteries (branching off the aorta), with each branch forming a network of arterioles covering the heart's surface. These vessels lie in the epicardium (heart surface tissue) and nourish the deeper areas of the myocardium (heart muscle tissue) by sending branches inward towards it.

Any abnormal deformation of an arterial segment can result in increased vascular resistance and often lead to very serious health risks. Occlusion of a blood vessel is an example of one such deformity and is usually caused by the build-up of cholesterol or fibrous tissue on the wall of the vessel, a condition commonly referred to as thrombosis (this change in vessel wall structure is often also termed atherosclerosis). Such an occlusion, when found restricting coronary circulation, prevents oxygen and nutrients from entering and nourishing a particular myocardial area (myocardial ischaemia). With the heart effectively starved in this area, contraction of cardiac muscle ceases and the heart is placed under increased strain. This strain can become very severe and build up to the dangerous and often fatal state of heart attack (myocardial infarction).

In 2003, 34% of Americans had some form of cardiovascular disease, with 6.3% of all Americans suffering from coronary heart disease and 3.5% experiencing myocardial infarction (Heart Disease and Stroke Statistics, 2006). In 2006, cardiovascular disease cost the American government a staggering $403 billion. According to a survey conducted by the Burden of Disease Research Unit in 2003 (Bradshaw *et al.,* 2003) the incidence of heart disease in South Africa is no different, with cardiovascular disease accounting for 17% of mortality in 2000. Despite increased awareness and the improvement of modern cardiovascular medication, invasive surgery to correct diseased vessels is inevitable.

Various surgical procedures exist to prevent or reverse the closure of coronary vessels, the most popular being arterial stenting. A stent is a small spring-like device designed to open and reinforce arterial sections. It is most commonly deployed by means of a balloon

catheter and, depending on its required location enters the body through the femoral or brachial artery. Once the stent has reached the desired location the balloon is inflated (or an expansion mechanism initiated, in the case of self expanding stents), causing both stent and artery to spring open. Stenting increases the flow of blood through congested arterial sections and, as such, prevents myocardial infarction.

Coronary stents fall under the broad classification of implanted medical devices and have various standards and requirements to which they must adhere. All implanted medical devices should retain full mechanical integrity for their intended duration of life within the human body. Through thorough testing and inspection of stents, the risk of premature degradation can be avoided.

1.1 Project Aim

Recent European standards require *in vitro* stent testing of at least 380 million cycles, to simulate 10 years of operation in the human body. The latest standard (BS EN 14299:2004) states that "Tests shall be conducted under conditions simulating *in vivo* radial, axial and other loads as appropriate". In order for stent manufacturing companies to comply with these and other standards, a testing device would be required to simulate these loads as accurately as possible.

It is therefore the aim of this project to design a machine capable of testing how well DISA Vascular's stents retain mechanical integrity over a simulated period of 10 years.

Furthermore, due to commercial time constraints and thus the need for relatively fast evaluation processes, the effective 10 year time period should be reduced to a few months. The machine should be designed to simulate physiological conditions (of the coronary arteries) as closely as possible and induce the required loading (BS EN 14299:2004). An investigation into stent fatigue characteristics and crack propagation will also be conducted. This will serve as the basis for evaluating the results obtained after the simulated 10 year period.

1.2 Project Goals

The goals of the project are to:

- Design a machine capable of subjecting coronary stents to cyclic loading while adequately simulating conditions they would normally experience in a human coronary artery. The machine would need to simulate at least 380 million cycles of loading (10 year lifespan at approximately 72 beats per minute).
- Study the motion of coronary arteries and understand the important parameters governing their behaviour. These motion parameters will serve as design criteria for the fatigue testing machine.
- Understand stent fatigue and the initiation and propagation of cracks across its structure.

1.3 Overview of Dissertation

The project starts off in Chapter 2 with a brief overview of the structure and functionality of the heart and its vessels. Chapter 3 is concerned with the history and evolution of stents, and then moves on to describe their fatigue characteristics and fracture mechanics. Chapter 4 describes stent fatigue testing considerations and presents an overview of current fatigue-testing trends. Chapters 5 through 8 discuss the design process implemented throughout the project, and neatly summarize the steps undertaken from start to finish. Chapter 9 presents the results of machine testing and evaluates them based on the engineering specifications adopted at the beginning of the project. Chapter 10 ends by discussing the project's outcome, draws conclusions and forms recommendations based on these conclusions.

Chapter Two

Anatomy and Physiology of the Heart and Coronary Vessels

2.1 Introduction

This chapter will briefly discuss the anatomical and physiological properties of the heart and its surface vessels.

2.2 Cardiovascular Anatomy

2.2.1 Anatomy of the Heart

The heart, situated within the thoracic cavity between the lungs, is roughly the size of a clenched fist and is responsible for circulating 5 litres of blood approximately 38 million times per year (Sherwood, 2004). Two-thirds of the heart lies to the left of the midline with its apex resting on the superior surface of the diaphragm. The heart and its main vessels (Figure 2.1) are held in place by the fibrous pericardium, a layer of connective tissue forming a 'sac' around the heart. This layer of parietal pericardium is responsible for producing the lubricating pericardial fluid (filling the pericardial cavity) in which the heart is suspended.

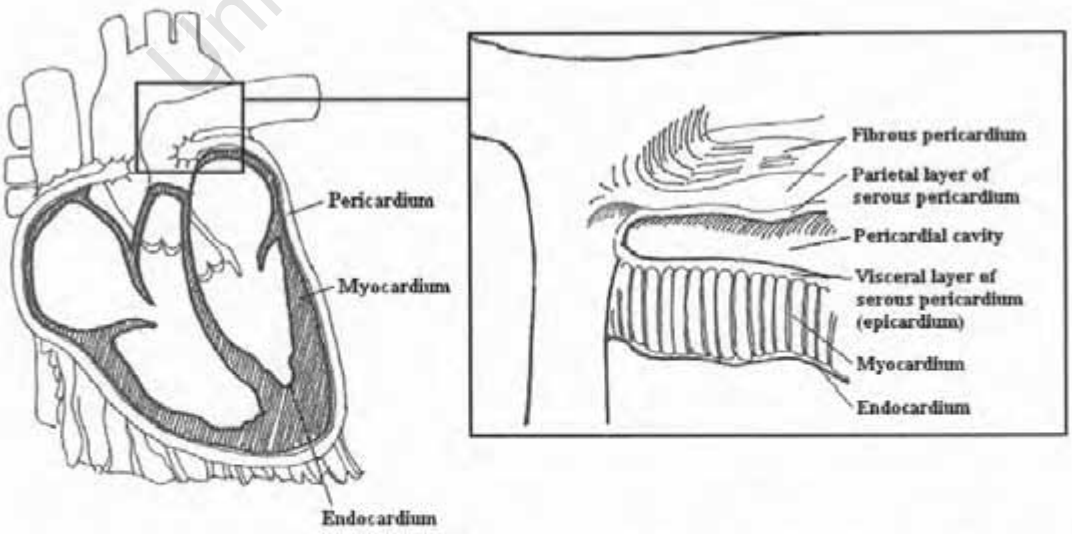

Figure 2.1 The heart and its layers [Adapted from Hatchett R and Thompson D, (2002)]

The heart wall can be divided into 3 layers: epicardium, myocardium and endocarium. The epicardium consists of a thin layer of smooth fibrous tissue, housing the heart muscle and providing a layer upon which the coronary arteries lie.

The myocardium is the thick muscular layer of the heart and is responsible for providing adequate contractile force to pump blood to various areas. The left ventricle must pump blood to all areas of the body and, as such, has the thickest layer of myocardial tissue. The endocardium forms the heart wall's internal layer and is composed of squamous epithelium bound to a thin layer of connective tissue.

The heart is internally divided into four distinct chambers: two atria (left and right) and two ventricles (left and right). Deoxygenated blood enters the right atrium through the superior and inferior vena cava, having been drained from upper and lower parts of the body respectively. The coronary circulatory system drains its deoxygenated blood into the right atrium through the coronary sinus. Once the right ventricle has been filled with blood arriving from the atrium, myocardial tissue of this chamber contracts and forces the blood out of the heart through the pulmonary arteries to be oxygenated in the alveoli of the lungs. Backflow of blood from the right ventricle to the right atrium is prevented by the tricuspid valves (Sherwood, 2004).

Once oxygenated, blood re-enters the heart via the pulmonary veins into the left atrium. Again, once sufficient blood had collected in the left ventricle, contraction occurs and forces nutrient-rich, oxygenated blood out through the aorta to the rest of the body. The bicuspid valves between the left atrium and ventricle prevent backflow between these two chambers. A small amount of oxygenated aortic blood branches off from the aorta at an early stage and is used to replenish the coronary circulatory supply.

2.2.2 Histology of Blood Vessels

The human circulatory system and its blood vessels serve a number of very important functions. Not only do they bring fresh supplies (nutrients, oxygen and various other dissolved substances) to the vicinity of all bodily cells for absorption (arterial branches), but they also remove their wastes (venous branches). The circulatory system is also of

crucial importance in maintaining homeostasis within the body. Due to its design, it is able to ensure correct pressure distributions and temperature gradients throughout the body.

2.2.2.1 Types of Blood Vessels and their various Layers

In order to maintain a steady flow and create appropriate pressure gradients, blood vessels leaving the heart become progressively smaller en route to their final destination (Van De Graaf, 2002). In addition to their gradual decrease in size, vessel composition also varies depending on its location in the vascular system. The vessels leaving the heart are referred to in order of decreasing diameter as arteries, arterioles and capillaries. At the microscopic capillary level, material exchange (between blood vessel and cell) occurs and the once fresh and nutrient-rich arterial flow begins its journey back towards the heart in the venous circuit. The vessels of the venous circuit are referred to in order of increasing diameter as capillaries, venules and veins.

The walls of blood vessels can be divided into 3 layers: tunica externa, tunica media and tunica interna. These layers, in addition to the gradual decrease in vessel diameter, are illustrated in Figure 2.2. With the exception of capillaries, all blood vessels are composed of these 3 layers to a greater or lesser extent.

Tunica Externa

The tunica externa (sometimes referred to as the adventitia) forms the outer layer of arteries and veins. Consisting of a network of connective tissue, collagen and elastic fibres, it enables vessel flexibility and anchors the vessel to the surrounding tissues. In the tunica externa of larger arteries and veins, vasa vasorum (literally meaning vessels of the vessels) are often present. These vessels enable blood flow to the cells of larger arteries and veins, a process not required in thinner walled vessels due to their ability to diffuse substances directly from the blood flowing through them.

Tunica Media

The tunica media forms the middle layer of arteries and veins and consists of smooth muscle cells and elastic tissue. Bound internally by the internal elastic layer (IEL) and

externally by the external elastic layer (EEL), it separates the tunica externa from the tunica interna. The combination of muscle and elastic fibre present within the layer allows for vessel expansion (when blood is pumped through them following ventricular contraction) and recoil (following ventricular relaxation). This behaviour is analogous to that of a rubber band.

Tunica Interna

The tunica interna, also called the tunica intema, forms the innermost layer of blood vessels and effectively creates the channel through which blood flows (lumen). Consisting predominantly of squamous epithelial cells and elastic fibres, it is the only layer that is present in all blood vessels.

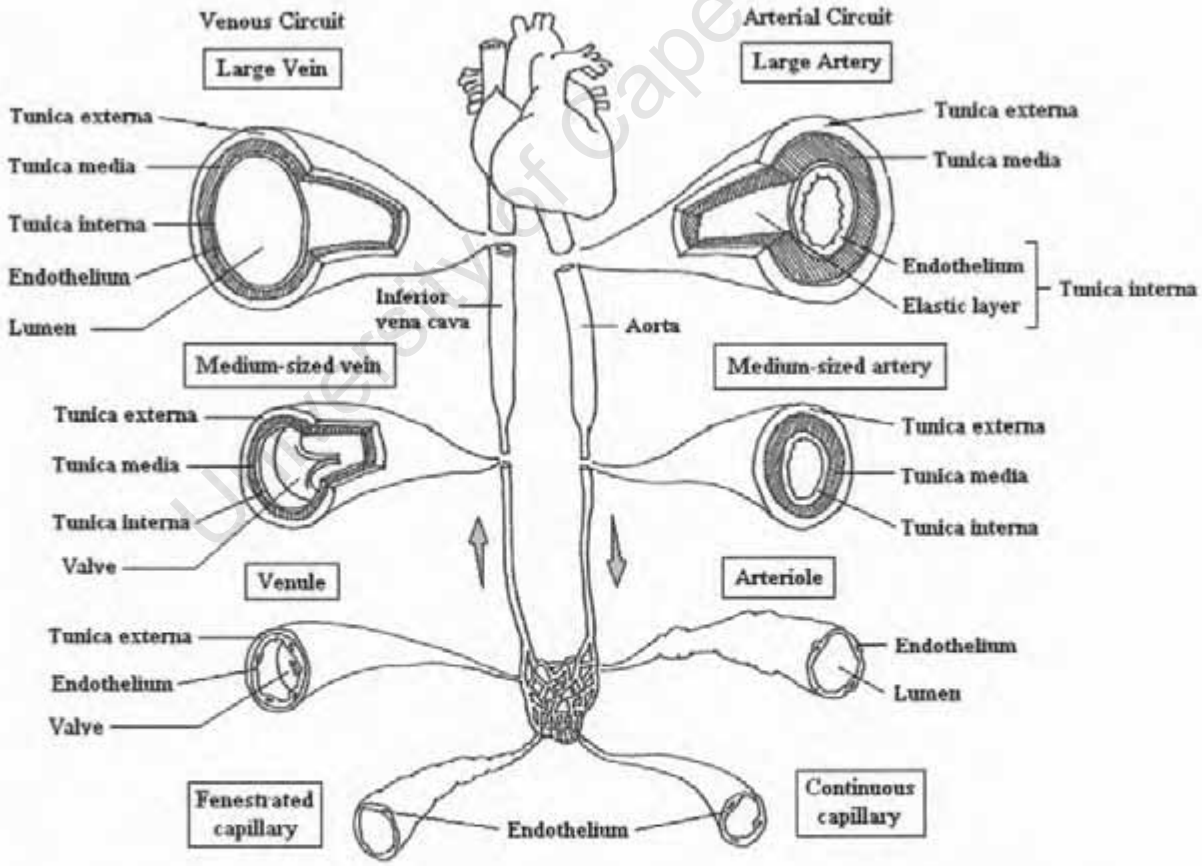

Figure 2.2 Type and variation of blood vessel structure [Adapted from Van De Graaf, (2002)]

2.2.2.2 Variation in Blood Vessel Structural Composition

Arteries, veins and capillaries vary in lumen size, wall thickness and structural composition. While the three layers mentioned in section 2.2.2.1 are common to most of these vessels, the proportion of these layers varies with vessel function. Table 2.1 summarizes the differences in vessel composition across the vascular range.

Vessel	Lumen diameter	Wall thickness	Tunica Externa	Tunica Media	Tunica Inerna
Large artery	25 mm	2 mm	Thinner than tunica media layer. Composed of lonely arranged collagen fibres. Vasa Vasorum present.	Thickest layer of the larger arteries. Very high elastic fibre content rendering the IEL and EEL not very distinctive.	Epithelial cells present with a relatively thick layer of sub-endothelial connective tissue.
Medium - sized artery	3 - **4** mm	**1** mm	Thinner than tunica media layer. Highly collagenous with fibroblasts present.	Very thick layer. Greater amount of smooth muscle tissue present and less elastic fibre. IEL and EEL more distinctive.	Epithelial cells with less of a sub-endothelial connective tissue layer than in larger arteries.
Arteriole	30 pm	20 pm	Thinner than tunica media layer. Not very distinct.	Very thin layer of smooth muscle cells (1-2 layers). IEL and EEL not very distinct.	Very thin epithelial layer. Sub-endothelial connective tissue seldom present.
Capillary	8 pm	1 pm	Absent	Absent	Single squamous epithelial layer. Could be of the continuous, fenestrated or disontinuous kind.
Venule	20 pm	2 pm	Thickest layer of the venule and is highly collagenous.	Not very distinct at all, consisting of only a few layers of smooth muscle cells.	Very thin epithelial layer. Sub-endothelial connective tissue seldom present.
Medium - sized vein	**4 -** 5 mm	0.5 mm	Slightly thicker than the media layer. Highly collagenous with some elastic fibres also present.	Several layers of circularly arranged smooth muscle cells.	Epithelial layer rather thin. Transition from interna to media not very distinct. Small amounts of sub-endothelial connective tissue present.
Large Vein	30 mm	1.5 mm	Thickest layer and consists of many longitudinally arranged smooth muscle bundles surrounded by collagen fibres. Vasa Vasorum also present.	Relatively thin layer consisting of circular arranged smooth muscle fibres.	Thin epithelial layer. Sub-endothelial connective tissue also present.

Table 2.1 Summary of different vessel compositions throughout the circulatory system [data obtained from Gray's Anatomy (1977), Van De Graaf (2002)]

2.2.3 The Coronary Circulatory System

The coronary artery circulatory system (see Figure 2.3) can be divided into two main branches, the left main coronary artery (LMCA) and right coronary artery (RCA). Each main branch services its respective side of the heart by further dividing into sub-branches and eventually finer arterioles, forming a network of circulation around the heart.

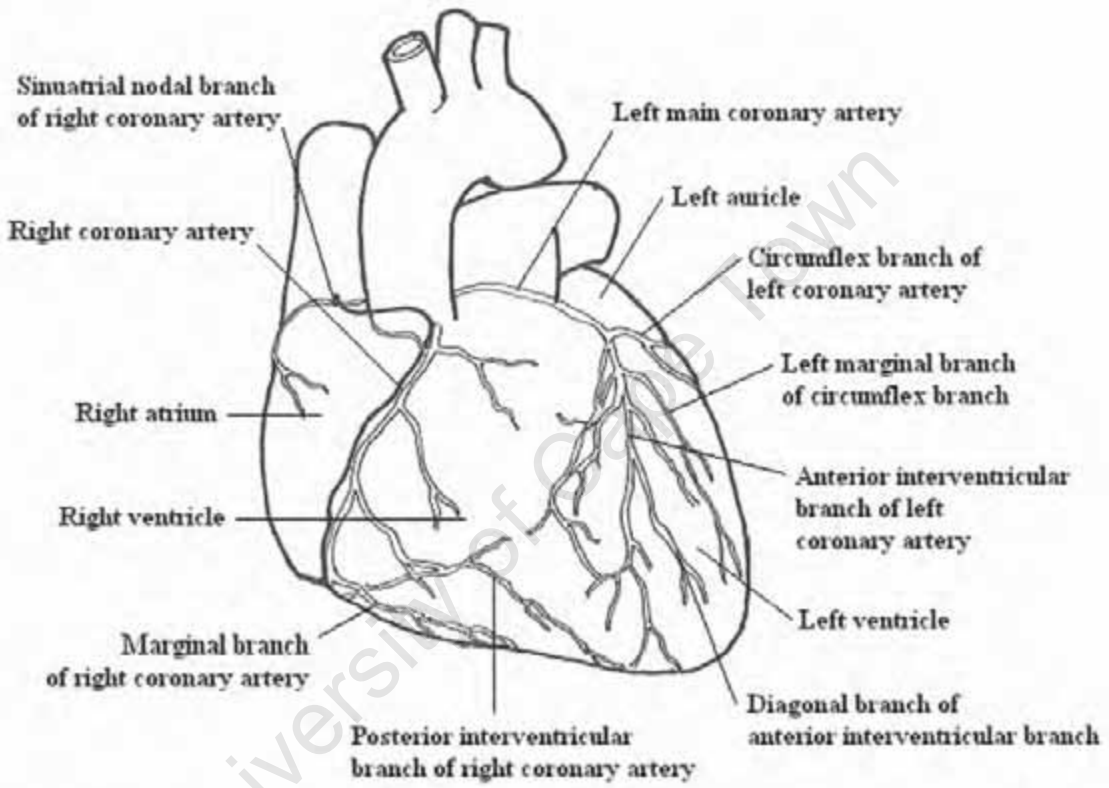

Figure 2.3 The coronary circulatory system [Adapted from Canby, (2006)]

The LMCA branches off from the base of the aorta and runs anteriorly towards the left side of the heart before branching into the left circumflex artery (LCX) and left anterior descending artery (LAD). The LCX primarily services the left posterior side of the heart while the LAD covers the left anterior surface. The LAD divides further into diagonal branches laterally and medially into the interventricular septal branches.

While the LMCA consists of two main arteries (LAD and LCX), the RCA is primarily a single vessel. Running anteriorly towards the right side of the heart, this vessel also originates from the base of the aorta. The RCA then travels down the right anterolateral surface of the heart before splitting and wrapping fully anteriorly and posteriorly at the

bottom. The LCX and posterior section of the RCA join in a capillary network on the heart's posterior surface.

2.2.3.1 Histology and Morphology of Coronary Arteries

This section presents a more in-depth look into: the histology (structural composition of biological organisms) and morphology (study of the form or shape of an organism or part thereof) of the coronary arteries; their clinical detection and reconstruction; and changes or irregularities that could be associated with the onset of coronary atherosclerosis.

Coronary arteries vary in lumen size and wall thickness depending on their location and can generally be regarded as having similar structural compositions to that of the medium-sized arteries listed in Table 2.1. Since the illustration of Figure 2.3 represents a general layout of the heart's surface coronary vessels, it is important to realize that the exact shape and length of the various coronary branches vary from person to person. With numerous medical imaging techniques available, the exact morphology of patients' coronary vessels can be visualized and interpreted in far greater detail. Ultrasound, angiograms, CT scans and MRI have all been used (Bourantas *et al.,* 2003; Hennemuth *et al.,* 2005; van Geuns *et al.,* 1999) in conjunction with various software algorithms to more accurately visualise the coronary arteries. Techniques of this kind are of vital importance to doctors in the accurate diagnosis of coronary artery disease. An example of an angiogram image is presented in Figure 2.4.

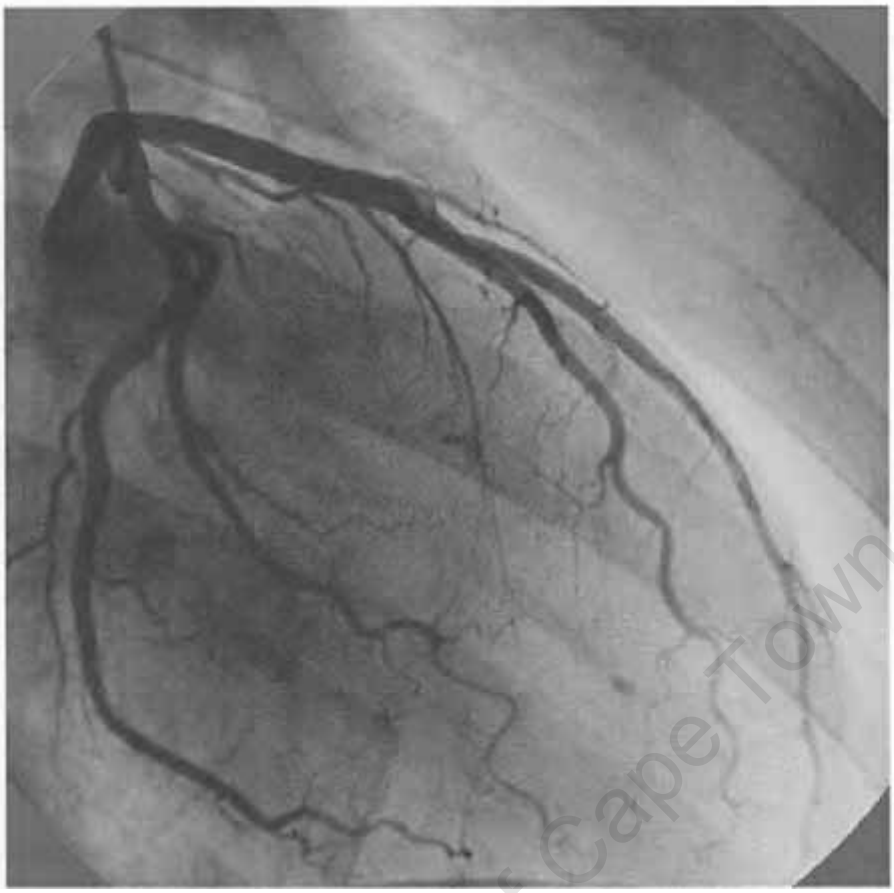

Figure 2.4 Angiogram illustrating the coronary vessels of the heart (Obtained through DISA Vascular from standard patient records at Groote Schuur hospital, Cape Town, South Africa)

Not only do the aforementioned imaging techniques lend themselves to the reconstruction of coronary arteries along their length, but they also serve as an excellent means of visualising the artery in cross-section (Sinha *et al.,* 2006; Shimamoto *et al.,* 2005; Fayad *et al.,* 2000). Localized plaque build-ups and inherent vessel weaknesses are just some of the important irregularities that can be detected using such techniques. As in the case with axial vessel imaging, doctors can more accurately diagnose cardiovascular ailments with these techniques.

It has been proven that certain geometric features increase the likelihood of atherosclerosis in coronary vessels (Friedman *et al.,* 1996). Branch angle, curvature, intima and media thickness and vessel length have all been proven to contribute to a higher coronary disease risk. Arbel *et al.* (2005) has also shown the significance of RCA shape (C or S-like vessel curve) on atherosclerosis development. Table 2.2 below summarizes some of the common

correlations between geometry and pathology as published in prior work findings by Friedman *et al.* (1996).

Correlations of geometry and pathology - Prior Work

Arterial Segment	Geometric feature(s) (superscript denotes method of measurement)	Pathological endpoint (superscript denotes method of measurement)	Geometric feature associated with higher risk	Ref.
Left anterior descending (LAD) and circumflex coronary (LCX)	Left main coronary artery (LM) length[a]	atherosclerosis'	Short LM	Gazetopoulos *et* a/. (1976) [num]
LAD and LCX	LM length[y]	Severity of lesions[a]	short LM	Gazetopoulos *et* (1976) [num]
LM, LAD, LCX	LM length, LAD-LCX branch angle[d]	Presence of severe lesions, particularly	Short LM, potentiated by large angle	Saltissi *et al.* (1979)
Aorto-iliac region	Aortic bifurcation angle	Presence of occlusive disease[a]	Small angle	Sharp *et al.* (1982)
Internal carotid artery (ICA) bifurcation	Turning angles of daughter vessels`	Incidence of lesions on outer walls at branch'	Smaller turning angle	Sakata *et al.* (1985)
LAD and first diagonal branch (D1)	Two projections of LAD-D1 branch angle'	Distribution of lesions'	Small or large angles	Endoh *et al.* (1988)
ICA	Radius of curvature'	Fibrous plaque involvement[a]	Small radius of curvature	Sakata and Takebayashi (1988)
Anterior inferior aorta	Aorto-renal branch angle	Plaque involvement relative to entire inferior aorta[a]	Large angle	Nguyen and Hague (1990)
ICA	ICA-common carotid artery area ratio; ICA external CA branch angle[d]	Percent diameter stenosise	Large area ratio; no effect of angle	Fisher and Fieman (1990)
LAD	Angles at LM bifurcation'	Any significant stenotic lesion[a]	Large LAD turning angle; no effect of other angles	Ikeda *et al.* (1993)
LAD and LCX	LAD-LCX branch angle'	Extent of proximal sudanophilias	Small angle	Friedman *et al.* (1993)
Superficial femoral	Tortuosity'	Roughness of lumen border'	High tortuosity	Smedby *et al.* (1993)

'Direct measurement

[b]Orthogonal biplane angiograms; Pythagorean theorem.

[c]Angiography.

[d]Single plane angiography.

'Not specified.

[f]Oualitative.

'Biplane angiograms; 3-D reconstruction.

LAD = Left anterior desc. coronary artery

LCX = Left circumflex coronary artery

LM = Left main coronary artery

RCA = Right coronary artery

Table 2.2 Correlations of geometry and pathology — prior work [Adapted from Friedman *et al.* (1996)]

Friedman *et al.* (1998) went on to provide more evidence as to how asymmetry of the intima and media in daughter vessels departing the LAD becomes greater with increased branch angle. The resultant asymmetric wall thickness distribution lends itself to increased lipid accumulation and thus greater coronary atherosclerotic risk (Stacy *et al.*, 1992)

From the above information it becomes clear that coronary arteries vary from person to person in both histology and morphology. Geometric and morphological factors have a great impact on the development of atherosclerosis in the coronary vessels and, with age, gender, health and heart condition having major effects on these factors (Kucher, 2001; Dodge, 1992), one cannot deny the importance of a healthy lifestyle.

2.3 Cardiovascular Physiology

2.3.1 Blood Flow Dynamics

As with any other fluid flow problem, blood flow can be modelled and expressed in terms of traditional fluid dynamic principles. One of the biggest differences though between flow through a coronary vessel and that of a water pipe (for example), is the fact that a vessel is a living tissue. Plaque build-ups on the vessel wall, aneurysms and thrombotic activity are just some examples of how the vessel geometry can be changed, potentially resulting in far greater fluid dynamic considerations than a simple water pipe.

2.3.1.1 Newtonian vs Non-Newtonian Flow

A fluid with a shear rate directly proportional to shear stress is known as a Newtonian fluid (Figure 2.5). Regardless of the amount of force induced on the fluid to set it in motion (viscosity), it will always respond in a linear manner.

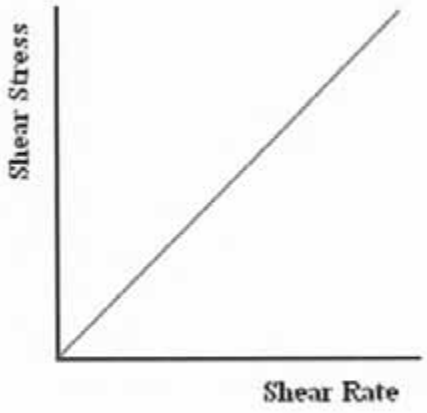

Figure 2.5 Newtonian flow

Some fluids have a non-linear shear stress vs shear rate and are said to be Non-Newtonian. The viscosity of such substances does not behave in the linear way Newtonian fluids do and can either be referred to as shear thinning of shear thickening (Figure 2.6). A shear thinning fluid has a viscosity that decreases with increased shear rate, while a shear thickening fluid's viscosity increases with increased shear rate.

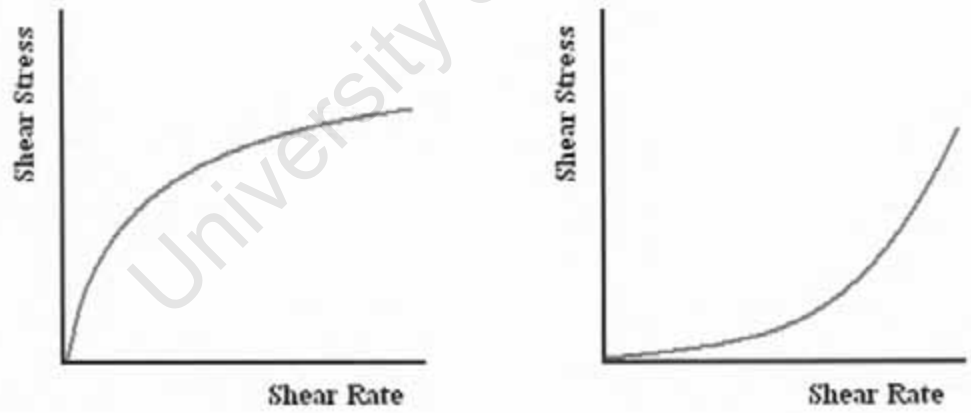

Figure 2.6 Non-Newtonian flow: shear thinning (left) and shear thickening (right)

There has been much debate as to whether blood should be approximated as a Newtonian or Non-Newtonian fluid. According to research conducted by Johnston *et al.* (2006), the error in treating it as a Newtonian fluid (for the relatively simple purpose of analysing wall shear stresses) was minimal despite concerns of it being more Non-Newtonian in nature at low flow rates (Pedley *et al.*, 1980). Non-Newtonian approximations can generally be

assumed when the microscopic properties of blood and its cells are being examined. For all other purposes however a simplistic Newtonian model is more than adequate.

For the purpose of this project, blood will be treated as a Newtonian fluid and simulated as water. Mineral composition and pH of the water will be adjusted to simulate physiological conditions as closely as possible (Section 8.2.1).

2.3.1.2 Laminar vs Turbulent Flow

Laminar flow, sometimes referred to as streamline flow, occurs when a fluid flows in parallel layers. This type of flow is very different from turbulent flow which is far more "violent" in nature, tending to form vortices and rapid pressure variations at very high speeds.

In most cases, blood flow can generally be regarded as being laminar in nature, with slight turbulent activity only really presenting itself in the larger arteries at peak systole (Section 2.3.2) and distal to areas of high stenotic activity.

2.3.2 Blood Pressure Distribution throughout the Body

As briefly mentioned in Section 2.2.2.1, blood vessels become progressively smaller as they find their way from the heart towards distal extremities of the body. The reduction of vessel diameter is of crucial importance in maintaining reasonably constant blood pressures throughout the body. If blood vessels were of constant cross-section throughout the body, frictional pressure losses would occur the further blood moved from the heart. Gravitational effects would also produce adverse pressure distributions.

The pumping action of the heart sets up pressure waves through the blood vessels as blood is forced through them. Maximal pressure (upper point of pulse wave) is known as systolic pressure while the lower boundary pressure is called diastolic pressure. Blood pressure readings are normally represented in mmHg and expressed as systolic/diastolic (120 mmHg/80 mmHg, for a healthy individual under 35 years of age). The difference between systolic and diastolic pressures is referred to as pulse pressure and is generally in the order

of about 40 mmHg. Figure 2.7 below illustrates the variation in blood pressure distribution throughout the body's vessels.

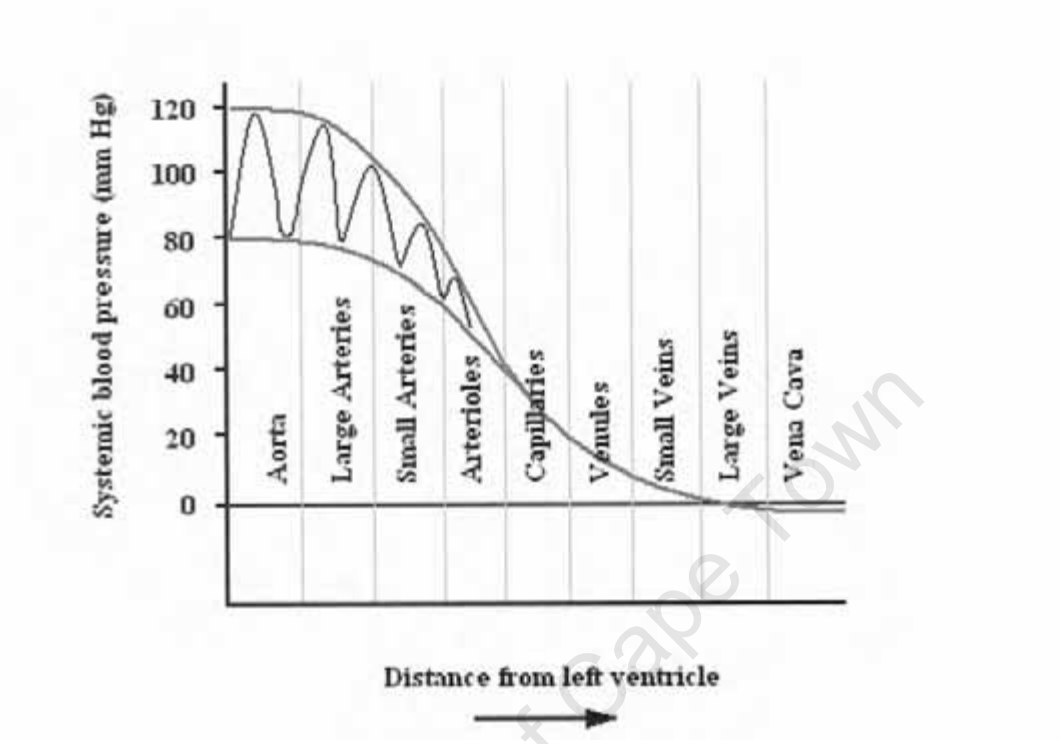

Figure 2.7 Variation in blood pressure distribution [Adapted from Van de Graaf, (2002)]

2.3.2.1 Coronary Blood Pressure

In normal healthy coronary arteries there is little pressure loss across the vessel length and coronary pressure can generally be regarded as aortic pressure minus central venous pressure (CVP). With CVP being close to zero, its effects on coronary pressure are generally ignored, resulting in healthy coronary pressures equal to that of aortic pressures (varying dependant on health, but generally regarded as 120/80 as mentioned in Section 2.3.2).

In the case of stenosis, pressure losses do occur and, depending on severity, can affect distal coronary pressure losses significantly. Pressure decrease as a result of stenosis is expressed in terms of a fractional flow reserve (FFR) and represents a percentage of normal perfusion distal segments are receiving due to proximal stenotic activity. An FFR

of 0.6 in a specific vessel segment would thus mean that distal portions of that vessel are only receiving 60% of their normal flow and, as a result, myocardial perfusion in that area is 40% lower than normal. Coronary stenting has the effect of increasing the FFR of congested vessels and combats the effect of reduced myocardial perfusion.

2.3.3 Coronary Artery Circulation

With coronary pressures and fluid flow considerations mentioned in previous sections, this section will attempt to gain some insight into the general physiology, motion and average compliance of the coronary vessels.

2.3.3.1 General Physiology

The coronary artery circulatory system nourishes the myocardium by sending smaller branches downward through the epicardial layer. In this way a supply of fresh oxygenated blood is carried directly to the heart muscle, eliminating the need for diffusion between the heart chamber and myocardium. These myocardially penetrating arteries actively deliver blood when the heart is in a relaxed state, but are squeezed close and generally restricted when the ventricles contract. This action results in an intermittent and pulsating flow of blood to the myocardium (Marieb, 1998).

After flowing through the capillary beds of the myocardium, deoxygenated blood is collected in the cardiac vein and transported to the main coronary sinus. This vessel empties the blood into the right atrium and in so doing completes the cardiac circulatory circuit.

Since the coronary arteries line the surface of the heart, average coronary blood temperature is equal to average human core temperature at 37°C. Although people generally exhibit slightly different core temperatures, it is important to realize that 37°C is the recognized average.

2.3.3.2 Motion of the Coronary Vessels

The motion of coronary arteries has recently seen an increase in interest amongst biomechanical and clinical investigators. This increased interest stems from a long believed notion that movement of these vessels might play a role in the development of coronary atherosclerosis (Friedman ***et al.,*** 1999). Regardless, the coronary artery motion parameters gathered in these and other tests (Ding ***et al.,*** 2002; Johnson ***et al.,*** 2004; Shechter ***et al.,*** 2006) are very useful in understanding their behaviour.

Motion of the coronary arteries, coupled with cyclic pressure fluctuations, is among the principal causes of vessel stresses and strains. It is therefore unsurprising that by understanding these properties one could quite accurately simulate their behaviour in a "mock artery".

Using various techniques (Hofman ***et al.,*** 998; Friedman ***et al.,*** 1999), the primary motion parameters identified and analyzed for both RCA and LAD are summarized in Table 2.3. All of the parameters listed below are a function of time and distance along the vessel axis.

Parameters	Definition
Displacement	3D displacement of a material point
Strain	Relative length change of a segment
Curvature (C)	Amount by which a geometric object deviates from being flat
Bending	Rate of change of curvature
Pulse Curvature	Cmax - C1- over a cardiac cycle
Torsion (T)	Measure of how sharply a curve is twisting
Twisting	Rate of change of torsion
Pulse Torsion	Tmax - TM;,, over a cardiac cycle

Table 2.3 Coronary artery motion parameters of primary interest [Adapted from Ding ***et al.,*** (2002)1

By making use of clinical biplane coronary cine-angiograms, Ding ***et al.*** (2002) quantified these parameters for both RCA and LAD (Table 2.4). These results are consistent with the

findings published by Hofman *et al.* (1998) who measured similar motions by means of MR'. It can be observed from the findings of Table 2.4 that mean total displacement (MTD) and mean total twisting (MTT) are the only parameters that exhibit a significant difference in magnitude between RCA and LAD (with p values less than 0.05). In addition to this, it should be noted that all values presented in Table 2.4 include one standard deviation (as apposed to a more conservative approximation of three standard deviations).

Parameters	Unit	RCA	LAD	p value
Mean total displacement (MTD)	cm	6.00 ± 2.59	2.91 ± 0.74	0.009
Mean total strain (MTS)	cm/cm	0.054 ± 0.020	0.040 ± 0.018	0.24
Mean average curvature (MAC)	cm^{-1}	0.39 ± 0.10	0.48 ± 0.17	0.35
Mean total bending (MTB)	cm	0.95 ± 0.35	1.16 ± 0.44	0.44
Mean pulse curvature (MPC)	cm^{-1}	0.33 ± 0.14	0.39 ± 0.12	0.29
Mean average torsion (MAT)	cm	1.50 ± 0.60	2.69 ± 0.79	0.03
Mean total twisting (MTT)	cm	12.13 ± 5.50	26.35 ± 14.60	0.09
Mean pulse torsion (MPT)	cm^{-1}	4.45 ± 2.59	8.65 ± 5.08	0.16

Table 2.4 Variability of coronary artery motion parameters [Adapted from Ding *et al.,* (2002)]

The above information, although very informative, represents average values over an entire cardiac cycle. Parameters like MTD and MTB are relative in this context and include cardiac motion (heart motion within the pericardial cavity) and respiratory effects. The problem with this approach is that although the RCA has a MTD of 6 cm, we have no way of accurately gauging its displacement independent of cardiac and respiratory motion. The averaged nature of the above information also does not lend itself to an understanding of local displacements across the entire vessel length.

Shechter *et al.* (2006) and Johnston *et al.* (2004), in attempting to produce clearer CT and MR angiography imaging techniques, produced data similar to the findings of Ding *et al.* (2002) and Hofman *et al.* (1998). Their data was expressed across a cardiac cycle and gave a clearer idea as to the arteries' motion parameters along their length. Again, however,

data was inclusive of cardiac and respiratory motion and very little information regarding pure coronary displacement could be obtained.

Due to the difficulty in separating pure coronary displacement (as a result of pressure through the vessel and cardiac surface motion) from cardiac and respiratory motion, attention was turned to the dynamics of coronary curvature throughout the cardiac cycle.

Curvature -- quantified in the findings of Ding *et al.* (2002) but again presented as an average value -- can be defined as the inverse of the radius of an osculating circle (drawn so as to touch closely) at a specific point on a curve. Figure 2.8 below illustrates this definition.

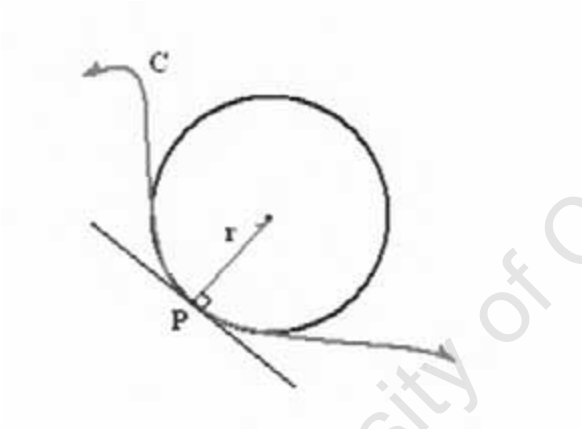

Figure 2.8 2-D illustration of curvature calculation

If the radius of the circle illustrated in Figure 2.8 (drawn to fit neatly into curve C at point P) has a radius of 5 cm for example, the curvature at point P could be expressed as 1/5 = 0.2 cm^{-1} . Straight lines have a curvature equal to zero, since any osculating circle drawn at a point on the line would be of infinite radius.

By making use of biplane cine-angiography, Gross *et al.* (1998) studied the dynamics of coronary artery curvature as pertaining to a segment of a human LAD. Plotting the difference between maximum and minimum curvatures (flexing) at each point along the vessel length, their results provide useful information. Figure 2.9 illustrates this flexing along the vessel length across two cardiac cycles.

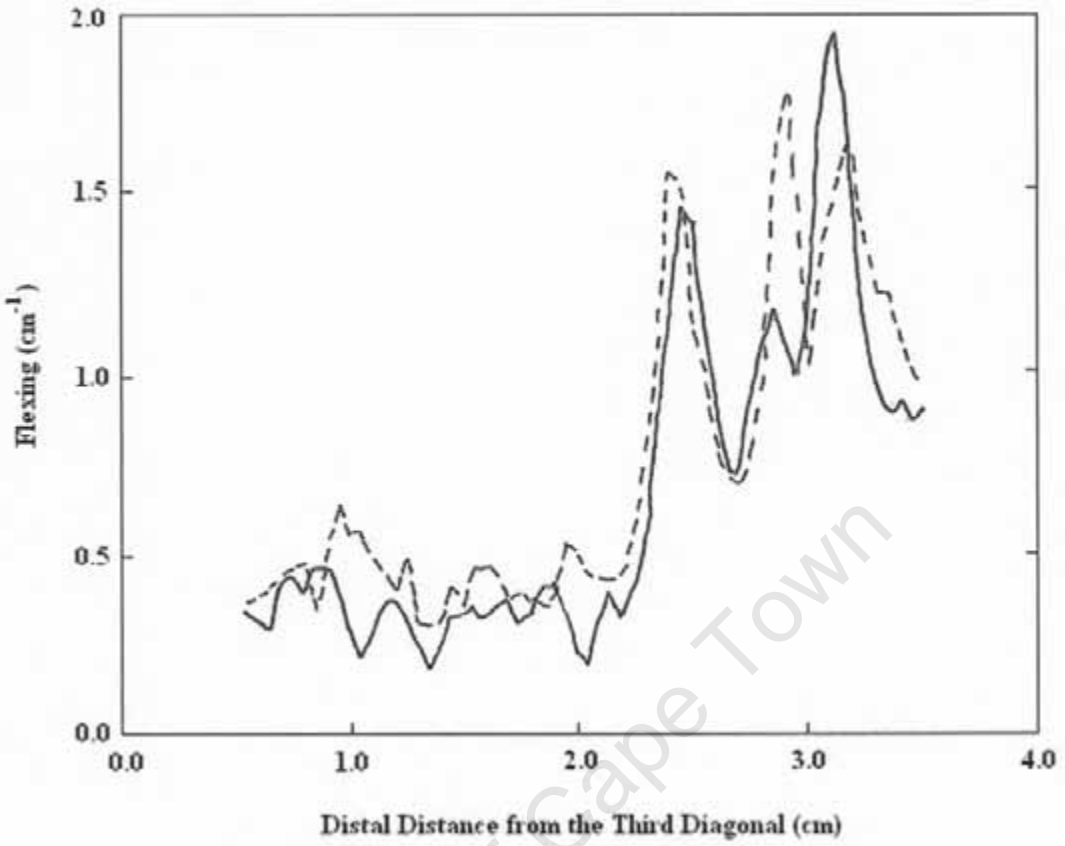

Figure 2.9 Flexing along LAD vessel segment for two cardiac cycles *(Gross et al.,* 2002)

From Figure 2.9 we can see that maximum flexing occurs approximately 3.2 cm distal to the third diagonal of the LAD vessel segment and measures roughly 1.8 cm^{-1}. The results agree with those of Prosi *et al.* (2004), who observed curvature variations of between 0.1 and 0.9 cm^{-1} along a 0.45 cm segment of human LAD. Pao *et al.* (1992) found that the dynamic change in curvature experienced by a coronary artery can be as high as 80 percent of the mean curvature. This finding, when applied to the average curvature values illustrated in Table 2.4 (Ding *et al.,* 2002), further supports the findings of Gross *et al.* (1998) and Prosi *et al.* (2004). Assuming a mean curvature of 0.5 cm^{-1}, a change of 80 percent would increase the curvature by 0.4 cm^{-1} (total flexing), and thus corresponds well with the results illustrated in Figure 2.9.

Vessels producing sharp curvatures are seldom stented, as these vessels most often lie very distally and contain lumen diameters too small to access. Another factor worth mentioning is that vessel flexion is also somewhat inhibited by the insertion of stents due to their slight longitudinal straightening effect (Gyöngyösi *et al.,* 2000).

Designing a machine capable of subjecting stents to curvatures of up to 1.8 cm^{-1} is not only extremely impractical, but generally unnecessary too. For this reason, flexing in the low level range (between 0.4 cm^{-1} and 0.5 cm^{-1}) was considered of primary design importance. For the purpose of this project, vessels will need to be bent to induce maximal curvature changes of at least 0.5 cm^{-1}.

2.3.3.3 Coronary Vessel Compliance

Another parameter of primary concern as pertaining to the scope of this project is that of coronary artery compliance. Compliance can be represented as a change in diameter (Cd) or in volume (C_v) per 100 mmHg with:

$$C_d = \frac{\Delta D}{D \times \Delta P} \tag{2.1}$$

and

$$C_v = \frac{\Delta V}{V \times \Delta P} \tag{2.2}$$

The two forms of compliance are quite different and should not be confused. From this point on, only diametric compliance (C_d) shall be considered.

According to research conducted by Conti *et al.* (2002), healthy arteries can generally be considered to be 3 — 4 percent compliant per 100 mmHg with diseased ones slightly less compliant. The range of 5 — 7 percent compliance per 100 mmHg has been accepted as the general standard for vessels simulating human arteries (discussed in greater detail in Chapter 4).

Chapter Three

Coronary Stents — Some Background

3.1 Introduction

This chapter briefly discusses the evolution of coronary stents, presents examples of various stent types and briefly details their method of insertion into the human body. Section 3.5 moves on to give a brief overview of recognized stent fatigue-life estimation methods.

3.2 Stent History

The concept of the stent developed during the 1980's around the time when interventional cardiologists were experiencing difficulties with early balloon angioplasty techniques (opening of a vessel with a balloon). In some of these early cases the opened vessels would collapse again after the procedure (possibly due to the localized weakening of the vessel wall) and require emergency bypass surgery as a last resort. Restenosis (the post-operative re-occurrence of stenotic activity) also proved problematic and in 1986 the first stent was implanted into a human coronary artery (Puel and Sigwart, 1986) in an attempt to reduce such re-occlusion of the vessel. By 1995 several generations of new stents were available to cardiologists as an alternative means of opening closed coronary vessels.

3.3 Types of Stents Available Today

Stents these days are available in various designs, lengths and material composition but can generally be divided into two groups: self expanding and balloon expanding varieties. Self expanding stents make use of specialized materials that when released; expand naturally to a predetermined size. Continued gradual expansion over time is one of the problems with such a stent, and for this and other reasons, the balloon expandable variety is normally preferred. This system, on the other hand, relies on a balloon catheter to expand the stent into place by pressurizing the balloon to a predetermined value.

There are numerous balloon expandable stents available today. DISA Vascular (situated in Cape Town, South Africa - www.disavascular.com), for example, produce 3 basic balloon expandable coronary stent varieties; stainless steel, cobalt chromium and stellium drug-eluting stents. Each variety is produced in varying lengths and cell numbers (referring to the number of circumferential scaffold "rings") depending on the type of coronary ailment and its location. Figure 3.1 below shows the basic design of a coronary stent, illustrating surface features like cells, s-links, struts and hairpins.

Figure 3.1 DISA Vascular's 'ChromoFlex' Cobalt Chromium coronary stent

3.4 Insertion and Operation of Coronary Stents

Before a coronary stent is deployed into a troublesome vessel, doctors ensure that the patient receives some form of blood thinning agent (usually Heparin). A thinning agent is necessary to reduce the chance of blood clots forming and clinging to the newly inserted stent. After adequate blood thinning has been achieved an incision is made in the patient's groin from where a small sheath enters the femoral artery. This sheath provides an opening through which the stent will be inserted and also enables a pathway for the injection of a radiocontrast agent needed to visualize the arteries via angiography.

To start off, a guidwire is fed up the femoral artery to the site of blockage in the coronary artery. Next, a thin balloon catheter is threaded onto the guidwire and fed to the blocked

area, inflated slightly and then removed. This initial balloon opening of the occluded area is necessary to pass the stent through. When the cardiologist is satisfied that the blocked area has been adequately prepared for stent insertion, the balloon catheter (with stent crimped around the deflated balloon portion) is fed to the site of vessel obstruction. With the stent positioned carefully in the centre of the blockage, the catheter is pressurized, causing the balloon to expand with the stent following (Figure 3.2). With inflation pressure and related balloon compliance closely linked and known by the cardiologist, the stent can be expanded to the exact required size. Once the stent has been successfully deployed, the balloon catheter is deflated (leaving the stent firmly in place against the vessel wall) and removed from the body. The stent will experience a very slight recoil (decrease in diameter) once the balloon is deflated due to the force exerted on it from the arterial segment and the stent's inherent elastic range. This recoil is however minimal and required deployment pressures take this property into account.

Within the first couple of days of coronary stenting, the internal wall of the artery forms a thin layer of epithelial cells across the surface of the stent. This layer gradually thickens with time and eventually incorporates the stent as part of the vessel wall.

According to DISA Vascular, coronary stents are generally not removed from problematic areas but are occasionally re-stented or, in severe cases, bypassed by grafting new arterial sections around the blocked area.

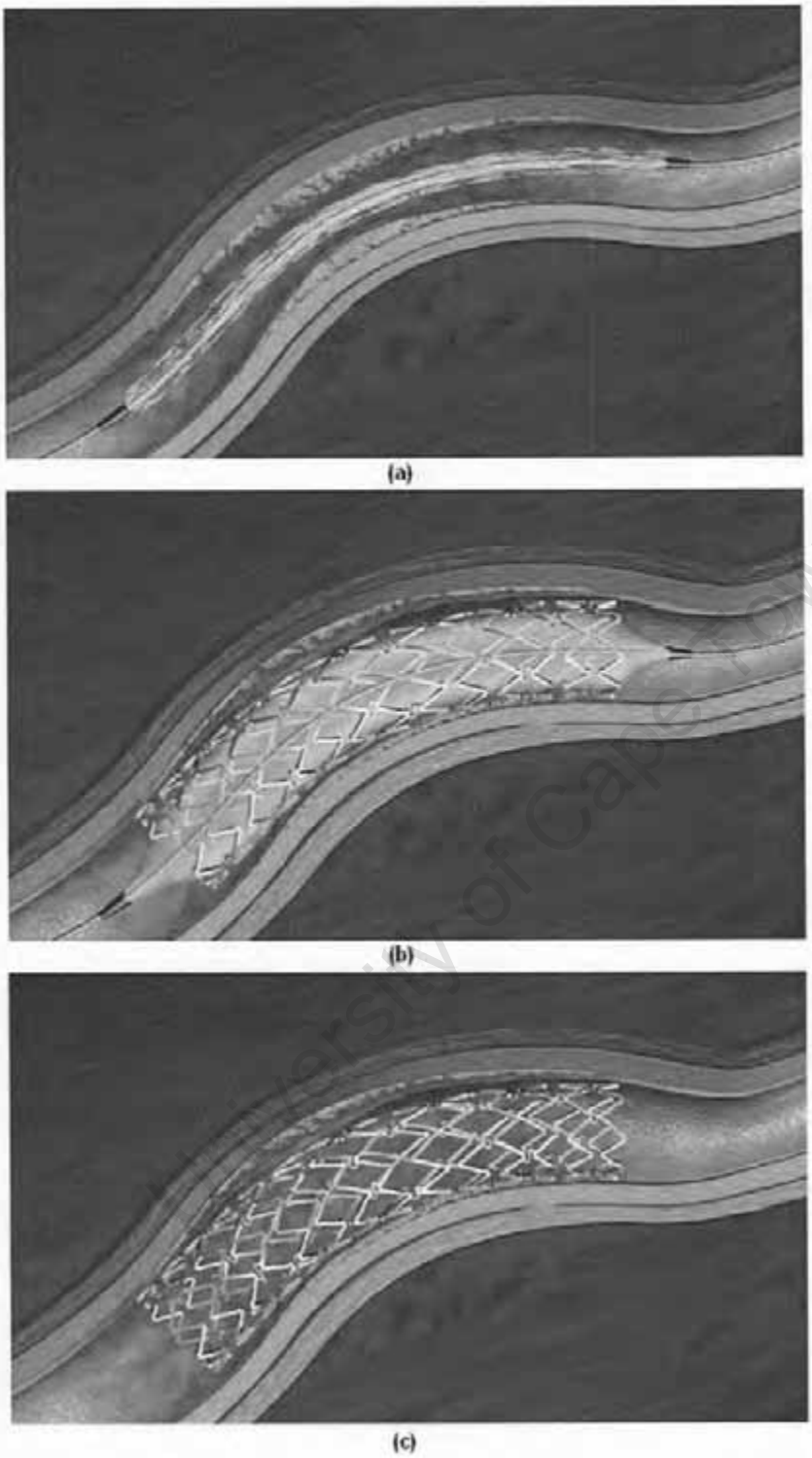

Figure 3.2 Insertion and operation of a coronary stent [Adapted from advertising media of DISA Vascular's ChromoFlex stent]

(a) Insertion of a stent into the middle of a blocked vessel.

(b) Expansion of the stent by means of a balloon.

(c) The newly stented artery with catheter removed.

3.5 Fatigue Considerations

3.5.1 Introduction

Medical standards require that coronary stents survive at least 380 million cycles of loading during their intended life span. Assuming an average heart rate of 72 beats per minute, this translates to approximately 10 years.

This section will discuss the general principles of fatigue and the various life estimation methods generally used to evaluate the performance of stents.

3.5.2 Definition of Fatigue

Metal fatigue can be defined as the progressive and often localised structural damage of a metal when subjected to cyclic loading. Even with an applied cyclic load much lower than that of the material's static yield strength, the metal can fail over time. This resultant failure can directly be attributed to the initiation and propagation of microscopic cracks within the metal during cyclic loading.

3.5.3 Fatigue Life Estimation Methods

There are numerous fatigue life estimation methods available today that can be used in the fatigue analysis of metals undergoing cyclic loading. This discussion will focus on two of the most generally accepted methods pertaining to fatigue life estimation of coronary stents, namely: Stress-Life fatigue analysis (generally illustrated by an S-N curve plotting stress versus number of cycles to failure) and Damage Tolerant analysis (Callister, 2000)

3.5.4 Stress-Life Fatigue Analysis

One of the most widely used high-cycle fatigue analysis techniques is Stress-Life analysis (S-N). The S-N approach (illustrated in Figure 4.1) plots nominal stress amplitude S versus cycles to failure N, producing a curve of constant life below which failure will not occur. The example curves illustrated in Figure 4.1 are presented purely for the purpose of understanding the S-N curve principle. Actual curve calculations obviously vary

dependant on the material tested and often require numerous tests at various stress amplitudes and cycles to generate.

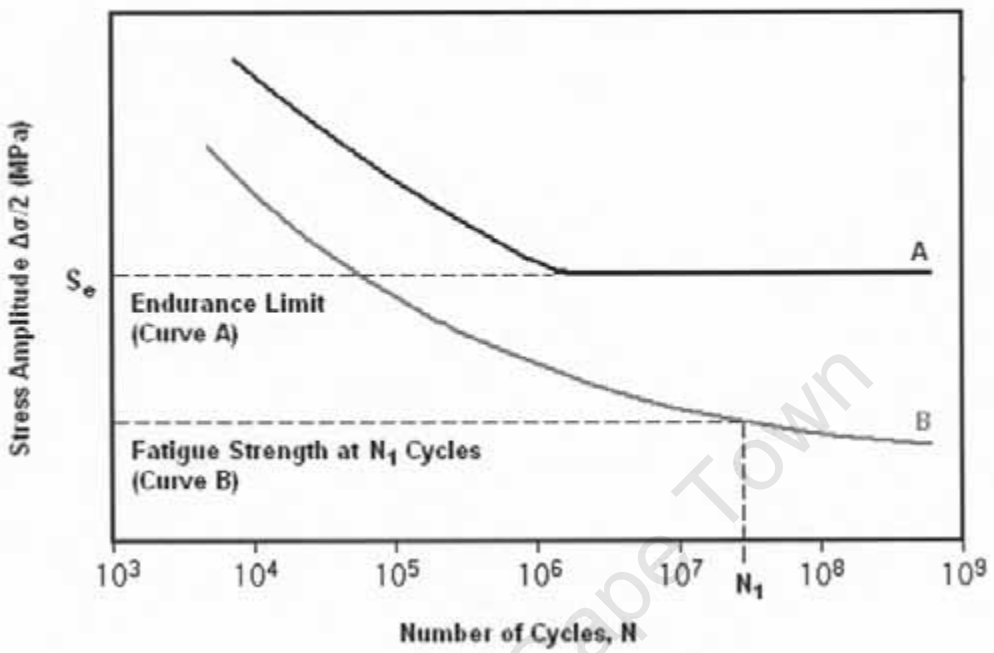

Figure 3.3 Examples of typical S-N curves (for materials A and B)

From the above illustration, numerous fatigue analysis properties can be explained, the first of which being the ability of certain materials to exhibit an endurance limit. This limit (clearly represented by the straight line of curve A) represents a stress level below which the material can be cycled infinitely without risk of failure. A second important factor to note is that the stress amplitude plotted on the y-axis is a nominal average and can be expressed as follows:

$$\sigma_a = \frac{\Delta \sigma}{2} = \frac{\sigma_{max} - \sigma_{min}}{2} \qquad (4.1)$$

with Figure 3.4 illustrating these common cyclic loading parameters.

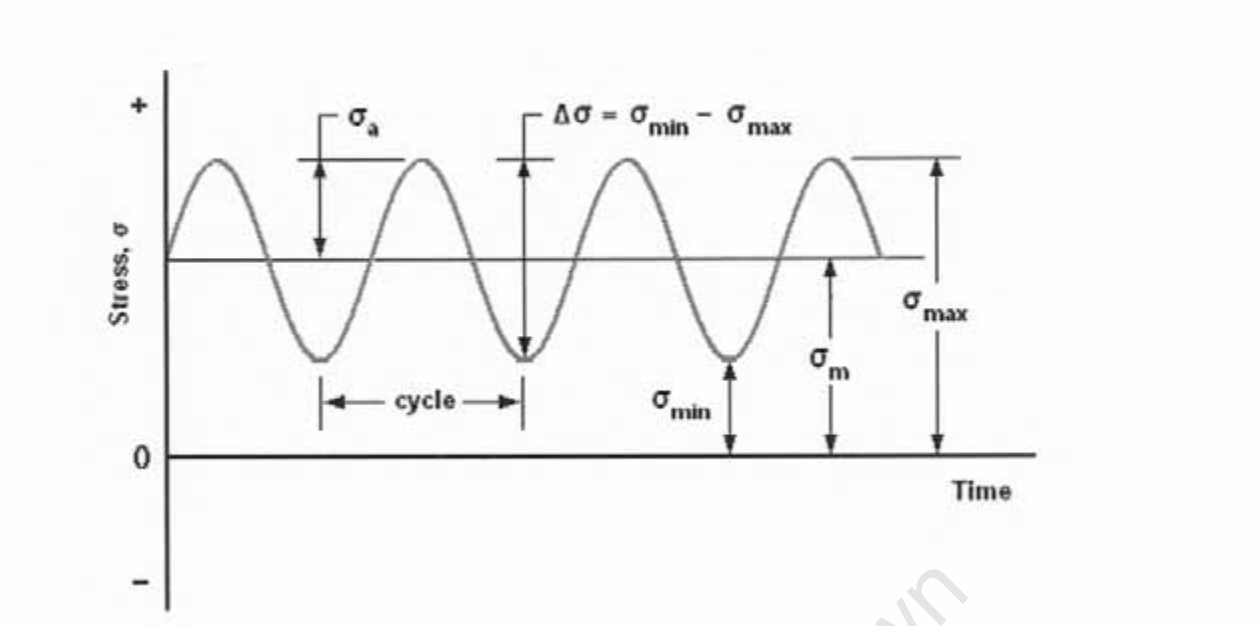

Figure 3.4 Common cyclic loading parameters in fatigue analysis.

In the design of a coronary stent, material selection and stent geometry are of utmost importance. Both of these parameters directly influence the stent's ability to survive cyclic loading (380 million cycles), with material selection influencing the S-N curve shape, and stent geometry affecting *cyclic* stress amplitude. A stent that is to survive 380 million cycles based on a Stress-Life Fatigue Analysis should be fatigued so as to remain in an area below its appropriate S-N curve.

3.5.5 Damage Tolerant Analysis

Stress-Life Fatigue analysis relates to the total fatigue life of the material and, as such, determines the stresses and number of cycles to initiate and propagate a crack through an initially crack-free material, until failure. Damage Tolerant analysis, on the other hand, considers the presence of pre-existing flaws in the material and calculates the total number of cycles required to propagate the largest crack to failure. Damage Tolerant analysis provides a more conservative approach to the prediction of material life. With crack propagation rate the key parameter in this analysis approach, stent geometry considerations become vitally important. Crack propagation rates predicted by this analysis method are best understood (in terms of a corresponding `cylces to failure') when compared to the thinnest stent surface the crack could potentially traverse.

Damage-Tolerant analysis (Figure 3.5) is generally illustrated by plotting crack growth rate (da/dN) versus a range of stress intensities (AK). Crack growth rate, measured in metres travelled per cycle, gives an indication of the crack's speed, while stress intensity defines the distribution of local stresses and strains near the crack tip in a linear elastic material.

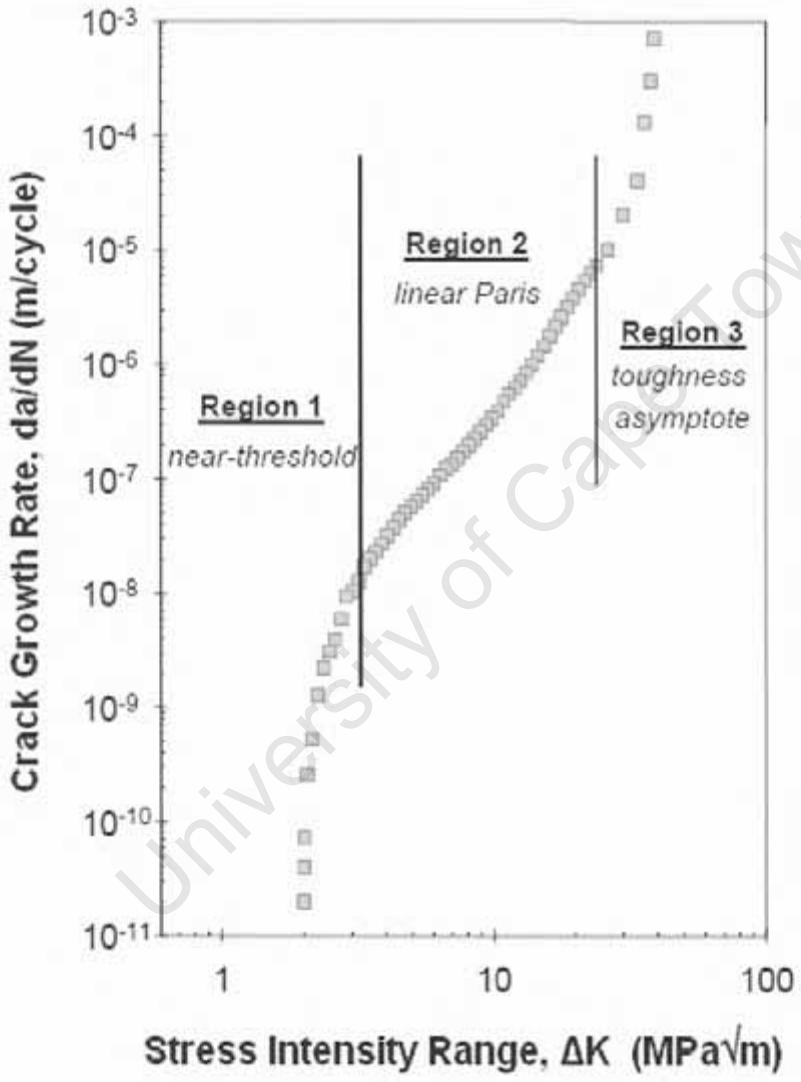

Figure 3.5 Variation in fatigue crack propagation rate (da/dN) as a function of stress intensity range (AK) [adapted from Forman *et al.,* 2005].

The plot of Figure 3.5 (once again, purely for illustrative purposes) illustrates the existence of a stress intensity threshold region below which cracks would not propagate. With increasing stress intensity, crack growth rate increases resulting in an obvious decrease in

the material's fatigue life. Different materials exhibit different crack propagation rates and for this reason stent-manufacturing companies must pay particular attention to Damage-Tolerant analysis.

Chapter Four

Fatigue Testing of Coronary Stents

4.1 Introduction

The aim of this project, as outlined in Chapter 1, is to design a machine capable of subjecting stents, at an accelerated frequency, to simulated physiological conditions as found in the human coronary arteries. Coronary motion parameters and compliance were discussed in Chapter 2 and, together with the fatigue principles mentioned in Chapter 3, form the foundation of this chapter.

With blood pressure, coronary motion and vessel compliance all responsible for inducing radial and axial stresses within a stent, appropriate simulation of the artery in some form of `mock artery' is of crucial importance.

4.2 The Need for Accelerated Testing

Recent European standards (BS EN 14299:2004) require *in vitro* stent testing of at least 380 million cycles, to simulate 10 years of operation in the human body. Since a stent manufacturing company in today's highly competitive world cannot possibly afford to wait 10 years for stent validation, the fatigue process should naturally be accelerated. In order to reduce validation time to between 2 and 3 months, cyclic loading of the stents would need to take place at frequencies of approximately 50 - 60 Hz. Elevated frequencies however run certain obvious physical risks and it is therefore important to note that the 50 - 60 Hz range is by no means a fixed project criteria.

4.3 Mock Artery Considerations

4.3.1 Simulation of Appropriate Arterial Motion

The coronary motion parameters of primary interest discussed in Chapter 2 are not all able to be satisfactorily simulated at elevated frequencies. A mock artery set to pulsate in

various directions (torsion, twisting and bending) at frequencies of between 50 and 60 Hz could give rise to unwanted effects, particularly if the mock artery is very flexible. Inherent resonant frequencies would cause random and unwanted motions and for this reason, while adhering to the motion parameters of Chapter 2 it would be more practical to focus on only one governing motion parameter. Such a parameter is without question *bending.* With a stent firmly deployed in the middle of a length of mock artery, symmetrical bending would subject it to displacement, induce both tensile and compressive axial loads and, at its midpoint, enable the simulation of appropriate curvature (0.5 cm^{-1}). There are of course numerous ways to bring about axial loading in such a stent (as presented and discussed in Chapter 6) but *bending* for the moment seems the most appropriate parameter for the aforementioned reasons.

4.3.2 Simulation of Appropriate Arterial Compliance

A second important requirement in the design of a Fatigue Tester of this nature is the adequate simulation of arterial compliance. It has been shown that mock artery compliance decreases with increased frequency (Conti *et al.,* 2002). This is of particular importance when deciding on suitable mock artery material, because increased test frequency will have adverse effects on the mock artery's ability to expand when subjected to internal or external pressure gradients. With the stent deployed against the inner wall of the mock artery, it is these pressure gradients that will be responsible for inducing radial stresses in the stent as it follows the inner wall's cyclic expansion and relaxation.

All balloon expandable stents exhibit elastic recoil ranges, supporting the assumption that stents would follow the inner wall of the mock artery as it expands. If, for example, a stent was deployed to 3.5 mm in a 3 mm mock artery, the vessel would resist this change in diameter by pushing back on the stent. With the stent exhibiting a 5% recoil range for example, the vessel would be successful in pushing the stent back to a smaller diameter of 3.325 mm (3.5 mm minus the 2% recoil range). The stent would still be firmly deployed in the 3 mm vessel (still under the pressure of the vessel wall) and, should the vessel increase in diameter due to internal pressurization, the stent will follow its change in diameter as it increases to diameters beyond 3.325 mm. The stent will however only follow the vessel due to the reduction in deployment resistance and will continue to increase in size while within its natural elastic recoil range.

Elastic recoil ranges for several of DISA Vascular's stents are illustrated in the *Hysteresis* (resultant strain response to applied forces) diagram of Figure 4.1. From the diagram it becomes clear that each stent possesses two distinct recoil ranges: Crimp recoil (horizontal force-strain line on the left hand side of the diagram) and deployment recoil (similar line on the right hand side).

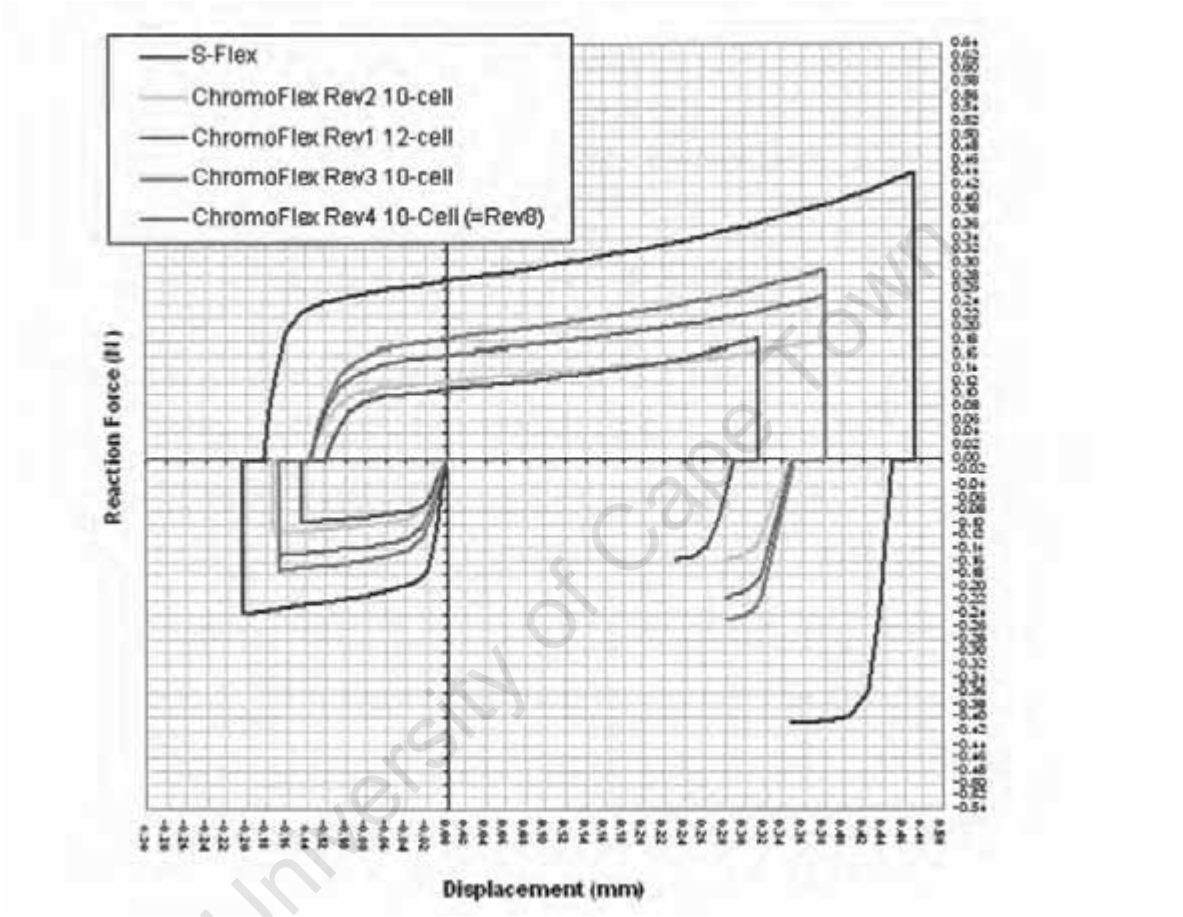

Figure 4.1 Hysteresis characteristics of several DISA Vascular stents [Obtained with permission from DISA Vascular]

It has been suggested (Conti *et al.,* 2002) that tubes with compliances ranging from 5-7% per 100 mmHg are ideal in the simulation of arterial conditions. With blood pressure fluctuations as high as 100 mmHg in unhealthy patients rather common, the machine will need to bring about changes in internal vessel diameter of approximately 5% at frequencies of up to 60 Hz to simulate a 'worst case' coronary artery compliance scenario. The effects of decreased vessel compliance and elastic recoil ranges (as previously mentioned) will form the basis of tube selection and design considerations to follow.

Chapter Five

The Design Process — Problem Understanding

5.1 Customer Requirements

One of the most important and often overlooked aspects of any successful design project is the clear understanding of its requirements. This section deals with the identification of customers and the full understanding of their requirements for such an accelerated stent fatigue testing machine.

5.1.1 Customer Identification

A "customer" can be defined as any person or organization that is likely to have an effect on a project's design requirements. The following customer classes were identified and targeted:

1. *Machine Operator* — all people responsible for machine operation, including; stent deployment and removal, machine operation and inspection.
2. *DISA Vascular Personnel* — All other DISA Vascular staff benefiting from the machine's capabilities although not directly involved in its use.
3. *Marketing* — Staff potentially responsible for the marketing of the machine, including; Sales of such machines and associated services.
4. *Manufacturing Personnel* — including; component manufacture, acquisition and assembly.
5. *European and American Standards Organizations* — all organizations responsible for the publication of new relevant standards to be upheld by DISA Vascular.
6. *Maintenance Staff* — staff responsible for the cleaning and routine upkeep of the machine.

5.1.2 Requirements for each Customer Group

5.1.2.1 Machine Operator requirements

1. Easy deployment of stents
2. Easy removal of stents
3. Easy to control
4. Ability to monitor various machine conditions
5. Maintain high level of sustainability
6. Reliable operation for 3 month period

5.1.2.2 DISA Vascular personnel requirements

1. Fastest possible stent evaluation time
2. Provide space for testing a number of stents
3. Allow testing of various stent sizes
4. Meet requirements of current EU and USA standards
5. Reasonable production time

5.1.2.3 Marketing Personnel

1. Meets customer requirements
2. Easy to package
3. Easy to store
4. Attractive
5. Competitive price

5.1.2.4 Production Personnel

1. Easy to manufacture
2. Easy to assemble and disassemble
3. Use of available resources
4. Use of standard parts
5. Produce minimum material waste

5.1.2.5 EU and USA Standards Organizations

I. Subject stents to 380 million cycles of testing
2. Test 6 stents of maximum and minimum diameter
3. Operate at a limited maximum speed
4. Induce axial forces
5. Induce radial forces
6. Induce displacements and strains recognized as being most severe according to literature studies
7. Maintain temperature within physiological range
8. Induce relevant change in stent diameter

5.1.2.6 Maintenance Staff

1. Should be durable
2. Standard components for easy maintenance
3. Easy to clean
4. Allow for easy oiling and lubrication

5.1.3 Additional (Non-Vital) Requirements

The following requirements were identified as being non-vital to successful project completion, although would be interesting to consider. They were as follows:

1. Quiet operation
2. Allow for stents to be visible during testing
3. Provide slight torsional stent deformation
4. Stent failure detection system

For each customer group, the relative importance of each requirement was analyzed and illustrated in the *Quality Function Deployment* diagram (QFD) of Table 5.1 illustrated in section 5.4.

5.2 Evaluation of Competition

The following current products were analyzed to determine how well each of them meets the requirements formulated in Section 5.1.2:

1 DISA Vascular's current Fatigue Tester

2 Enduratec Model 9110-12 Coronary and Peripheral Stent Fatigue Tester

The aforementioned products were evaluated by rating their ability to satisfy specific requirements on a scale of 1 to 5 (A score of 5 representing the complete fulfilment of a particular requirement). Evaluation results are illustrated in Table 5.1 of Section 5.4.

5.3 Engineering Requirements

The customer requirements of Section 5.1.2 were transformed into a list of engineering specifications and illustrated in Table 5.1. By generating engineering specifications,

customer requirements are restated in measurable terms, thus providing a better understanding of the problem from the physical design viewpoint.

5.4 Quality Function Deployment (QFD)

The QFD diagram (Ullman, 1997) of Table 5.1 illustrates and summarizes the activities undertaken in the previous 3 sections. The following properties can be evaluated through use of this technique:

1. Relative importance of requirements for each customer group (1 to 37)
2. Evaluation of competition (scale 1 to 5)
3. Measurement of the relationship between customer requirements and engineering specifications (9 = strong relationship; 3 = medium relationship; 1 = weak relationship; blank = no relationship)
4. Relationships between various engineering specifications (9,3,1)
5. Development of Engineering Targets

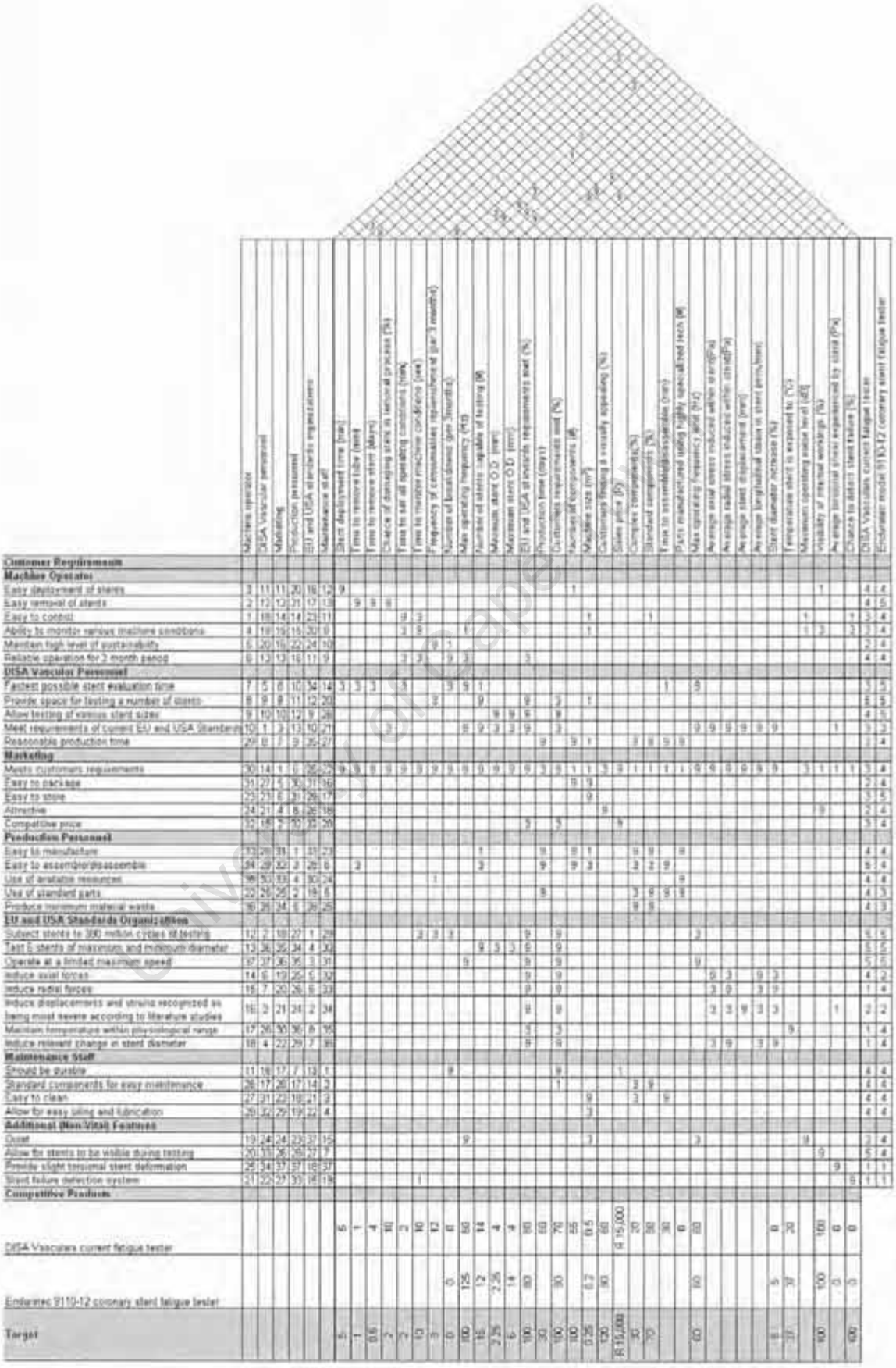

Table 5.1 QFD Diagram for Fatigue Tester project

Chapter Six

The Design Process — Concept Generation

6.1 Patent Searches

Analyzing patents can be a very useful source of conceptual ideas. The following two documents have been located:

1. Edwards Lifesciences LLC [US 2003011 0830A1 — Patent Application Publication]
2. Endura-Tec Systems Corporation [US Patent Number — 5,670,708]

The vital information pertaining to their functionality is presented in Appendix D.

6.2 Functional Decomposition

To start off with, the overall design problem was broken down into a series of smaller sub-systems (following a tree-like configuration), the idea being to formulate multiple conceptual solutions for each subsystem. Figure 6.1 illustrates the functional decomposition of the Fatigue Tester design problem.

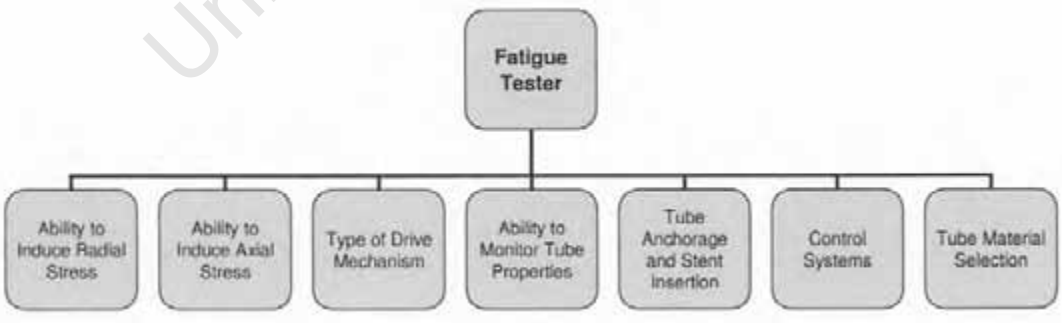

Figure 6.1 Functional decomposition of the Fatigue Tester

The next step was to perform similar functional decomposition for each of the 7 sub-functions illustrated in Figure 6.1, narrowing each function down to a list of clearly understandable and potentially viable solutions. Each conceptual branch was labelled A to N to avoid unnecessary confusion.

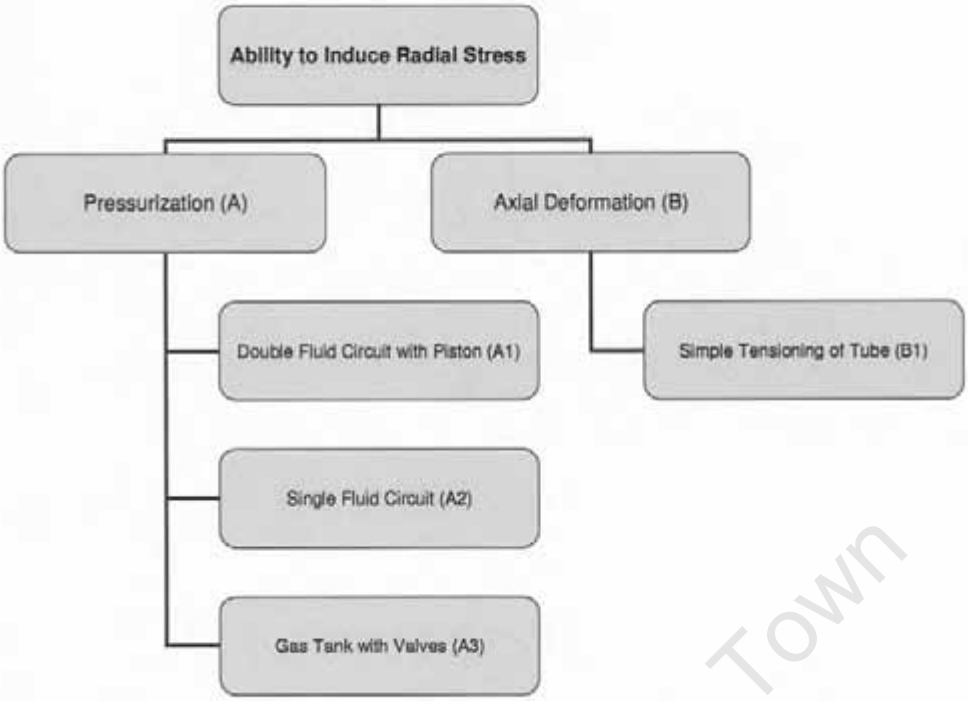

Figure 6.2 Functional decomposition: ability to induce radial stress

The ability to induce radial stress was divided into two possible solutions (Figure 6.2); tube pressurization and pure axial deformation. Concepts Al to A3 (illustrated in section 6.3.1) deal with pressurization while concept B 1 (section 6.3.2) induces radial stress by pure tensioning.

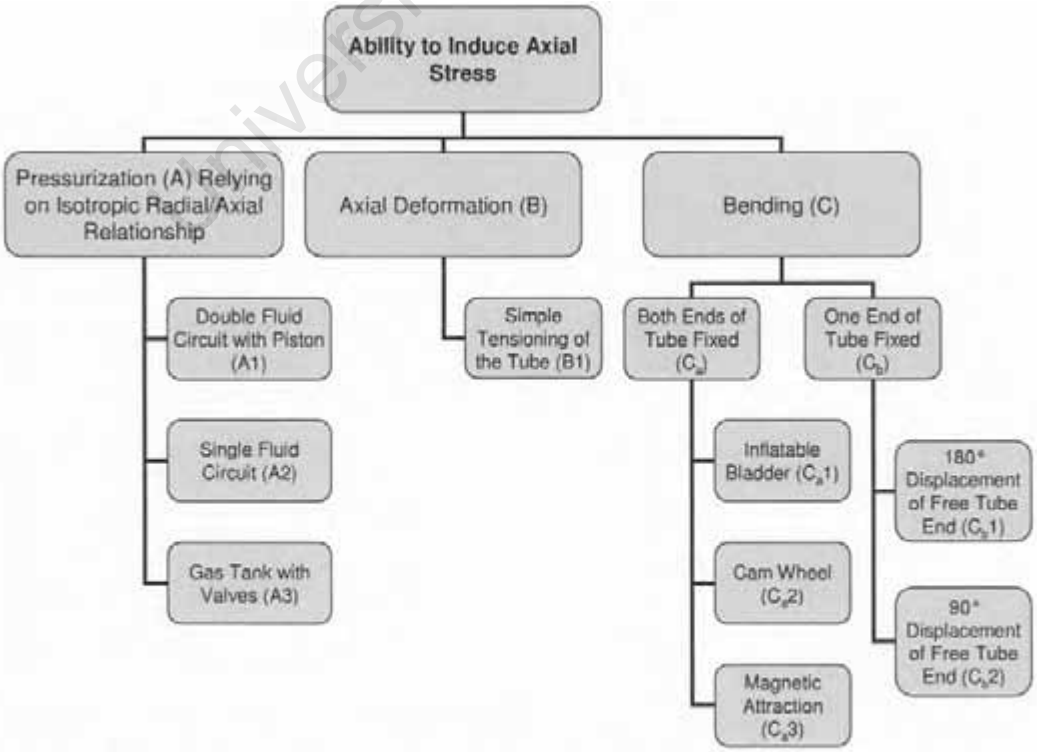

Figure 6.3 Functional decomposition: ability to induce axial stress

Figure 6.3 illustrates the various conceptual solutions generated to induce axial stresses within the stent. Again, as in Figure 6.2, pressurization and axial deformation could be considered appropriate solutions. Numerous bending concepts (C, illustrated in section 6.3.3), with sub-branches *a* and *b* were also considered.

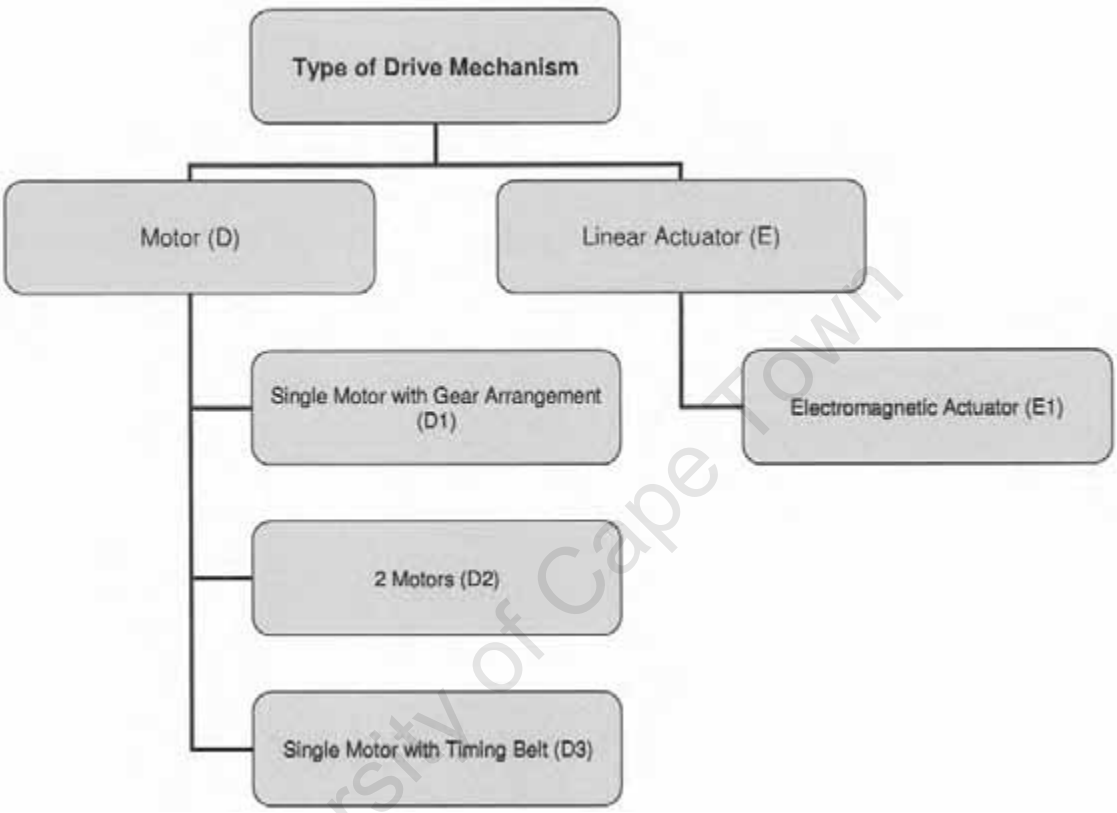

Figure 6.4 Functional decomposition: type of drive mechanism

Whatever the choice of tube motion and pressurization, some form of driving mechanism would be needed. Conceptual solutions generated for this application are presented in Figure 6.4 and were divided into two categories; motor drive and linear actuation. Concepts D1 to D3 (illustrated in section 6.3.4) deal with motor drive while concept El (section 6.3.5) makes use of a linear actuator.

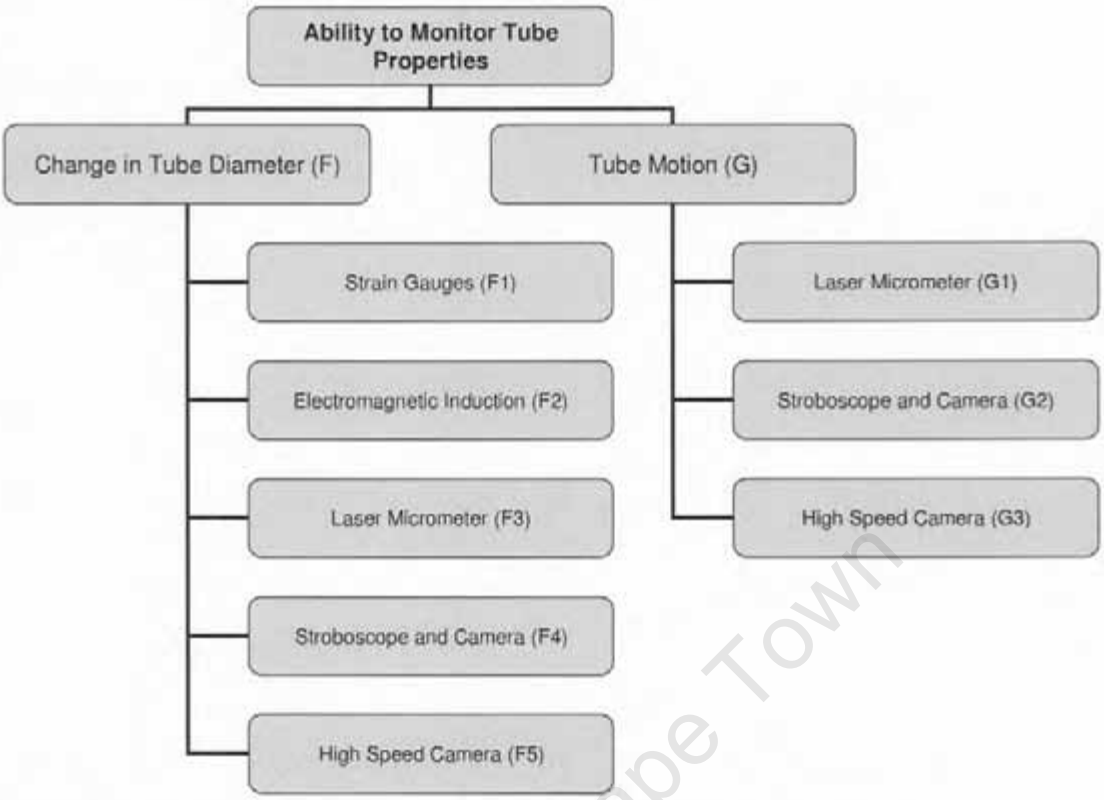

Figure 6.5 Functional decomposition: ability to monitor tube properties

Concepts generated for the monitoring of tube motion at high frequencies are illustrated in Figure 6.5. Concepts F1 to F5 (section 6.3.6) deal primarily with the ability to detect a change in tube (mock artery) diameter, while concepts GI to G3 (section 6.3.7) enable the viewing of general tube motion.

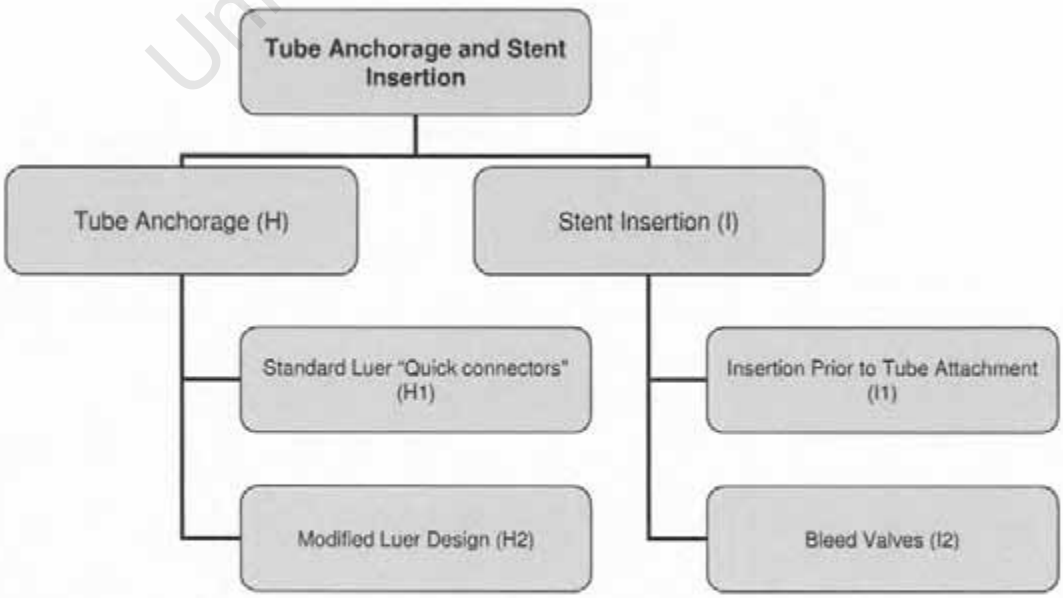

Figure 6.6 Functional decomposition: tube anchorage and stent insertion

The functional decomposition of Figure 6.6 illustrates concepts pertaining to tube anchorage (H) and stent insertion (I). Tube anchorage concepts are discussed and illustrated in section 6.3.8, with stent insertion dealt with in section 6.3.9.

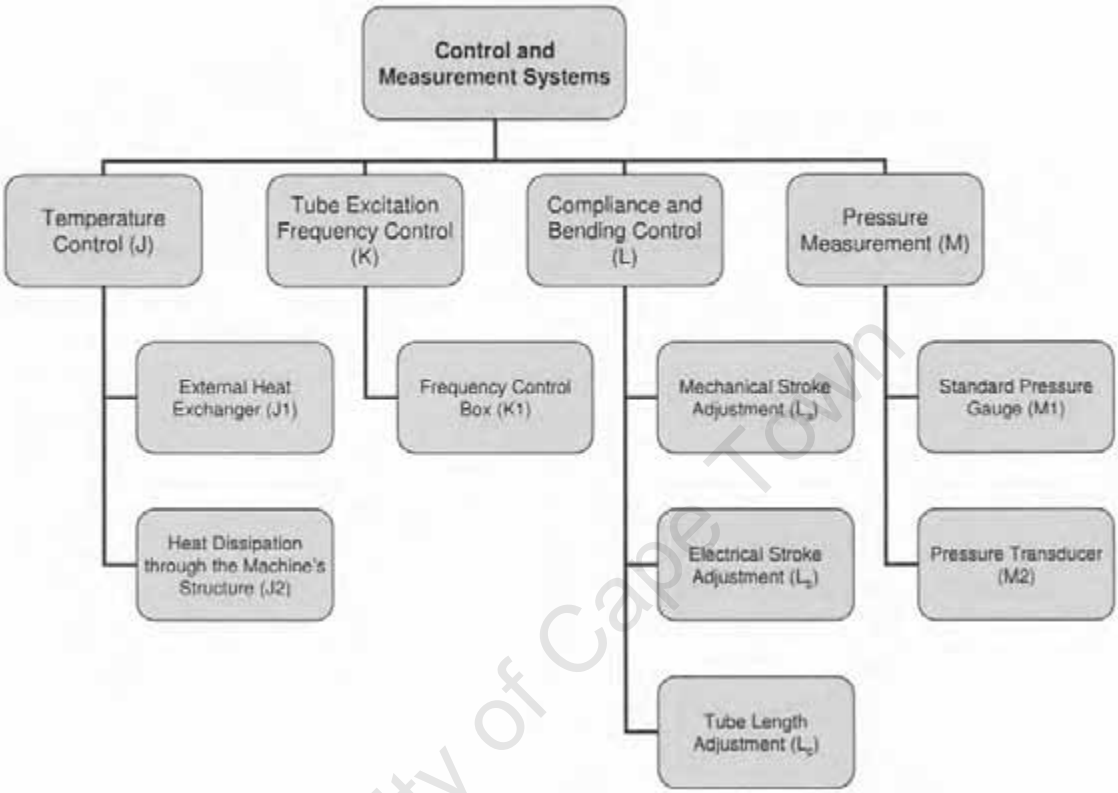

Figure 6.7 Functional decomposition: control and measurement systems

Control of certain parameters is vital in the design of an accelerated fatigue tester. Fluid temperature, frequency and compliance are just some of these parameters, and Figure 6.7 illustrates the potential solutions generated. Temperature control (J1 to J2) is discussed in section 6.3.10, with frequency control (K) presented in section 6.3.11. Compliance and bending control considerations (L) are discussed in section 6.3.12 with pressure measurement concepts (M) being addressed in section 6.3.13.

Figure 6.8 on the following page performs further functional decomposition of conceptual branch L.

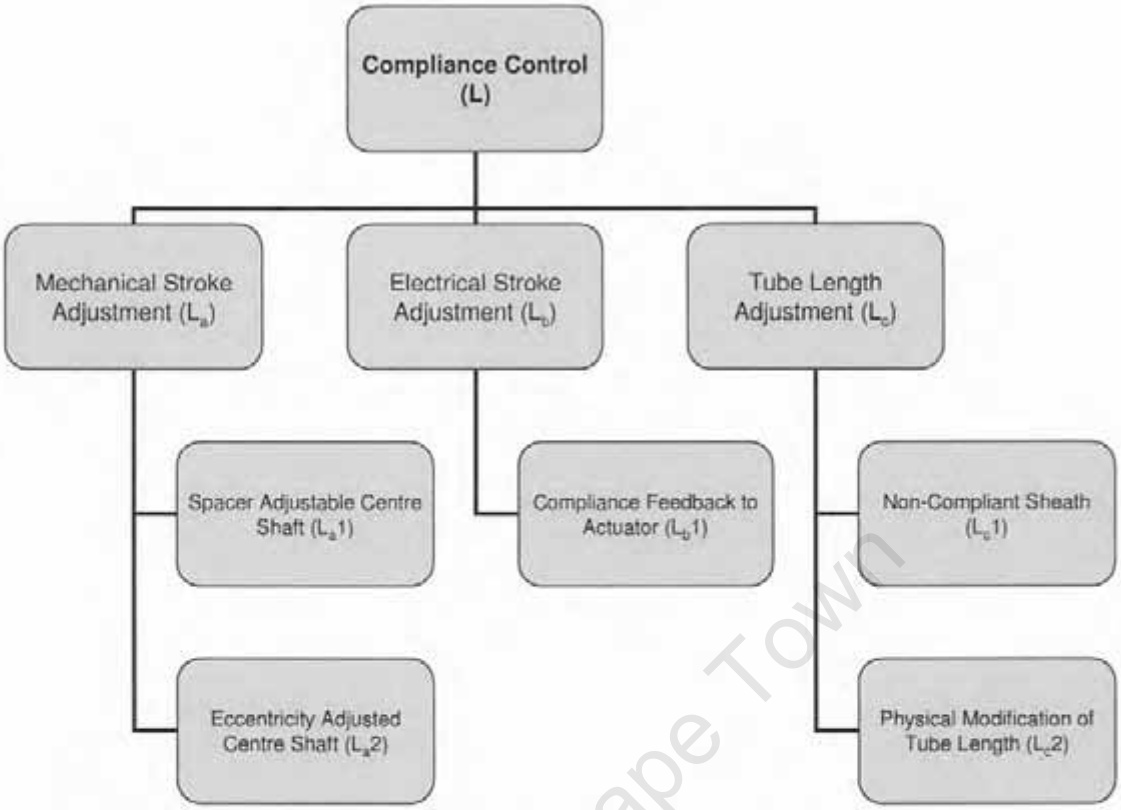

Figure 6.8 Functional decomposition: compliance control

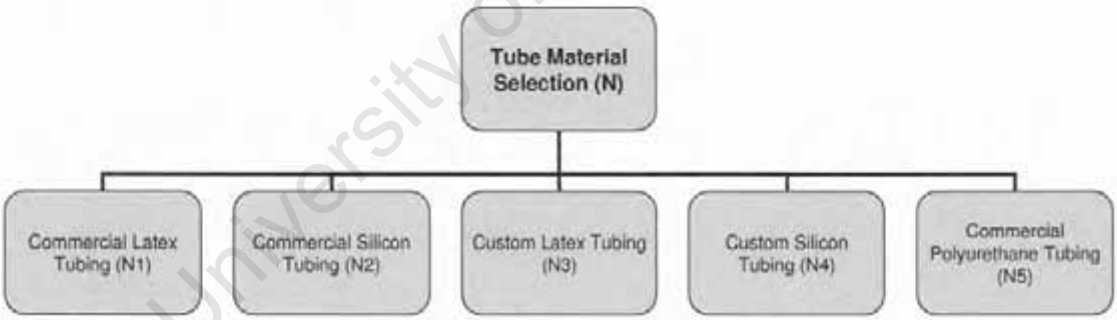

Figure 6.9 Functional decomposition: tube material selection

The various material choices considered in the simulation of a coronary artery are presented in Figure 6.9. Concepts N1 to N5 are presented in section 6.3.14.

6.3 Generated Concepts for Individual Sub-Functions

This section briefly discusses and illustrates all the different conceptual solutions generated from the aforementioned functional decomposition process. Starting with the Pressurization concepts illustrated in branch 'A' of Figure 6.2, it presents all concepts in sufficient detail so as to be made available for adequate evaluation in Chapter 7.

6.3.1 Pressurization Concepts (A)

6.3.1.1 Double Fluid Circuit with Piston (Al)

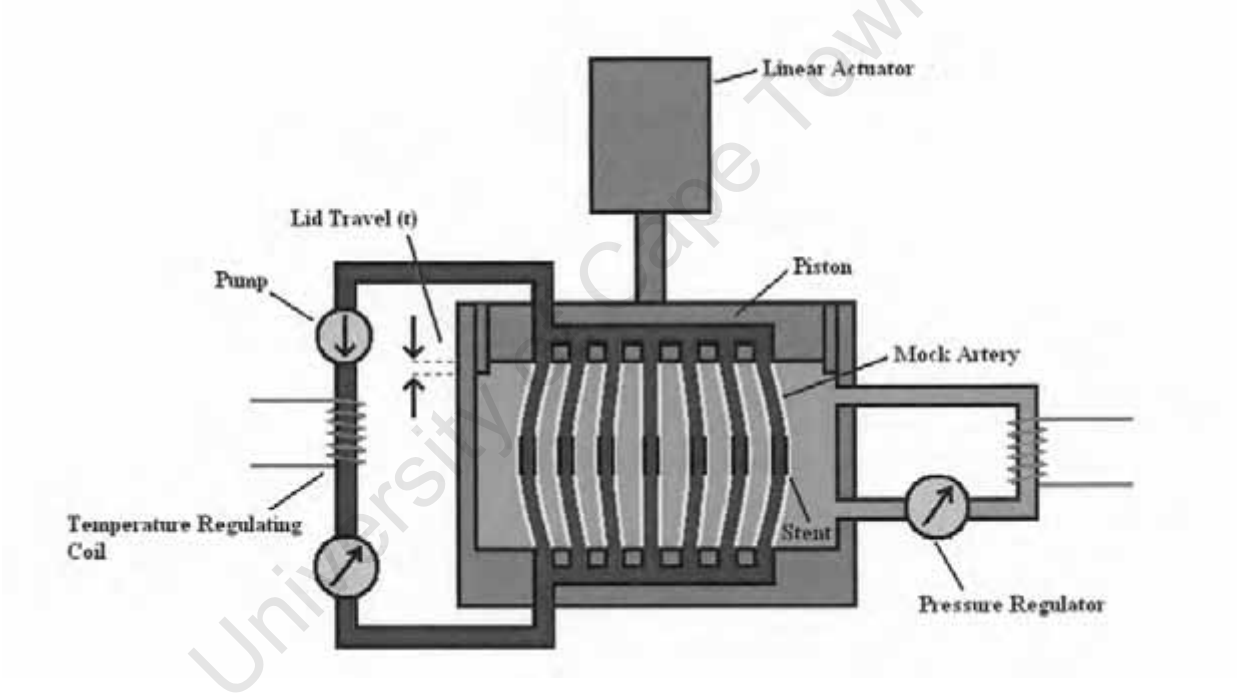

Figure 6.10 Concept Al — Double fluid circuit with piston

By making use of two separate fluid chambers, this concept relies on the external fluid (orange) to induce a negative pressure on the tubes, thereby 'sucking' them open. A piston, driven by some form of linear actuator, would be used to induce this negative pressure and at the same time be responsible for bending the tubes. An independent second fluid circuit (blue) would, in this way, be free to circulate an appropriate liquid through the inside of the tubes, constantly bathing the stents deployed within them.

6.3.1.2 Single Fluid Circuit (A2)

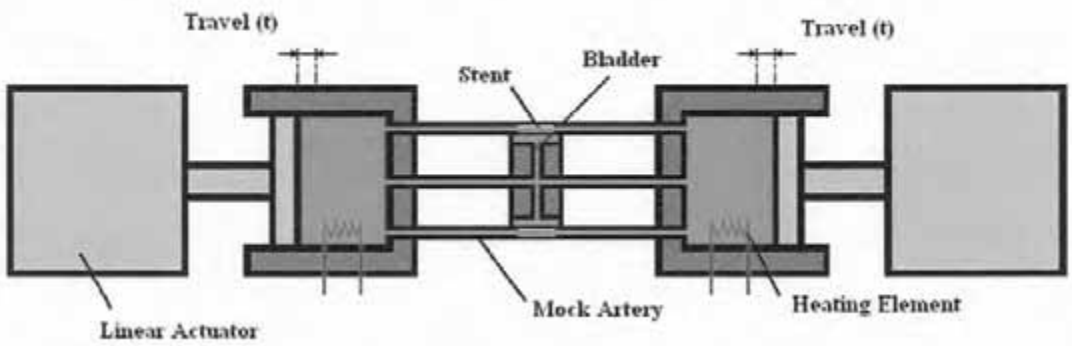

Figure 6.11 Concept A2 — Single fluid circuit

This concept brings about internal pressurization of the tubes by means of a single, internal fluid circuit. With all of the tubes connected to a pressurizable reservoir (two represented here), radial stress can be induced in the tubes by simply driving the piston.

6.3.1.3 Gas Tank with Valves (A3)

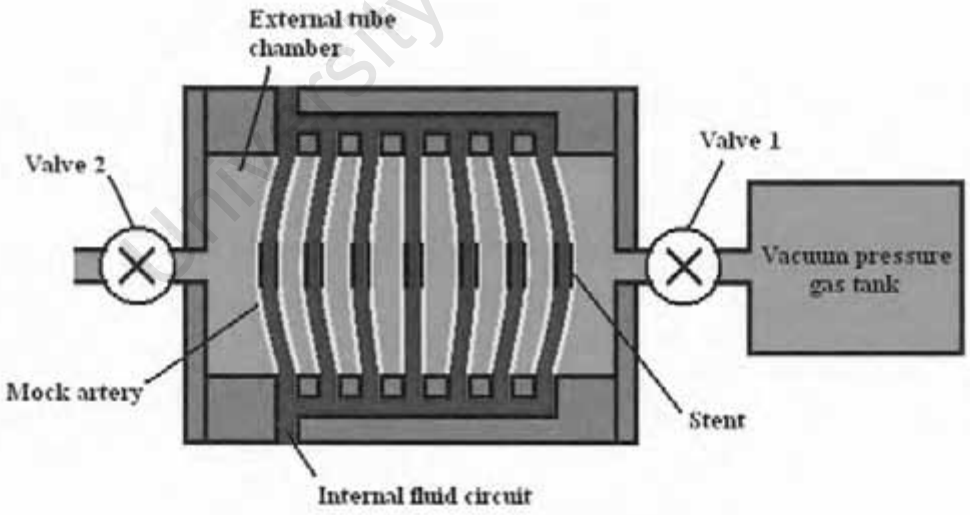

Figure 6.12 Concept A3 — Gas tank with valves

Instead of using pistons, this conceptual solution would make use of high speed pressure valves to bring about changes in tube pressure (internal or external). Figure 6.12 illustrates how the system could be connected to a vacuum tank (external tube chamber) by means of

two valves. When valve 1 is opened (with valve 2 remaining closed), the pressure surrounding the tube will decrease until tank and chamber pressure are equal. After equilibrium of the two pressures, valve 1 could be closed and valve 2 (atmosphere) opened, returning the pressure to its initial state. By timing these valves to fire in such a way at elevated frequencies, cyclic tube compliance changes could be obtained. A high pressure gas tank could alternatively be connected to the tube fluid circuit (blue) to achieve similar results.

6.3.2 Axial Deformation Concepts (B)

6.3.2.1 Simple Tensioning of the Tube (B1)

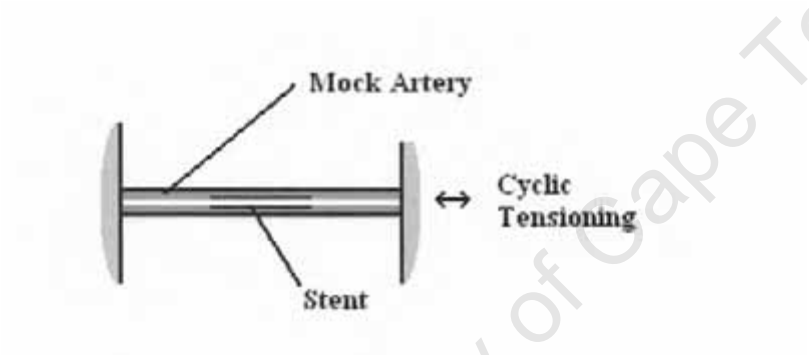

Figure 6.13 Concept B 1 — Simple tensioning of the tube

A stent deployed within a tube could also experience radial and axial loads if the tube was stretched. Since a stretched tube not only becomes longer but also thinner, this action could bring about both forms of loading simultaneously.

6.3.3 Bending Concepts (C)

Bending concepts, as illustrated in Figure 6.3 of section 6.2, were divided into two conceptual branches: bending with both ends fixed (C_a); and bending with one end fixed (Cb). The following two sections illustrate and describe the conceptual solutions generated for both C_a and C_b.

6.3.3.1 Both Ends of Tube Fixed Concepts (Ca)

The following concepts induce bending of tubes with their end points fixed. Bending of this nature was considered important since internal pressurization of the tubes might require their end points to be fixed.

Inflatable Bladder (C_a1)

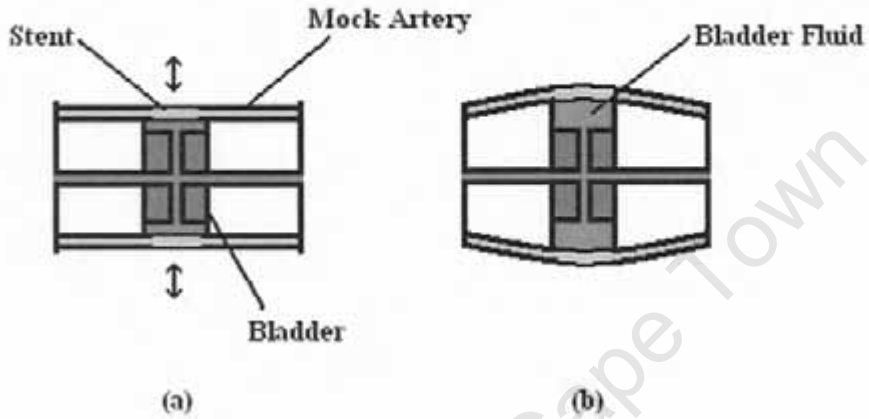

Figure 6.14 Concept C_a1 — Inflatable bladder. (a) Initial deflated bladder scenario. (b) Inflation of the bladder and resultant tube bending.

Concept C_a1 produces tube bending by inflating a central bladder and forces the tubes outward. With the tubes secured to the surface of the bladder, cyclic inflation would result in bending of the tubes at the same frequency.

Cam Wheel (C_a2)

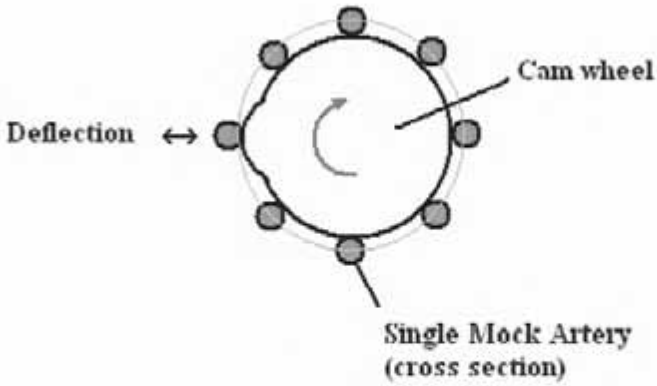

Figure 6.15 Concept C_a2 – Cam wheel

Concept C_a2 produces tube bending by means of a rotary cam wheel. With numerous tubes arranged around the cam wheel (so as to brush up against its surface), rotation would cause tubes in the area of the cam to displace due to its profile. Bending would take place one tube at a time and its frequency would be dependent on the rotary speed of the cam wheel.

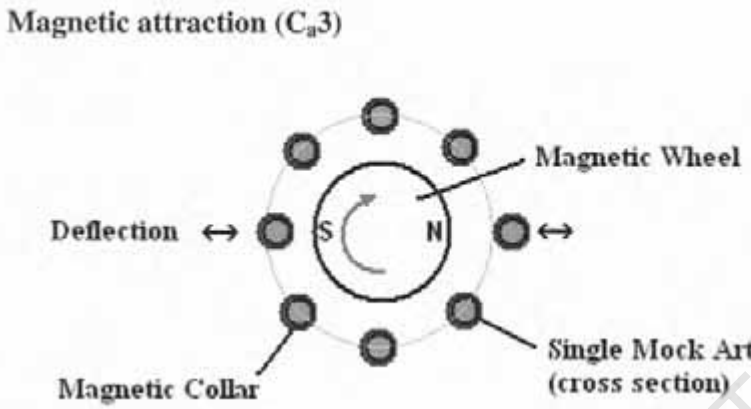

Figure 6.16 Concept C_a3 — Magnetic attraction

This concept makes use of a similar principle to that of concept C_a2, but does so by using a magnet. A magnet with north and south poles (as illustrated in Figure 6.16) set to rotate inside an array of tubes with magnetic 'collars' would cause cyclic bending by means of magnetic attraction.

6.3.3.2 One End of Tube Fixed Concepts (Cb)

This section discusses and illustrates various tube bending possibilities when one end is free to move.

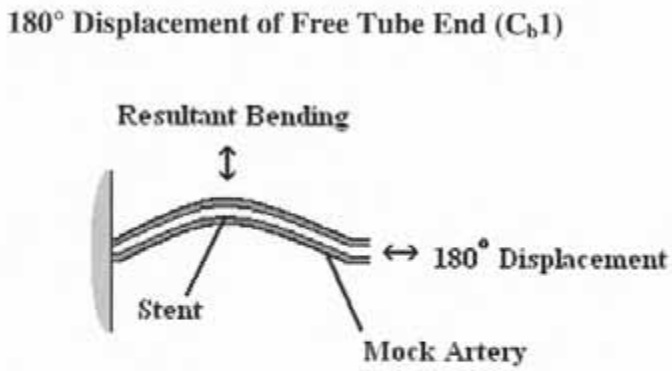

Figure 6.17 Concept C_b1 - 180° displacement of free tube end

Concept Cb 1 brings about tube bending by displacing the free tube end back and forth. With the tube pre-bent, the bend plane can to a certain extent be set, allowing further bending to occur in a predictable direction.

90° Displacement of Free Tube End (Cb2)

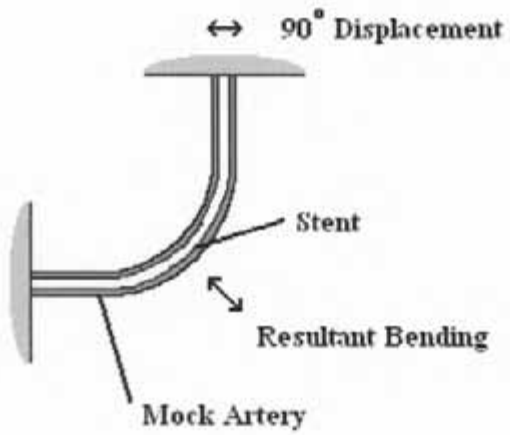

Figure 6.18 Concept C_b2 - 90° displacement of free tube end

Should spatial constraints prevent tube bending from occurring at 180°, 90° bending (as illustrated in Figure 6.18) could also be implemented. Again, as with concept Cb 1 , initial bending of the tube can help position and direct further cyclic bend directions.

6.3.4 Motor Drive Concepts (D)

Since tube motion and pressurization will need to be induced simultaneously by the fatigue tester, some form of drive mechanism will be required. This section suggests the use of a simple electric motor as the drive mechanism, and presents conceptual solutions as to how two independent and synchronized activities (motion and pressurization) could be controlled.

6.3.4.1 Single Motor with Gear Arrangement (Dl)

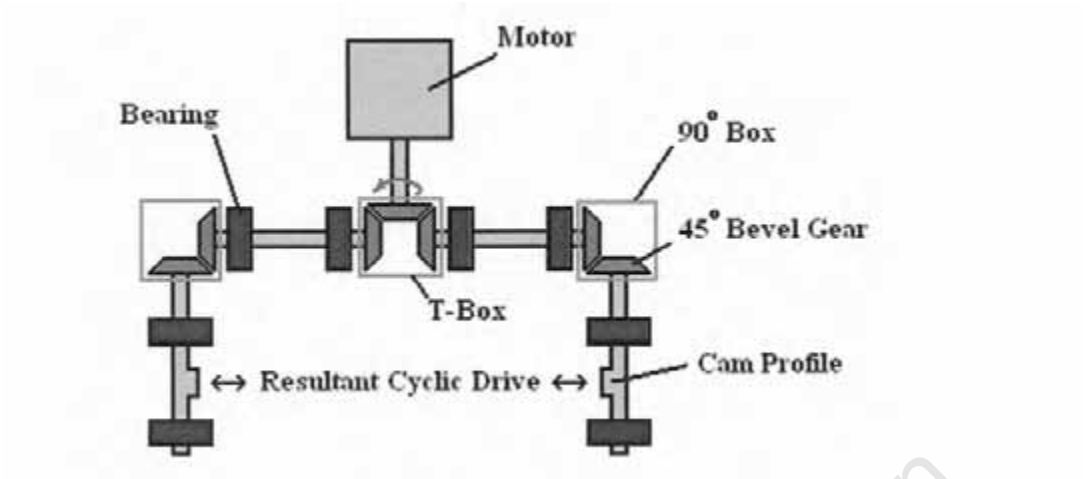

Figure 6.19 Concept Dl — Single motor with gear arrangement

This concept imparts cyclic drive to both motion and pressurization driven ends through an arrangement of bevel gears (T-Box and 90° Box) and bearings. The motor's torque would first be transferred through a T-Box (effectively splitting the drive into two directions) after which a 90° Box would pass it onto some form of cam profile, producing cyclic stroke at both ends.

6.3.4.2 Two Motors (D2)

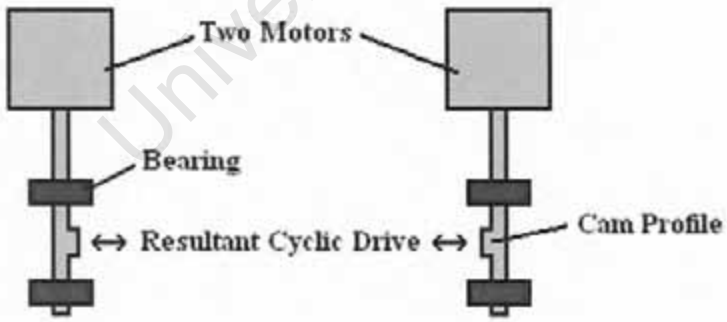

Figure 6.20 Concept D2 — Two motors

This concept makes use of two motors to bring about cyclic strokes at both ends. The two motors would need to be of the same specifications in order to keep both strokes perfectly synchronized.

6.3.4.3 Single Motor with Timing Belt (D3)

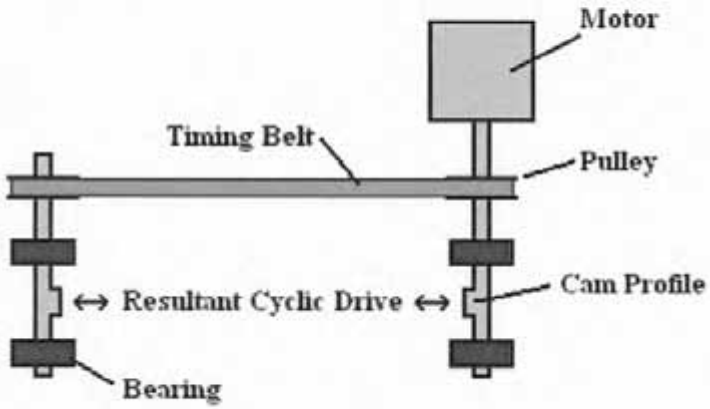

Figure 6.21 Concept D3 – Single motor with timing belt

Instead of making use of gears, this concept relies on a timing belt to transfer motor torque to the opposite drive shaft.

6.3.5 Linear Actuation Concepts (E)

6.3.5.1 Electromagnetic Actuator (E1)

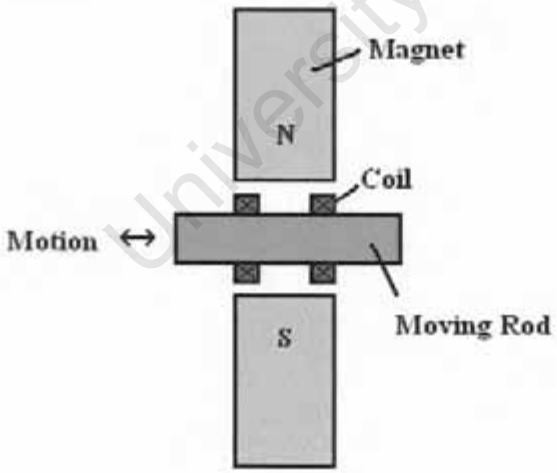

Figure 6.22 Concept El — Electromagnetic actuator

Cyclic stroke can also be produced at both motion and pressurization ends by making use of an electro-magnetic actuator, as used by the Endura-Tec system design illustrated in Appendix E. By sending the coil in Figure 6.22 an alternating current signal, the electro-

motive force (EMF) induced in the moving rod would cause cyclic motion back and forth. This concept operates in the same way as that of a speaker.

6.3.6 Concepts for Detecting a Change in Tube Diameter (F)

6.3.6.1 Strain Gauges (F1)

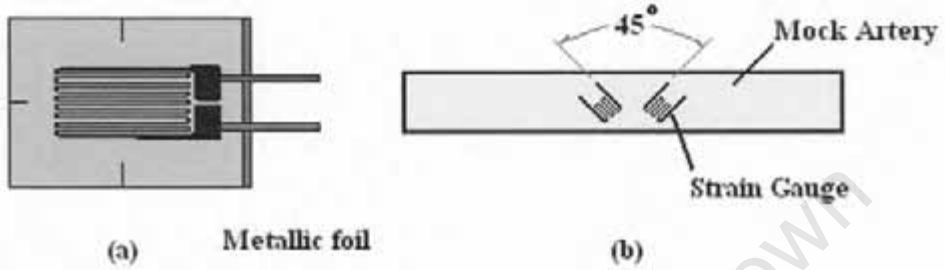

Figure 6.23 Concept Fl — Strain gauges. (a) A typical strain gauge. (b) Two strain gauges applied on the surface of the mock artery at 45°.

A strain gauge consists of a metallic foil arranged in a grid pattern. When attached to the surface of an object, the metallic foil's electrical resistance varies as the underlying object is stretched or compressed. Strain gauges are normally used in pairs and the varying resistances produced during testing are displayed as a strain value. Applying two strain gauges to the surface of the tube would give an indication of its motion and resultant strains.

6.3.6.2 Electromagnetic Induction (F2)

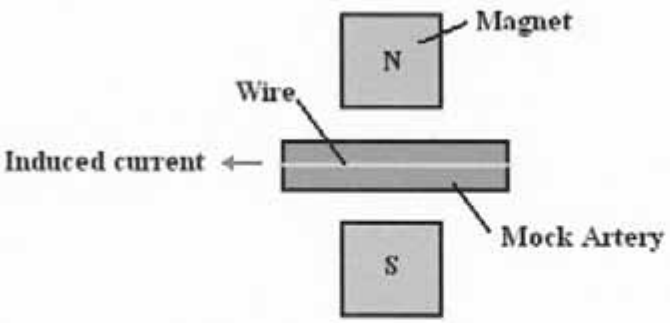

Figure 6.24 Concept F2 – Electromagnetic induction

This concept makes use of electromagnetic induction to give an indication of tube expansion. With the tube expanding and raising the wire (attached to it) into and out of the page (Figure 6.24) through the magnetic field, the varying current induced could be used to determine the cyclic change in tube diameter.

6.3.6.3 Laser Micrometer (F3)

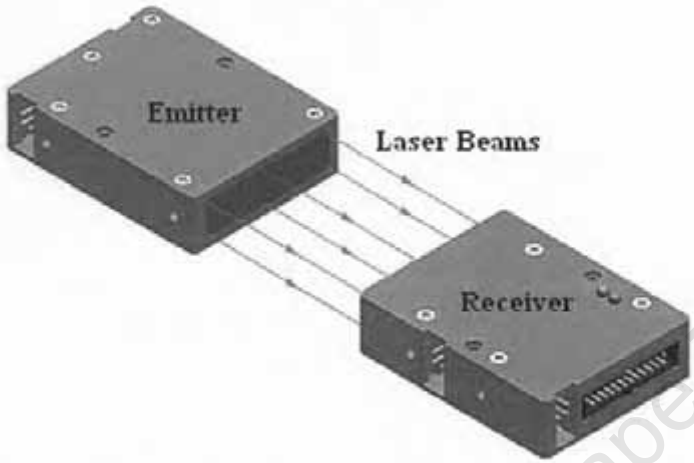

Figure 6.25 Concept F3 – Laser micrometer

Concept F3 makes use of a laser micrometer to detect changes in mock artery diameter. Laser micrometers function by emitting an array of parallel laser beams onto some form of receiver (Figure 6.25). When an object is passed through the laser, the detector (using various edge and position detection algorithms) is able to 'visualize' its motion. Laser micrometers (depending on type) offer exceptional resolution (- 3 microns) and excellent sampling frequencies (- 2000 Hz). They would definitely be capable of detecting changes in mock artery diameter at elevated frequencies.

6.3.6.4 Stroboscope and Camera (F4)

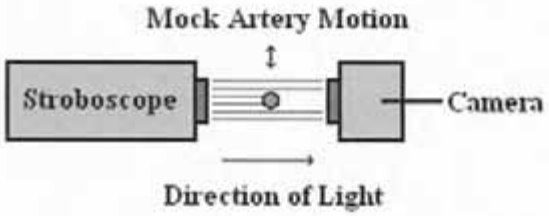

Figure 6.26 Concept F4 – Stroboscope and camera

Tube motion and diameter detection could also be accomplished by using a camera (capturing either videos or photos) in conjunction with a stroboscope (flashing light source). Firing the stroboscope at a frequency close to that of tube motion would produce a slower moving resultant image. This image is produced by means of an effect known as aliasing, and is more clearly defined and discussed in Chapter 7.

6.3.6.5 High Speed Camera (F5)

Use of standard video cameras and stroboscopes can be avoided by filming the mock arteries motion using a high speed camera. There are various types of high speed cameras, but most are capable of capturing images at up to 8,000 frames per second. With the mock artery adequately illuminated, a high speed camera could photograph its motion and diameter variation at 60 Hz with relative ease.

6.3.7 Concepts for Viewing Tube Motion **(G)**

Concepts Fl to F5 were specifically generated to enable the detection of diameter variation in the mock arteries. Concepts F3, F4 and F5 however could also enable the detection of general tube motion and for this reason were used again in this conceptual branch and labelled Gl, G2 and G3 respectively.

6.3.8 Tube Anchorage Concepts **(H)**

Since the mock arteries will be subjected to both bending and internal pressurization at up to 60 Hz, secure anchorage is vital. The following two options regarding their anchorage were generated.

6.3.8.1 Standard Luer "Quick Connectors" **(H1)**

Possibly one of the easiest ways to attach vessels of varying diameter securely to a fixed surface is by making use of standard Luer connectors. These pneumatic connectors provide an excellent seal (collar and tapered profile design as illustrated in Figure 6.27) and can be coupled and tightened very easily.

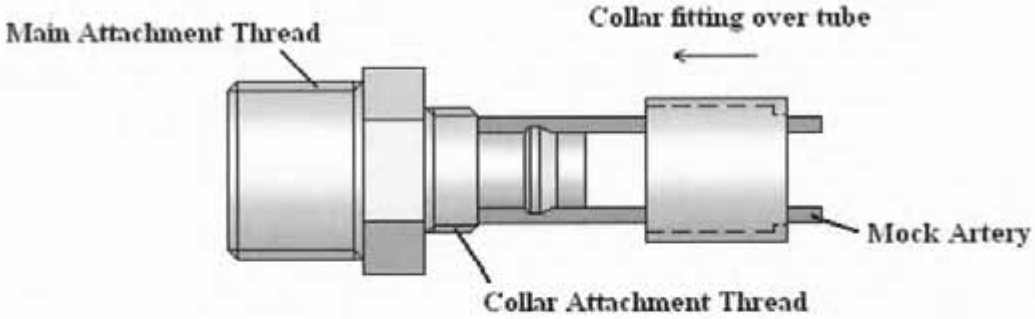

Figure 6.27 Concept H1 – Standard Luer "quick connectors"

6.3.8.2 Modified Luer Design (H2)

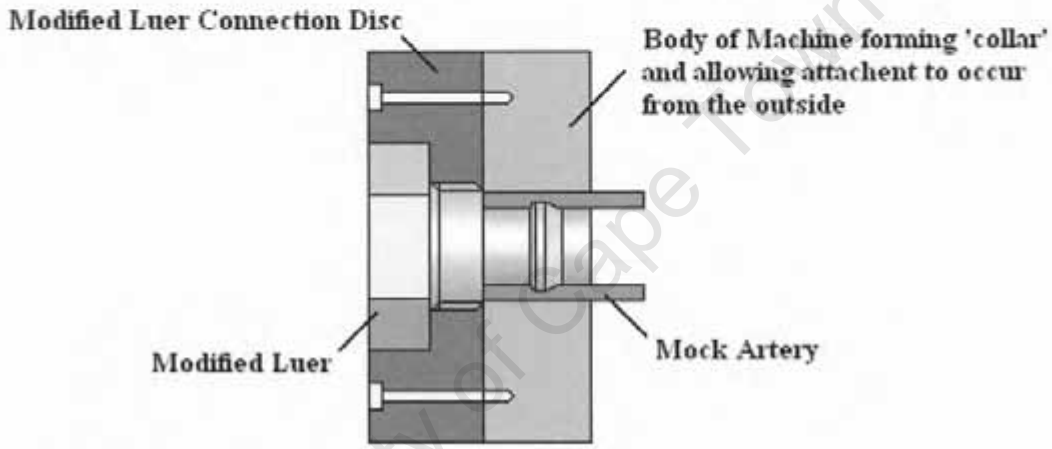

Figure 6.28 Concept H2 – Modified Luer design

Depending on the type of system designed, spacing requirements might prevent the use of standard Luer connectors and require a modified Luer design. Figure 6.28 illustrates a possible adaptation of the Luer connector principle, when internal connection space is limited (tube channel for example — as used in Prototype Al of chapter 7).

6.3.9 Stent Insertion Concepts (I)

The final design will need to enable simple, yet effective deployment of stents into the mock arteries. The following two conceptual solutions address this requirement.

6.3.9.1 Insertion Prior to Tube Attachment (I1)

This concept requires that the stents be deployed into the mock artery before they are attached to the machine.

6.3.9.2 Bleed Valves (12)

This conceptual solution makes use of bleed valves opposite each connected mock artery. Not only could this valve be used to bleed air from the system to ensure adequate operational pressures, but it could also serve as a deployment pathway for the stents. Once the stents have been deployed the valves can be closed.

6.3.10 Temperature Control Concepts (J)

Since blood flows though the coronary vessels at 37°C, adequate temperature regulation of the simulated fluid medium might prove necessary. The following two concepts address the issue of fluid temperature regulation within the fatigue tester.

6.3.10.1 External Heat Exchanger

This conceptual solution ensures fluid temperature regulation at 37°C by making use of some form of external heat exchanger. With the fluid circuits (either internal or external — as illustrated in the example conceptual sketch of Figure 6.10) allowed to continuously circulate, warm fluid flowing out of the system could be passed through a heat exchanger and cooled before re-entering the system, thereby ensuring a constant operating temperature.

6.3.10.2 Heat Dissipation through the Machine's Structure

By making use of materials with good heat conductivity, excess heat generated during the high frequency pulsation of fluid could be dissipated through the machine's structure. Such dissipation would eliminate the need for external fluid circuit cooling.

6.3.11 Tube Excitation Frequency Control Concepts (K)

6.3.11.1 Frequency Control Box (K1)

Since DISA Vascular already possess a frequency controller box (illustrated in Figure 6.29), this device will be used to send either the electric motor or linear actuator a

controlled frequency signal. The device can be programmed to any desired operational frequency and once initiated, achieves this frequency in a gradually accelerated manner. In addition to providing accurate frequency control, the device also records testing duration and displays it on the cover panel in hours. This provides the operator with an indication as to how many cycles the machine has completed.

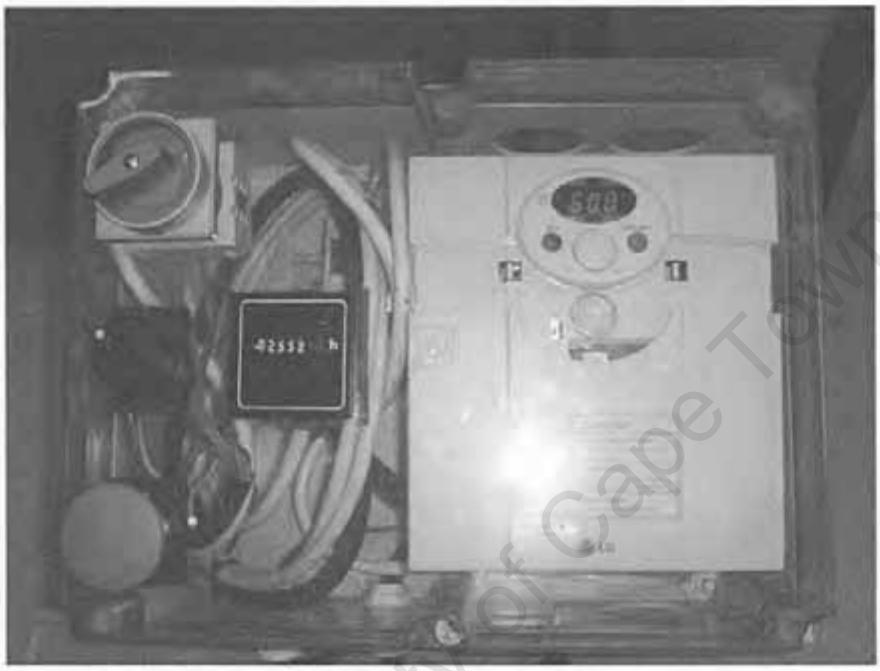

Figure 6.29 Concept K1 – Frequency control box

6.3.12 Compliance and Bending Control Concepts (L)

Whether using mechanical cams or electrical linear actuation, the stroke produced should be adjustable and thus enable the operator to have control over the amount of tube expansion (compliance) and bending. The following conceptual sub-braches describe various compliance and bending control concepts.

6.3.12.1 Mechanical Stoke Adjustment Concepts (La)

The following concepts enable the adjustment of a mechanical cam (as illustrated in the conceptual sketches of Figures 6.19 to 6.21) to achieve control over compliance and bending parameters.

Spacer Adjustable Centre Shaft (L_a1)

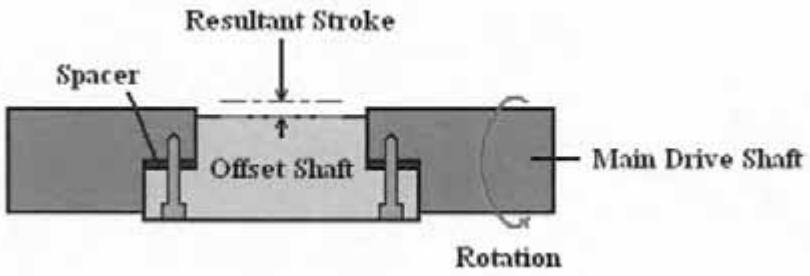

Figure 6.30 Concept L_a1 — Spacer adjustable centre shaft

An adjustable stroke is produced in this concept by making use of spacers to separate main drive shaft and offset shaft centrelines. With the offset centre shaft raised in this way, rotation of the main shaft would cause it to rotate in a cam-like manner. Connecting a bearing around the centre shaft would transfer its offset into a physical stroke at a frequency perfectly in-phase with the rotation of the main shaft.

Eccentricity Adjusted Centre Shaft (L_a2)

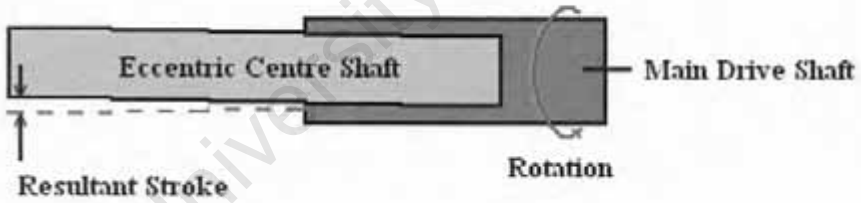

Figure 6.31 Concept L_a2 — Eccentricity adjusted centre shaft

This concept relies on an eccentric shaft to produce variable strokes. With the main shaft threaded internally at a slight angle, a shaft screwed inside it would rotate in a cam-like manner as the main shaft turns. Screwing the eccentric shaft deeper into the main drive shaft would result in a smaller stroke, while unscrewing the shaft would produce larger strokes. This principle is employed by DISA Vascular's current fatigue test bench.

6.3.12.2 Electrical Stroke Adjustment Concepts (Lb)

Concepts falling under this sub-branch of compliance and bending control do so by generating electrical signals that are responsible for increasing or decreasing stroke amplitudes.

Compliance Feedback to Actuator (Lb1)

Should an electro-magnetic actuator be used in conjunction with a laser micrometer, electrical compliance feedback (output from the micrometer) could be used to increase or decrease the amplitude of actuation. If the micrometer for example was to detect a gradual decrease in tube expansion (increase in stent diameter of less than 5%) it could trigger the electro-magnetic actuator to increase its stroke slightly. This increased stroke would lead to increased pressure fluctuations and improve tube expansion. The process would continue until the 5% range had been restored.

6.3.12.3 Tube Length Adjustment Concepts (L_c)

Varying the extent by which the mock arteries expand can also be controlled by adjusting their length. With the mock arteries being flexible in nature, shorter arteries will expand more than longer arteries when subjected to the same internal pressure variations.

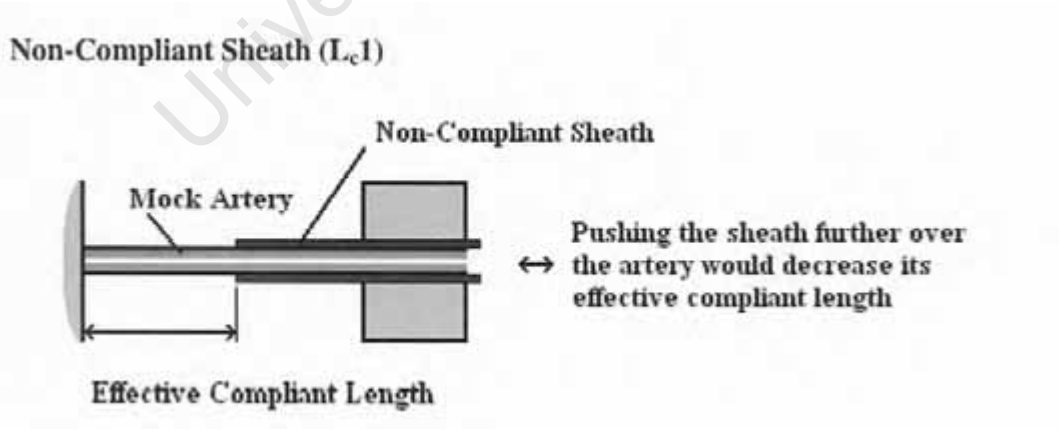

Figure 6.32 Concept 1_„1 — Non-compliant sheath

This concept enables the modification of effective tube length by sliding a non-compliant tube over it. The shorter the effective tube length, the greater its change in diameter for the same internal pressure.

Physical Modification of Tube Length (1,2)

One of the more obvious ways to vary the tube length would be to physically cut it to the new desired size. This would however require the tube attachment sides to be adjustable so that the new tube length could be connected in a naturally and unstressed state.

6.3.13 Pressure Measurement Concepts (M)

Since cyclic internal pressure variations are of vital importance in the expansion of the mock arteries, some form of pressure measurement device would be required to record these changes. The following two concepts suggest possible solutions.

Standard Pressure Gauge (M1)

Figure 6.33 Concept Ml — Standard pressure gauge

Standard pressure gauges record pressure changes with a small internal diaphragm and generally output the results (psi, kPa or atm) by means of a needle and dial.

Pressure Transducer (M2)

Pressure transducers work on a similar principle, but generally output pressure readings as a current (mA) or voltage (V) signal. After interpretation of the signal by a computer or similar processor, representative pressure readings are derived and can be plotted as a function of time. Plots of this nature are very useful, as they provide the user with instantaneous pressure readings even at very high frequencies.

6.3.14 Tube Material Selection (N)

The following materials were identified and considered for use as mock arteries in the fatigue testing machine:

1. Commercial Latex Tubing (N1)
2. Commercial Silicon Tubing (N2)
3. Custom Latex Tubing (N3)
4. Custom Silicon Tubing (N4)
5. Commercial Polyurethane Tubing (N5)

Custom latex and silicon tubes can be produced to any size by painting layers of liquid silicon or latex onto a glass rod. The more layers painted, the thicker the final tube.

Chapter Seven

The Design Process — Concept Evaluation

Concept Evaluation involves an in-depth analysis of all concepts generated (Chapter 6) and should, through the use of logical hierarchical evaluation techniques, present one with the most feasible concepts in the end. The following techniques (in this order) were applied to the generated concepts, leading to the final conceptual design discussed and illustrated in Section 7.5.

1. Feasibility Evaluation (instinctive response)
2. Evaluation making use of relevant calculations and / or testing results obtained
3. Final Decision matrix (using the results obtained in 1 and 2)

7.1 Feasibility Evaluation

Feasibility was scored on a scale of 1 to 3: (1) it is not feasible and will never work, or is too expensive or impractical to consider; (2) it might work if something else happens; (3) it is worth considering.

This initial step of concept evaluation analyses all generated conceptual solutions and by means of the aforementioned scoring technique, passes only those concepts worth considering (score > 2) on to the next level of evaluation. The technique could be viewed as somewhat of an instinctive response and, as the name implies, strives to evaluate the concepts as simplistically as possible. Table 7.1, on the following page illustrates this evaluation process as applied to the concepts generated in Chapter 6. Feasibility scores and general comments regarding conceptual feasibility are included in the illustration.

Concept	Feasibility	General Comments
Pressurization concepts (A)		
Double fluid circuit with piston (Al)	2	Would need to test vacuum ability
Single fluid circuit (A2)	3	To be considered
Gas tank with valves (A3)	1	Reliability of gas valves at high frequencies doubtful. Air is also less dense than water and could cause inertia-related problems.
Axial deformation concepts (B)		
Simple tensioning of tube (B1)	1	Would cause the tube to creep with time
Bending concepts (C)		
Both ends of tube fixed (C.)		
Inflatable bladder (C.1)	2	Was considered appropriate if tubes could be secured to bladder surface, preventing them from 'bouncing' at high frequencies.
Cam wheel (C.2)	1	Cyclic knocking of the stent considered undesirable
Magnetic attraction (C.3)	1	Magnetic ring around the mock artery would reduce its ability to expand
One end of tube fixed (DO		
180° displacement of free tube end (al)	3	To be considered
90° displacement of free tube end (C_b2)	3	To be considered
Motor-drive concepts (D)		
Single motor with gear arrangement (D1)	1	Very cumbersome and expensive. Gears would all require oil baths.
2 motors (D2)	1	No two motors are exactly the same and, as such, perfect synchronization over 3 months will not be possible
Single motor with timing belt (D3)	3	To be considered
Linear actuation concepts (E)		
Electromagnetic actuator (El)	1	Very specialized unit, requiring design and manufacture of its own
Concepts for detecting a change in tube diameter (F)		
Strain gauges (F1)	1	The wire coil one would need would restrict tube compliance
Electromagnetic induction (F2)	1	Specialized unit, and it is doubtful as to how well the wire could be adhered to the tube surface
Laser micrometer (F3)	1	Very appropriate but due to their price, not considered an appropriate solution
Stroboscope and camera (F4)	2	Would need to test the resolution of such a measuring technique. If sufficient quality is attainable, the concept is worth considering
High speed camera (F5)	3	Very appropriate solution. The equipment would need to be borrowed for testing (Denel Landsystems: Somerset West, South Africa)
Concepts for viewing tube motion (G)		
Laser micrometer (31)	1	Very appropriate but due to their price, not considered an appropriate solution
Stroboscope and camera (G2)	2	Would need to test the resolution of such a measuring technique. If sufficient quality is attainable, the concept is worth considering

Concept	Feasibility	General Comments
High speed camera (G3)	3	Very appropriate solution. The equipment would need to be borrowed for testing (Denel Landsystems: Somerset West, South Africa)
Tube anchorage concepts (H)		
Standard luer "quick connectors"	3	To be considered
Modified luer design	2	Suitability dependant on final design and application
Stent insertion concepts (I)		
Insertion prior to tube attachment (H)	1	Tube attachment would produce excessive stress on the stent
Bleed valves (12)	3	To be considered
Temperature control concepts (J)		
External heat exchanger (J1)	1	Too expensive
Heat dissipation through the machine's structure (J2)	3	To be considered
Tube excitation frequency control concepts (K)		
Frequency control box (K1)	3	To be considered
Compliance and bending control concepts (L)		
Mechanical stroke adjustment concepts (L)		
Spacer adjustable centre shaft (L$_a$1)	3	To be considered
Eccentricity adjusted centre shaft (L$_a$2)	2	Chance that the shaft would loosen during loading, thereby changing the stroke
Electrical stoke adjustment concepts (L$_b$)		
Compliance feedback to actuator (L^{b1})	1	Since an actuator was considered unfeasible, this conceptual solution is no longer appropriate
Tube length adjustment concepts (L$_b$)		
Non-compliant sheath (L$_a$i)	3	To be considered
Physical modification of tube length (1$_{_o}$2)	3	To be considered
Pressure measurement concepts (M)		
Standard pressure gauge (M1)	1	Unable to display pressure fluctuations at high frequencies
Pressure transducer (M2)	3	To be considered
Tube material selection (N)		
Commercial latex tubing (N1)	3	To be considered
Commercial silicon tubing (N2)	3	To be considered
Custom latex tubing (N3)	1	Considered inappropriate
Custom silicon tubing (N4)	1	Considered inappropriate
Commercial polyurethane tubing (N5)	1	Very low compliance, inappropriate for vessel expansion

Table 7.1 Feasibility analysis of generated concepts

7.2 Evaluation Based on Calculations and / or Testing Results Obtained

This section further analyzes the concepts passed by section 7.1 by means of prototype testing and / or preliminary calculations. The type of evaluation technique performed

depends on the nature of the concept, but all techniques strive to provide a clearer understanding of the concept's suitability to successful project implementation.

7.2.1 Tube Material Selection (concepts N)

Tube material selection (although labelled 'N' in the concept generation chapter) was evaluated first as it forms the basis for most of the conceptual solutions. With polyurethane tubing already being rejected during feasibility evaluation, this section deals with the evaluation of commercially available latex and silicon tubes.

Testing and Results

With coronary artery lumen diameters ranging from between 3 to 4 mm (as presented in chapter 2), standard commercially available 3mm latex and silicon tubes were acquired for evaluation purposes. Latex tubes measured 2.8 mm in inner diameter and 5.8 mm in outer diameter, while silicon tube's inner and outer diameters measured 3.1 and 6.1 mm respectively. The tubes were subjected to internal pressurization and their external diameters recorded as a result. It was assumed that the wall thickness of both tube varieties did not change with increased pressure, and the relationship between inner diameter (d1) and outer diameter (d_o) was therefore calculated as follows:

$$d_{i,pressurized} = \sqrt{d^2_{o,pressurized} - \frac{4 \times A_{cross\ section}}{\pi}} \tag{7.1}$$

with

$$A_{cross\ section} = \frac{\pi}{4}(d^2_{o,unpressurized} - d^2_{i,unpressurized}) \tag{7.2}$$

Figures 7.1 and 7.2 on the following page illustrate the results obtained during static pressurized testing. Figure 7.1 plots recorded outer diameter variations for both silicon and latex tubes across a range of pressures; while Figure 7.2 plots theoretically calculated inner diameter changes (using equations 7.1 and 7.2) across the same pressure ranges. Linear trend lines were added to both figures as their equations were considered important in making compliance modifications at higher frequencies, based on the results obtained from Ramesh *et al.* (2005).

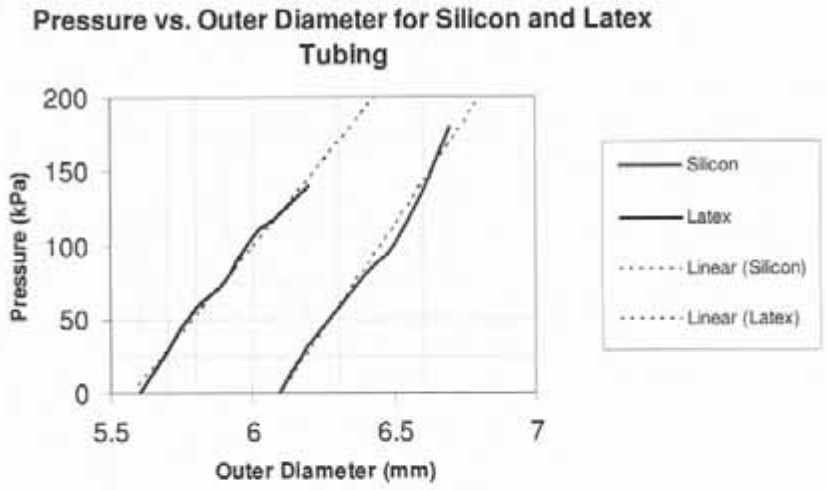

Figure 7.1 Pressure vs. outer diameter for silicon and latex tubing under static conditions

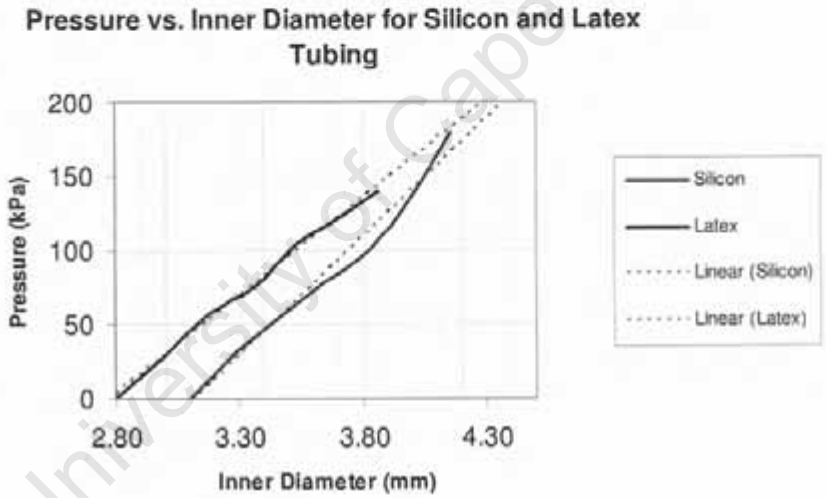

Figure 7.2 Pressure vs. inner diameter for silicon and latex tubing under static conditions

Figures 7.1 and 7.2 illustrate the slightly superior compliance characteristics of latex tubes over that of silicon. Latex tube exhibits an internal diameter change of 5% at approximately 18 kPa, while silicon reaches a 5% change at about 25 kPa.

With compliance characteristics for silicon and latex tubes known, the data was adapted based on the findings of Ramesh *et al.* (2005) to produce theoretical variations in tube compliance at elevated frequencies. The findings (illustrated in Figures 7.3 and 7.4) plot change in internal diameter for both silicon and latex tubes against pressure at frequencies

ranging from 0 Hz (static) to 25 Hz. Data generated in formulating these findings are presented in Appendix A-1.

Since the findings of Ramesh ***et al.*** (2005) only supplied compliance reduction data up to 25 Hz, the predicted behaviour illustrated in Figure 7.3 cannot be extrapolated up to 60 Hz. Accurate analysis of silicon and latex tube compliance at frequencies higher than 25 Hz will require physical machine testing and can thus not be discussed at this point.

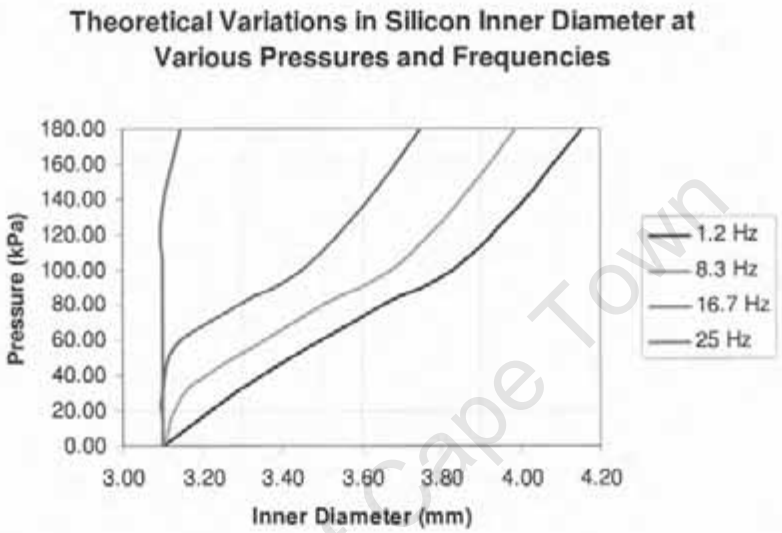

Figure 7.3 Theoretical variations in silicon inner diameter at various pressures and frequencies.

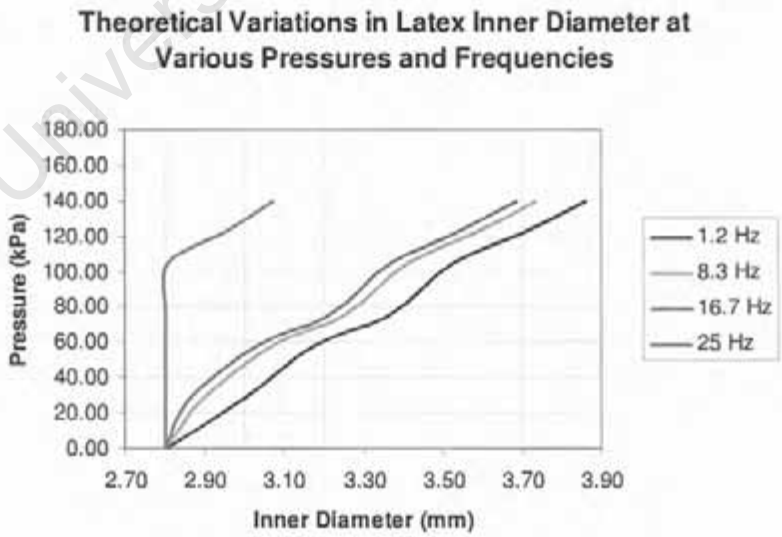

Figure 7.4 Theoretical variations in latex inner diameter at various pressures and frequencies.

The findings seem to suggest that at frequencies of 25 Hz approximately 180 kPa is required to cause 5% inner diameter expansion of 3 mm silicon tubes, with 120 kPa being required to achieve the same relative expansion in latex. In addition to these calculated results, it was found that latex tubes (being softer than silicon) vibrated in an uncontrollable fashion at frequencies above 40 Hz. Testing of this nature was conducted on DISA Vascular's Fatigue test bench (illustrated in section 7.2.3) and thus only gave an indication of the tube's motion.

Conclusion

Silicon tubes display relatively similar compliance characteristics to that of latex and, with increased motional stability at frequencies above 40 Hz seemed a more appropriate tube for selection. Theoretical data has suggested pressures of approximately 180 kPa to produce acceptable vessel expansion at 25 Hz. With this design parameter in mind, and the inclusion of various stoke adjustment features present (capable of adjusting pressure gradients), there is little doubt that silicon tubes could produce acceptable deformations at frequencies up to 60 Hz.

7.2.2 Pressurization (concepts Al and A2)

Both of these conceptual solutions induce tube deformation by causing a pressure gradient across the vessel wall. With the stent being deployed up against the inner wall of the mock artery, a change in vessel diameter would induce various stresses on the deployed stent. The ability of the stent to follow a changing vessel wall diameter is evaluated in Section 7.2.3 (based on the findings presented in chapter 4). For now, however, pressurization and its effects on a mock artery will be evaluated. Concept Al (double fluid circuit with piston) makes use of a negative pressure to "suck" the vessel open, while Concept A2 (single fluid circuit with piston) causes the same deformation by means of positive internal pressure. Both concepts were evaluated by making use of DISA Vascular's fatigue test bench (Figure 7.5), which provided a stationary and pivoting plate between which the prototypes could be connected. The pivoting plate was driven by an offset shaft coupled to an electric motor and set to vibrate at any user-defined frequency controlled by a custom made control system.

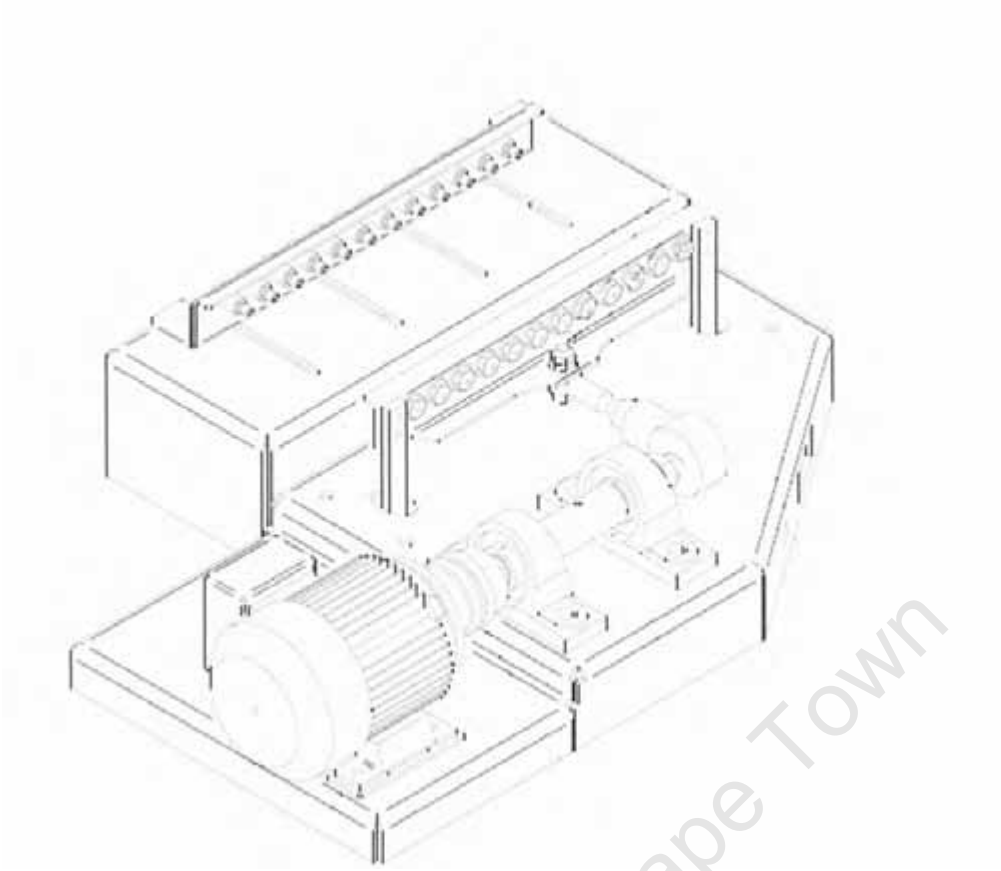

Figure 7.5 An illustration of DISA Vascular's fatigue test bench

To aid in the understanding of how concepts Al and A2 would achieve appropriate stent deformation, the following properties will need to be discussed: isotropic material, poisson's ratio and thin-walled vessels.

Isotropic Material

An isotropic material can be defined as any material displaying identical properties in all directions. One such property is the *Elastic Modulus* (E), relating a material's stress (G) and strain (c) in the following way:

$$\sigma = E \times \epsilon \tag{7.3}$$

An isotropic material would thus display identical stress/strain relationships in every direction.

Poisson's Ratio

Poisson's ratio suggests that at right angles to an applied load, a certain amount of lateral expansion or contraction occurs. This effect is illustrated in Figure 7.6 and shows that

when an object is subjected to a tensile force the lateral sides will contract, while subjecting it to a compressive force will force the lateral sides out.

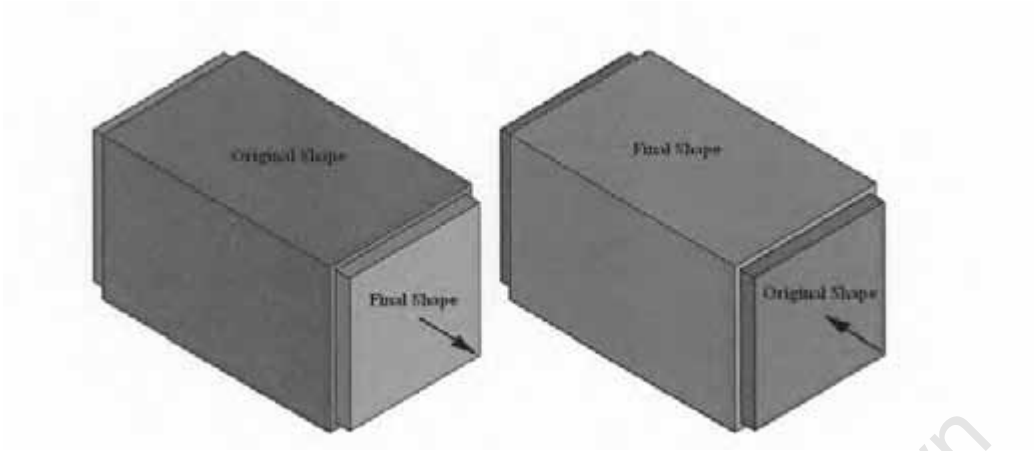

Figure 7.6 Lateral contraction and expansion of solid bodies subjected to axial loads

The ratio of change in lateral strain to axial strain is expressed by v (poisson's ratio) and is a definite property of the material:

$$\nu = -\frac{Lateral\ strain}{Axial\ strain} \tag{7.4}$$

Thin-walled vessels

A thin-walled vessel is one in which its outer and inner radius are assumed to be equal ($r_i \approx r_o$). Many cylindrical and spherical pressure vessel calculations make use of this assumption and even with wall thicknesses ($t = r_o - r_i$) reaching one-tenth of the internal radius the approximation yields satisfactory results.

Concepts Al and A2 subject the stent deployed within the "mock arteries" to appropriate deformations by making use of the aforementioned principles. Assuming isotropic and thin-walled tubes, axial stress (øa) can be shown to relate to radial stress (ør) in the following way:

$$\sigma_r = 2\sigma_a = \frac{pr}{t} \tag{7.5}$$

With the parameters p, r and t representing internal pressure, tube radius (with $I_, = r_i = r$ due to our thin-walled assumption) and wall thickness, respectively.

For an isotropic material, by substituting Equation 7.3 into Equation 7.5 we find that a similar relationship can be derived for the tube's strain:

$$\epsilon_r = 2\epsilon_a = \frac{pr}{t} \tag{7.6}$$

A pressurized tube experiencing a resultant increase in diameter would also increase in length by a respective ratio of 2:1. The radial and axial stresses required to fatigue a stent could thus potentially be achieved by merely inducing tube expansion.

7.2.2.1 Concept Al (Double fluid circuit with piston)

The general idea behind this concept is very sound. Inducing a negative pressure around the tube would cause it to expand while at the same time allowing for independent fluid flow through the centre of the tube. Since the simulation of physiological conditions is one of the primary project goals, an uninterrupted and separate internal circulation has many advantages. Controlled flow rate (potentially necessary in the future fatigue testing of drug-eluting stents) and temperature regulation are examples of these advantages and would prove difficult to achieve when pressurizing the tube internally (concept A2).

Prototype Design and Construction

The concept was tested by constructing a prototype out of perspex (Figure 7.7) that separated the two fluid circuits while at the same time restricted the tube to a limited channel in which to oscillate. The creation of a channel was found to be necessary due to the less rigid tube's tendency to "flap" at increased oscillation frequencies. By confining the tube to a limited channel (only slightly wider than its diameter of 6 mm) a more controlled environment was ensured and photography of the tube was made easier.

Pressure reduction around the tube was achieved by creating two discs at one end (similar to that of a piston) enclosed by a rubber band to make them airtight. The rubber band was securely fastened to the circumferential surface of both perspex discs by means of hose clamps and tightened to ensure a watertight seal. Early prototype design made use of discs with smooth surfaces which upon testing were found to leak. The problem was corrected

by machining "steps" into the disc surface, effectively placing the rubber bands under greater pressure and significantly reducing the risk of leakage (Figure 7.8).

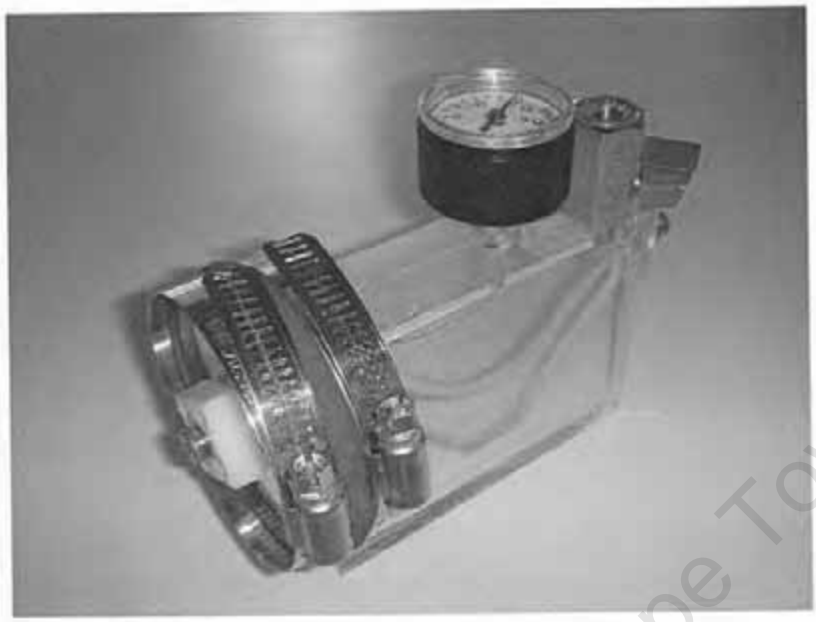

Figure 7.7 Concept A1 prototype

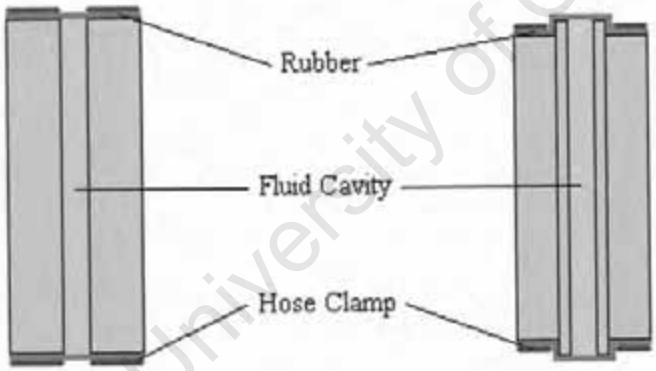

Figure 7.8 *Smooth* (left) and *Stepped* (right) circumferential disc surface design

Construction of the prototype body was problematic, with early prototypes made from polyethylene and perspex (bonded with silicon and screws) leaking. Perspex, while providing the required transparency for examination purposes, was later found to produce the best possible seal when bonded together using a plastic adhesive such as *Tensol* 7. This adhesive, after being activated by a catalysing agent, bonds two pieces of perspex together into a seamless monolithic structure, thereby creating a perfectly airtight seal.

The unit was provided with 10 mm attachment threads at each end to connect between the pivoting and stationary plates of the fatigue test bench. Final design drawings for the prototype of concept Al are presented in Appendix B.

Testing, Calculations and Conclusions

Concept Al was evaluated both theoretically and experimentally and provided much insight into the mock arteries ability to expand due to pressure gradients at elevated frequencies. Although much was known about silicon and latex tube compliance when exposed to static (low frequency) pressure variations (section 7.2.1), this test was the first conducted at higher frequencies.

Figure 7.9 illustrates the theoretical pressure gradients the prototype was able to induce for various piston strokes and fluid compositions (calculations presented in Appendix A-2). Increased piston stroke (displacement of circular discs) led to increased pressure gradients (dP), while increased gas content reduced the total pressure gradient. The best results were thus achieved with no air present in the cavity housing the tube, and with maximal piston strokes.

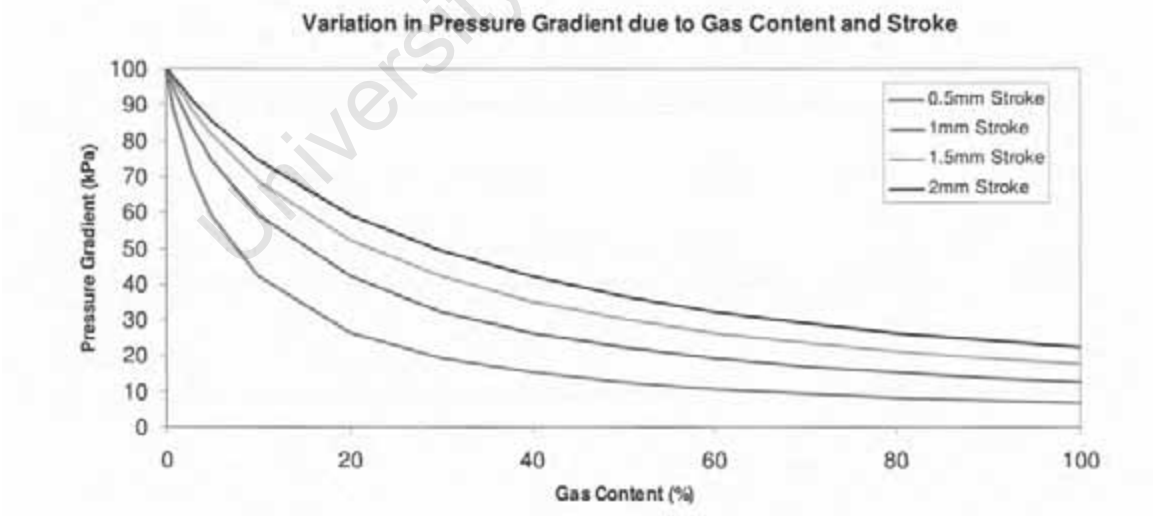

Figure 7.9 Prototype Al - Theoretical variation in pressure gradient due to gas content and stroke

During testing, while able to produce reasonable pressure gradients at low frequencies, the prototype failed at higher frequencies. The force required to pull the circular discs apart

seemed too great and the high frequency pressure gradients were too low to induce a 5% change in vessel diameter.

With approximately 180 kPa required to induce a **5%** change in internal silicon tube diameter (Section 7.2.1), information acquired during testing suggested that the prototype of concept Al would not work.

7.2.3.2 Concept A2 (Single fluid circuit with piston)

Concept A2 differs from that of concept Al in that tube deformation is induced solely by internal pressurization. Due to the small internal volume of mock arteries, pressurization of this kind is advantageous because greater pressure gradients can be achieved from considerably less force. As noted in the previous section, larger pressure gradients are vital in obtaining our targeted 5% compliance, a requirement further intensified by the tube's reduction in compliance at elevated frequencies.

Prototype Design and Construction

Initial prototype design and construction of concept A2 was very similar to that of Al. Perspex was again used to house the tubes and modifications were made to ensure that fluid was only contained inside the tubes. The outer perspex plates now served purely as a tube guide and were not responsible for holding fluid at all.

The design of Prototype A2 went through two revisions before taking on the final shape of Figure 7.10, the main change being the increase in piston diameter from 75 mm to 150 mm (producing greater pressure gradients). Learning from the problems experienced in prototype Al, prototype A2 also made use of *steps* on the circular disc surface (piston) and used *Tensol-7* in the monolithic bonding of the perspex structure. Detailed design drawings for prototype A2 are presented in Appendix C.

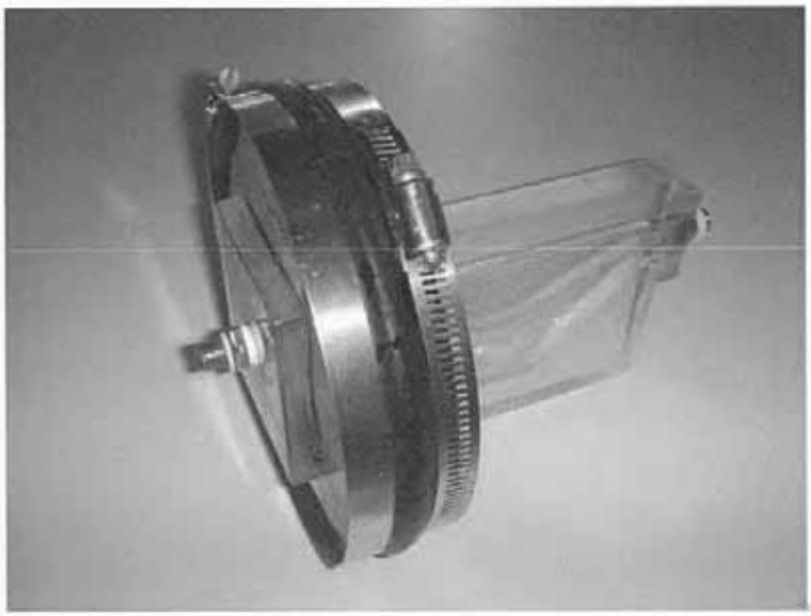

Figure 7.10 Concept A2 prototype

Testing, Calculations and Conclusions

Prototype A2 was evaluated both theoretically (Appendix A-3) and experimentally and produced much better results than that of prototype Al. Experimental evaluation was conducted using both high speed video camera and stroboscope / camera techniques (section 7.2.4) to analyse the tubes, while making use of the *WIKA S-10* pressure transducer setup presented in Section 7.2.5 to record pressure variations.

Before presenting the results of theoretical and experimental evaluation, shock wave generation and fluid selection considerations will be addressed.

Shock Wave generation

Since the piston of prototype A2 would be compressing fluid into the mock artery at frequencies of — 60Hz and doing so across a stroke of up to 2 mm, the question of whether this action would induce shock waves was raised. A shock wave (in either a gas or liquid) is caused when an object is set in motion through a fluid faster than the speed of sound in that fluid. Such motion can cause waves of high pressures and varying densities behind the object and would obviously cause errors in the interpretation of results obtained by this prototype. The speed of sound in water and air at 15.5°C is 1482 m/s and 340 m/s respectively. With a piston set in motion at 60 Hz its velocity when covering a distance of

2 mm per half-stroke (one full stroke being defined as the forward and return motion of the piston) can be calculated as follows:

$$\text{Time per half-stroke} = (1 / 60) / 2 = 0.00833 \text{ s}$$
$$\text{Distance per half-stroke} = 2 \text{ mm} = 0.002 \text{ m}$$
$$V = 0.002 / 0.00833 = 0.24 \text{ m/s}$$

With piston speed per half-stroke being significantly lower than the speed of sound in both water and air, the risk of shock wave generation is insignificant and can for all intents and purposes be ignored.

Fluid Selection

There was much speculation as to whether air or water would be a better choice of fluid within the tube. Water (or a similar fluid) would be advantageous to use from a physiological simulation point of view, but the incorporation of air into the system would be decidedly easier. After considerable thought however and a few trial runs, water was chosen above air for the following reasons:

1. Water, being a fluid, has far more densely packed molecules than that of air. When pressurized by means of a piston, molecules far from this displacing point would feel the motion (compressing each other to increase pressure) faster and more synchronously than that of air.
2. Water (or a similarly fluid medium, i.e. a saline solution) would simulate physiological conditions more accurately than air, and ensure constant flow over the deployed stent.
3. Water's temperature would be easier to control than that of air and its thermal characteristics might prove more suited to cooling a stent being fatigued at high frequencies.

Evaluation of Prototype A2

Figure 7.11 illustrates the theoretical pressure gradients that prototype A2 was able to induce for a tube length of 130 mm at various piston strokes. These pressure gradients are

far greater than those generated by prototype Al and are were achievable for considerably less stroke.

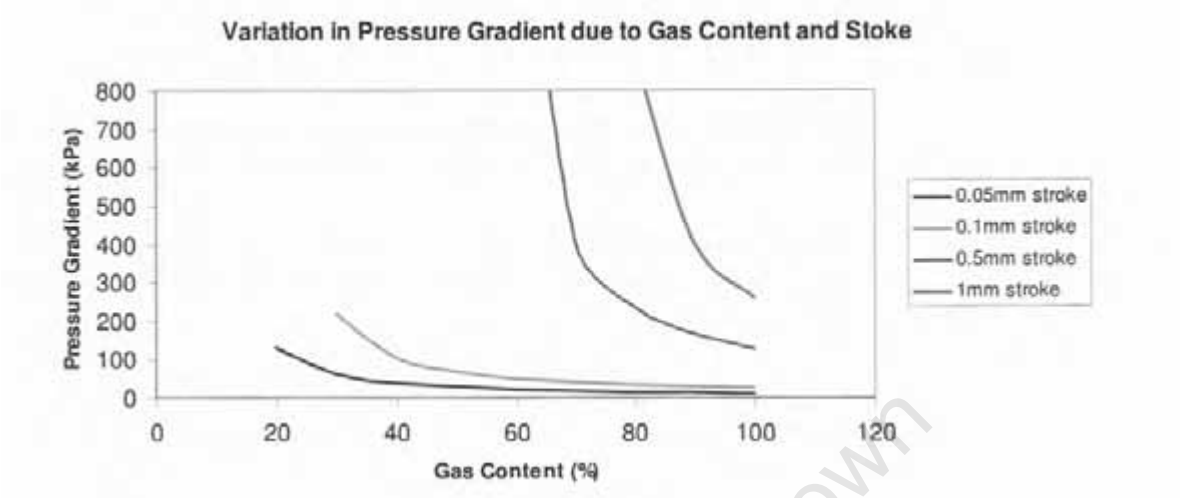

Figure 7.11 Prototype A2 - Theoretical variation in pressure gradient due to gas content and stroke

As previously mentioned, the prototype was evaluated by means of high speed video camera and stroboscope / camera configurations. Images generated from the testing procedures were analyzed with professional graphic measurement software by recording changes in vessel outer diameter during maximum and minimum periods of internal pressurization. Using the uniform cross-sectional area assumption of section 7.2.1, the measured changes in outer diameter were used to predict internal diameter changes. This was found to be necessary since the silicon tubes were not transparent enough to accurately visualize their inner diameter boundary.

Prototype A2 contained a great deal of air during testing cycles and although numerous attempts were made to increase water content, the design simply didn't allow for its removal. Induced pressure gradients were very high at 60 Hz (despite the presence of air) and resultant tube expansion was greater than the required 5%. A 150 mm piston diameter was found to be too great and air content would need to be considerably lowered in the final design. However the prototype suggested the suitability of this concept to induce cyclic pressure variations and tube expansion.

7.2.3 Stent Expansion Analysis

The stent's ability to expand with increasing vessel diameter was analysed under static conditions with both photography and x-ray imaging (*Lodox* system). Experimental testing was performed to verify the theoretical assumptions described in Chapter 4, and produced successful results. With scaling effects producing slightly distorted images during x-ray imaging, x-ray evaluation of the tubes was performed with a 22 mm washer (outer diameter) in the background as a calibration tool. The photographic and x-ray images obtained are presented in Figures 7.12 and 7.13 below and their results are summarized in Table 7.3.

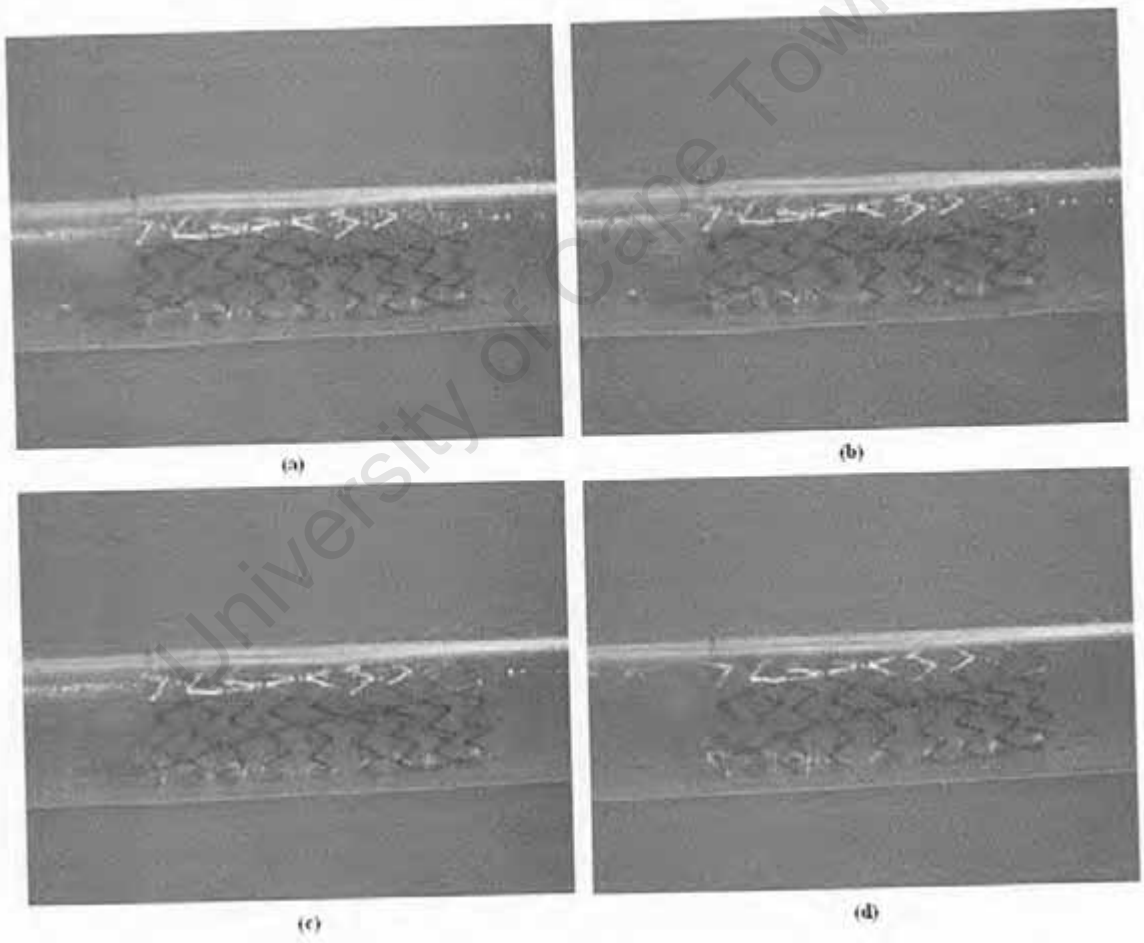

Figure 7.12 Photographs illustrating the expansion of a stent deployed inside a silicon tube when exposed to various internal pressures (a) 0 kPa (b) 20 kPa (c) 40 kPa (d) 90 kPa

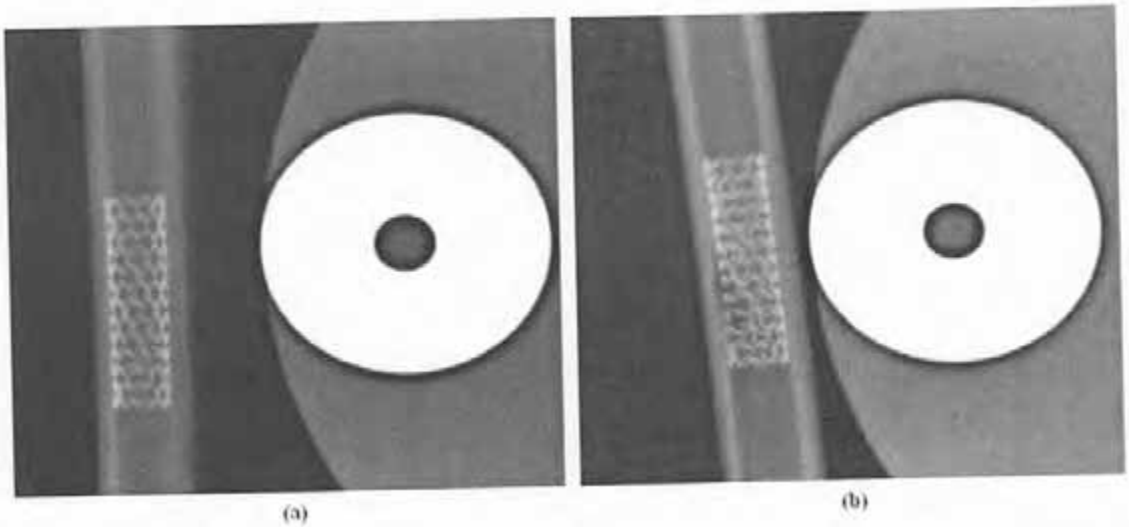

Figure 7.13 X-rays illustrating the expansion of a stent deployed inside a silicon tube when exposed to various internal pressures (a) 0 kPa (b) 90 kPa

Photographic Evaluation				
Frame	(a)	(b)	(c)	(d)
Wall Adherance	Good	Good	Good	Slight Separation
Pressure (kPa)	0	20	40	90
Outer Diameter Expansion (%)	0	0.6	2.1	5.7
Inner Diameter Expansion (%)	0	2.3	8.1	21.3
Stent Expansion (%)	0	2.0	4.6	7.1

X-Ray Evaluation		
Frame	(a)	(b)
Wall Adherance	Good	Slight Separation
Pressure (kPa)	0	90
Outer Diameter Expansion (%)	0	5.1
Stent Expansion (%)	0	6.1

Table 7.2 Summary of stent expansion results obtained from photographic and x-ray evaluation.

The results presented in Table 7.2 reinforce the theoretical assumptions made in Chapter 4 and suggest that expansion of a stent deployed within a mock artery is possible provided the stent remains within its elastic range.

7.2.4 Tube Compliance Measurement and Motion Tracking (concepts F4 and F5)

The measurement of tube compliance and motion at high frequencies is no easy task. Budgetary constraints, lack of specialized equipment and technical know-how all contributed to these difficulties. The following section evaluates concepts F4 (stroboscope and camera) and F5 (high speed camera), and provides a clearer understanding of how tube expansion and motion were captured using these methods.

General Methodology

The bending of a 6 mm tube stops being clearly discernable to the human eye at approximately 6 Hz. For this reason a system would need to be implemented to make viewing of the tubes possible, even at frequencies of 60 Hz and above. The general idea behind conceptual solution F4 (stroboscope and camera) was to subject the mock artery to a 60 Hz oscillation while illuminating it with a high frequency light source (stroboscope). If allowed to occur in a darkened room, with the light from the high frequency light source as the only light, a slower moving tube would be observed. This reduction in apparent movement speed is directly related to the relative difference in frequency between light source and tube motion. This phenomenon is due to an effect known as *aliasing* and is graphically illustrated in Figure 7.14.

To aid in the understanding of this phenomenon, one should imagine that the flash being emitted from the light source is instantaneous and is responsible for illuminating the tube at that exact moment. Figure 7.14a illustrates this pulsatile nature of the stroboscope. With the motion of the tube represented by a sinusoidal wave (Figure 7.14b), one full wavelength would represent the tube's motion from start to finish once. If we now were to imagine illuminating the tube at a specific point once every wavelength, it becomes quite clear from Figure 7.14c that the resultant shadow image produced would appear stationary. Hence, setting the tube in motion at the same frequency as that of the light source (60 Hz for example) would produce a static image.

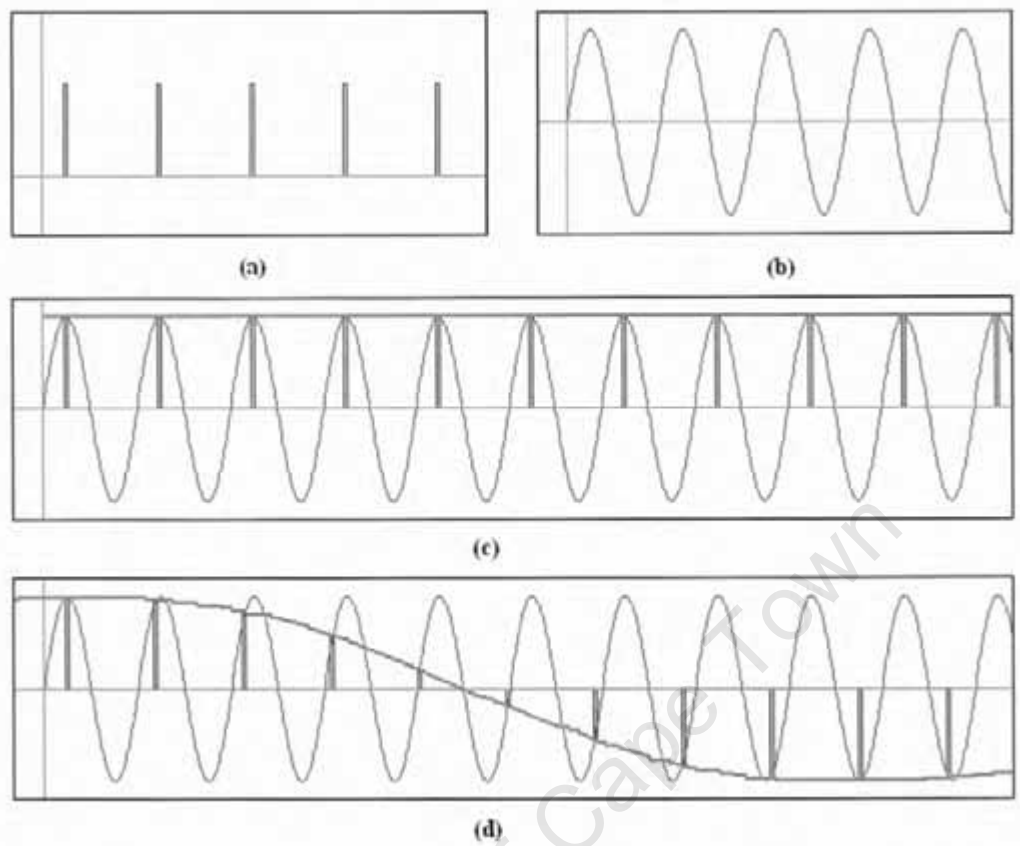

Figure 7.14 The effect of aliasing in visualizing high frequency tube motion
(a) Pulsatile nature of stroboscope
(b) Sinusoidal motion of tube
(c) Creation of a stationary tube image
(d) Creation of a "slow motion" tube image

Of the two potential solutions discussed in the following sections, only concept F3 makes use of this phenomenon, with concept F4 relying on high speed photography to analyse tube motion.

7.2.4.1 High Speed Camera (concept F5)

Most standard general purpose digital video cameras are capable of capturing images at up to 30 frames per second (fps) although normal filming is generally achieved at a rate of 24 fps. Increased frame rate however leads to decreased spatial resolution with most cameras only supporting resolutions of 320 x 240 at 30 Hz. For this project's application, not only

would the camera be unable to film tube motion at 60 Hz but also not film it at an acceptable spatial resolution. Low resolutions would result in pixelation errors and thus undermine the results obtained from tube diameter measurements.

High speed cameras, on the other hand, are perfectly suited to shooting film at very high frame rates (up to 10,000 fps) and offer exceptional resolution, their only drawbacks being limited film time and very high cost. Denel Landsystems (Somerset West, Western Cape) very kindly agreed to offer the use of their camera for the analysis of tube motion during the prototype and final design evaluation stages. This camera provided a resolution of 1280 x 1024 at frame rates ranging from 120 to 8,000 fps. With a camera of this type capable of filming at speeds far greater than that of tube motion, the need for a flashing light source (making use of an aliased image) becomes redundant. Use of Denel's *MotionScope® PCI high speed digital imaging system* was purely for evaluative purposes, as such a camera would be far too expensive to incorporate in the final design.

During prototype testing the camera performed very well and provided a clear view of the silicon tube's motion at 60 Hz. Figure 7.15 illustrates an example of the images achieved during prototype evaluation.

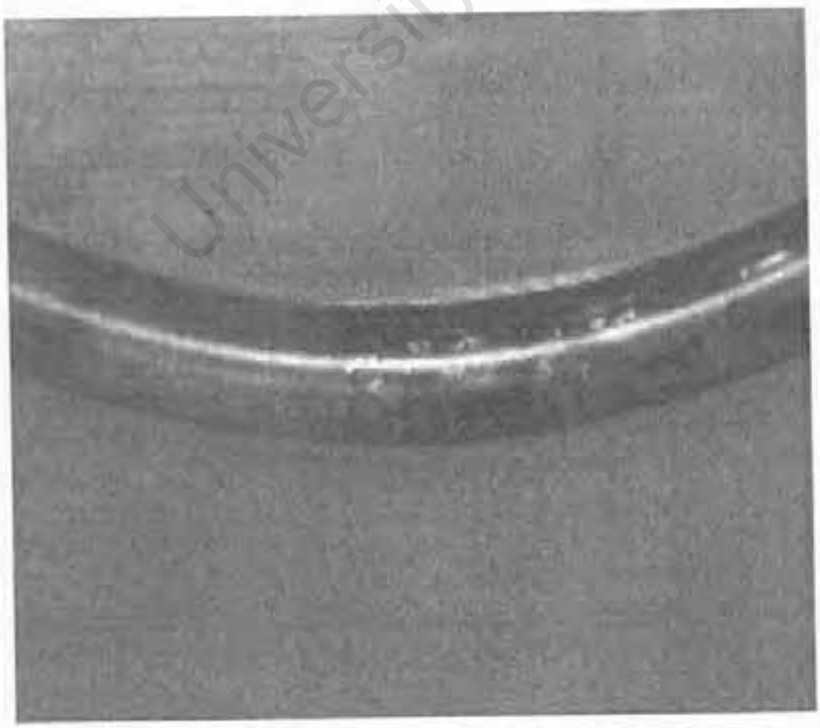

Figure 7.15 Image obtained using the *MotionScope® PCI high speed digital imaging system*

7.2.4.2 Stroboscope and Camera (concept F3)

A *Lutron DT — 2269* stroboscope was used in conjunction with a *Sony Cybershot* to evaluate the suitability of this method for testing purposes. Results produced very pixelated images and were not considered appropriate for detecting tube diameter variation. The technique was however considered suitable for measuring tube bending and could be used in the evaluation of vessel curvature in the final machine.

7.2.5 Pressure Measurement (concept M2)

Concept M2 achieves high speed pressure measurement by making use of a pressure transducer and computer acquisition card. For the purpose of this evaluation, a WIKA S-10 pressure transducer was used in conjunction with a PCI-730 analogue data acquisition board. The pressure transducer was connected to a 24 V power supply and, depending on the pressure it was recording, generated a 4 to 20 mA signal. With the PCI-730 card unable to interpret current signals (designed for 0 to 5 V), a circuit was built to perform the necessary current to voltage conversion. The circuit responsible for this conversion is illustrated in Figure 7.16.

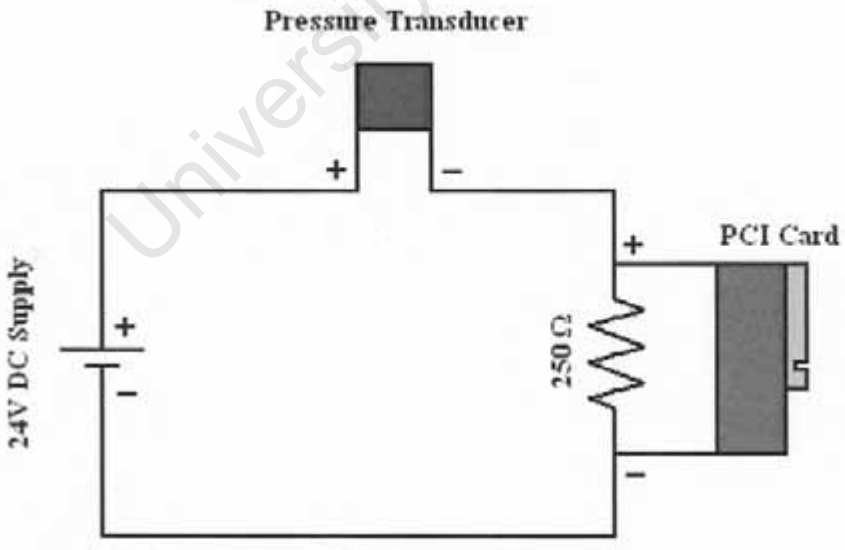

Figure 7.16 0 to 5 V conversion circuit

The voltage signals received by the PCI-730 card were interpreted by WaveView for Windows © 2002 (Eagle Technology) and plotted at a frequency of 1000 Hz. After

recording pressure variations for a suitable time period the program was stopped and the data generated converted to an Excel spreadsheet. In order to accurately correlate the generate voltage readings with the pressures detected by the transducer, a calibration curve was produced (Figure 7.17). With the pressure transducer connected to a known and variable pressure source, voltage readings produced in the Excel spreadsheet were matched with their corresponding pressures. The calibration curve of Figure 7.17 was very accurate and would be used for all future pressure measurements.

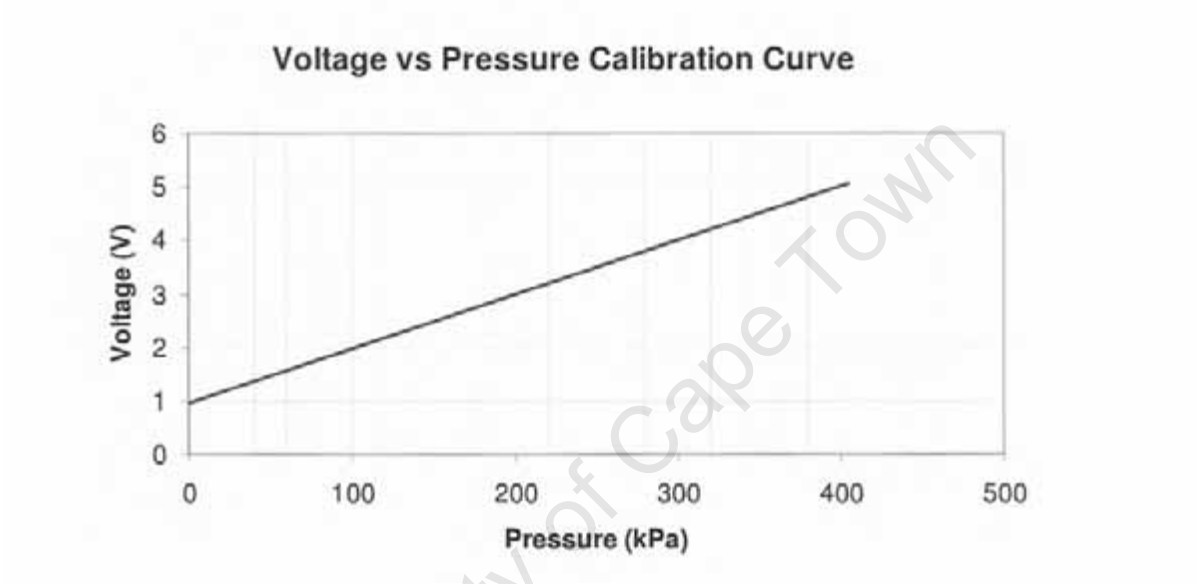

Figure 7.17 Calibration curve for pressure measurement

Concept M2 proved very capable of interpreting pressure fluctuations at high frequencies and, despite occasional voltage spikes (as a result of noise) produced very satisfactory results. Figure 7.18 illustrates the pressure measurements achievable at 50 Hz using the aforementioned technique.

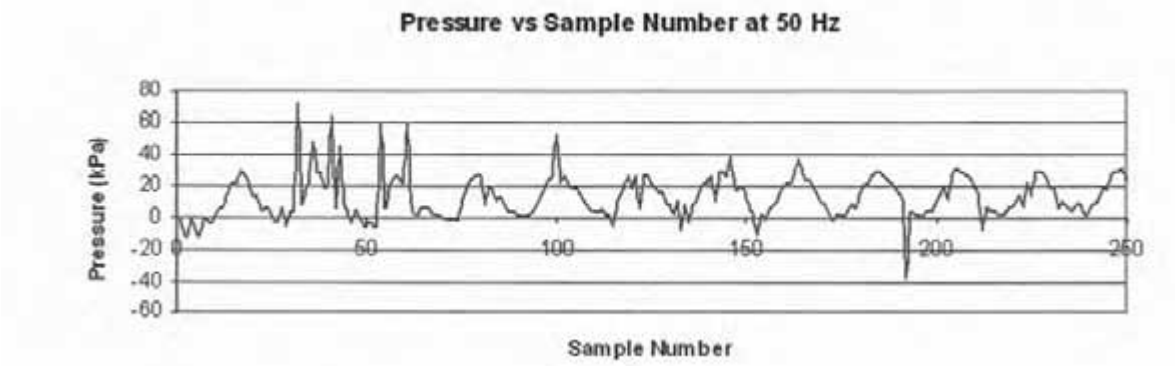

Figure 7.18 Example 50 Hz pressure variation

7.3 Final Decision Matrix

All conceptual solutions considered feasible by sections 7.2 and 7.3 were subjected to final evaluation based on their suitability in meeting the list of customer requirements (weighted in order of average customer importance) presented in Chapter 5. The results are illustrated in the Decision Matrix of Table 7.3 and provide an indication as to which concepts should be combined to form the best possible final design (Ullman: *The mechanical design process,* 1997).

7.4 The Final Design

The selected conceptual solutions forming the foundation of the final design are highlighted in yellow in the Decision Matrix of Table 7.3.

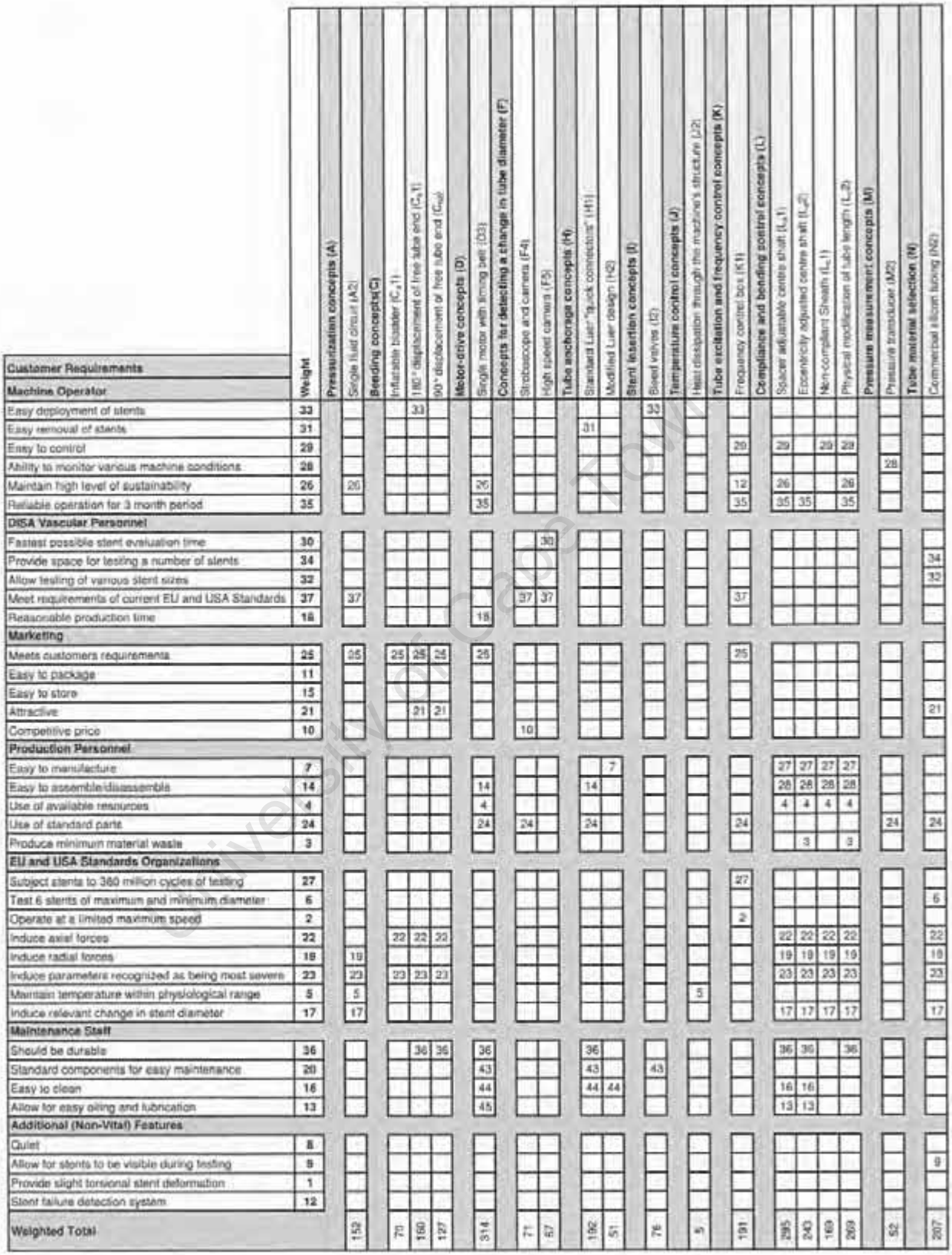

Customer Requirements	Weight	Pressurization concepts (A)		Bleeding concepts(C)			Motor-drive concepts (D)	Concepts for detecting a change in tube diameter (F)		Tube anchorage concepts (H)		Stent insertion concepts (I)	Temperature control concepts (J)	Tube excitation and frequency control concepts (K)	Compliance and bending control concepts (L)				Pressure measurement concepts (M)	Tube material selection (N)	
Machine Operator		Single fluid circuit (A2)		Inflatable bladder (C_{11})	180° displacement of free tube end (C_{12})	90° displacement of free tube end (C_{13})	Single motor with timing belt (D3)	Stroboscope and camera (F4)	High speed camera (F5)	Standard Luer-Tapack connectors* (H1)	Modified Luer design (H2)	Bleed valves (I2)	Heat dissipation through the machine's structure (J2)	Frequency control box (K1)	Spacer adjustable centre shaft (L_A1)	Eccentricity adjusted centre shaft (L_A2)	Non-compliant Sheath (L_N1)	Physical modification of tube length (L_L2)	Pressure transducer (M2)	Commercial silicon tubing (N2)	
Easy deployment of stents	33				33							33									
Easy removal of stents	31									31											
Easy to control	29													29	29		29	29			
Ability to monitor various machine conditions	28																		28		
Maintain high level of sustainability	26	26					26							12	26			26			
Reliable operation for 3 month period	35						35							35	35	35		35			
DISA Vascular Personnel																					
Fastest possible stent evaluation time	30								30												
Provide space for testing a number of stents	34																			34	
Allow testing of various stent sizes	32																			32	
Meet requirements of current EU and USA Standards	37	37						37	37					37							
Reasonable production time	18						18														
Marketing																					
Meets customers requirements	25	25		25	25	25	25							25							
Easy to package	11																				
Easy to store	15																				
Attractive	21				21	21														21	
Competitive price	10							10													
Production Personnel																					
Easy to manufacture	7										7				27	27	27	27			
Easy to assemble/disassemble	14						14			14					28	28	28	28			
Use of available resources	4						4								4	4	4	4			
Use of standard parts	24						24	24		24				24					24	24	
Produce minimum material waste	3															3		3			
EU and USA Standards Organizations																					
Subject stents to 360 million cycles of testing	27													27							
Test 6 stents of maximum and minimum diameter	6																			6	
Operate at a limited maximum speed	2													2							
Induce axial forces	22			22	22	22									22	22	22	22		22	
Induce radial forces	19	19													19	19	19	19		19	
Induce parameters recognized as being most severe	23	23		23	23	23									23	23	23	23		23	
Maintain temperature within physiological range	5	5											5								
Induce relevant change in stent diameter	17	17													17	17	17	17		17	
Maintenance Staff																					
Should be durable	36				36	36	36			36					36	36		36			
Standard components for easy maintenance	43						43			43		43									
Easy to clean	16						44			44	44				16	16					
Allow for easy oiling and lubrication	13						45								13	13					
Additional (Non-Vital) Features																					
Quiet	8																			8	
Allow for stents to be visible during testing	9																			9	
Provide slight torsional stent deformation	1																				
Stent failure detection system	12																				
Weighted Total		152		70	160	127	314	71	67	192	51	76	5	191	295	243	169	269	52	207	

Table 7.3 Decision Matrix for the Fatigue Tester Project

Chapter Eight

The Design Process — Final Machine Design and Manufacture

8.1 Design of the Fatigue Tester

Final machine design was based on the conceptual solutions presented in Chapter 7 and is illustrated in the assembly drawing of Figure 8.1.

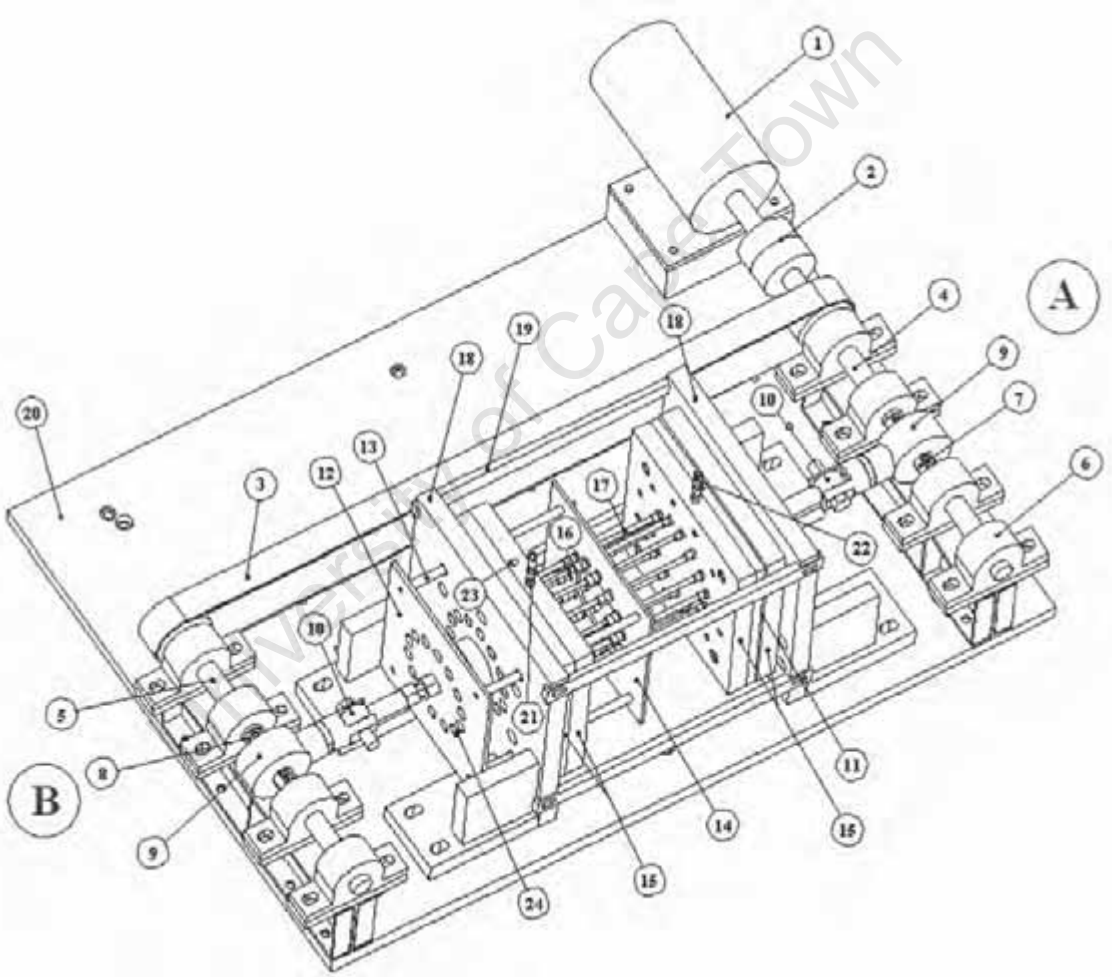

Figure 8.1 Final design of the fatigue tester

Sections 8.1.1 to 8.1.9 below, briefly discuss the various components of the final design using the numbered referencing of Figure 8.1, and aim to establish a relationship between these components and the findings produced through concept evaluation (Chapter 7). All descriptions below make references to relevant part numbers illustrated in Figure 8.1.

8.1.1 Motor Drive

A 1.5kW synchronous motor (1) was used to drive the fatigue tester and received its driving frequency from the controller box illustrated and discussed in Chapter 6 (6.3.11.1). Torque was transferred to the timing belt pulley by means of a standard 25mm **I.D.** (inner diameter) dog clutch (2).

8.1.2 Synchronous Torque Transfer

Main drive shafts *4* and *5* were synchronously driven by an 8M 30mm wide (2400mm pitch length) *Fenner* timing belt *(3)* connected to two 44-8M-30 *Fenner* pulleys. These pulleys made use of standard taper lock and keyway fittings, and transferred torque from the motor to the two 25mm drive shafts *(4* and *5)* very reliably. Main drive shafts were supported by four 25mm pillow blocks (6) to allow for the insertion of a spacer adjustable centre shaft (concept **LI).** A guard would be built to cover the timing belt and reduce the risk of accidental injury.

8.1.3 Stroke Generation

The design of Figure 8.1 induced two variable strokes at each end by means of two spacer adjustable centre shafts (7 and *8).* The shafts were supported by the main drive shafts as illustrated in Figure 6.30 of Chapter 6, and their offset was controlled by inserting spacers of various thicknesses between their mounting surfaces. Offset shaft 7 was responsible for producing the stroke driving fluid pressurization, while shaft 8 induced stroke for tube bending. Both shafts 7 and *8* transferred rotational stroke into pure linear stroke by means of a UCECH 205 (model number) hanger block *(9)* and **PHS** 18 EC rod end *(10)* configuration.

8.1.4 Fluid Pressurization

Two fluid cavities (one at each end) were formed by an arrangement of aluminium plates *(15)* and connected via a radial array of silicon *(16)* and polyethylene tubes *(17).* The fluid cavity was pressurized by a 40mm piston and gasket *(11)* arrangement receiving cyclic strokes from the configuration mentioned in section 8.1.3. The exact dimensions of the

piston and internal gasket chamber are presented in the detail drawings of Appendix F, but Figure 8.2 below provides a basic illustration of its functionality. Calculations leading to the design of this particular arrangement are presented in Appendix E-1, and Figure 8.2 illustrates some of the important parameters used in these calculations. The effect of gasket motion on pressurization was evaluated for both best and worst case scenarios, with the greatest pressures being induced during conical gasket following of the piston and lowest pressures occurring due to water back-pressure. The effect of water back-pressure was approximated by taking only piston motion into account (gasket not contributing to pressure increase at all) and therefore volume change was calculated by multiplying the piston surface area by the stroke.

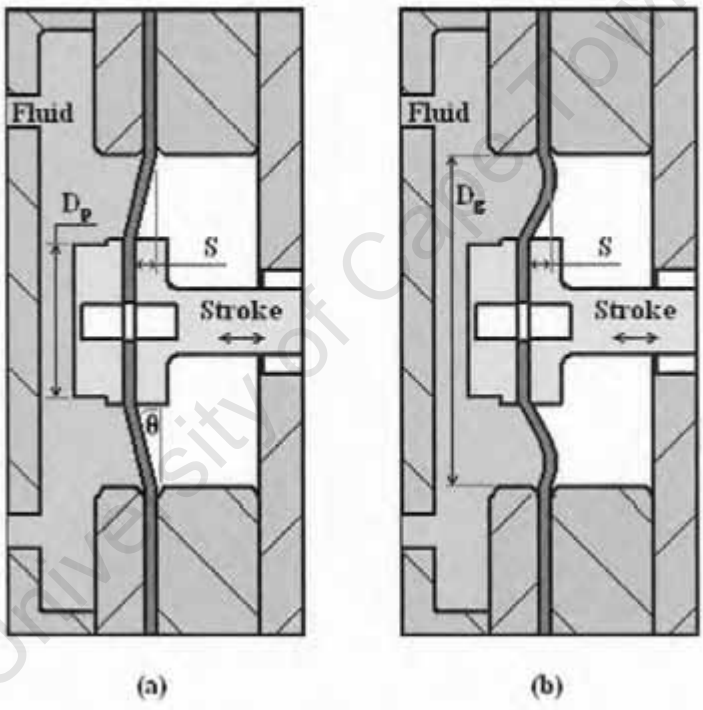

Figure 8.2 Basic functioning of piston and gasket induced pressurization (a) conical gasket motion (b) gasket motion due to water back-pressure.

Figure 8.3 summarizes the theoretical pressure gradients attainable from such a design during static conditions and illustrates the effects of increased stroke and gas content on its performance. Figure 8.4 illustrates the theoretical change in silicon inner diameter achievable during low frequencies. Information obtained during analysis of the final machine at high frequencies could be used to make necessary adjustments in achieving appropriate tube expansion.

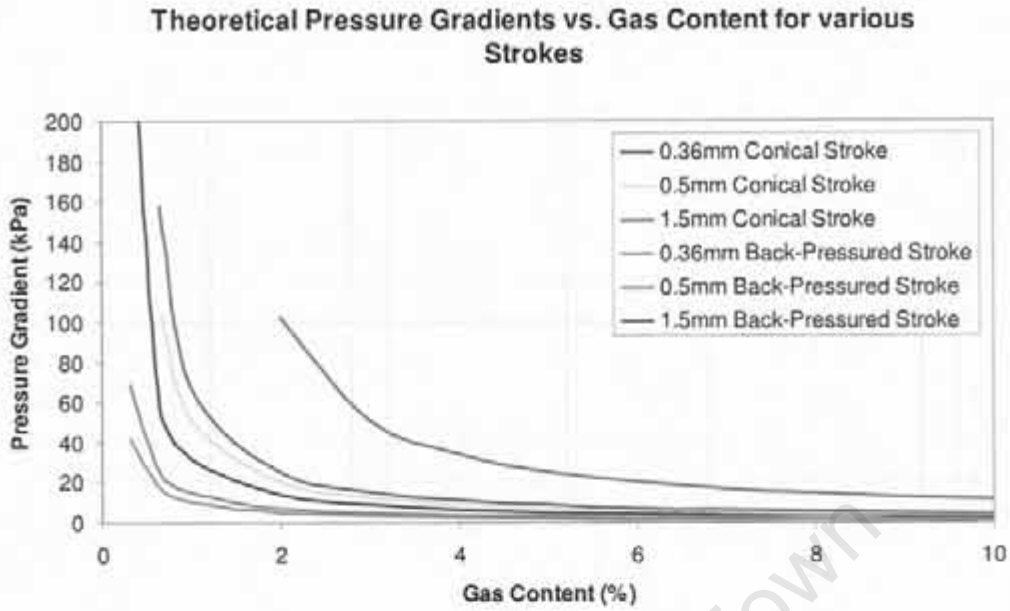

Figure 8.3 Theoretical pressure gradients attainable by the final design at low frequencies

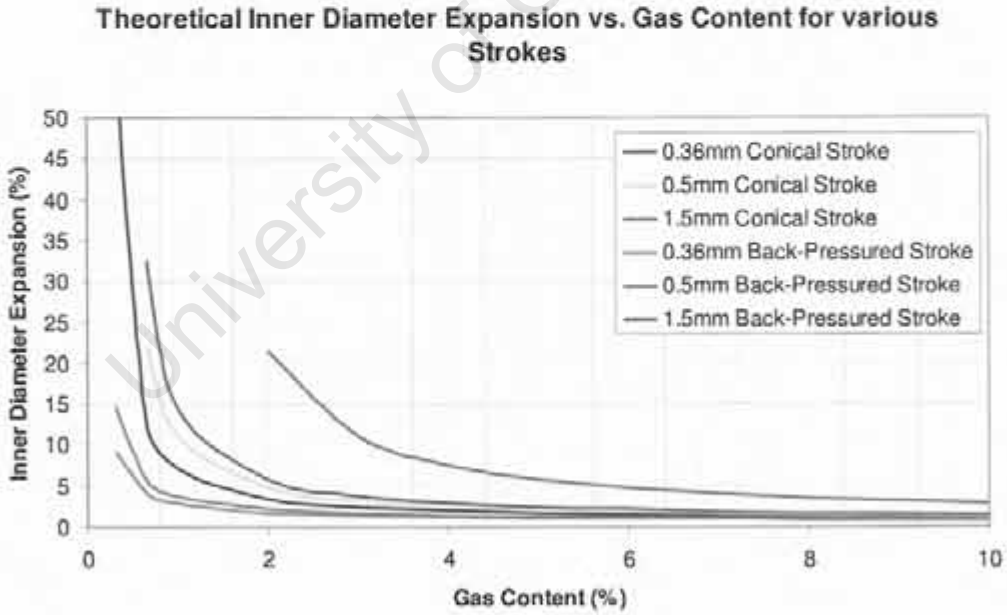

Figure 8.4 theoretical diameter expansions attainable by the final design at low frequencies

8.1.5 Tube Bending

Offset shaft *8* and its corresponding stroke-producing configuration are responsible for driving the unit causing tube bending. This unit consisted of an inner (12) and outer *(14)* plate connected via four guide rods *(13),* and caused both silicon *(16)* and polyethylene (17) tubes to bend by displacing them back and forth by 180°. With the stroke produced by shaft 8 being transferred to the outer plate, the guide rods ensured that the inner plate moved at the same frequency and amplitude as that of its driving stroke. Radial arrays of pneumatic "quick connectors" were attached to the aluminium plate configurations at each end (Figure 8.5), and these provided the opening through which fluid flowed (from cavity B, through tubes *16* and 17, to cavity A). Bulkhead connectors were fastened to plate *14* in the same radial configuration, and provided the "middle" attachment points for tubes *16* and *17.*

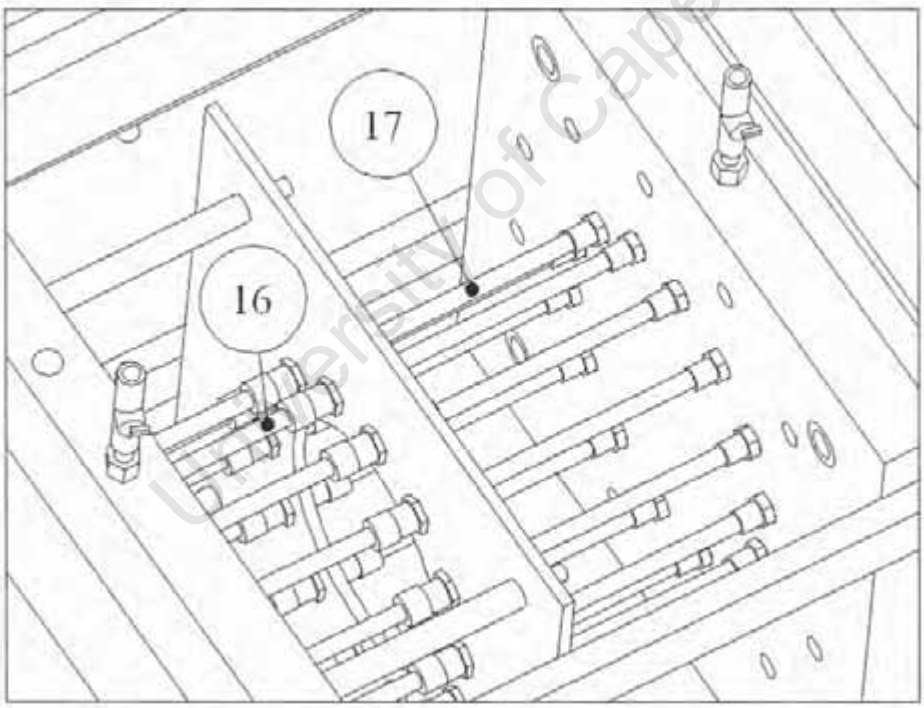

Figure 8.5 Illustration of internal bend-plate with tubes and pneumatic connectors

A 2 mm motion of the inner plate induced maximal curvature variations in the silicon tubes of approximately 0.47 cm^{-1} by bending them from a 4 mm amplitude sinusoidal shape to a shape of 6.9 mm amplitude. Figure 8.6 illustrates these initial and final sinusoidal vessel shapes.

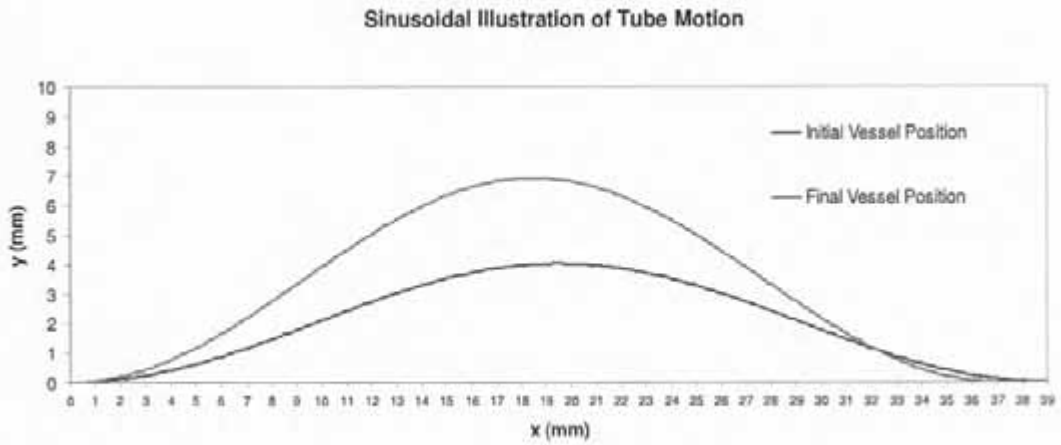

Figure 8.6 Sinusoidal illustration of tube motion for a 2 mm stroke

Due to the required initial vessel bend and geometries of both "quick connectors" and bulkhead attachment points, silicon tubes had to be cut to 52.8 mm and connected to the pneumatic fittings as illustrated in Figure 8.7. Bulkhead and "quick connector fittings" needed to be set 39 mm away from each other at maximal stroke and 37 mm away during minimum stroke (corresponding to a total stroke of 2 mm).

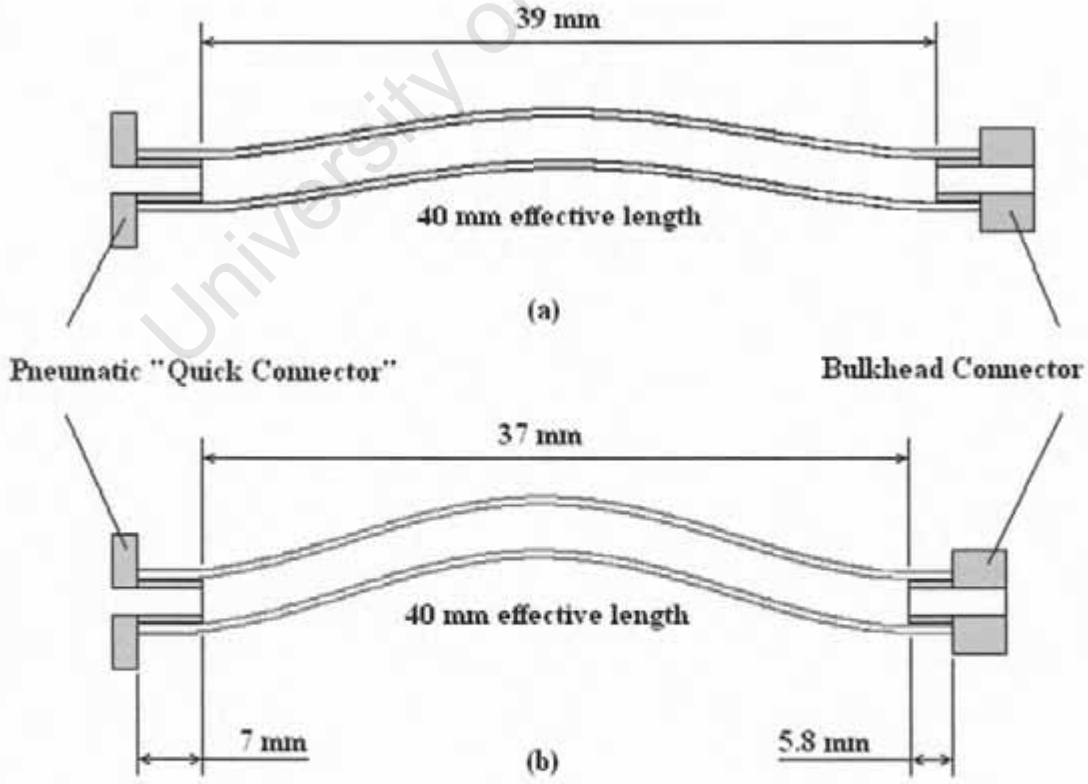

Figure 8.7 Silicon tube attachment considerations to induce 0.5 cm^{-1} maximal curvature variation (a) initial vessel position; and (b) final vessel position

Non-compliant polyethylene tubes were inserted purely to complete the fluid circuit, and their length was not of crucial importance. Design calculations leading to the selection of these geometries and configurations are illustrated in Appendix E-2.

8.1.6 Fluid Chamber Support and Stroke Guide

The fluid chambers contained within aluminium plates 15 were supported by means of two machined angle-block constructs (18). These angle blocks were bolted firmly to base plate 20 and braced together by means of four cross-beams (19). Support of this magnitude was considered important since high frequency machine oscillation would have led to vibrations that could misalign shaft sections if not secured properly.

Another important requirement of the angle-blocks was their ability to guide the 16 mm shafts (connected to the piston on side A and outer bend plate on side **B)** receiving cyclic stroke thrust from the unit mentioned in section 8.1.3. Vesconite bushes were positioned in the centre of each angle-block to facilitate the guiding of these shafts.

8.1.7 Fluid Cavity Inlets, Outlets and Bleed Valves

Saline fluid was fed into the system through a ball-valve at 21 and, after filling the fluid cavity on side B, flowed through the connecting tubes and exited through another ball-valve at 22. Unwanted gas present in the system was bled via fourteen pneumatic plugs (24). These plugs also served as the entrance through which stents were deployed into the silicon vessels (16).

8.1.8 Pressure Monitoring

The WIKA S-10 pressure transducer responsible for detecting pressure changes was connected to a 1/8 BSP fitting at 23. The transducer was connected to a computer as discussed in section 7.2.5, from where pressure readings were displayed in an Excel spreadsheet.

8.1.9 Base Plate Mounting

The main base plate *(20)* was supported by five 100 x 100 x 30 mm rubber blocks and securely bolted to a steel cabinet. The cabinet was used to house the frequency controller box and any extra machine components.

8.2 Manufacture of the Final Machine

T.K. Manufacturing (Port Elizabeth, South Africa) was commissioned with the manufacture of the final machine and all detail and assembly drawings referred to during this period are presented in Appendix F. Other machine components (saline fluid and current to voltage converter) were produced locally and are presented in the following two sections.

8.2.1 Creation of Saline Fluid (Phosphate Buffer Solution)

Phosphate Buffer Solution (PBS) was created and used to simulate the physiological properties of blood. Saline has an electrolyte balance very similar to that of blood and, with its pH set to 7.4, serves as an excellent medium for simulation.

A 500m1 Phosphate Buffer Solution having a pH of 7.4 at 37°C can be prepared as follows:

Required Equipment/Ingredients:

1) 1L glass measuring beaker
2) Pipette
3) Scale (Calibrated)
4) Potassium Chloride (0.1g)
5) Potassium Dihydrogenphosphate (0.1g)
6) Sodium Chloride (4.0g)
7) Sodium Hydrogenphosphate (0.58g)
8) 1M Sodium Hydroxide
9) 1M Hydrochloric acid
10) pH meter (Calibrated)
11) 1L glass storage container
12) Water bath (set to 37°C)

Preparatory Steps:

1) To ensure accuracy of results, thoroughly check that all glassware and equipment is clean and that all necessary calibrations are done beforehand
2) Charge 450m1 distilled water into a beaker and stir at room temperature
3) To the stirring water add Potassium Chloride (0.1g); Potassium Dihydrogenphosphate (0.1g); Sodium Chloride (4.0g); Sodium Hydrogenphosphate (0.58g)
4) Cover and Stir the mixture until all the solids have dissolved
5) Place the solution in the water bath and allow equilibrating
6) Once 37°C has been reached, adjust pH to7.4 using Sodium Hydroxide or Hydrochloric acid
7) Bring the solution up to the required 500mL by adding distilled water (in the order of approximately 50mL — depending on pH balancing process)

5 Litres of PBS was mixed up in this way and would be used within the fatigue tester.

8.2.2 Current to Voltage Converter

The simple conversion circuit discussed and illustrated in section 7.2.5 was built and housed in a plastic circuit container box, as illustrated in Figure 8.8.

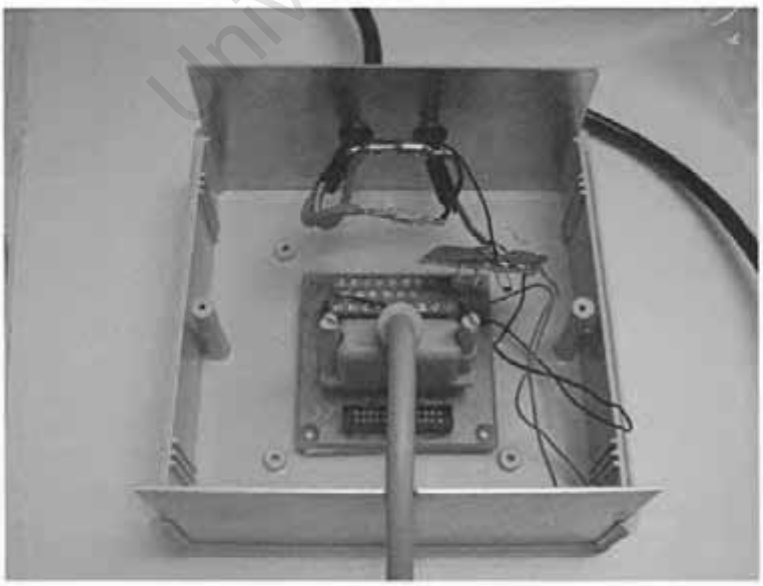

Figure 8.8 The final current to voltage conversion circuit

8.3 The Final Machine

The final machine (connected to various measurement components) is illustrated in Figures 8.9.

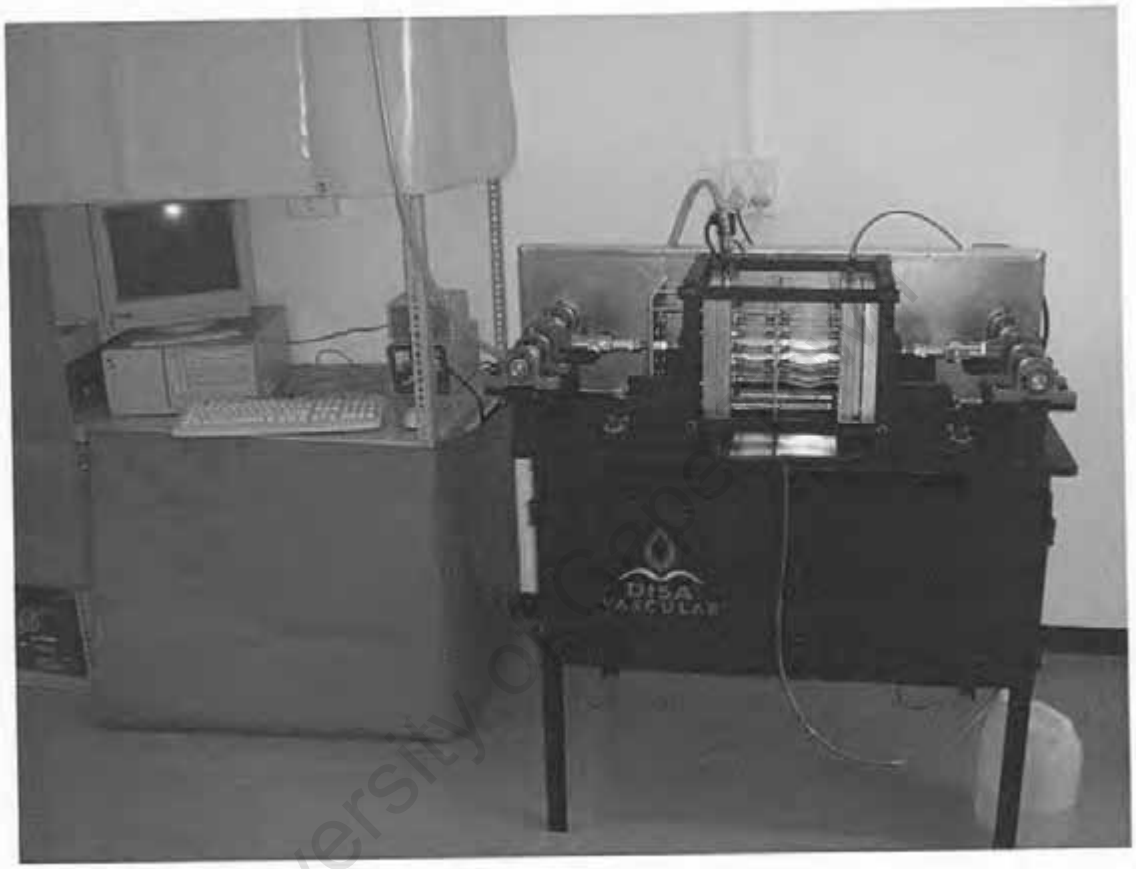

Figure 8.9 The final accelerated fatigue testing machine

Chapter Nine

Testing and Results

Testing of the fatigue tester was performed to gauge how well the machine was meeting the requirements outlined in Chapter 5 and whether the relevant vessel motions and expansion documented in Chapter 2 were being met. The following criteria were considered important in the evaluation of the fatigue testing machine.

- Stent deployment
- The variation in average pressure gradients from 0 Hz to 60 Hz for various stroke amplitudes
- Vessel expansion achievable at 50, 55 and 60 Hz
- Mock artery motion at 50, 55 and 60 Hz
- The machine's ability to perform reliable testing of a sample stent over a 3 day period
- Stent removal

The following sections document the testing performed in evaluating the aforementioned criteria. All tests were conducted with a 10 cell, 24 mm *Chromoflex* stent deployed in one of the silicon tubes (described in section 9.1).

9.1 Stent Deployment

9.1.1 Testing

A 10 cell, 24 mm *Chromoflex* stent was deployed in one of the 14 silicon tubes by means of a 3.5 mm stent delivery catheter. This particular balloon catheter required a pressure of 7 bars to deploy the stent to a diameter of 3.37 mm inside the 3.1 mm silicon tube (approximately 10% over deployed). The stenting system was inserted into the centre of the silicon vessel through the appropriate bleed valve and deployed such that the middle of the stent coincided with the point of maximum vessel curvature. Initial rotation of the main drive shaft ensured that the silicon tube was in a state of minimum vessel curvature

(39 mm clearance) to facilitate easy deployment. The stent insertion procedure is illustrated in Figure 9.1.

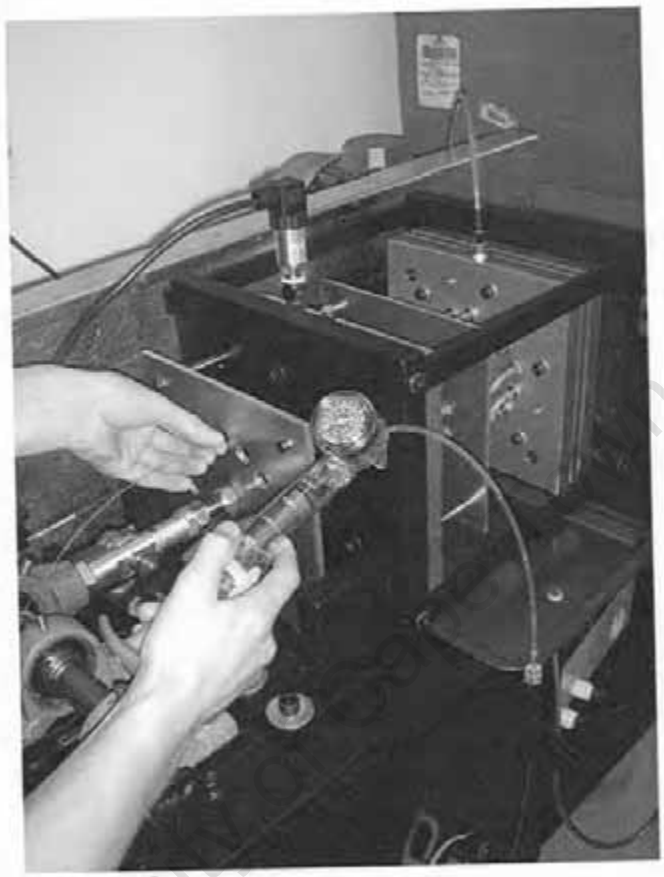

Figure 9.1 Stent insertion

With the stent guided by the catheter and in the appropriate vessel position, inflation of the balloon was achieved by a hand-held inflation device. Pressure was increased to 7 bar (resulting in 3.37 mm stent expansion) and maintained for approximately 1 minute to ensure adequate deployment pressure. With the stent firmly deployed, the balloon was deflated and the catheter removed.

In order to test adequate deployment of the stent within the tube, the machine was filled with fluid (bleeding as much air out as possible) and run at frequencies up to 60 Hz.

9.1.2 Results

The stent adhered to the inner vessel wall very well and, even at frequencies of 60 Hz did not move in the tube. Movement of this type could be caused by excessive post-

deployment recoil or tube expansion. With no motion present, the extent of stent expansion was calculated based on the results of high frequency pressure monitoring (section 9.2.2) and vessel expansion (section 9.3.2).

9.2 Average Pressure Gradients at various Frequencies and Stroke Amplitudes

9.2.1 Testing

The machine's ability to induce appropriate pressure gradients (sufficient to induce 5% vessel expansion) was tested for various strokes and frequencies. Starting with a 1.5 mm piston stroke, pressure readings transmitted by the pressure transducer at frequencies from 5 to 60 Hz were interpreted using WaveView for Windows © 2002 (Eagle Technology) and plotted in Excel as a function of time. Similar results were obtained for 0.5 and 0.36 mm strokes.

9.2.2 Results

Figure 9.2 illustrates the cyclic pressure gradients (difference between recorded maximum and minimum pressures) achievable as a function of machine frequency and offset stroke.

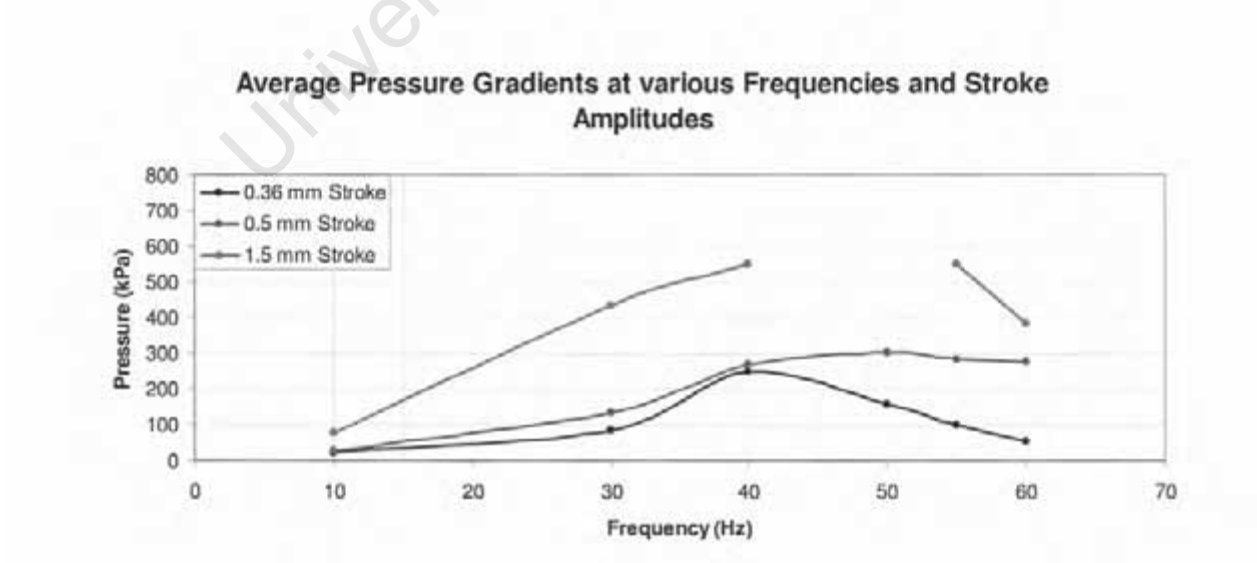

Figure 9.2 Average pressure gradients at various frequencies and stroke amplitudes

Pressure gradients displayed a significant maximum value for 0.36, 0.5 and 1.5 mm strokes at various frequencies, with pressure gradients seeming to decrease in a linear manner after these maximum values. Pressure gradients reached a maximum of 250 kPa at 40 Hz with the machine stroke set to 0.36 mm. A 0.5 mm stroke reached a maximum of 300 kPa at 50 Hz. With the machine set to a stroke of 1.5 mm, pressure gradients became so high that the pressure transducer reached its maximum output voltage between 40 and 50 Hz, making accurate reading of higher pressures impossible.

9.3 Vessel Expansion Achievable at 50, 55 and 60 Hz

9.3.1 Testing

Vessels were subjected to pressurization at 50, 55 and 60 Hz with a 0.36 mm stroke and monitored using a *MotionScope® PCI high speed digital imaging system*. Image sampling was conducted at 1000 frames per second and interpreted using *MScope Player* 2.21 image capture software. The test setup is illustrated in Figure 9.3 below.

Figure 9.3 Vessel expansion and motion test setup

Images acquired during the testing process (50, 55 and 60 Hz) were used to measure vessel outer diameter at the point of maximum vessel curvature (middle of the stent). Outer diameter was measured during periods of maximum and minimum vessel curvature for all three test frequencies and the results used to calculate outer diameter changes at these frequencies. Since periods of maximum and minimum curvature correspond to maximum and minimum pressures respectively, the images obtained would be used for both motion and expansion evaluation. *MScope Player* 2.21 was used to perform the physical measurements with each image calibrated before measurement using a steel ruler placed just behind the tubes during testing.

9.3.2 Results

Images obtained during the aforementioned test procedure are illustrated in Figures 9.4 to 9.6 below.

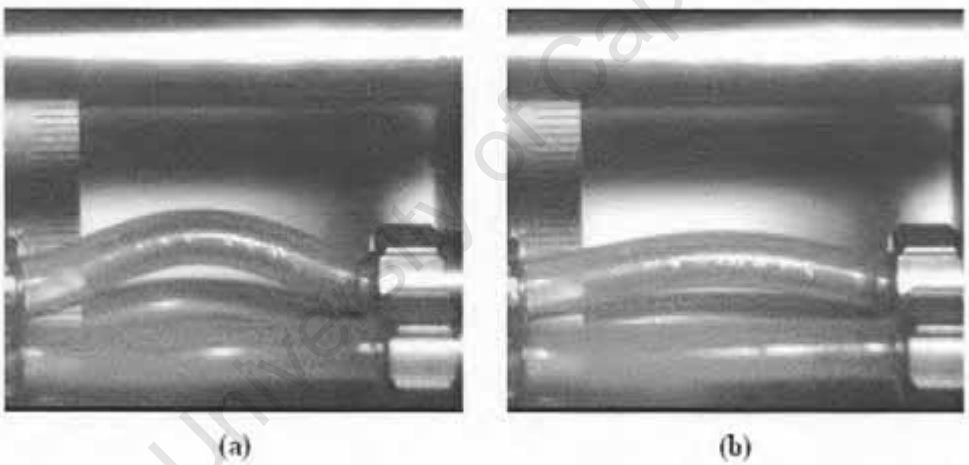

Figure 9.4 Images obtained at 50 Hz during (a) maximum curvature (b) minimum curvature

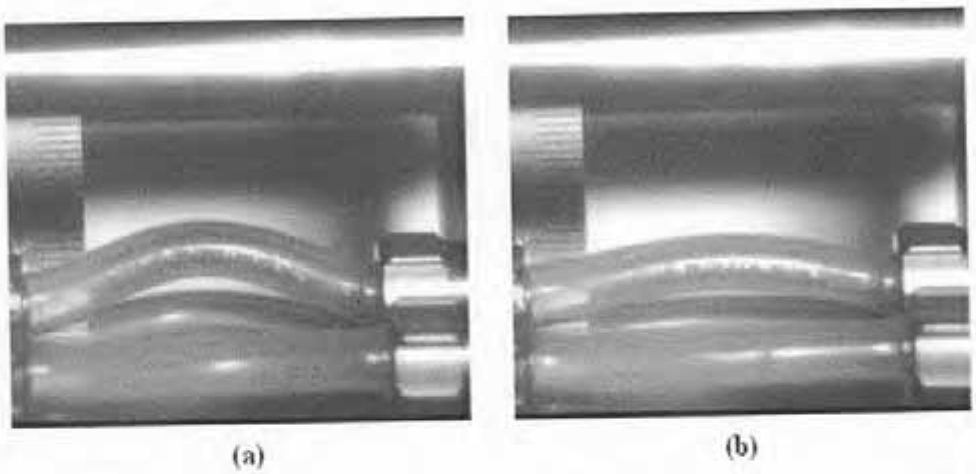

Figure 9.5 Images obtained at 55 Hz during (a) maximum curvature (b) minimum curvature

Figure 9.6 Images obtained at 60 Hz during (a) maximum curvature (b) minimum curvature

During the test runs, internal system pressure was monitored and found to be identical to the values illustrated in Figure 9.2. Outer diameter measurements recorded during image evaluation are summarized in Table 9.1.

Frequency (Hz)	50	55	60
Maximum Bend Outer Diameter (mm)	6.15	6.07	6.19
Minimum Bend Outer Diameter (mm)	6.07	5.93	6.06
Outer Diameter Change (%)	1.20	2.41	2.09

Table 9.1 Measured vessel outer diameter changes at 50, 55 and 60 Hz

With initial vessel geometry (prior to stent insertion) measuring approximately 3.1 mm inner diameter and 6.1 mm outer diameter, vessel wall area was calculated using Equation 9.1 below and measured as 21.68 mm^2.

$$A_{cross\ section} = \frac{\pi}{4}(d^2_{o,unpressurized} - d^2_{i,unpressurized}) \quad (9.1)$$

Since vessel outer diameter was measured across the area of stent deployment, a new wall area would need to be calculated using a 3.4 mm inner diameter (deployment size) and 6.1 mm outer diameter (assuming insignificant outer diameter change due to deployment). The new stent wall cross-sectional area was measured as 20.15 mm^2.

Using this newly determined cross-sectional wall area, the results of Table 9.1 were converted to theoretical inner diameter changes using the methods presented in section 7.2.1. These results are presented in Table 9.2 below.

Frequency (Hz)	50	55	60
Maximum Bend Inner Diameter (mm)	3.48	3.35	3.56
Minimum Bend Inner Diameter (mm)	3.35	3.08	3.33
Inner Diameter Change (%)	3.90	8.68	6.78

Table 9.2 Theoretical vessel inner diameter changes at 50, 55 and 60 Hz

9.4 Mock Artery Motion at 50, 55 and 60 Hz

9.4.1 Testing

Mock artery motion was analysed using the images produced from vessel expansion testing (Figures 9.4 to 9.6) by measuring amplitude and attachment distance changes (from minimum to maximum vessel curvature conditions) and relating these values to the design calculations presented in Appendix E-2 (described in section 8.1.5). The vessels were subjected to a 2 mm stoke amplitude based on the findings presented in Chapter 8 to give rise to curvature variations of approximately 0.47 cm^{-1}. The purpose of this testing procedure was to gauge how closely the physical model was simulating its theoretical counterpart.

9.4.2 Results

Measured and calculated values for attachment distance, amplitude and curvature are summarized in Table 9.3 below for each condition. These results were used to calculate average curvature variation which would need to be compared to the literature findings discussed in section 2.3.3.2.

Frequency (Hz)	**50**	**55**	**60**
Maximum Tube Attachment Distance (mm)	39.30	39.82	39.68
Minimum Amplitude (mm)	3.06	3.19	2.95
Minimum Curvature (cm^{-1})	0.39	0.40	0.37
Minimum Tube Attachment Distance (mm)	36.99	37.85	37.31
Maximum Amplitude (mm)	5.44	5.63	5.85
Maximum Curvature (cm^{-1})	0.78	0.77	0.83
Stroke (mm)	2.31	1.97	2.38
Amplitude Variation (mm)	2.37	2.45	2.90
Maximum Curvature Variation (cm^{-1})	0.39	0.38	0.46

Table 9.3 Measured mock artery motion parameters at 50, 55 and 60 Hz

Maximum test vessel curvature variation measured 0.39 cm^{-1} at 50 Hz for a measured bending stroke of 2.31 mm. 55 Hz produced a curvature variation measurement of 0.38 cm^{-1} at 1.97 mm stroke, with 60 Hz giving rise to 0.46 cm^{-1} curvature variation for a measured stroke of 2.38 mm.

9.5 Stent Testing over a Three Day Period

9.5.1 Testing

After conducting the test procedures discussed in the previous sections, the machine was prepared for a 3 day trial run. Testing of this nature was considered important for the following two reasons:

- Machine drive shafts and bearings were identified as the primary focal point of machine failure with operational temperatures and test duration directly affecting their optimal performance. A 3 day simulation period would give an indication as

to the machine's ability to survive highly repetitive motions at maximal operating temperatures.

- A 3 day simulation period, if conducted at 50 Hz, would subject a deployed stent to approximately 13 million cycles of loading. Testing of this kind, although not meeting the required 380 million cycle requirement, would give some indication as to the stent's ability to withstand these test loads.

Prior to initial stent insertion, the 10 cell, 24 mm *Chromoflex* stent was inspected under a microscope and photographed to document its initial surface characteristics. These photographs would serve as a comparative tool after testing, with the following structural sites being focused on:

- Centre S-Link
- Struts at both ends of the stent
- Hairpins at both ends of the stent

The machine was set to a frequency of 50 Hz and allowed to run for a full 3 day period. It was inspected twice a day for the test duration and monitored for signs of any abnormal operation. At the end of the 3 day testing period, the stent was removed from the silicon mock artery (section 9.6) and analysed again to determine any change in structural integrity.

9.5.2 Results

Initial stent microscopy of the 5 sites referred to in the previous section revealed satisfactory results (Figure 9.7 on the following page). The stent surfaces were of a very good quality, with no major surface defects present and only slight "crimp" scratches identified in a few places. The stent was of an acceptable weight and surface geometry and met all of Di sa Vascular's quality standards.

Three day simulation (13 million cycles) was very successful and the machine performed well, subjecting the deployed stent to the equivalent of 4 months of average coronary artery load conditions. No noticeable differences in operating conditions were displayed during the test period and the stent remained firmly deployed within the silicon vessel for

the entire period. The bearings appeared to reach maximum operation temperatures within the first hour of testing and thereafter remained reasonably constant. Over lubrication of the bearings appeared to have an increased effect on their operating temperatures with those bearings running with less grease operating at slightly cooler temperatures. Unsurprisingly, bearing temperatures were higher the closer the bearings were to the main drive pulley, with these bearings transferring greater torques than those guiding distal shaft segments.

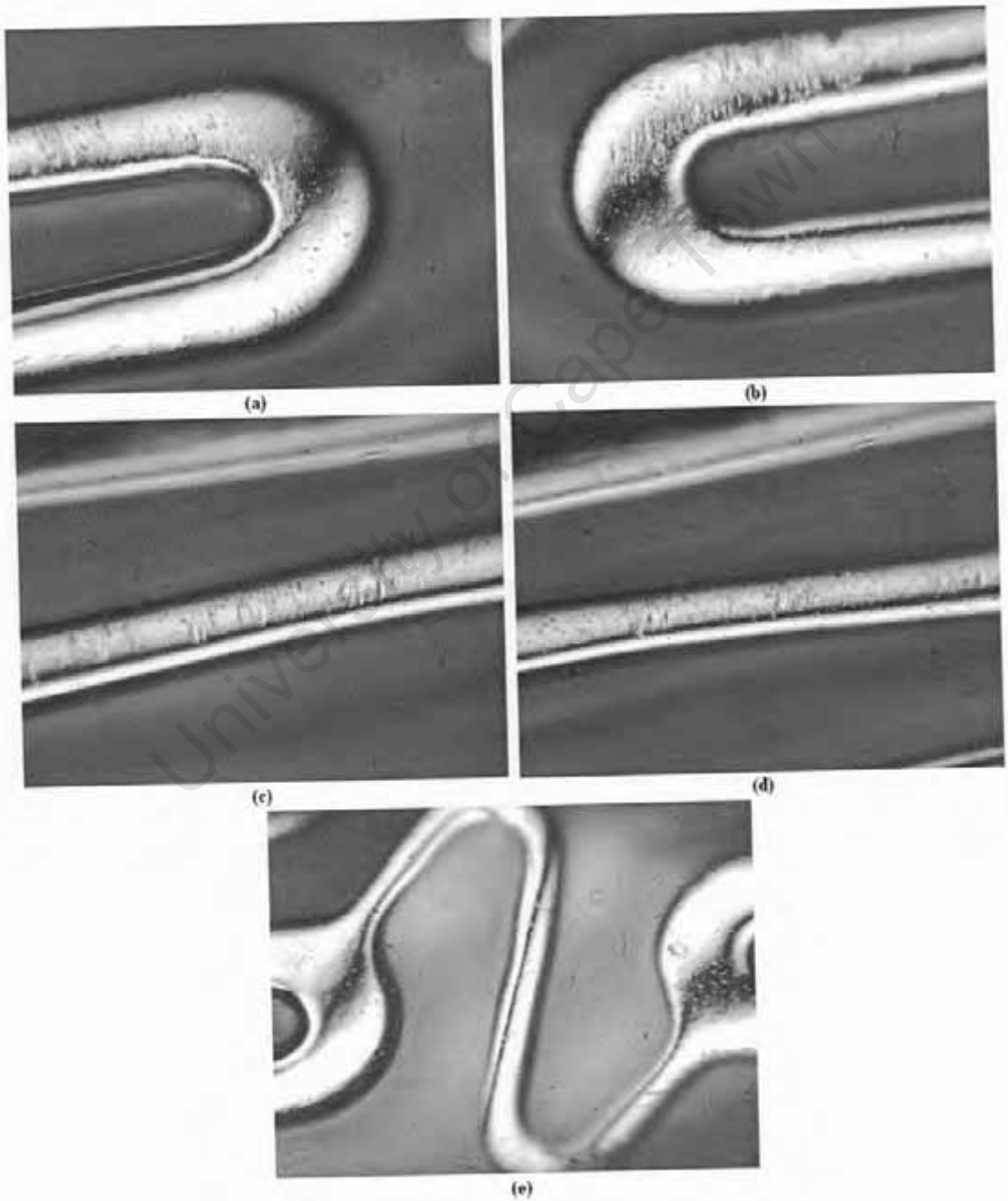

Figure 9.7 Initial stent surface microscopy images for (a) left hairpin (b) right hairpin (c) left strut (d) right strut (e) centre S-Link

Initial microscopy of the fatigued stent (after 3 days) produced images with trace amounts of silicon scattered all over the stent surface. The stent was placed in a beaker containing commercial dish-washing liquid and agitated at high frequencies for approximately 15 minutes in an attempt to remove these silicon particles. Agitation proved relatively unsuccessful and final microscopy of the stent surface produced images that would not make final surface evaluation very easy. The final microscopy images obtained are illustrated in Figure 9.8 below.

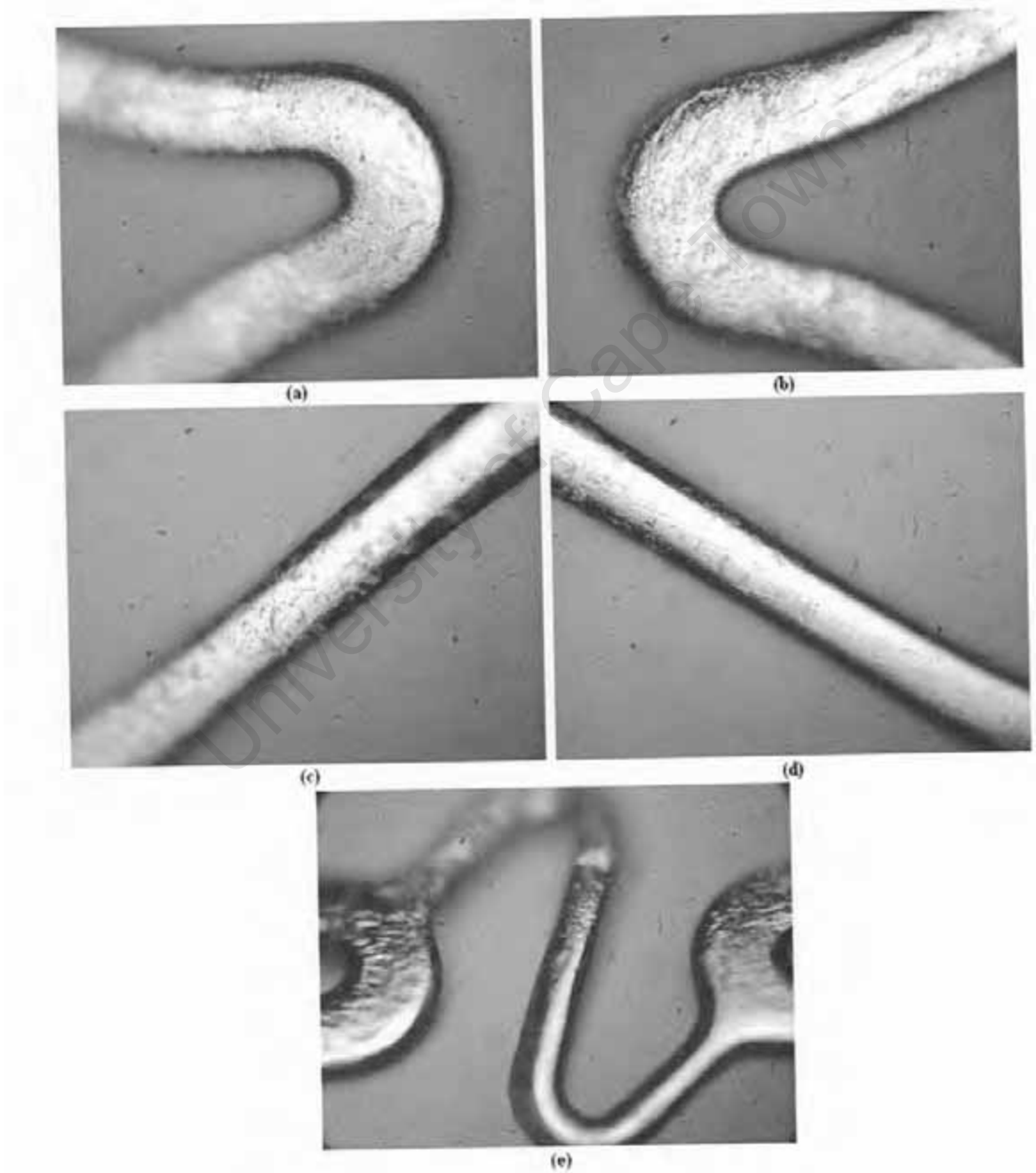

Figure 9.8 Final stent surface microscopy images for (a) left hairpin (b) right hairpin (c) left strut (d) right strut (e) centre S-Link

The images illustrated in Figure 9.8 make it difficult to distinguish silicon deposits from damage as a result of plastic deformation. From the images it is however clear that there were no obvious signs of cracking, breaking or splitting. Figure 9.8 appeared to display signs of plastic deformation on the stent surface although, as previously mentioned, this could not be confirmed due to what appears to be a thin film of silicon residue.

9.6 Stent Removal

9.6.1 Testing

Stent removal is obviously vital in order to evaluate fatigue results as described in the previous section. With appropriate testing completed, vessel removal would be achieved by cutting the tube at each end, taking care not to induce unnecessary extra loading on the stent while doing so. Removal of the vessel by loosening the luer connectors was not considered an appropriate solution as this would cause twisting of the tube, placing excessively large loads on the stent.

The stent was freed from the silicon tube by carefully making a longitudinal incision with a scalpel down the vessel length. Care was taken so as not to cut the stent during this process. With the incision made, the silicon vessel was peeled open with pliers and the stent removed.

9.6.2 Results

Stent removal was a relatively straightforward process, but did leave the stent with microscopic silicon residue on its surface (as described and illustrated in section 9.5.2). Removal did not damage the stent, and any scratches that might have been caused on the stent surface as a result of vessel incision were positioned "face down" when evaluating it under the microscope.

Chapter Ten

Discussion, Conclusions and Recommendations

This chapter will discuss the results presented in Chapter 9 and compare them to the requirements outlined in Chapters 2 and 5. Conclusions will also be drawn regarding the machine's abilities and / or limitations, with suggested recommendations for future machine improvements outlined in section 10.3.

10.1 Discussion

10.1.1 Stent Deployment

Stent insertion was found to be a time consuming exercise, with catheter guidance causing the greatest problems. The pneumatic connector openings are very small and a steady hand is required to feed the catheter guide wire through the bleed valves and into the mock arteries. Once in place however, deployment of the stents is very straightforward and the transparent silicon tubes allow visualisation of the entire deployment process.

10.1.2 Average Pressure Gradients at various Frequencies and Stroke Amplitudes

Pressure gradients measured at low frequencies agreed well with the theoretical values predicted in section 8.1.4, with measured data suggesting a total gas content (after bleeding) of approximately 1 %. The data also suggests that the shape of gasket motion lies somewhere between ***conical*** (best case) and ***back pressured*** (worst case) profiles.

With increased frequency, generated pressure variations displayed a "bell-shaped" profile for all three driving strokes. The stroke of 1.5 mm unsurprisingly produced the greatest pressure variations, with a 0.36 mm stroke producing the smallest profile. The shape of this profile seems to suggest that tube compliance actually begins decreasing at frequencies above 40 Hz, with the effects of increased compliance clearly visible in the 10 to 40 Hz region. Since a less compliant tube opposes expansion far more than a tube of high compliance, an increase in pressure can be directly attributed to a decrease in compliance (with the stroke remaining constant). This decreased compliance seems to

agree with the findings of Conti *et al.* (2002) and Ramesh *et al.* (2005), who measured significantly lower vessel compliance at increased frequencies. Data collected by Conti *et al.* (2002) and Ramesh *et al.* (2005) was limited however to the 72 bpm (1.2 Hz) to 1500 bmp (25 Hz) range and, as such, was not suitable to validate higher frequency findings.

With average pressure gradients at 60 Hz gradually approaching static pressure readings, it might be safe to assume that compliance considerations at even higher frequencies could be predicted using static condition compliance results. This assumption would need to be experimentally tested however and, until such time, vessel compliance should still be verified by means of an image capture technique.

10.1.3 Vessel Expansion Achievable at 50, 55 and 60 Hz

When comparing the expansion achievable by silicon tubes during static pressurization (section 7.2.1) to the results documented from high speed imaging at high frequency, one can quite clearly see a decrease in total vessel compliance with increased frequency. Static pressurization of **6.1** mm outer diameter silicon tubes required approximately 40 kPa to increase their outer diameter by 2 %. At 60 Hz the silicon tube required approximately 70 kPa to achieve a similar diameter increase. These findings further support the generally accepted decrease in vessel compliance at increased frequencies (10.1.2).

As summarized in Table 9.1, a 0.36 mm stroke produced outer diameter variations in a 6.1 mm silicon tube of 1.2, 2.4 and 2.1% at frequencies of 50, 55 and 60 Hz respectively. Outer diameters measured during periods of low pressure did not quite equal the expected 6.1 mm and this can probably be attributed to inaccuracies during the measurement process. High speed photography produced images with resolutions of 700 x 600 pixels and this was considered one of the main reasons for poor measurement results. The effects of these slightly inaccurate readings could possibly also explain the "spike" of 2.4% expansion at 55 Hz. Assuming that compliance actually decreases at these high frequencies (as proposed in section 10.1.2) one would expect expansion at 55 Hz to fall between 1.2 and 2.1%.

Predicted internal diameter expansion (illustrated in Table 9.2) yielded very promising results, with pressurization between 50 and 60 Hz producing expansion in the targeted 5%

range. Seeing as though inner diameter expansion was derived from that of measured outer diameter changes, a similar "spike" of 8.7% can be seen at 50 Hz. Theoretical estimation of internal diameter based on outer diameter was very important since high speed imaging did not produce a clear picture of the vessel's inner boundaries.

Although tubes with compliances of 5-7% per 100 mmHg are generally accepted as being suitable for simulating human arteries, this project focused on the expansion range more than the pressure required to induce it. Since this project not only required internal pressurization of the vessels but also controlled bending, vessels with compliances of 5-7% per 100 mmHg would be too flexible. Pressures required to bring about the 3.9 to 6.8% change in silicon inner diameters (Table 9.2) are thus unsurprisingly higher than 100 mmHg (13.3 kPa), with pressures ranging from 16 to 50 kPa respectively.

10.1.4 Mock Artery Motion at 50, 55 and 60 Hz

The photographic inaccuracies mentioned in section 10.1.3 along with non-planar motion tube motion, could also have given rise to slightly unreliable tube motion measurement. Despite these potential inaccuracies, results presented in 9.4.2 seem very promising. Curvature calculations based on the measurements obtained from high speed imaging varied between 0.38cm^{-1} (55 Hz) and 0.46cm^{-1} (60 Hz), coming close to the target of 0.5 cm^{-} (Gross *et al.,* 2002). If tube motion occurred even fractionally outside of the plane of imaging, these recorded values would be lower than the actual reading, possibly even reaching the 0.5 cm^{-1} mark.

The results of Table 9.3 show that minimum vessel curvatures (at stent midpoint) range from 0.37 cm^{-1} to 0.4 cm^{-1}, while maximum curvatures fall in the 0.77 cm^{-1} to 0.83 cm^{-1} range. These values fall well within the mean average curvature ranges proposed by Ding *et al.* (2002), who measured values of 0.39 ± 0.1 $cm^{-'}$ in the RCA and 0.48 ± 0.17 $cm^{-'}$ in the LAD by means of clinical biplane coronary cine-angiograms.

10.1.5 Stent Testing over a Three Day Period

Testing over the 3 day period demonstrated the machine's ability to withstand high operating temperatures and cyclic forces. Although a 3 day period only subjects the

machine to approximately 14 million cycles (380 million required), a test of this kind does give some indication of its long term capabilities.

Microscopy images of the stent surface taken before and after machine simulation produced rather inconclusive results. Microscopic silicon particles prevented thorough evaluation of the stent surface after testing, making the detection of plastic deformation and crack propagation difficult. Even after agitation in a soapy medium, silicon particles remained on the stent surface.

10.1.6 Stent Removal

The way in which the stents are removed from the silicon tubes might play a significant role in the presence of silicon particles on their surface thereafter. Cutting the tube down its length was relatively successful, but could be considered a rather forceful removal technique. An operation of this kind would prove time consuming when needing to be repeated for 14 stents and could result in the stents being damaged if considerable care is not taken.

10.2 Conclusions

Accurate simulation of physiological conditions is vitally important in the fatigue testing of coronary stents. With the incidence of heart disease in the modern world ever increasing and cardiologists turning to these devices as the preferred treatment, the importance of their long term durability is undeniable. International standards are constantly enforcing more stringent requirements on coronary stents for these very reasons and it is up to the stent manufacturers to see to it that these requirements are being met. Accelerated fatigue testing is without question one very important aspect in the improvement of the coronary stent's performance.

The work presented in this project provides a means of simulating the physiological conditions experienced in the average coronary artery at an accelerated frequency of 60 Hz. With such a machine, one is capable of analyzing a coronary stent's performance over a simulated 10 year period in approximately 3 months.

The fatigue tester described in this thesis simulates coronary artery conditions by inducing relevant curvature variations and expansions on a mock artery. With a stent requiring testing while deployed inside this mock artery, relevant arterial simulation must subject the stent to appropriate physiological loading.

Testing conducted to prove the suitability of this machine to inducing appropriate vessel motion proved successful. Curvature variations ranging from 0.38 cm^{-1} to 0.46 cm^{-1} were measured in the midpoint of the vessel during testing, with these values comparing well with the literature. Although 0.5 cm^{-1} was targeted as the main motion requirement, measurement inaccuracies could have contributed to the machine's inability to achieve this goal.

The fatigue tester produced satisfactory levels of tube expansion and thus resultant stent expansion at 50, 55 and 60 Hz, with a 3 day test run successfully subjecting a 24 mm *Chromoflex* stent to over 13 million cycles of loading. Final inspection of the stent surface proved difficult due to the presence of silicon particles, but did not however reveal any major damage to the stent.

The accelerated fatigue tester presented in this project is capable of subjecting coronary stents to simulated physiological loading at elevated frequencies of up to 60 Hz.

10.3 Recommendations

Much can be done to improve the functionality and performance of this accelerated fatigue tester. From results presented throughout this document and the aforementioned discussions and conclusions, the following areas could potentially be addressed.

10.3.1 Vessel Selection and Compliance Analysis

- A thorough investigation into the compliance characteristics and suitability of various tubes in the simulation of arterial conditions. This should include the effects of increased frequency on the vessel's ability to expand and bend in a suitable manner.

- Evaluation of tube expansion should be performed more reliably. One such solution (presented in section 6.3.6) would be to make use of a laser micrometer. Such a device would provide far greater measurement accuracy and, as such, enable precise vessel expansion.

- **If** a high speed camera is to be used in the measurement process again, ensure that resolutions greater than 700 x 600 pixels are achievable.

- Experimentation with various pressurization stokes could lead to improved compliance capabilities.

10.3.2 Control Systems

- Should a laser micrometer be available for tube measurement, information regarding vessel expansion should be used to drive pressurization stoke amplitude. Feedback of this kind would ensure the long term accuracy of stent expansion in the 5% range.

10.3.3 Stent Removal

- A new technique should be developed to successfully remove the deployed stent from the mock artery after testing. Dissolving the vessel in a suitable fluid medium might provide the best results with minimal stent damage.

APPENDIX A

Concept Evaluation Calculations

Al — Tube Material Selection Calculations and Data

Outer Diameter Measurements

O.D. (mm)	Silicon Pressure (kPa)	Latex Pressure (kPa)
5.6		0
5.7		28
5.8		58
5.9		75
6		105
6.1	0	122
6.2	32	140
6.3	57	
6.4	80	
6.5	100	
6.6	135	
6.7	180	

Inner Diameter Calculations

O.D. (mm)	Silicon Pressure (kPa)	Latex Pressure (kPa)
1.94		0
2.21		28
2.46		58
2.69		75
2.90		105
3.10	0	122
3.29	32	140
3.48	57	
3.66	80	
3.83	100	
3.99	135	
4.16	180	

Predicted Diameter change for various frequencies					
Silicon					
Frequency (Hz)		1.20	8.30	16.70	25.00
Reduction Factor (%)		100.00	95.93	90.15	75.68
Pressure (kPa)	0.00	3.10	3.10	3.10	3.10
	32.00	3.29	3.16	3.10	3.10
	57.00	3.48	3.34	3.13	3.10
	80.00	3.66	3.51	3.30	3.10
	100.00	3.83	3.67	3.45	3.10
	135.00	3.99	3.83	3.60	3.10
	180.00	4.16	3.99	3.75	3.15

Latex					
Frequency (Hz)		1.20	8.30	16.70	25.00
Reduction Factor (%)		100.00	96.67	95.46	79.57
Pressure (kPa)	0.00	2.80	2.80	2.80	2.80
	28.00	2.99	2.90	2.86	2.80
	58.00	3.18	3.08	3.04	2.80
	75.00	3.36	3.25	3.21	2.80
	105.00	3.53	3.41	3.37	2.81
	122.00	3.70	3.58	3.53	2.94
	140.00	3.86	3.73	3.69	3.07

A2 – Prototype A1 calculations

Housing Cavity Volume Calculation				
A_{top}	2000	mm^2		
A_{bottom}	2400	mm^2		
Cavity Width	7.5	mm		
$V_{cntrcavity}$	33000	mm^3		
V_{extra}	667.5884389	mm^3		
V_{pghole}	911.0618695	mm^3		
Tube Length	130	mm		
Tube Diameter	6	mm		
V_{tube}	3675.663405	mm^3	3.67566E-06	m^3
V_{cavity}	30902.9869	mm^3	3.0903E-05	m^3
For Air				
Piston Stroke	1	mm		
Gasket Diameter	75	mm		
Gasket Start Volume			0	m^3
Gasket End Volume			4.41786E-06	m^3
V1			3.0903E-05	m^3
P1	101	kPa		
V2			3.53209E-05	m^3
P2	88.36711286	kPa		
Pressure Gradient (dP)	12.63288714	kPa		
For Water				
Piston Stroke	1	mm		
Gasket Diameter	75	mm		
Gasket Start Volume			0	m^3
Gasket End Volume			4.41786E-06	m^3
V1			0.0000001	m^3
P1	101	kPa		
V2			4.51786E-06	m^3
P2	2.235569398	kPa		
Pressure Gradient (dP)	98.7644306	kPa		
Calculation of Pressure Gradient for varying Gas concentrations				
Gas %	1	%		
Piston Stroke	2	mm		
Gasket Diameter	75	mm		
Gasket Start Volume			0	m^3
Gasket End Volume			8.83573E-06	m^3
V1			3.0903E-07	m^3
P1	101	kPa		
V2			9.14476E-06	m^3
P2	3.413104278	kPa		
Pressure Gradient (dP)	97.58689572	kPa		

Gas Content (%)	Piston Stroke (mm)			
	0.5	1	1.5	2
100	6.738	12.633	17.834	22.457
90	7.431	13.844	19.434	24.351
80	8.284	15.312	21.350	26.593
70	9.358	17.129	23.685	29.290
60	10.752	19.434	26.593	32.596
50	12.633	22.457	30.315	36.744
40	15.312	26.593	35.249	42.101
30	19.434	32.596	42.101	49.286
20	26.593	42.101	52.259	59.429
10	42.101	59.429	68.879	74.829
5	59.429	74.829	81.903	85.967
4	64.760	78.919	85.122	88.604
3	71.142	83.481	88.604	91.409
2	78.919	88.604	92.384	94.397
1	88.604	94.397	96.500	97.587
0	101.000	101.000	101.000	101.000

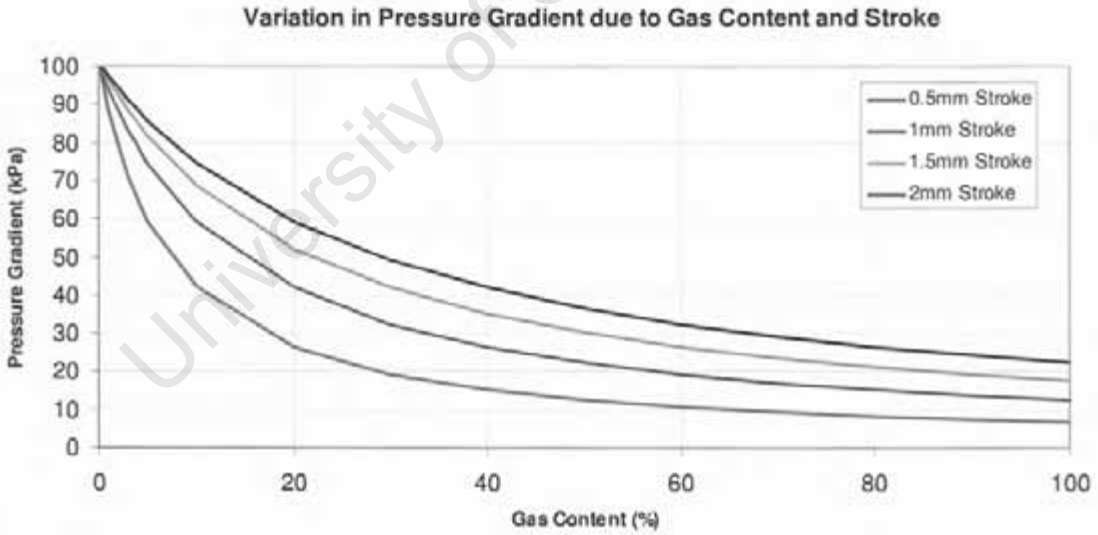

A3 - Prototype A2 calculations

Volume Calculations

Number of Tubes	1.00	
Tube Length	130.00 mm	5.00 mm
Tube Initial I.D.	3.00 mm	
Tube Volume	918.92 mm^3	35.34
Inner Cap Volume	1366.59 mm^3	
Connector Volumefe	141.37 mm^3	
Gasket Hole	7068.58 mm^3	
Inner Leur Volume	346.38 mm^3	
Gasket Diameter	145.00 mm	
Stroke	1.00 mm	
Gasket Volumedosed	6415.89 mm^3	
Gasket Volume$_{00}$	22928.89 mm^3	

For Air

Piston Stroke	1.00 mm	
Gasket Diameter	145.00 mm	
Gasket Start Volume		0.00 m^3
Gasket End Volume		0.00 m^3
V1		0.00 m^3
P1	101.00 kPa	
V2		0.00 m^3
P2	360.95 kPa	
Pressure Gradient (dP)	259.95 kPa	

For Water (with air content X)

Air Content	80.00 %	
Piston Stroke	1.00 mm	
Gasket Diameter	145.00 mm	
Gasket Start Volume		0.00 m^3
Gasket End Volume		0.00 m^3
Vi		0.00 m^3
P1	101.00 kPa	
V2		0.00 m^3
P2	1012.32 kPa	
Pressure Gradient (dP)	911.32 kPa	

Gas Content (%)	Piston Stroke (mm) 0.05	0.1	0.5	1
100	12.998	25.995	129.975	259.950
90	14.651	29.734	168.512	404.514
80	16.78695529	34.72833229	239.531	911.315
70	19.652	41.740	414.019	*
60	23.695	52.299	1524.684	*
50	29.834	70.009	*	*
40	40.267	105.854	*	*
30	61.917	216.921	*	*
20	133.927	*	*	*

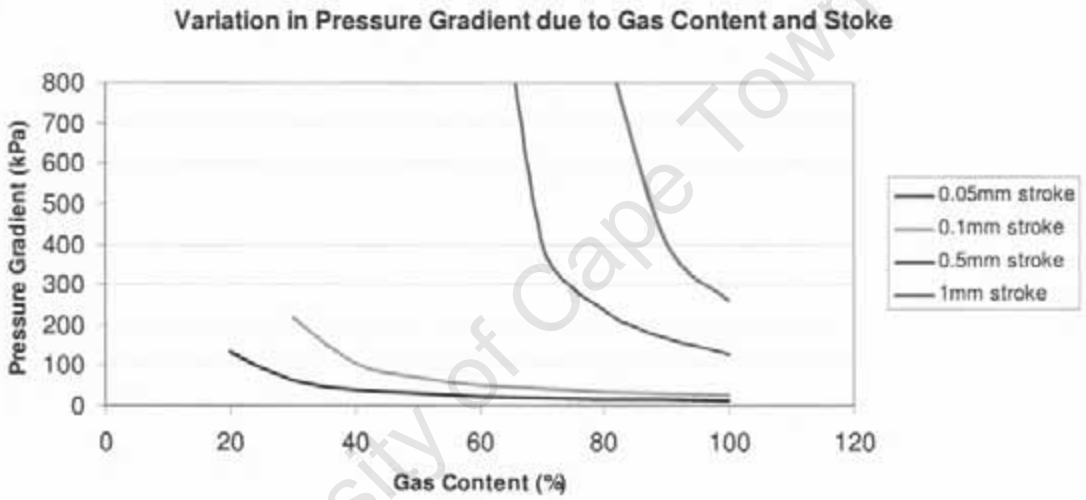

APPENDIX B

Prototype Al Detail Drawings

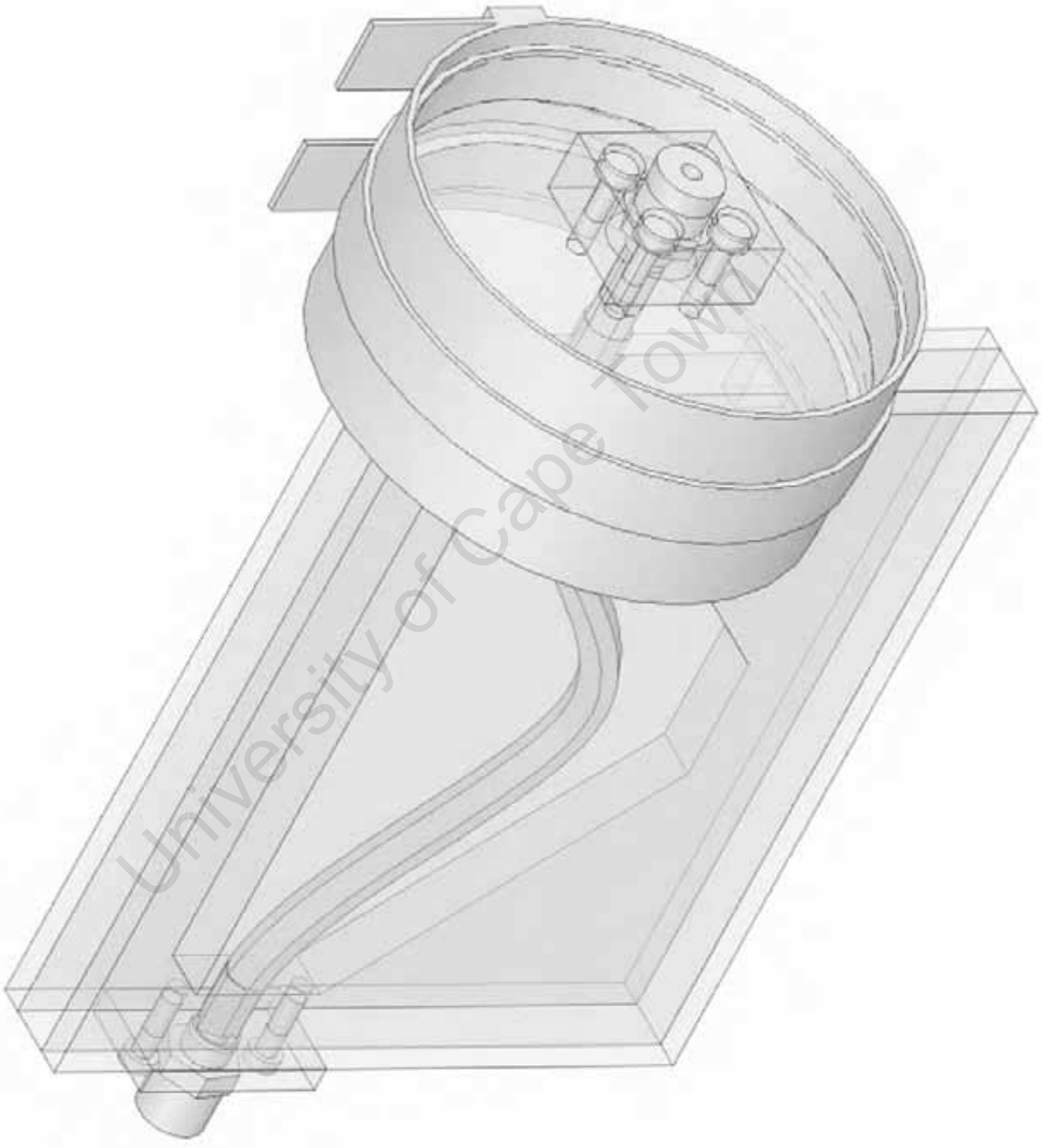

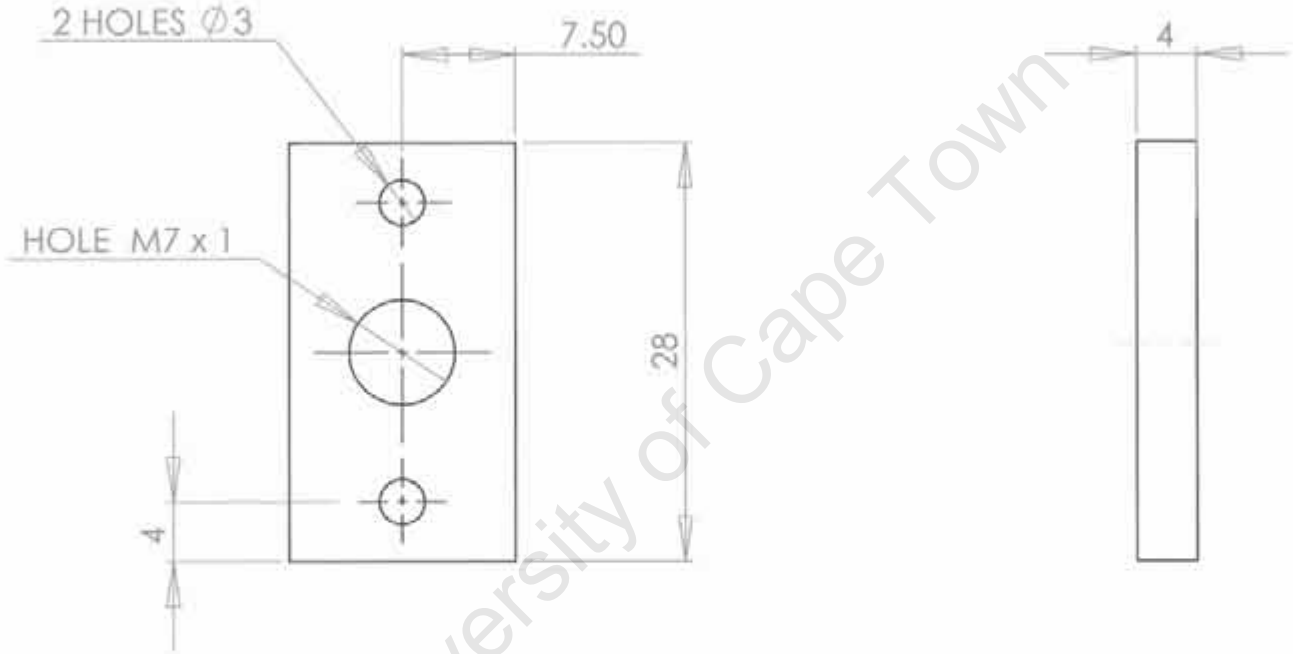

126

1	1	FIXED END CAP		PERSPEX	30 x 15 x 4
ITEM	QUANTITY	DESCRIPTION		MATERIAL	SPECIFICATION

UNLESS OTHERWISE SPECIFIED:
DIMENSIONS ARE IN MILLIMETERS
REMOVE ALL SHARP EDGES
TOLERANCES:
LINEAR: ± 0.1mm
ANGULAR: ± 1°

A4	NAME	DATE
DRAWN	MARTIN HOOLE	28/09/06
CHECKED	MARTIN HOOLE	28/09/06
SCALE:2:1		

TITLE: FIXED END CAP

DWG NO: FATIGUE - B - 01

SHEET 1 OF 1

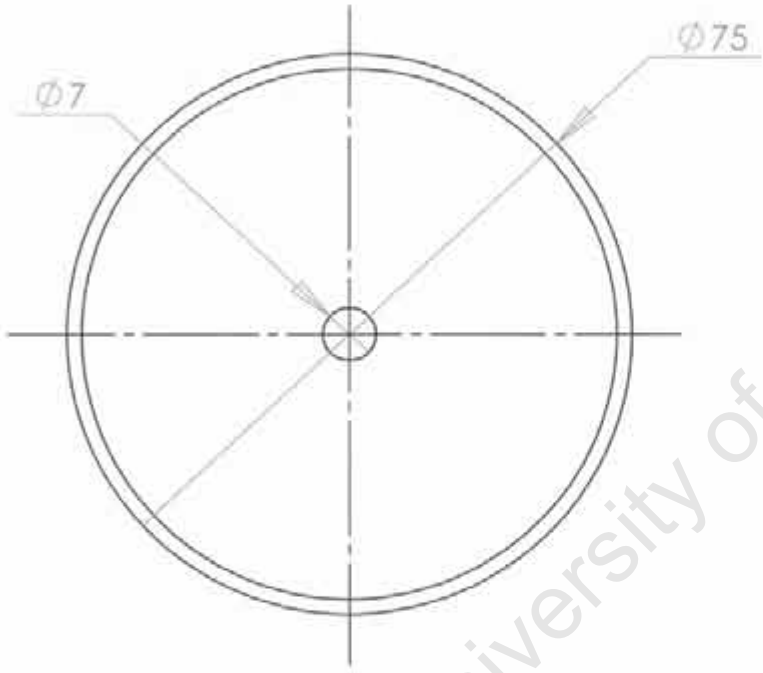

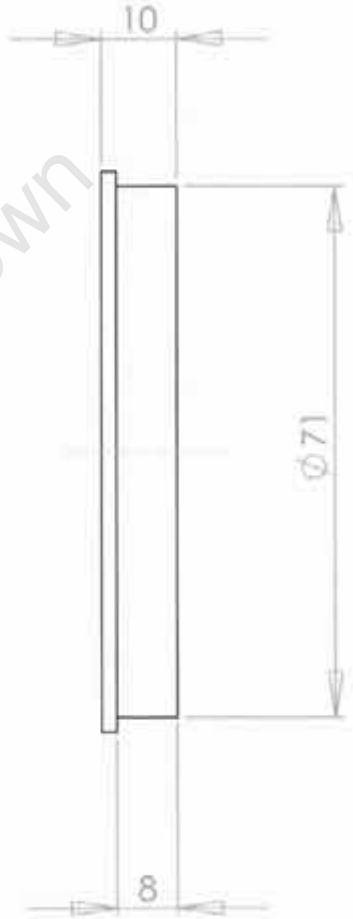

127

ITEM	QUANTITY	DESCRIPTION	MATERIAL	SPECIFICATION
1	1	FIXED END PISTON	PERSPEX	Ø 75 x 10

UNLESS OTHERWISE SPECIFIED:
DIMENSIONS ARE IN MILLIMETERS
REMOVE ALL SHARP EDGES
TOLERANCES:
LINEAR: ± 0.1mm
ANGULAR: ± 1°

A4	NAME	DATE
DRAWN	MARTIN HOOLE	28/09/06
CHECKED	MARTIN HOOLE	28/09/06
SCALE:1:1		

TITLE: FIXED END PISTON

DWG NO: FATIGUE - B - 02

SHEET 1 OF 1

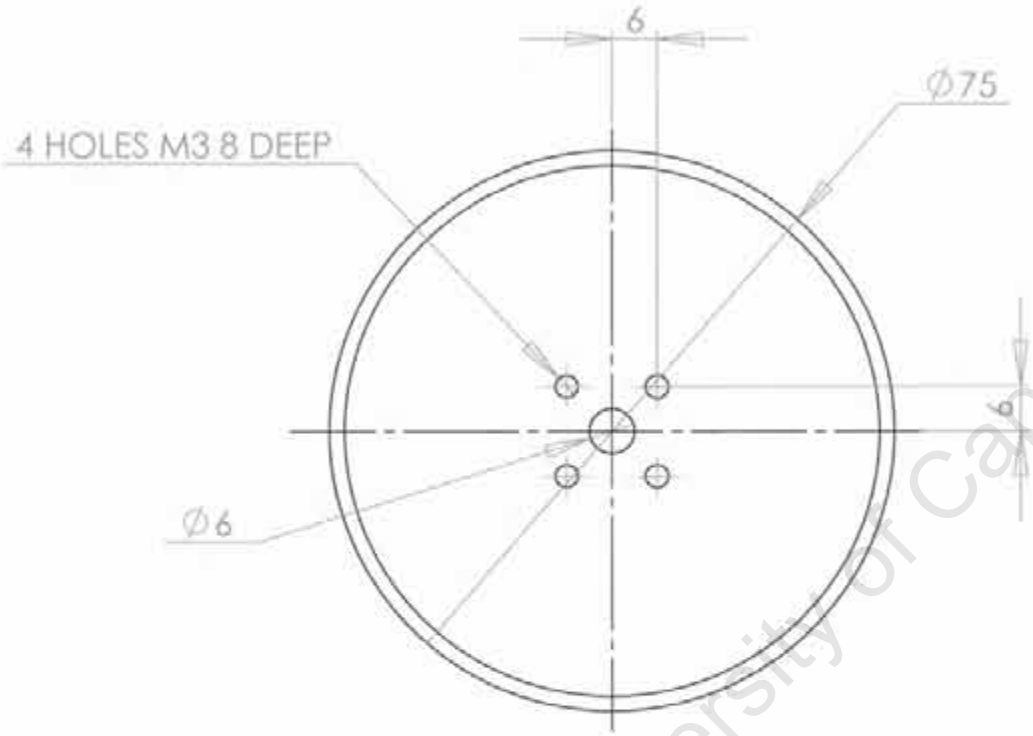

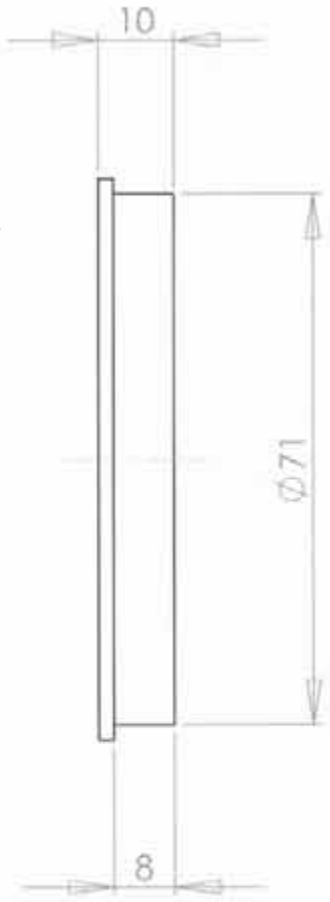

128

1	1	MOVING END PISTON			PERSPEX	Ø 75 x 10
ITEM	QUANTITY	DESCRIPTION			MATERIAL	SPECIFICATION
UNLESS OTHERWISE SPECIFIED: DIMENSIONS ARE IN MILLIMETERS REMOVE ALL SHARP EDGES TOLERANCES: LINEAR: ± 0.1mm ANGULAR: ± 1°		A4	NAME	DATE	TITLE: MOVING END PISTON	
		DRAWN	MARTIN HOOLE	28/09/06		
		CHECKED	MARTIN HOOLE	28/09/06	DWG NO:	FATIGUE - B - 03
		SCALE:1:1			SHEET 1 OF 1	

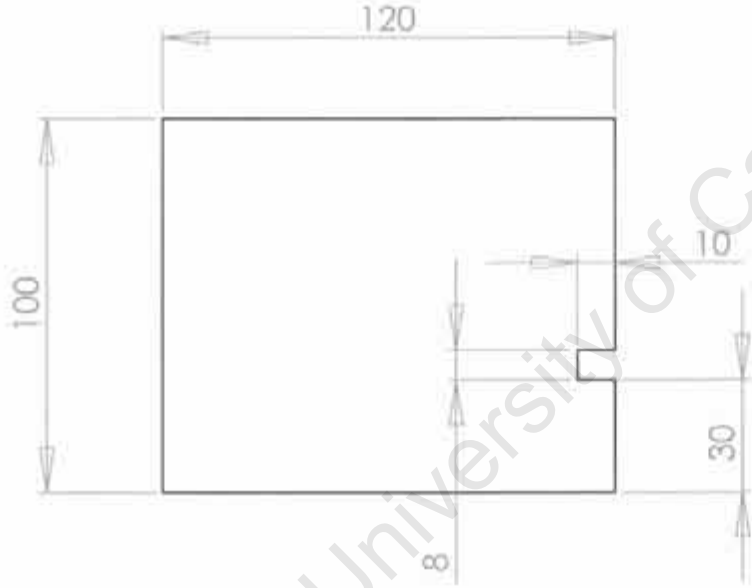

129

1	2	PERSPEX SIDE COVER			PERSPEX	120 x 100 x 4
ITEM	QUANTITY	DESCRIPTION			MATERIAL	SPECIFICATION
UNLESS OTHERWISE SPECIFIED: DIMENSIONS ARE IN MILLIMETERS REMOVE ALL SHARP EDGES TOLERANCES: LINEAR: ± 0.1mm ANGULAR: ± 1°		A4	NAME	DATE	TITLE:	PERSPEX SIDE COVER
		DRAWN	MARTIN HOOLE	28/09/06		
		CHECKED	MARTIN HOOLE	28/09/06	DWG NO:	FATIGUE - B - 04
		SCALE:1:2			SHEET 1 OF 1	

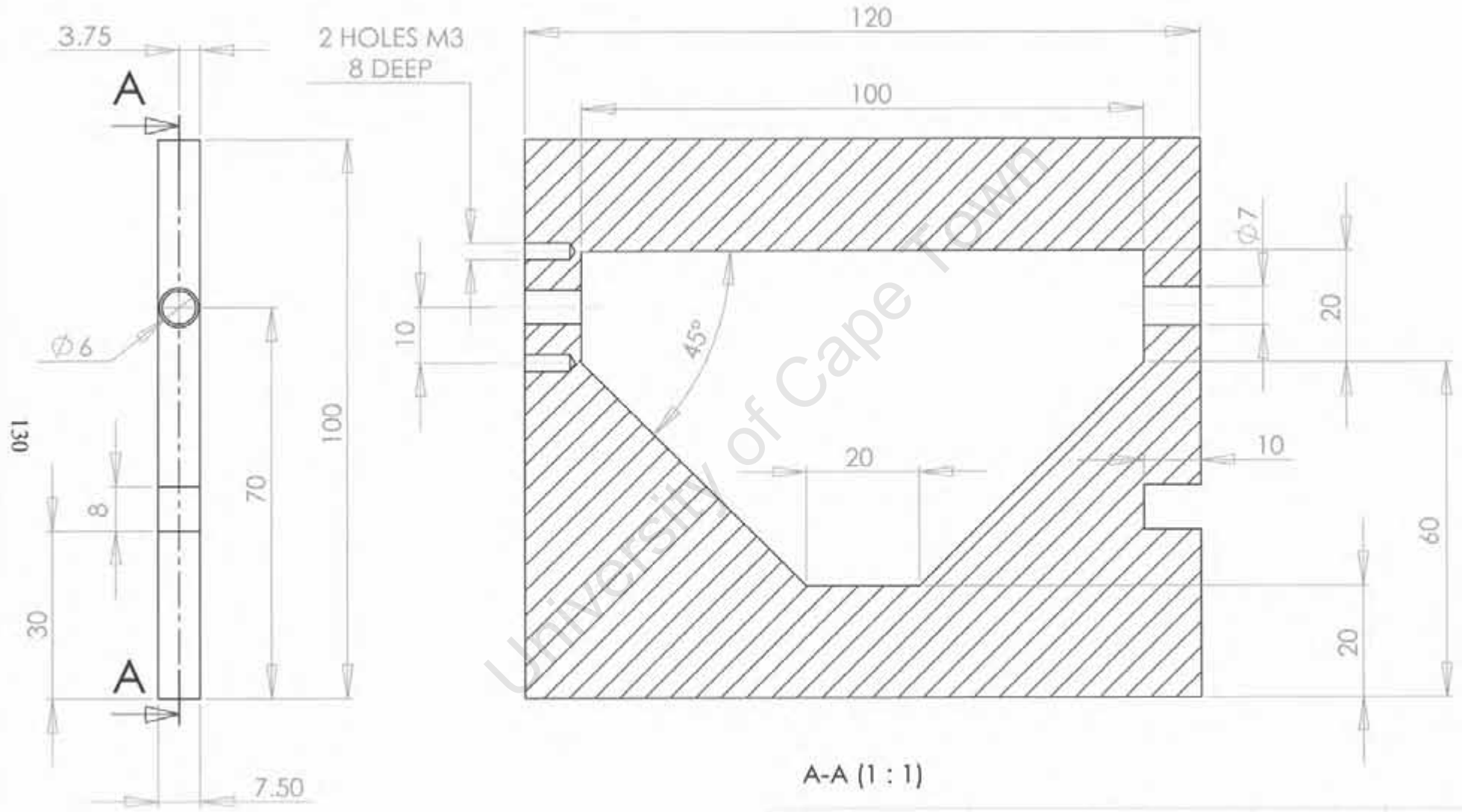

1	1	PERSPEX SPACER		PERSPEX	120 x 100 x 7.5
ITEM	QUANTITY	DESCRIPTION		MATERIAL	SPECIFICATION
UNLESS OTHERWISE SPECIFIED: DIMENSIONS ARE IN MILLIMETERS REMOVE ALL SHARP EDGES TOLERANCES: LINEAR: ± 0.1mm ANGULAR: ± 1°		A4	NAME	DATE	TITLE: PERSPEX SPACER
		DRAWN	MARTIN HOOLE	28/09/06	
		CHECKED	MARTIN HOOLE	28/09/06	DWG NO: FATIGUE - B - 05
		SCALE: 1:1			SHEET 1 OF 1

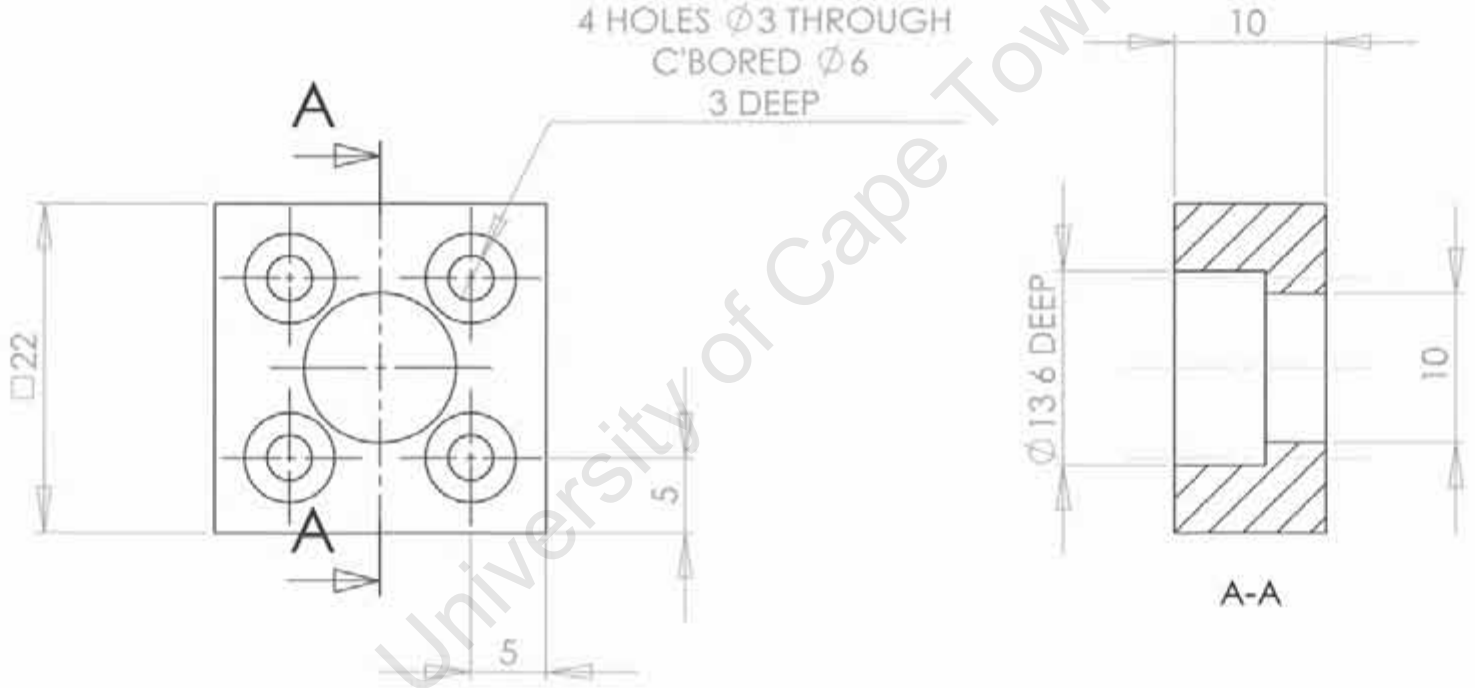

131

1	1	PISTON END CAP			PERSPEX	22 x 22 x 10
ITEM	QUANTITY	DESCRIPTION			MATERIAL	SPECIFICATION
UNLESS OTHERWISE SPECIFIED: DIMENSIONS ARE IN MILLIMETERS REMOVE ALL SHARP EDGES TOLERANCES: LINEAR: ± 0.1mm ANGULAR: ± 1°		A4	NAME	DATE	TITLE:	PISTON END CAP
		DRAWN	MARTIN HOOLE	28/09/06		
		CHECKED	MARTIN HOOLE	28/09/06	DWG NO:	FATIGUE - B - 06
		SCALE:2:1			SHEET 1 OF 1	

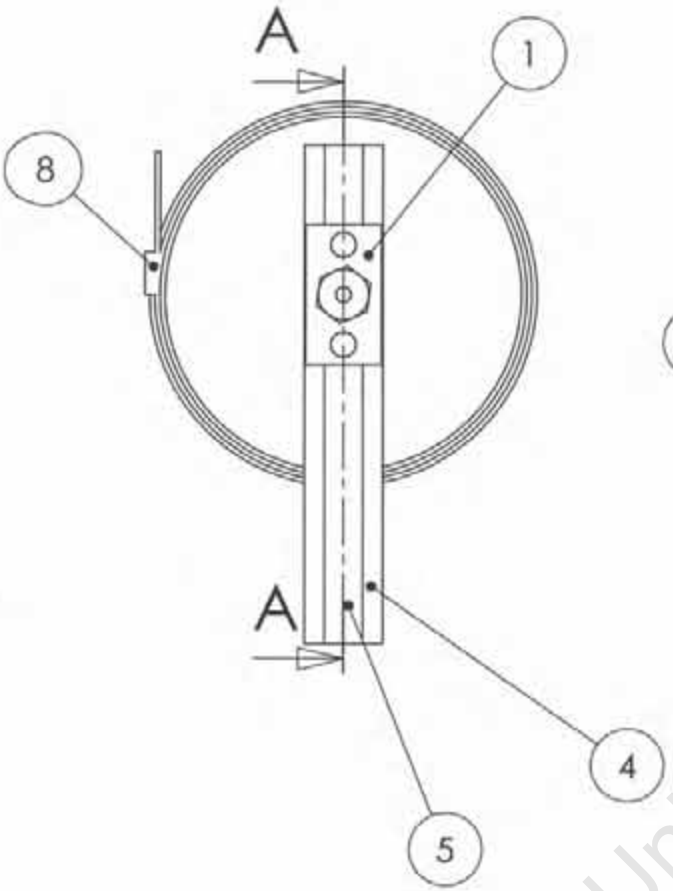

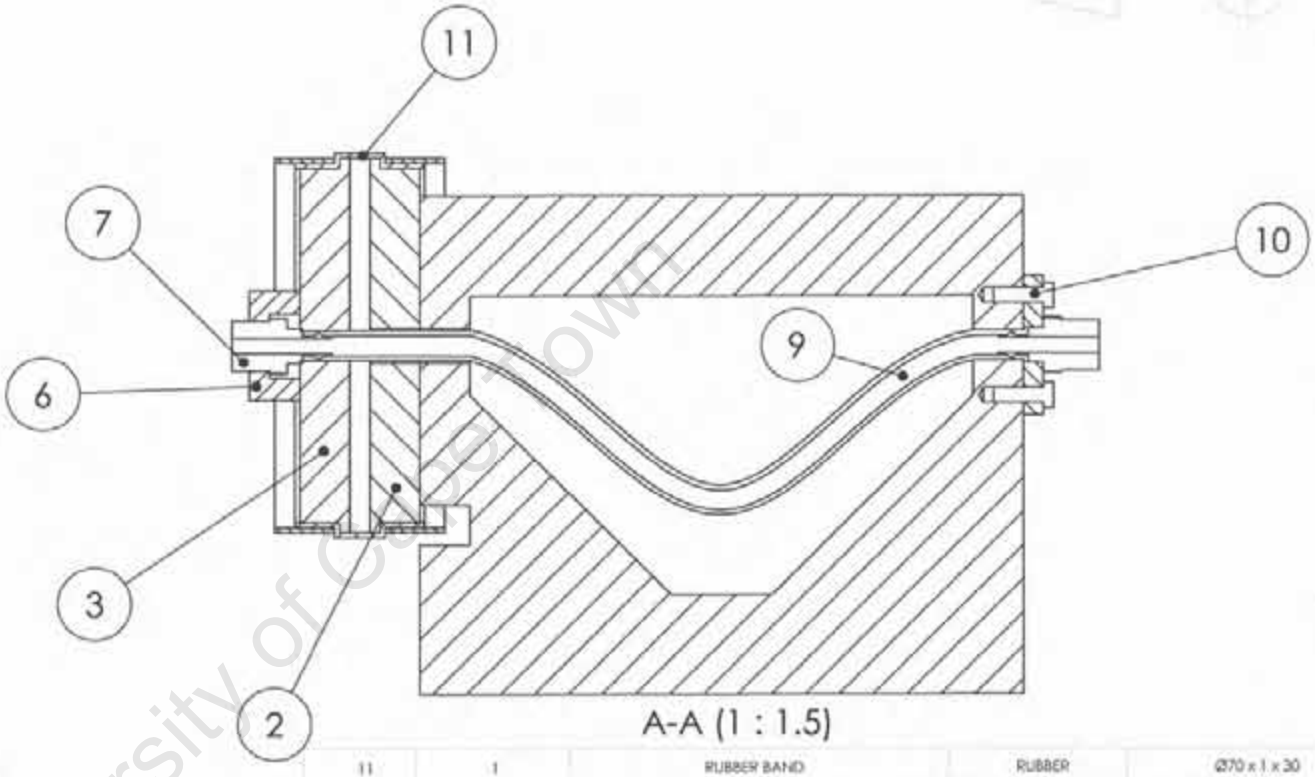

A-A (1 : 1.5)

132

ITEM	QUANTITY	DESCRIPTION	MATERIAL	SPECIFICATION
11	1	RUBBER BAND	RUBBER	Ø70 x 1 x 30
10	6	M3 CAPHEAD SCREW	STEEL	65 - 89mm (12.5mm wide)
9	1	TUBE	LATEX / SILICON	Ø6 x 100
8	2	HOSE CLAMP	STAINLESS STEEL	65 - 89mm (12.5mm wide)
7	2	PNEUMATIC LEUR CONNECTOR	BRASS	6mm 1/8 BSP
6	1	PISTON END CAP	PERSPEX	FATIGUE - A1 - 06
5	1	PERSPEX SPACER	PERSPEX	FATIGUE - A1 - 05
4	2	PERSPEX SIDE COVER	PERSPEX	FATIGUE - A1 - 04
3	1	MOVING END PISTON	PERSPEX	FATIGUE - A1 - 03
2	1	FIXED END PISTON	PERSPEX	FATIGUE - A1 - 02
1	1	FIXED END CAP	PERSPEX	FATIGUE - A1 - 01

UNLESS OTHERWISE SPECIFIED:
DIMENSIONS ARE IN MILLIMETERS
REMOVE ALL SHARP EDGES
TOLERANCES:
LINEAR: ± 0.1mm
ANGULAR: ± 1°

A4	NAME	DATE
DRAWN	MARTIN HOOLE	28/09/06
CHECKED	MARTIN HOOLE	28/09/06
SCALE:1:1.5		

TITLE: B - ASSEMBLY

DWG NO: FATIGUE - B - ASSEMBLY

SHEET 1 OF 1

APPENDIX C

Prototype A2 Detail Drawings

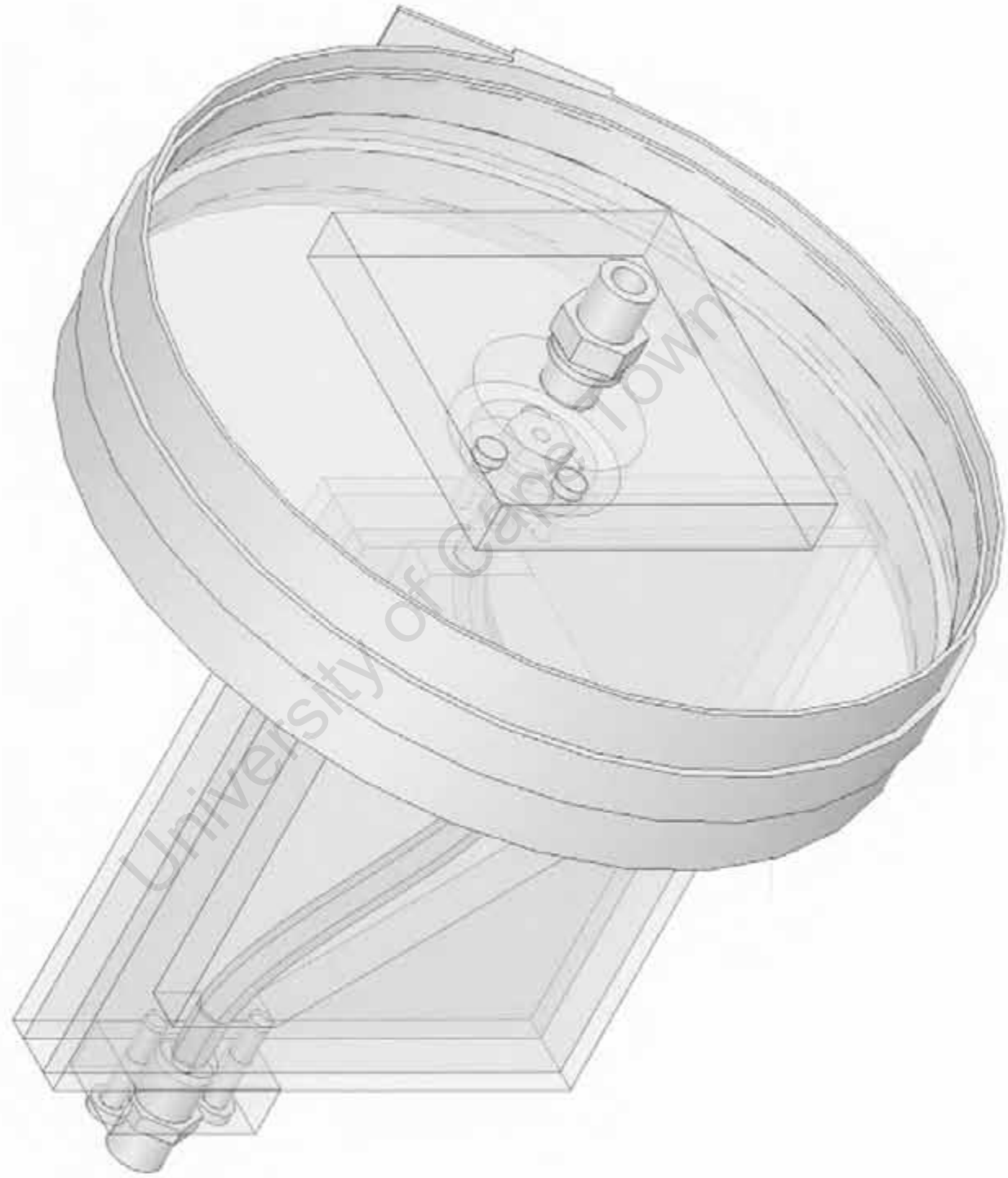

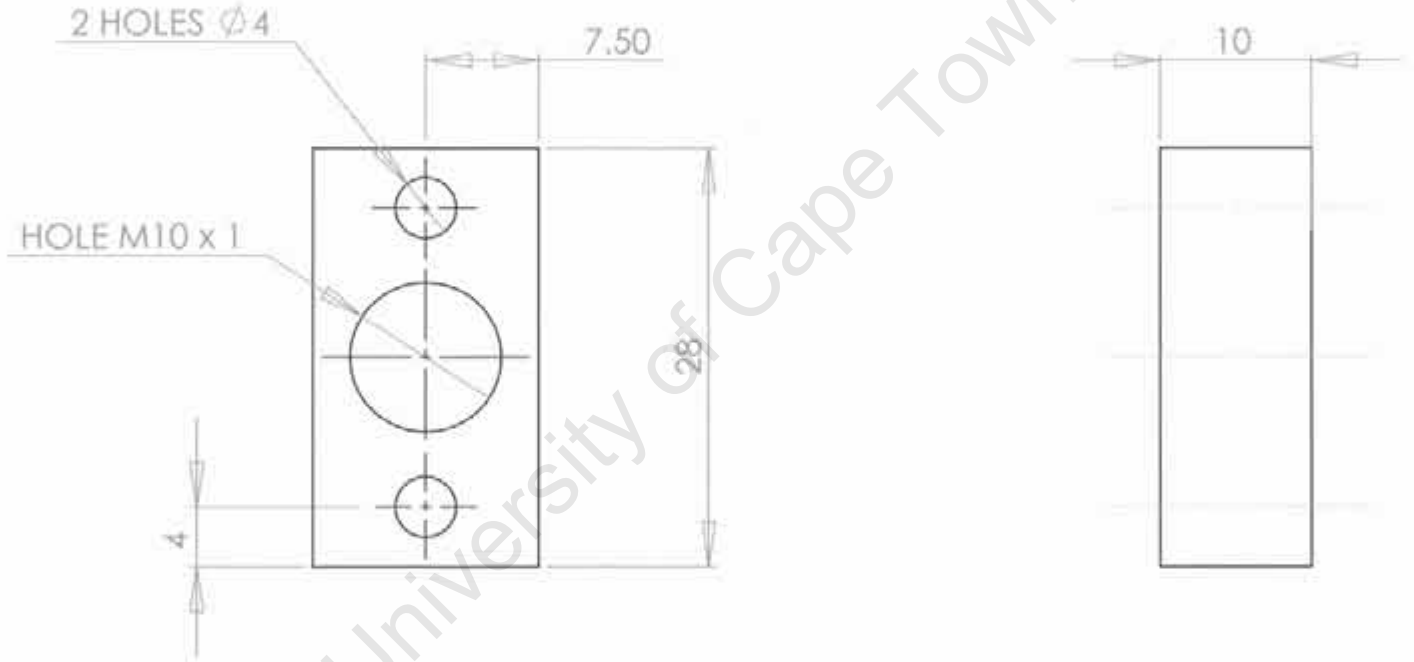

135

1	1	FIXED END CAP			PERSPEX	30 x 15 x 10
ITEM	QUANTITY	DESCRIPTION			MATERIAL	SPECIFICATION

UNLESS OTHERWISE SPECIFIED:
DIMENSIONS ARE IN MILLIMETERS
REMOVE ALL SHARP EDGES
TOLERANCES:
LINEAR: ± 0.1mm
ANGULAR: ± 1°

A4	NAME	DATE
DRAWN	MARTIN HOOLE	28/09/06
CHECKED	MARTIN HOOLE	28/09/06
	SCALE:2:1	

TITLE: FIXED END CAP

DWG NO: FATIGUE - C - 01

SHEET 1 OF 1

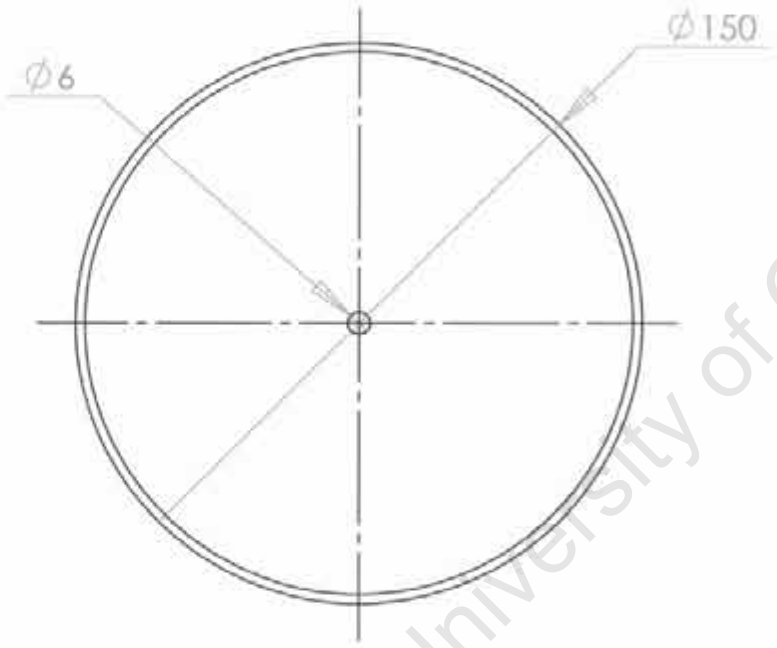

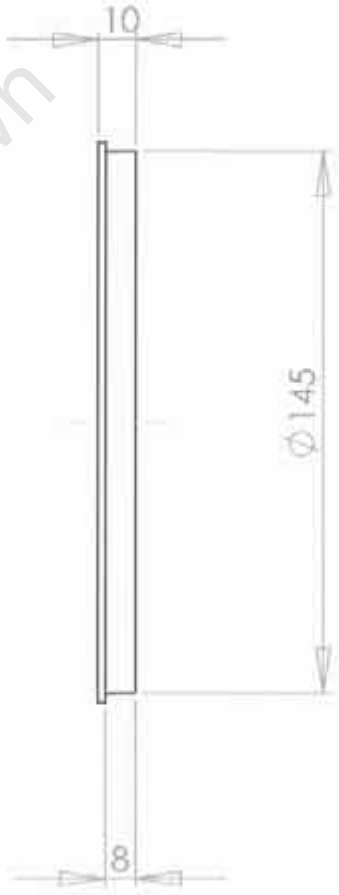

136

ITEM	QUANTITY	DESCRIPTION	MATERIAL	SPECIFICATION
1	1	FIXED END PISTON	PERSPEX	Ø 150 x 10

UNLESS OTHERWISE SPECIFIED:
DIMENSIONS ARE IN MILLIMETERS
REMOVE ALL SHARP EDGES
TOLERANCES:
LINEAR: ± 0.1mm
ANGULAR: ± 1°

A4	NAME	DATE
DRAWN	MARTIN HOOLE	28/09/06
CHECKED	MARTIN HOOLE	28/09/06
SCALE: 1:2		

TITLE: FIXED END PISTON

DWG NO: FATIGUE - C - 02

SHEET 1 OF 1

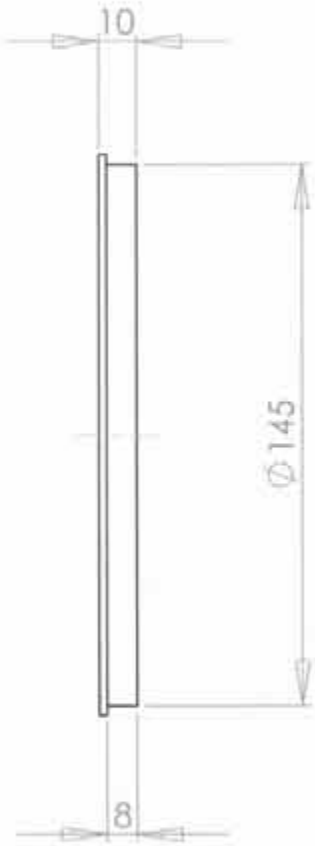

137

1	1	MOVING END PISTON			PERSPEX	Ø 150 x 10
ITEM	QUANTITY	DESCRIPTION			MATERIAL	SPECIFICATION
UNLESS OTHERWISE SPECIFIED: DIMENSIONS ARE IN MILLIMETERS REMOVE ALL SHARP EDGES TOLERANCES: LINEAR: ± 0.1mm ANGULAR: ± 1°		A4	NAME	DATE	TITLE: MOVING END PISTON	
		DRAWN	MARTIN HOOLE	28/09/06		
		CHECKED	MARTIN HOOLE	28/09/06	DWG NO: FATIGUE - C - 03	
		SCALE: 1:2			SHEET 1 OF 1	

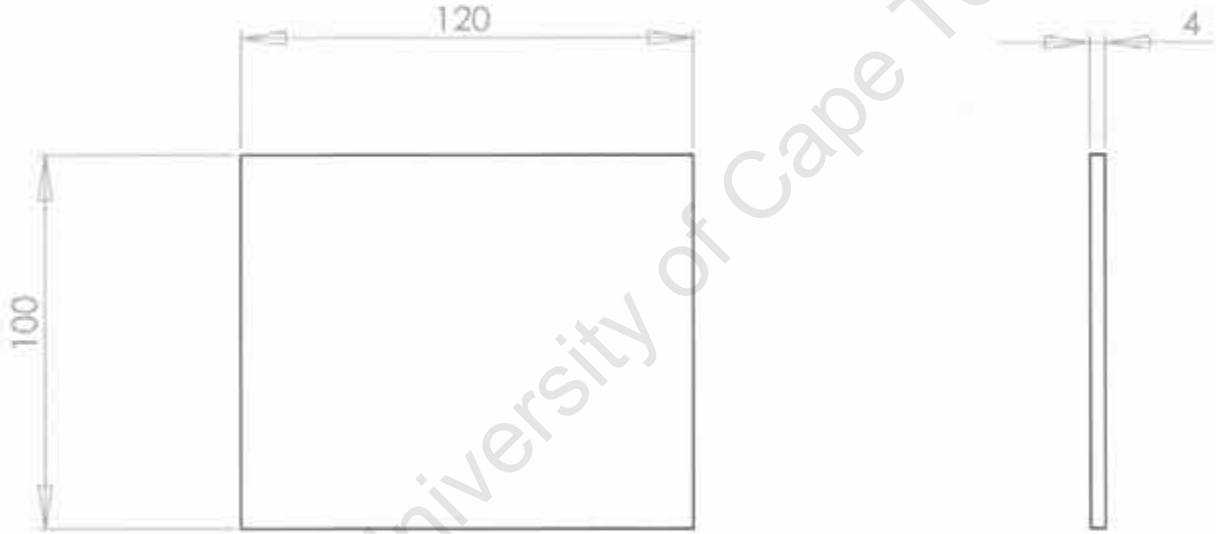

ITEM	QUANTITY	DESCRIPTION	MATERIAL	SPECIFICATION
1	2	PERSPEX SIDE COVER	PERSPEX	120 x 100 x 4

UNLESS OTHERWISE SPECIFIED:
DIMENSIONS ARE IN MILLIMETERS
REMOVE ALL SHARP EDGES
TOLERANCES:
LINEAR: ± 0.1mm
ANGULAR: ± 1°

A4	NAME	DATE
DRAWN	MARTIN HOOLE	28/09/06
CHECKED	MARTIN HOOLE	28/09/06
SCALE:1:2		

TITLE: PERSPEX SIDE COVER

DWG NO: FATIGUE - C - 04

SHEET 1 OF 1

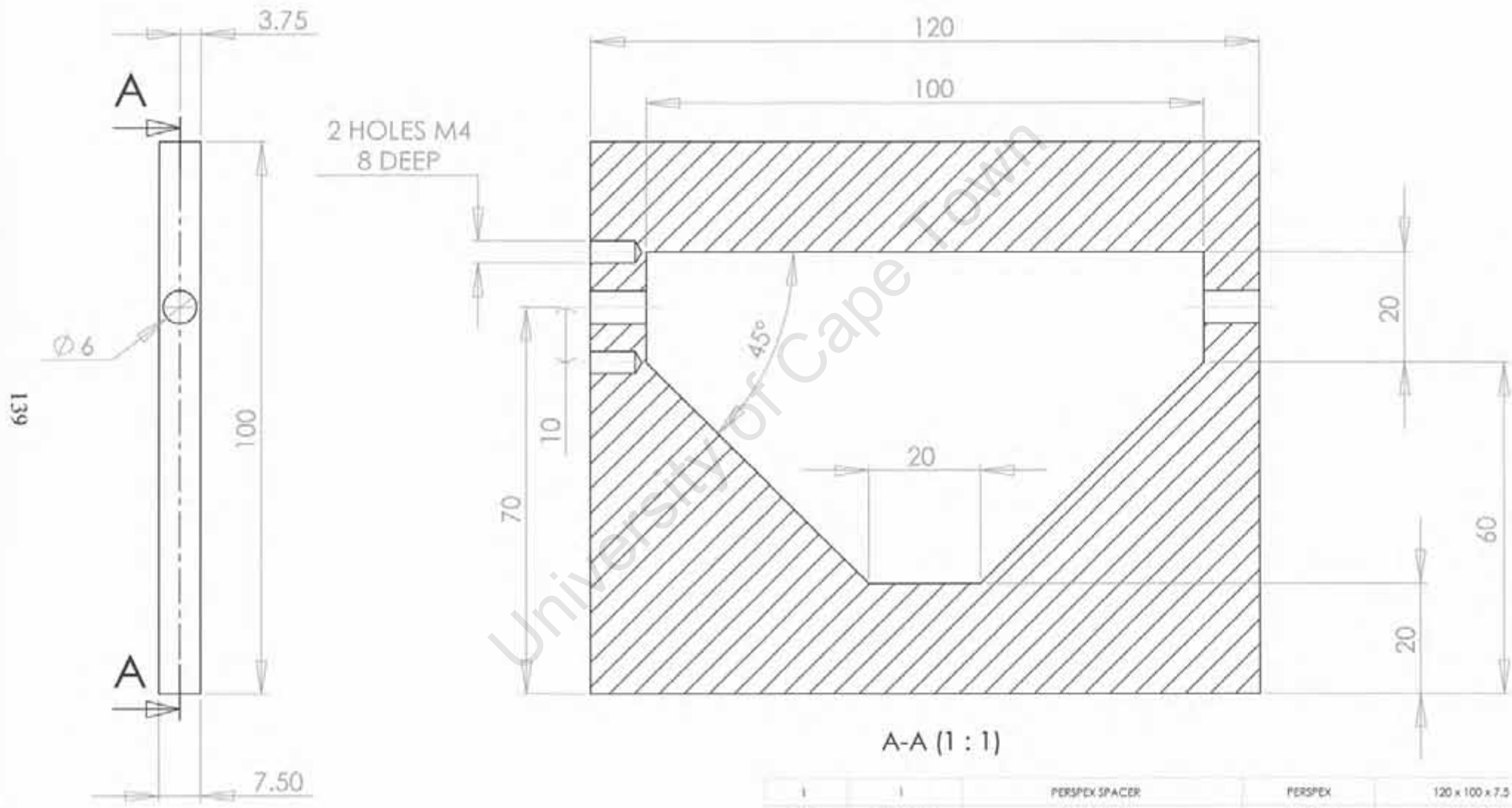

1	1	PERSPEX SPACER			PERSPEX	120 x 100 x 7.5
ITEM	QUANTITY	DESCRIPTION			MATERIAL	SPECIFICATION
UNLESS OTHERWISE SPECIFIED: DIMENSIONS ARE IN MILLIMETERS REMOVE ALL SHARP EDGES TOLERANCES: LINEAR: ± 0.1mm ANGULAR: ± 1°		A4	NAME	DATE	TITLE:	PERSPEX SPACER
		DRAWN	MARTIN HOOLE	28/09/06		
		CHECKED	MARTIN HOOLE	28/09/06	DWG NO:	FATIGUE - C - 05
		SCALE: 1:1			SHEET 1 OF 1	

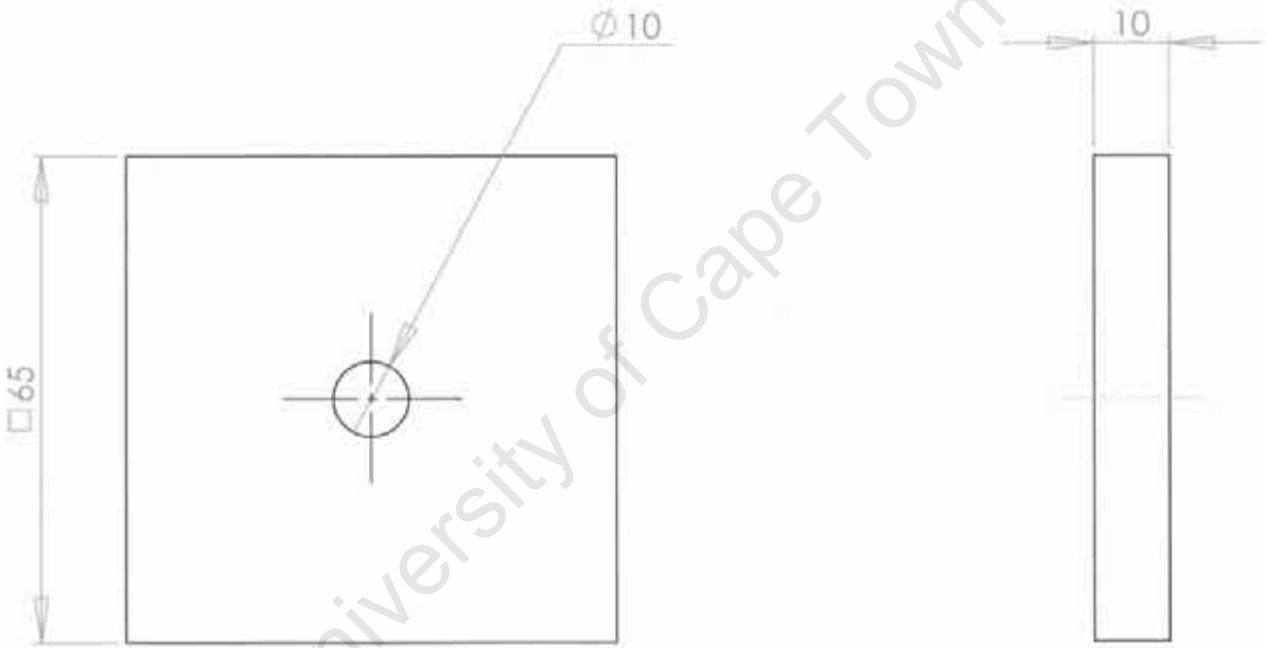

140

ITEM	QUANTITY	DESCRIPTION	MATERIAL	SPECIFICATION
1	1	PISTON END CAP	PERSPEX	65 x 65 x 10

UNLESS OTHERWISE SPECIFIED:
DIMENSIONS ARE IN MILLIMETERS
REMOVE ALL SHARP EDGES
TOLERANCES:
LINEAR: ± 0.1mm
ANGULAR: ± 1°

A4	NAME	DATE
DRAWN	MARTIN HOOLE	28/09/06
CHECKED	MARTIN HOOLE	28/09/06
SCALE: 1:1		

TITLE: PISTON END CAP

DWG NO: FATIGUE - C - 06

SHEET 1 OF 1

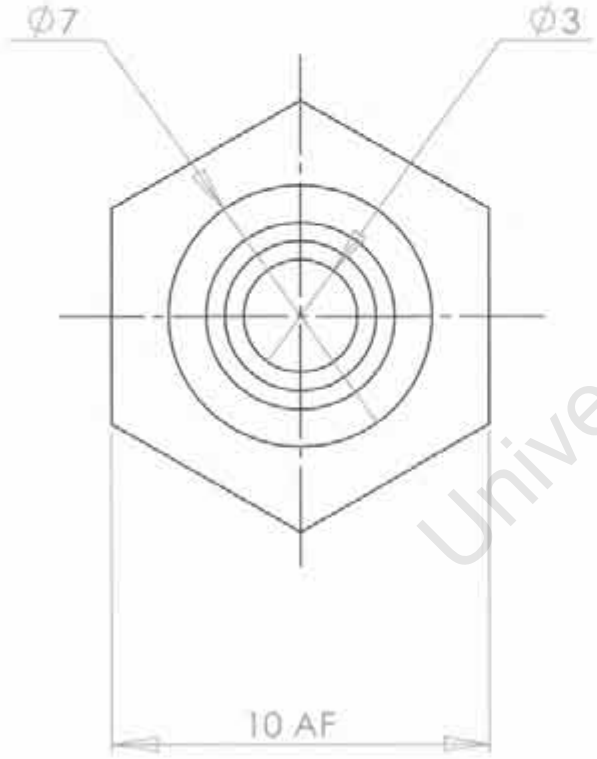

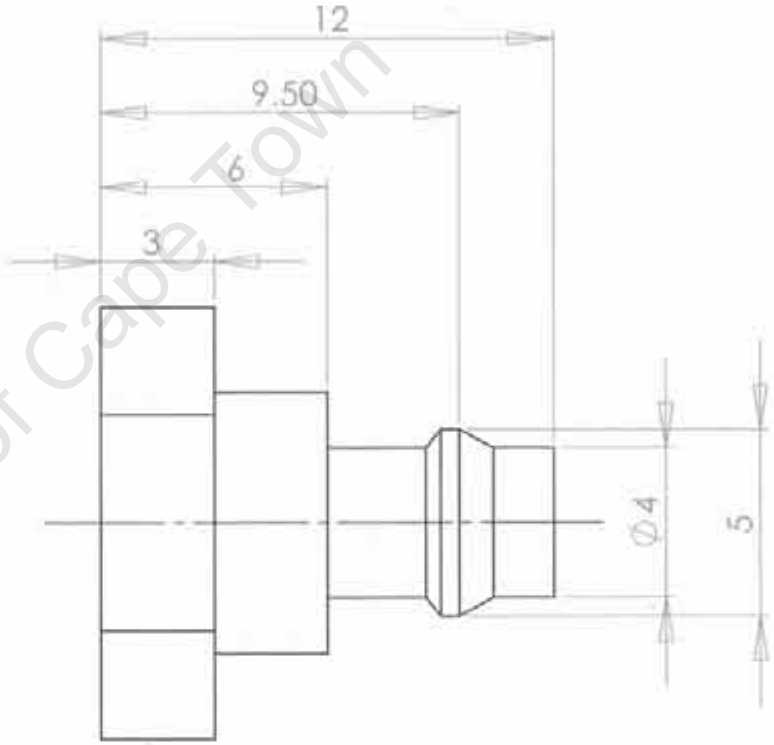

141

ITEM	QUANTITY	DESCRIPTION	MATERIAL	SPECIFICATION
1	1	FIXED END CAP	BRASS	Ø 12 x 12

UNLESS OTHERWISE SPECIFIED:
DIMENSIONS ARE IN MILLIMETERS
REMOVE ALL SHARP EDGES
TOLERANCES:
LINEAR: ± 0.1mm
ANGULAR: ± 1°

A4	NAME	DATE
DRAWN	MARTIN HOOLE	28/09/06
CHECKED	MARTIN HOOLE	28/09/06
SCALE:5:1		

TITLE: INNER LEUR CONNECTOR
DWG NO: FATIGUE - C - 07
SHEET 1 OF 1

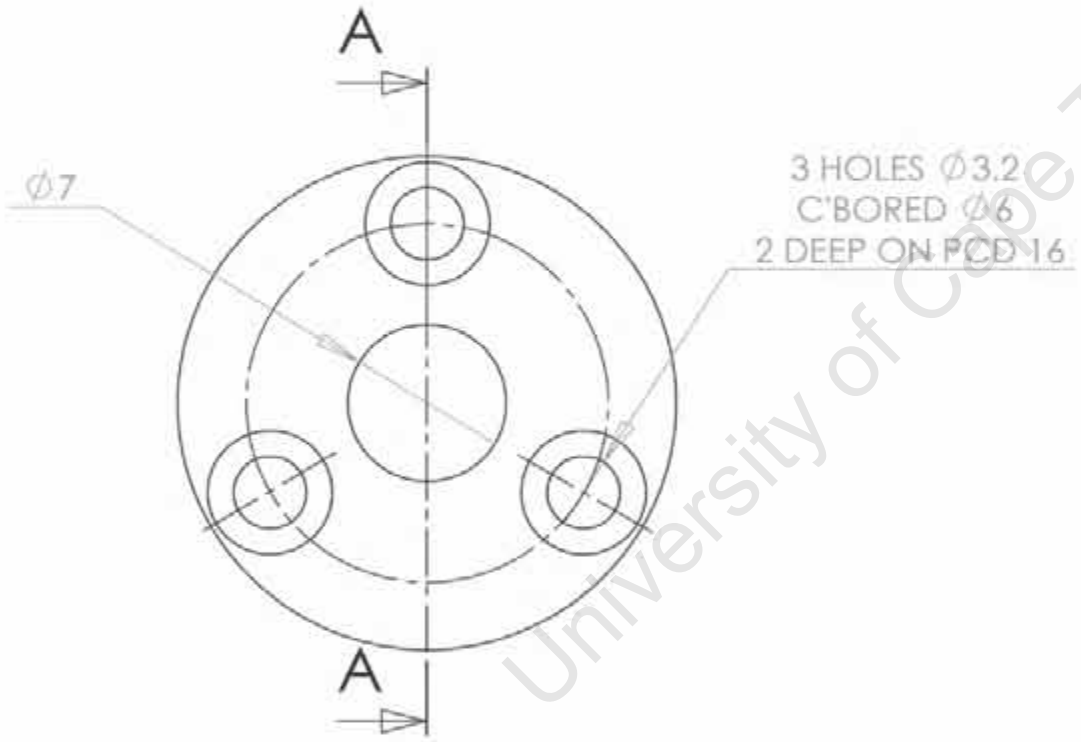

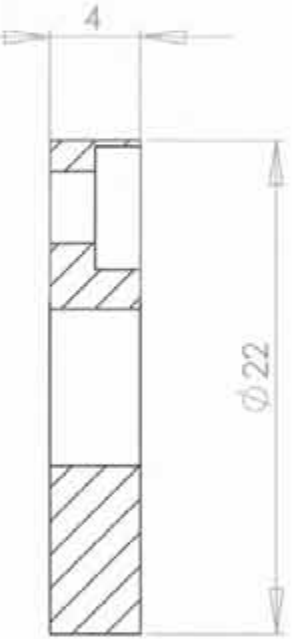

A-A (3 : 1)

142

1	1	FIXED END CAP		PERSPEX	Ø 20 x 4
ITEM	QUANTITY	DESCRIPTION		MATERIAL	SPECIFICATION
UNLESS OTHERWISE SPECIFIED: DIMENSIONS ARE IN MILLIMETERS REMOVE ALL SHARP EDGES TOLERANCES: LINEAR: ± 0.1mm ANGULAR: ± 1°	A4	NAME	DATE	TITLE:	INNER CAP
	DRAWN	MARTIN HOOLE	28/09/06		
	CHECKED	MARTIN HOOLE	28/09/06	DWG NO:	FATIGUE - C - 08
	SCALE:3:1			SHEET 1 OF 1	

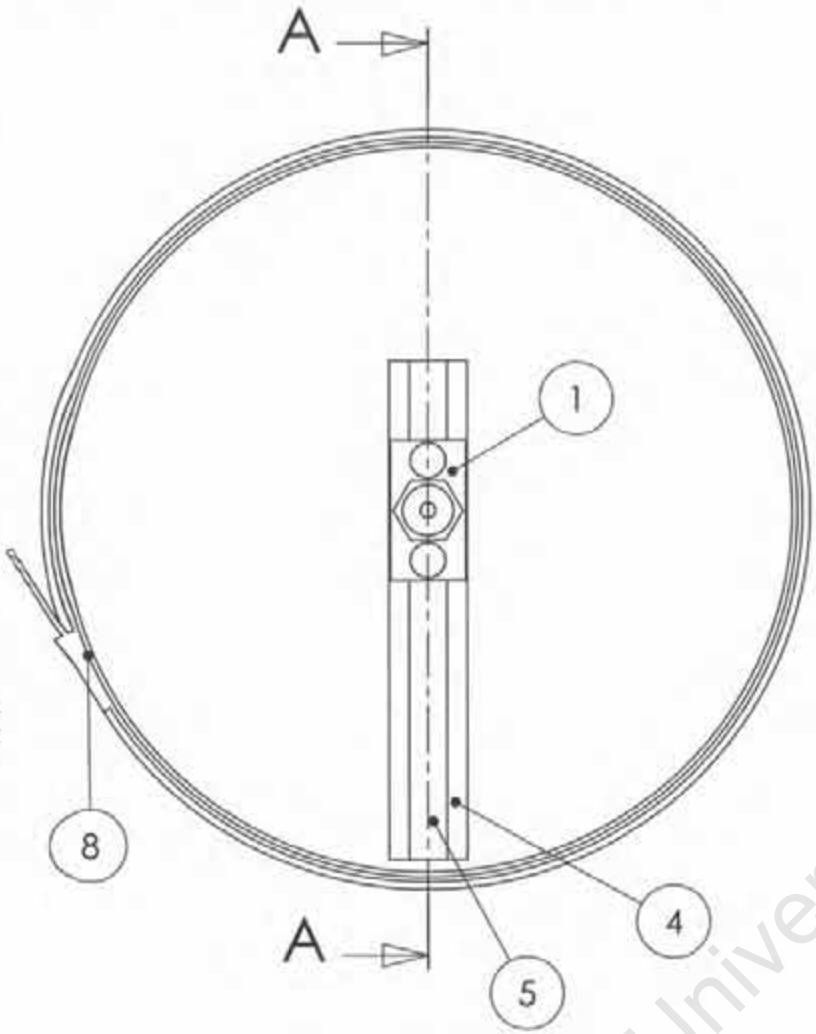

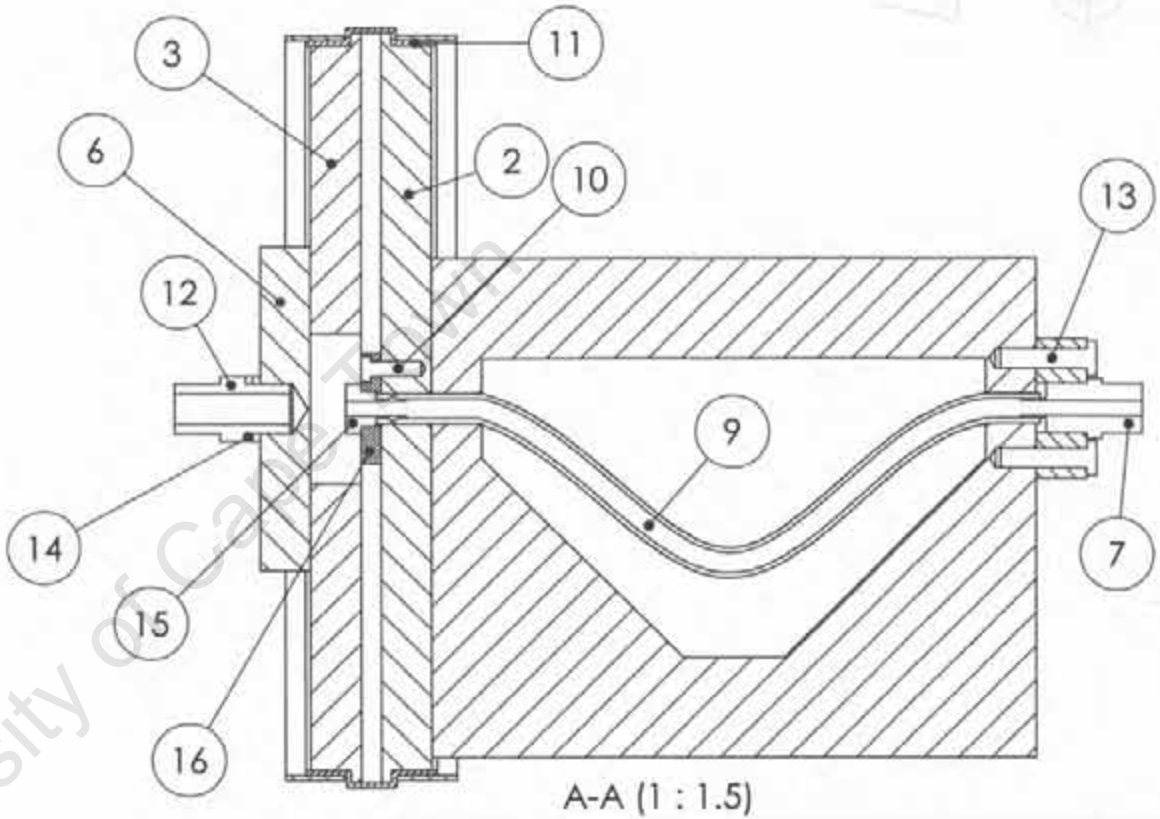

A-A (1 : 1.5)

ITEM	QUANTITY	DESCRIPTION	MATERIAL	SPECIFICATION
16	1	INNER CAP	PERSPEX	FATIGUE - A2 - 08
15	1	INNER LEUR CONNECTOR	BRASS	FATIGUE - A2 - 07
14	2	WASHER	PLASTIC	13-OD x 10-ID x 2
13	2	M4 CAPHEAD SCREW	STEEL	M4 x 17
12	1	M10 CONNECTOR	STEEL	M10 x 23 long
11	1	RUBBER BAND	RUBBER	Ø150 x 1 x 30
10	3	M3 CAPHEAD SCREW	STEEL	M3 x 10
9	1	TUBE	LATEX / SILICON	Ø6 x 100
8	2	HOSE CLAMP	STAINLESS STEEL	130 - 155mm (12.5mm wide)
7	1	PNEUMATIC LEUR CONNECTOR	BRASS	6mm 1/8 BSP
6	1	PISTON END CAP	PERSPEX	FATIGUE - A2 - 06
5	1	PERSPEX SPACER	PERSPEX	FATIGUE - A2 - 05
4	2	PERSPEX SIDE COVER	PERSPEX	FATIGUE - A2 - 04
3	1	MOVING END PISTON	PERSPEX	FATIGUE - A2 - 03
2	1	FIXED END PISTON	PERSPEX	FATIGUE - A2 - 02
1	1	FIXED END CAP	PERSPEX	FATIGUE - A2 - 01
ITEM	QUANTITY	DESCRIPTION	MATERIAL	SPECIFICATION

UNLESS OTHERWISE SPECIFIED:
DIMENSIONS ARE IN MILLIMETERS
REMOVE ALL SHARP EDGES
TOLERANCES:
LINEAR: ± 0.1mm
ANGULAR: ± 1°

A4	NAME	DATE
DRAWN	MARTIN HOOLE	28/09/06
CHECKED	MARTIN HOOLE	28/09/06
SCALE:1:1.5		

TITLE: C - ASSEMBLY

DWG NO: FATIGUE - C - ASSEMBLY

SHEET 1 OF 1

APPENDIX D

Patent Search Results

US 20030110830A1

(19) **United States**

(12) **Patent Application Publication** (10) **Pub. No.: US 2003/0110830 A1**

Dehdashtian et al. (43) **Pub. Date: Jun. 19, 2003**

(54) **METHODS AND APPARATUSES FOR MEASURING THE COMPLIANCE OF STENTS AND STENTED GRAFTS**

(76) Inventors: **Mark Dehdashtian**, Costa Mesa, CA (US); **William E. Krams**, Downey, CA (US); **Sanjay Shrivastava**, Newport Beach, CA (US); **Nareth Dy**, Tustin, CA (US); **Adnan Nabulsi**, South Gate, CA (US)

Correspondence Address:
Edwards Lifesciences LLC
Law Dept.
One Edwards Way
Irvine, CA 92614 (US)

(21) Appl. No.: **09/911,353**

(22) Filed: **Jul. 23, 2001**

Publication Classification

(51) **Int. Cl.**[7] **G01M 3/02**

(52) **U.S. Cl.** **73/37**

(57) **ABSTRACT**

Methods and apparatuses for testing the compliance of stents and stented grafts, including pre-testing them in a pre-tester tube prior to accelerated fatigue testing. The pre-tester tube is a simulated human vessel that may be made of animal tissue having approximately the same size as the human target vessel. The pre-test involves pressurizing the pre-tester tube at various normal and abnormal physiologic pulsed pressures with the stent or stented graft in place. By measuring the expansion of the pre-tester tube, the proper expansion rate of the stent or stented graft is determined. Those data are then used in a feedback loop to control the amount of expansion of a synthetic tester tube in the accelerated fatigue tests. The tester regulates the pressure in the tester tube to attain the proper expansion magnitude during the test. The animal tissue may be porcine tissue, in particular a porcine aorta to simulate the human abdominal aorta. Any side branches of the porcine aorta are tied off.

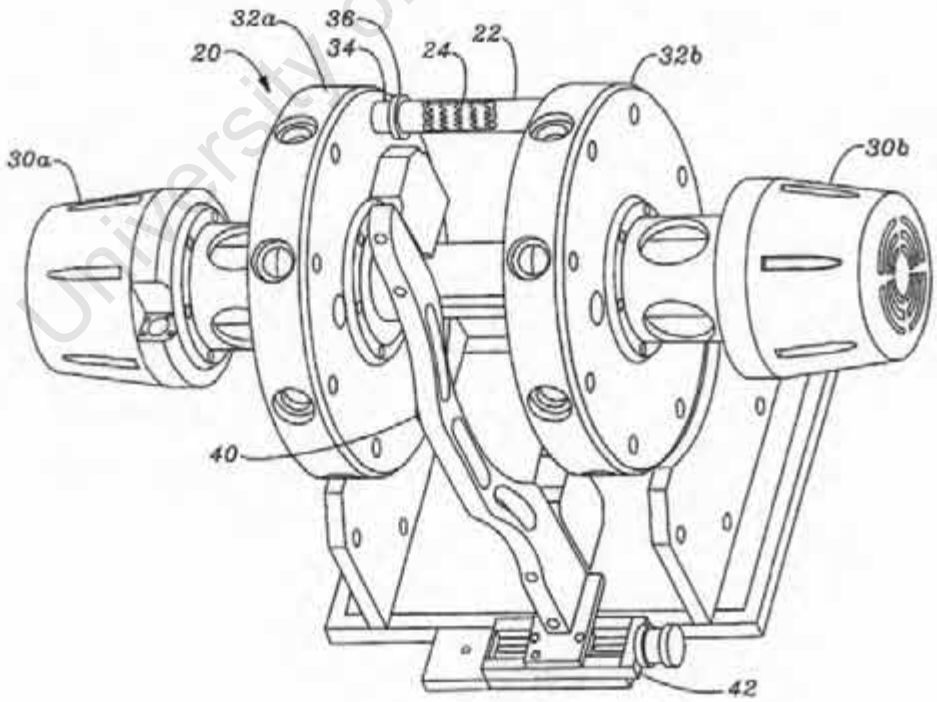

ELectroForce® Stent/Graft Series

Higher performance, greater precision, unmatched durability

Bifurcated 9120-4B
Stent/Graft Test Instrument

Ten Year FDA in-vitro tests take only weeks with the 9100 Series Stent/Graft Test Instrument. Using a patented high-bandwidth, low distortion linear actuator from Bose®, the instrument reduces test time and provides multi-billion cycle reliability.

The Stent/Graft Test System verifies the fatigue life of intravascular prostheses such as stents, grafts, occluders and shunts under simulated physiological strain conditions. The system consists of mock arteries, closed-loop pulsatile pumps and manifolds and a laser measurement system. It is operated to achieve mock artery diametric displacements that are equivalent to in-vivo conditions. The patented direct measurement approach allows you to map the diametric displacement at various locations along each stent length, thereby ensuring that the desired conditions are met. No other test instrument offers this capability.

The WinTest® Control System offers real-time control and integrated data acquisition. Amplitudes and frequency are easily adjusted throughout the test without the need for stopping. Built-in monitoring software also looks for unexpected conditions and automatically stops the test if trouble is detected. A UPS power back-up system ensures a smooth shut-down in the event of a power failure.

Our application engineers are available to assist you with your specific test needs. They can configure systems for testing special geometries, such as bifurcations, aneurysms and more. Contact us with your particular device requirements.

System Features

- Accelerated performance to 60 Hz and above*
- 6, 8, 12 or 20 mock arteries for testing multiple specimens
- 2.5 mm to 44 mm standard device range
- Twin Bose linear actuator driven pump assemblies for accelerated frequency and multi-billion cycle reliability
- Direct diametric distention measurement via laser micrometer
- Volumetric displacement control and pressure readout provide precision and flexibility
- WinTest advanced control algorithms mean real-time system adjustment without stopping the test. The test is continually monitored and controlled within preset limits.
- Digital temperature control
- Uninterruptible Power Supply (UPS) to ensure smooth system shutdown in the event of power loss
- Configurations available for testing complex geometries such as bifurcations and aneurysms

* Depends on specimen and tube configurations

The "heart" of the system is the Bose high performance linear actuators. Featuring performance to several hundred Hertz and tested to over 10 billion cycles, the capabilities of this motor are unprecedented. When combined with the WinTest Control System, diametric displacement amplitudes are easily created and adjusted in real-time without the need to stop and restart the test.

EnduraTEC
Life Enhancing Test Solutions

BOSE
Technology Alliance

APPENDIX E

Final Design Calculations

E1 – Fluid Pressurization Calculations

Theoretical Calculations

	Symbol	Value	Unit	Equation
Number of Tubes	N	14		
Tube I.D.	d_1	3	mm	
Tube Length	L_t	40	mm	
Non-Compliant Tube Length	L_{nc}	185	mm	
Piston Diameter	D_p	40	mm	
Gasket Diameter	D_g	84	mm	
Stroke	S	1.5	mm	
Gasket Angle	θ	0.07	rad	$\text{atan}(S / (D_g/2 - D_p/2)$
Cone Projected Height	h_c	2.86	mm	$(D_g/2) \times (\tan\theta)$
Back Pressure Disc Motion				
Back Pressure Stroke Volume Change	dV_{bp}	1884.96	mm^3	$\pi \times (D_p/2)^2 \times S$
Tube I.D.	d_2	3.64	mm	$\sqrt{[(4 \times dV_{bp}) / (\pi \times N \times L_t) + d_1^2]}$
Tube I.D. change	%	21.50	%	$(d_2/d_1 \times 100) - 100$
Conical Gasket Motion				
Conical Stroke Volume Change	dV_c	4718.67	mm^3	$(\pi/4) \times (d_2^2 - d_1^2) \times L$
Tube I.D.	d_2	4.44	mm	$\sqrt{[(4 \times dV_c) / (\pi \times N \times L_t) + d_1^2]}$
Tube I.D. change	%	48.06	%	$(d_2/d_1 \times 100) - 100$
Air Content	%	10.00	%	
Cavity Volume	V_{cav}	467864.80	mm^3	
Air Volume	V_{air}	46786.48	mm^3	
Initial Pressure	P_i	101.00	kPa	
Back Pressure Disc Motion				
Back Pressure Stroke Volume Change	dV_{bp}	1884.96	mm^3	$\pi \times (D_p/2)^2 \times S$
Pressurized Air Volume	V_{p_air}	44901.52	mm^3	$V_{air} - dV_{bp}$
Final Pressure	P_f	105.24		
Pressure Gradient	dP	4.24	kPa	
Conical Gasket Motion				
Conical Stroke Volume Change	dV_c	4718.67	mm^3	$(\pi/4) \times (d_2^2 - d_1^2) \times L$
Pressurized Air Volume	V_{p_air}	42067.81	mm^3	$V_{air} - dV_c$
Final Pressure	P_f	112.33		
Pressure Gradient	dP	11.33	kPa	
Pressure		200.00	kPa	
Tube Inner Area		5277.88	mm^2	
Force		1055.58	N	
		107.60	kg	

Experimental Results obtained

Stroke (mm)			0.36	0.5	1.5
10 Hz	Voltage (V)	Max	1.24	1.25	1.7
		Min	1.01	0.99	0.93
		Gradient	0.23	0.26	0.77
	Pressure (kPa)	Max	27.62376	28.61386	73.16832
		Min	4.851485	2.871287	-3.06931
		Gradient	22.77228	25.74257	76.23762
30 Hz	Voltage (V)	Max	1.69	2.12	5
		Min	0.85	0.77	0.61
		Gradient	0.84	1.35	4.39
	Pressure (kPa)	Max	72.17822	114.7525	399.901
		Min	-10.9901	-18.9109	-34.7525
		Gradient	83.16832	133.6634	434.6535
40 Hz	Voltage (V)	Max	3.06	3.3	5
		Min	0.55	0.57	0.45
		Gradient	2.51	2.73	4.55
	Pressure (kPa)	Max	207.8218	231.5842	399.901
		Min	-40.6931	-38.7129	-50.5941
		Gradient	248.5149	270.297	450.495
50 Hz	Voltage (V)	Max	2.2	3.46	5
		Min	0.61	0.41	0.4
		Gradient	1.59	3.05	4.6
	Pressure (kPa)	Max	122.6733	247.4257	399.901
		Min	-34.7525	-54.5545	-55.5446
		Gradient	157.4257	301.9802	455.4455
55 Hz	Voltage (V)	Max	1.73	3.3	5
		Min	0.71	0.43	0.37
		Gradient	1.02	2.87	4.63
	Pressure (kPa)	Max	76.13861	231.5842	399.901
		Min	-24.8515	-52.5743	-58.5149
		Gradient	100.9901	284.1584	458.4158
60 Hz	Voltage (V)	Max	1.38	3.2	4.29
		Min	0.85	0.42	0.41
		Gradient	0.53	2.78	3.88
	Pressure (kPa)	Max	41.48515	221.6832	329.604
		Min	-10.9901	-53.5644	-54.5545
		Gradient	52.47525	275.2475	384.1584

E2 – Vessel Bending Calculations

Start Tube Position											
Significant Data			x	Sine	f'(x)	f''(x)	1+f'^2	√(1+f'(x)^2)	Integrate	Curvature	Radius
x-total	39	mm	0	0.000	0.000	0.052	1.000	1.000		0.052	19.198
x-mid point	19.5	mm	5	0.617	0.233	0.036	1.054	1.027	0.103	0.033	30.005
Height	4.01	mm	10	2.088	0.323	-0.002	1.104	1.051	0.105	-0.002	553.338
Whole pipe length	40	mm	15	3.509	0.214	-0.039	1.046	1.023	0.102	-0.036	27.437
Start Curvature	0.521	cm^{-1}	20	4.007	-0.026	-0.052	1.001	1.000	0.100	-0.052	19.280
			25	3.276	-0.250	-0.033	1.063	1.031	0.103	-0.030	33.256
			30	1.765	-0.321	0.006	1.103	1.050	0.105	0.005	184.507
			35	0.402	-0.194	0.042	1.038	1.019	0.102	0.039	25.386
			39	0.000	0.000	0.052	1.000	1.000	0.100	0.052	19.198

End Tube Position											
Significant Data			x	Sine	f'(x)	f''(x)	1+f'^2	√(1+f'(x)^2)	Integrate	Curvature	Radius
x-total	37	mm	0	0.000	0.000	0.100	1.000	1.000		0.100	10.043
x-mid point	18.5	mm	5	1.172	0.440	0.066	1.194	1.093	0.109	0.050	19.826
Height	6.91	mm	10	3.891	0.582	-0.013	1.338	1.157	0.116	-0.008	122.408
Whole pipe length	40	mm	15	6.314	0.328	-0.082	1.108	1.053	0.105	-0.071	14.134
End Curvature	0.996	cm^{-1}	20	6.794	-0.148	-0.096	1.022	1.011	0.101	-0.093	10.719
			25	5.007	-0.524	-0.045	1.274	1.129	0.113	-0.031	32.083
			30	2.165	-0.544	0.037	1.296	1.138	0.114	0.025	39.741
			35	0.197	-0.195	0.094	1.038	1.019	0.102	0.089	11.267
			37	0.000	0.000	0.100	1.000	1.000	0.100	0.100	10.043

Total Flexing	0.47	cm^{-1}

APPENDIX F

Final Design Detail Drawings

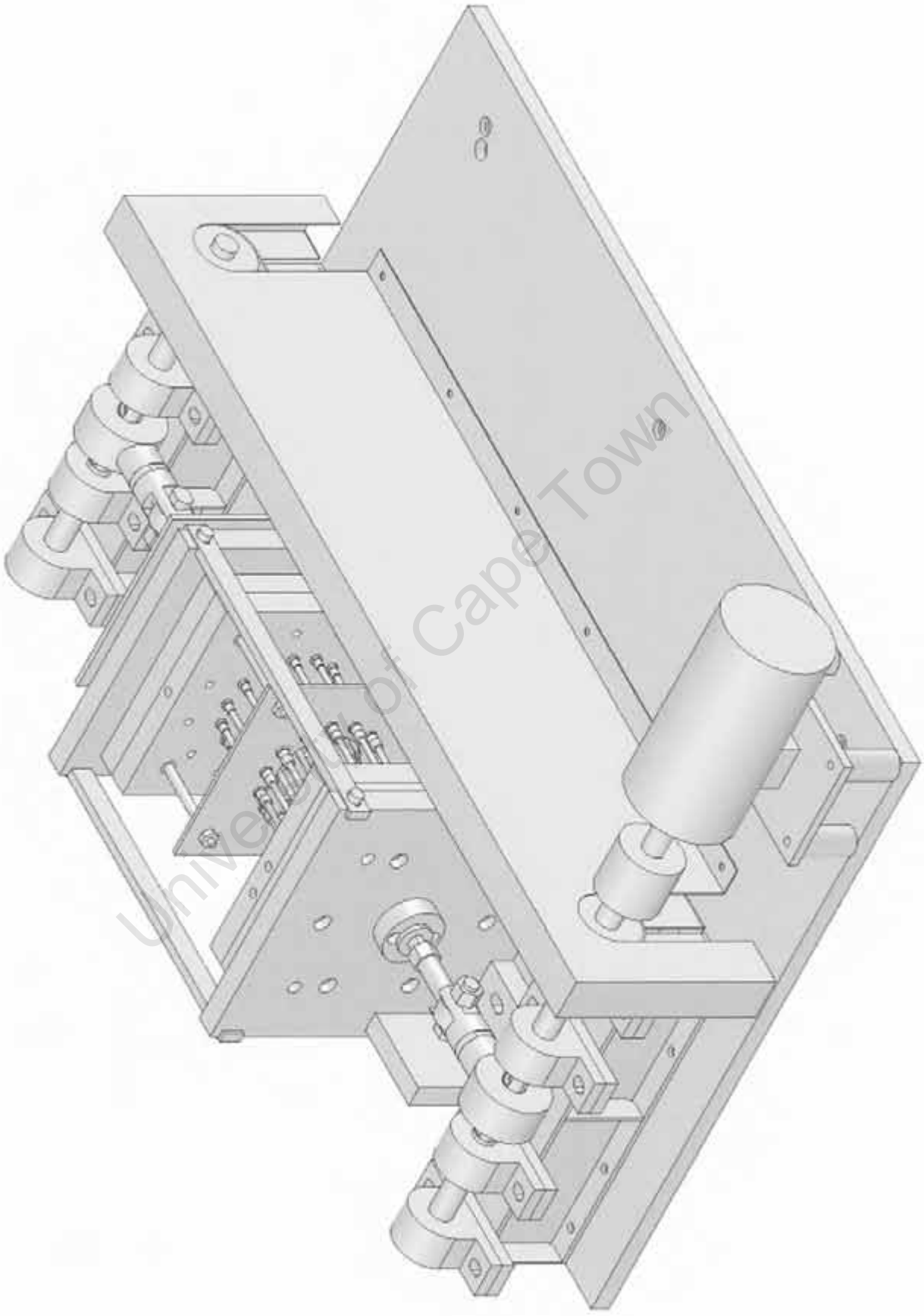

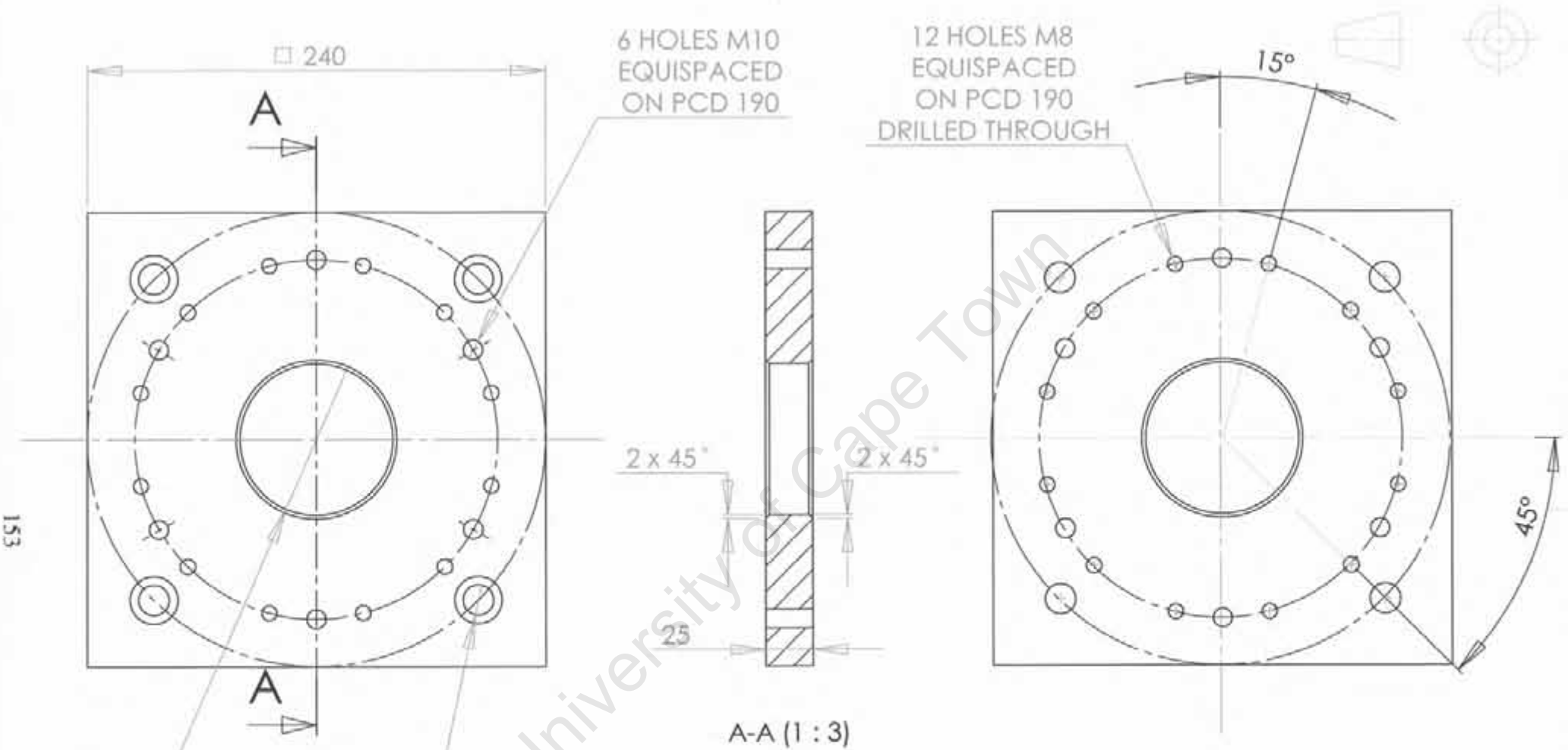

1	1	PISTON END OUTER PLATE			ALUMINIUM	240 x 240 x 25
ITEM	QUANTITY	DESCRIPTION			MATERIAL	SPECIFICATION
UNLESS OTHERWISE SPECIFIED: DIMENSIONS ARE IN MILLIMETERS REMOVE ALL SHARP EDGES TOLERANCES: LINEAR: ± 0.1mm ANGULAR: ± 1°		A4	NAME	DATE	TITLE: PISTON END OUTER PLATE	
		DRAWN	MARTIN HOOLE	28/09/06		
		CHECKED	MARTIN HOOLE	28/09/06	DWG NO:	FATIGUE - F - 01
		SCALE:1:3			SHEET 1 OF 1	

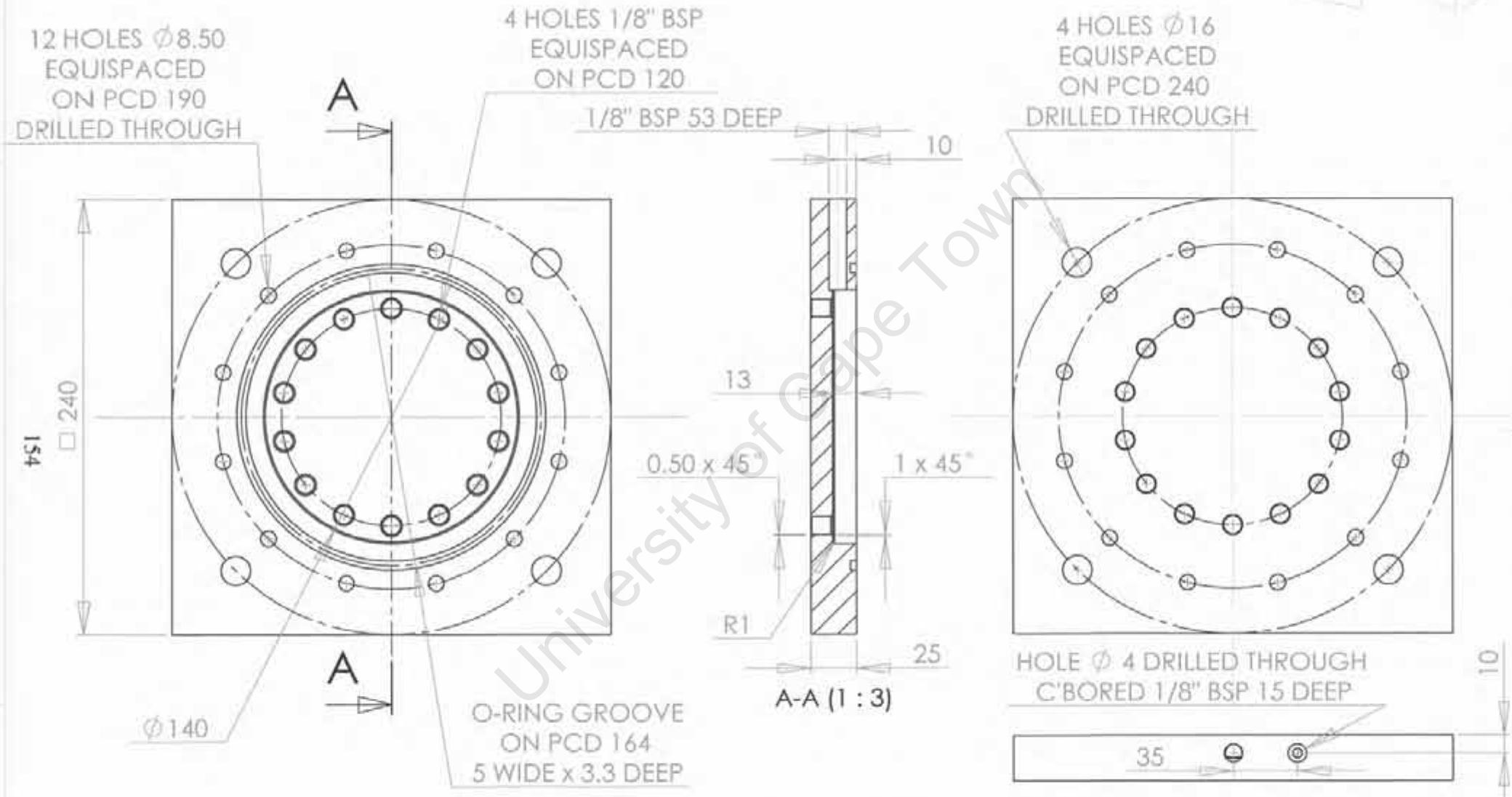

ITEM	QUANTITY	DESCRIPTION	MATERIAL	SPECIFICATION
1	1	BEND END INNER PLATE	ALUMINIUM	240 x 240 x 25

UNLESS OTHERWISE SPECIFIED:
DIMENSIONS ARE IN MILLIMETERS
REMOVE ALL SHARP EDGES
TOLERANCES:
LINEAR: ± 0.1mm
ANGULAR: ± 1°

A4	NAME	DATE
DRAWN	MARTIN HOOLE	28/09/06
CHECKED	MARTIN HOOLE	28/09/06
SCALE:1:3		

TITLE: BEND END INNER PLATE

DWG NO: FATIGUE - F - 02

SHEET 1 OF 1

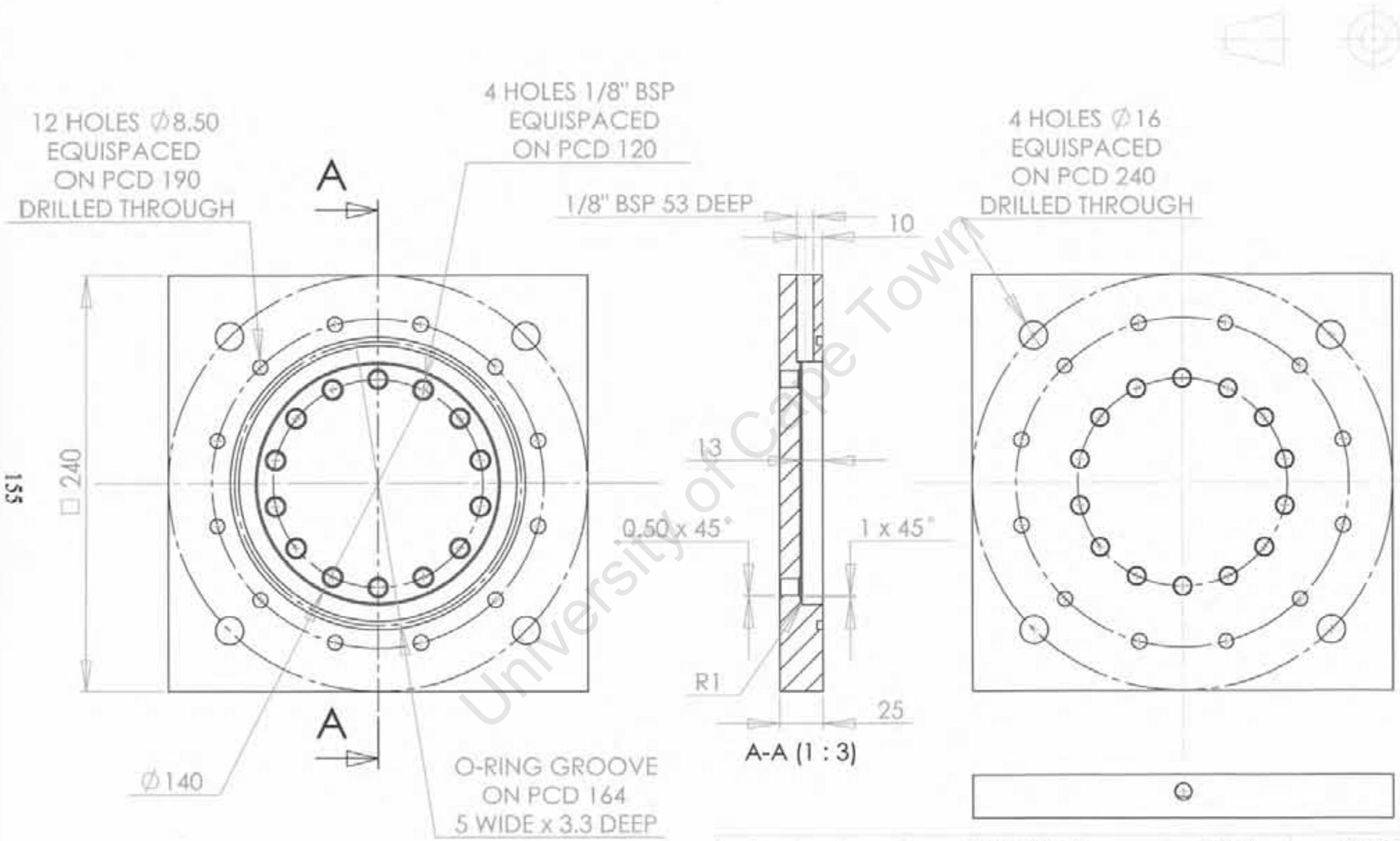

155

1	1	PISTON END INNER PLATE			ALUMINIUM	240 x 240 x 25
ITEM	QUANTITY	DESCRIPTION			MATERIAL	SPECIFICATION

UNLESS OTHERWISE SPECIFIED:
DIMENSIONS ARE IN MILLIMETERS
REMOVE ALL SHARP EDGES
TOLERANCES:
LINEAR: ± 0.1mm
ANGULAR: ± 1°

A4	NAME	DATE
DRAWN	MARTIN HOOLE	28/09/06
CHECKED	MARTIN HOOLE	28/09/06
SCALE:1:3		

TITLE: PISTON END INNER PLATE

DWG NO: FATIGUE - F - 03

SHEET 1 OF 1

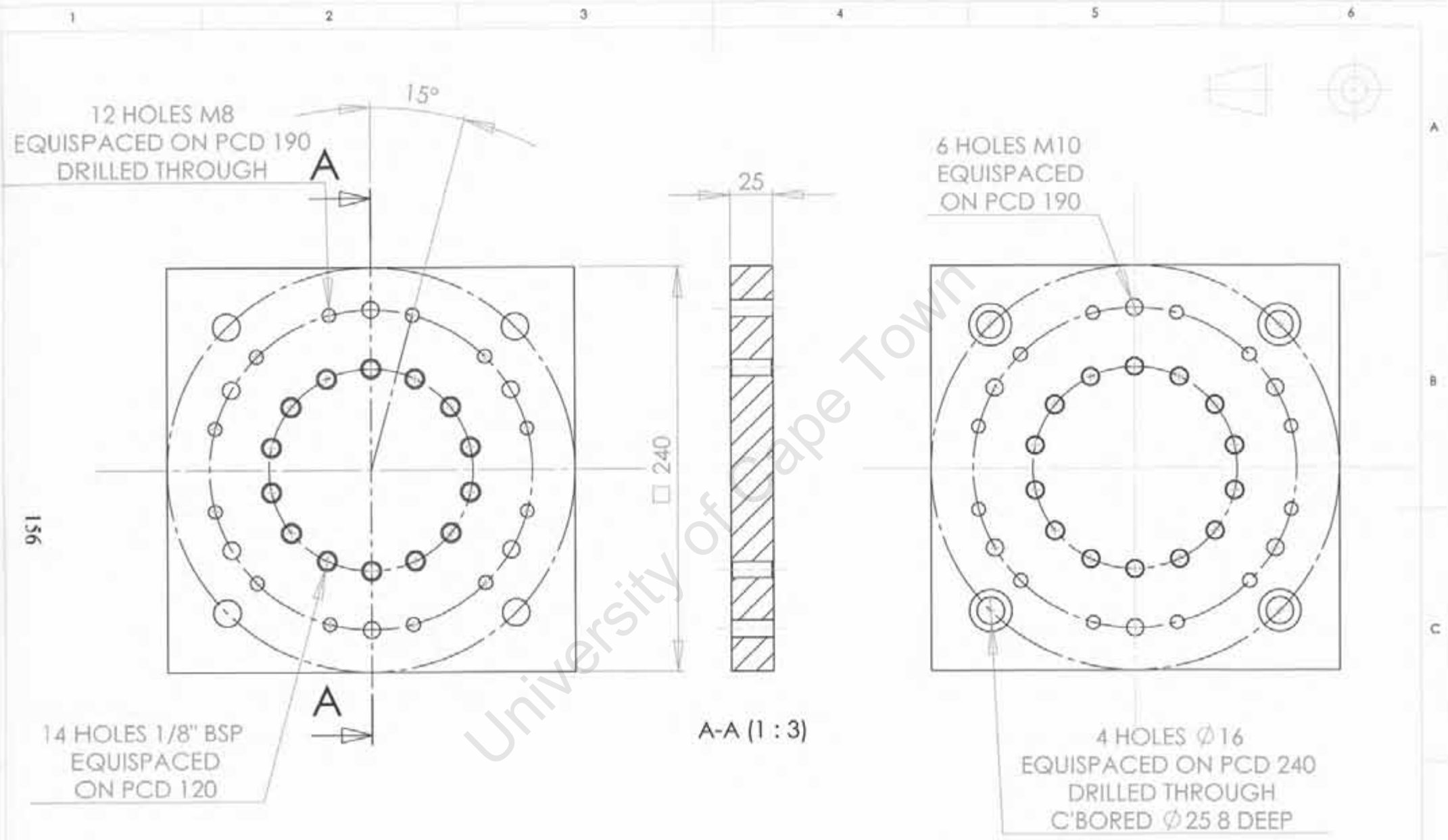

1	1	BEND END OUTER PLATE			ALUMINIUM	240 x 240 x 25
ITEM	QUANTITY	DESCRIPTION			MATERIAL	SPECIFICATION
UNLESS OTHERWISE SPECIFIED: DIMENSIONS ARE IN MILLIMETERS REMOVE ALL SHARP EDGES TOLERANCES: LINEAR: ± 0.1mm ANGULAR: ± 1°		A4	NAME	DATE	TITLE:	BEND END OUTER PLATE
		DRAWN	MARTIN HOOLE	28/09/06		
		CHECKED	MARTIN HOOLE	28/09/06	DWG NO:	FATIGUE - F - 04
		SCALE:1:3			SHEET 1 OF 1	

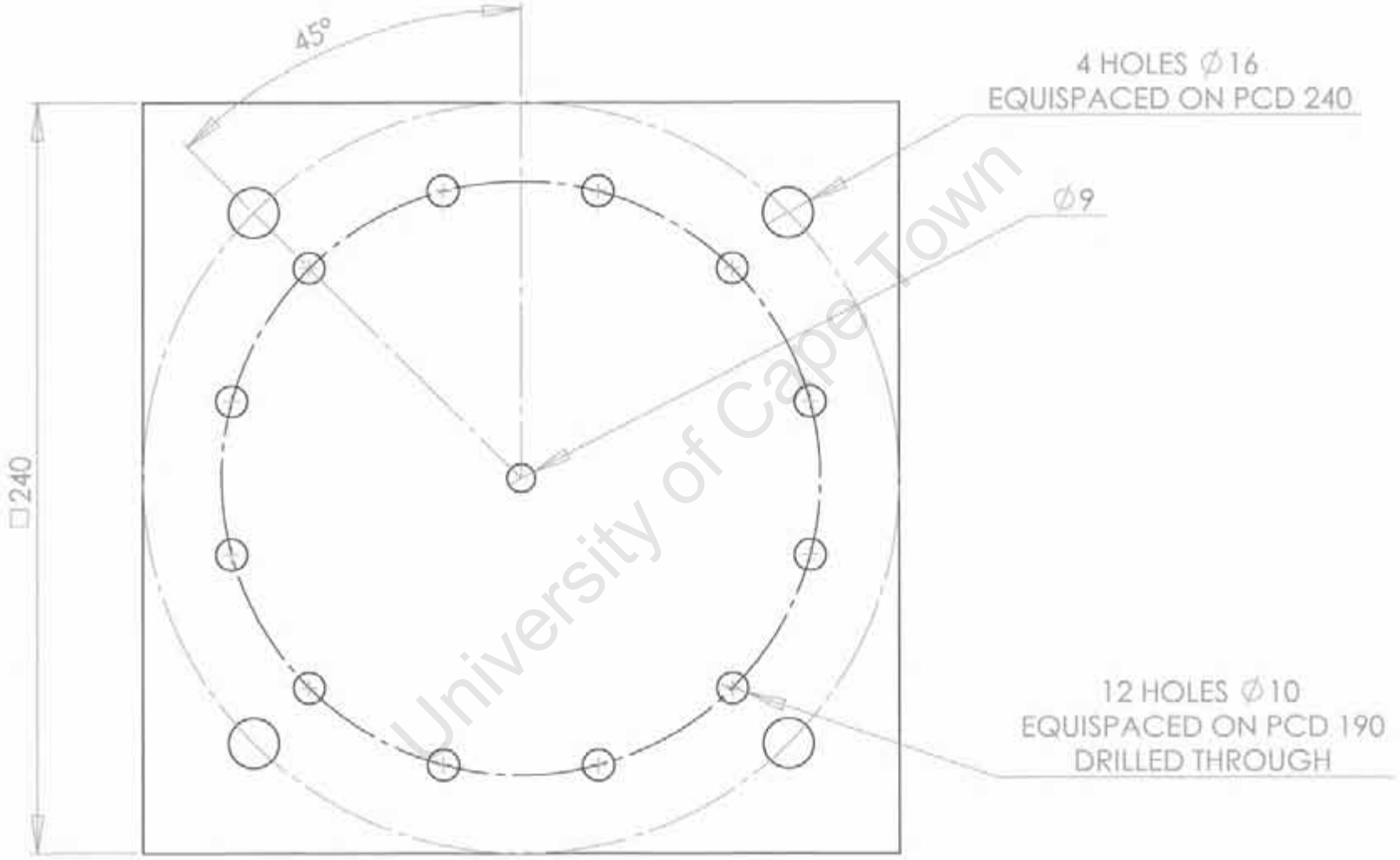

157

ITEM	QUANTITY	DESCRIPTION	MATERIAL	SPECIFICATION
1	1	PISTON END GASKET	REINFORCED GASKET	Ø220 x 3

UNLESS OTHERWISE SPECIFIED:
DIMENSIONS ARE IN MILLIMETERS
REMOVE ALL SHARP EDGES
TOLERANCES:
LINEAR: ± 0.1mm
ANGULAR: ± 1°

A4	NAME	DATE
DRAWN	MARTIN HOOLE	28/09/06
CHECKED	MARTIN HOOLE	28/09/06
SCALE:1:2		

TITLE: PISTON END GASKET

DWG NO: FATIGUE - F - 05

SHEET 1 OF 1

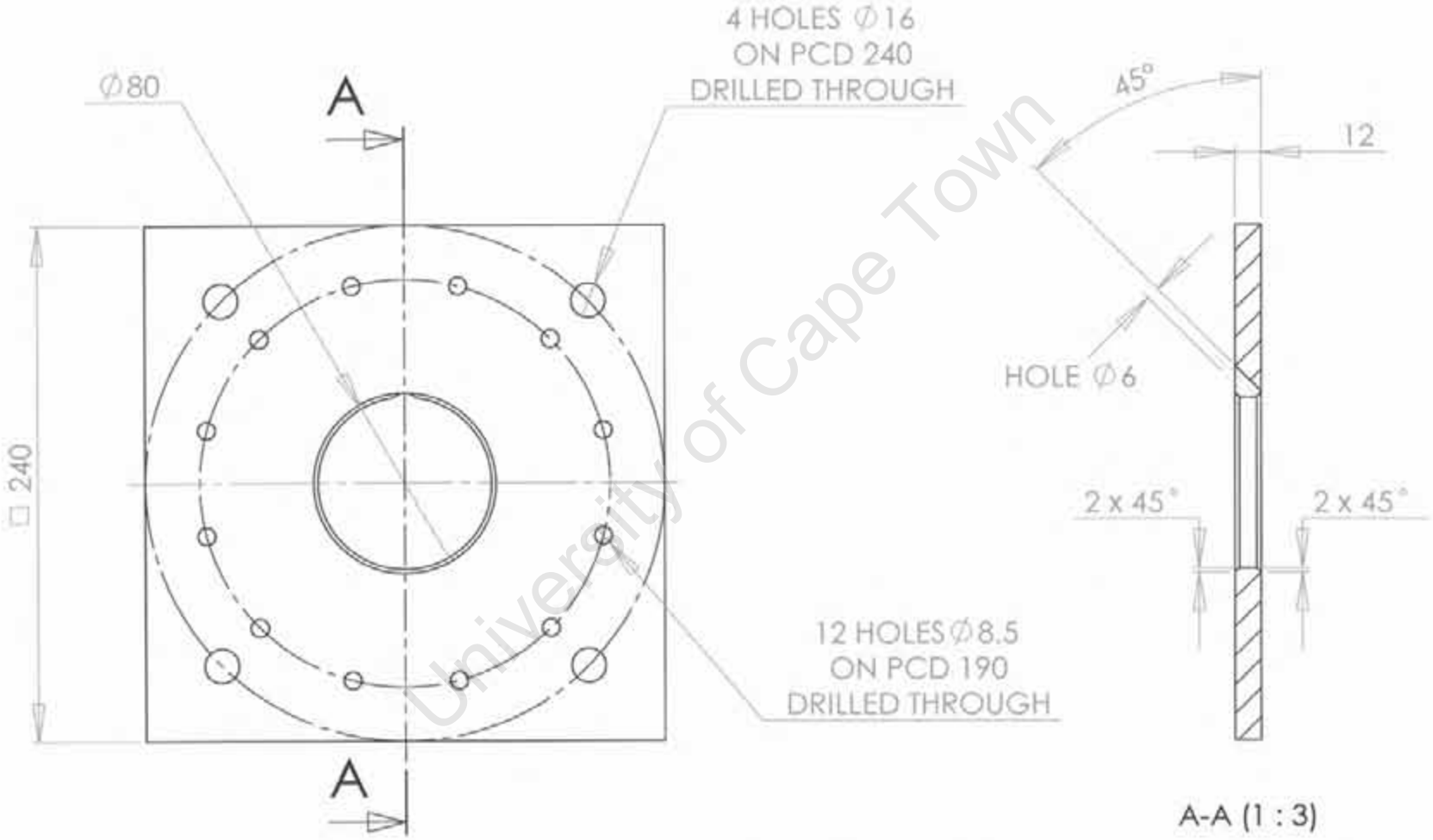

A-A (1 : 3)

158

ITEM	QUANTITY	DESCRIPTION	MATERIAL	SPECIFICATION
1	1	PISTON END SPACER	ALUMINIUM	240 x 240 x 12

		NAME	DATE
A4	DRAWN	MARTIN HOOLE	28/09/06
	CHECKED	MARTIN HOOLE	28/09/06
	SCALE: 1:3		

UNLESS OTHERWISE SPECIFIED:
DIMENSIONS ARE IN MILLIMETERS
REMOVE ALL SHARP EDGES
TOLERANCES:
LINEAR: ± 0.1mm
ANGULAR: ± 1°

TITLE: PISTON END SPACER

DWG NO: FATIGUE - F - 06

SHEET 1 OF 1

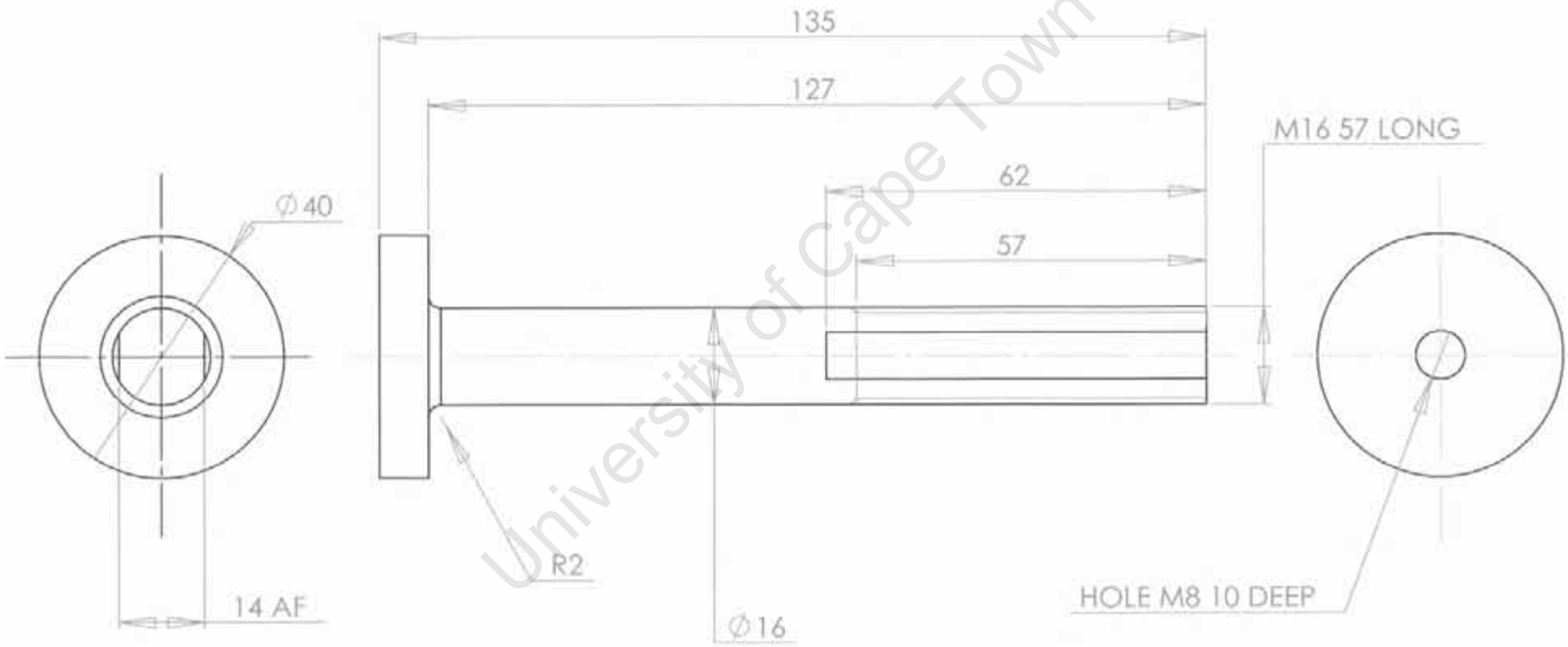

1	1	PISTON END ARM			V155	Ø 40 x 135
ITEM	QUANTITY	DESCRIPTION			MATERIAL	SPECIFICATION
UNLESS OTHERWISE SPECIFIED: DIMENSIONS ARE IN MILLIMETERS REMOVE ALL SHARP EDGES TOLERANCES: LINEAR: ± 0.1mm ANGULAR: ± 1°		A4	NAME	DATE	TITLE:	PISTON END ARM
		DRAWN	MARTIN HOOLE	28/09/06		
		CHECKED	MARTIN HOOLE	28/09/06	DWG NO:	FATIGUE - F - 07
		SCALE:1:1			SHEET 1 OF 1	

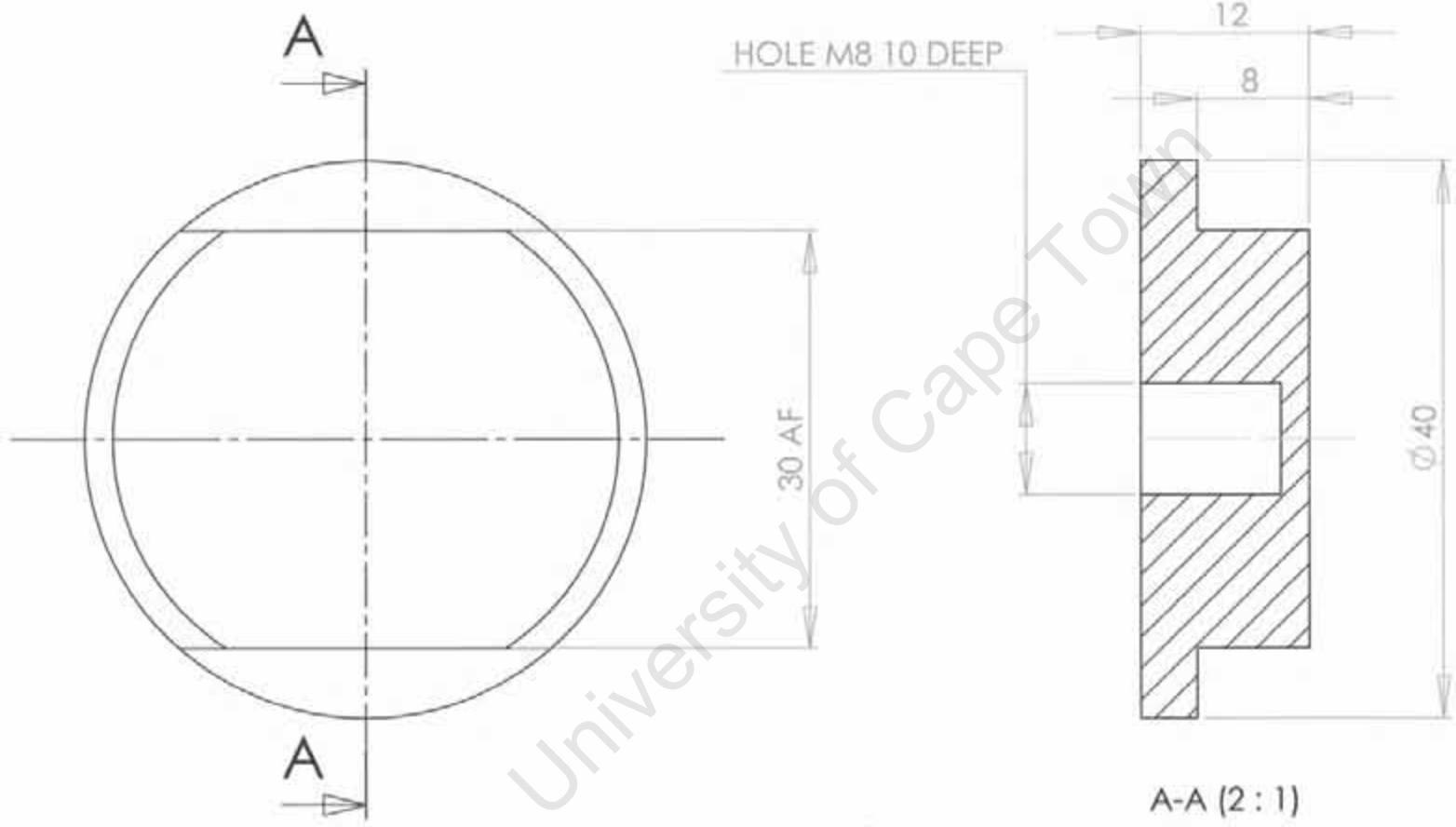

A-A (2 : 1)

1	1	GASKET INNER DISC			ST. STEEL	Ø 40 x 10
ITEM	QUANTITY	DESCRIPTION			MATERIAL	SPECIFICATION
UNLESS OTHERWISE SPECIFIED: DIMENSIONS ARE IN MILLIMETERS REMOVE ALL SHARP EDGES TOLERANCES: LINEAR: ± 0.1mm ANGULAR: ± 1°		A4	NAME	DATE	TITLE:	GASKET INNER DISC
		DRAWN	MARTIN HOOLE	28/09/06		
		CHECKED	MARTIN HOOLE	28/09/06	DWG NO:	FATIGUE - F - 08
		SCALE:2:1			SHEET 1 OF 1	

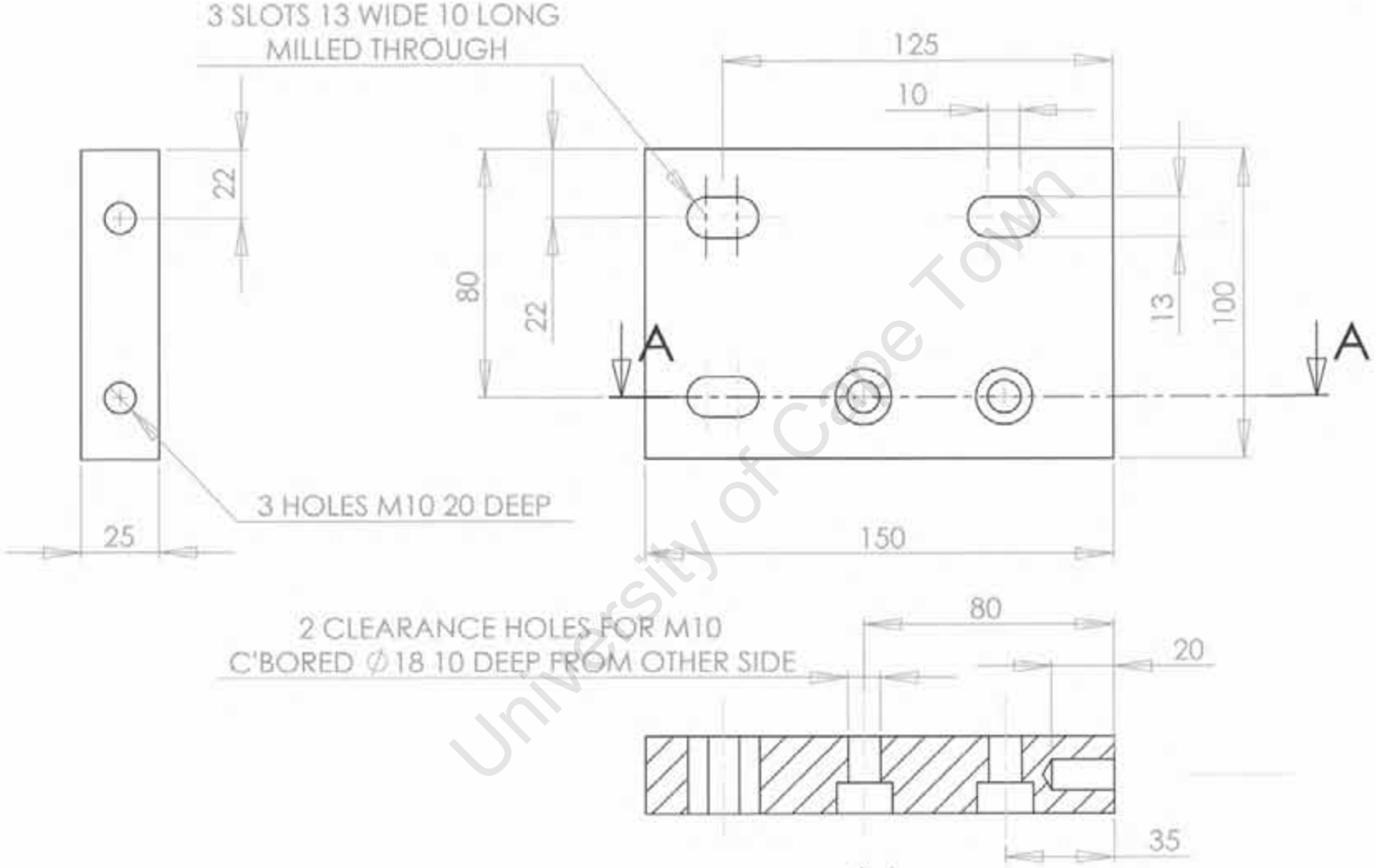

1	2	LEFT ANGLE PLATE BASE			MILD STEEL	200 x 100 x 25
ITEM	QUANTITY	DESCRIPTION			MATERIAL	SPECIFICATION
UNLESS OTHERWISE SPECIFIED: DIMENSIONS ARE IN MILLIMETERS REMOVE ALL SHARP EDGES TOLERANCES: LINEAR: ± 0.1mm ANGULAR: ± 1°		A4	NAME	DATE	TITLE: LEFT ANGLE PLATE BASE	
		DRAWN	MARTIN HOOLE	28/09/06		
		CHECKED	MARTIN HOOLE	28/09/06	DWG NO:	FATIGUE - F - 09
		SCALE:1:2			SHEET 1 OF 1	

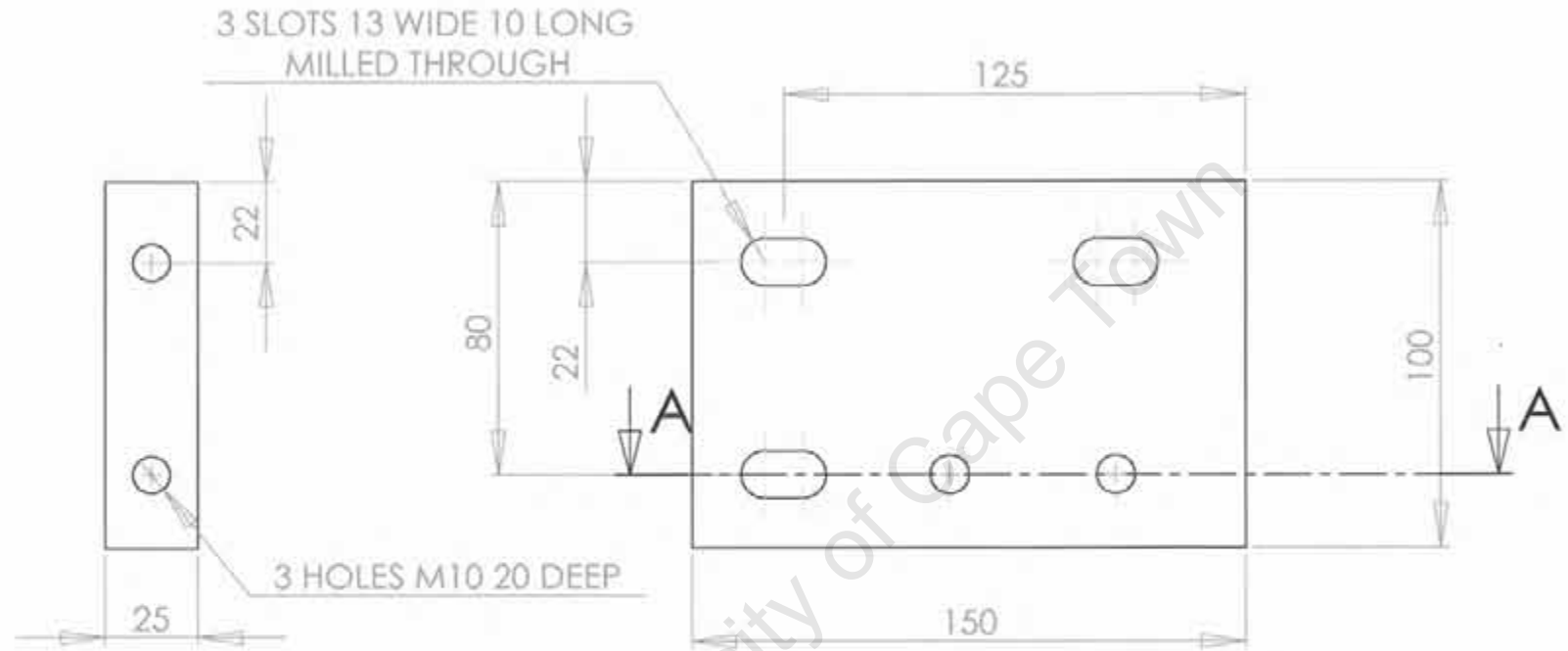

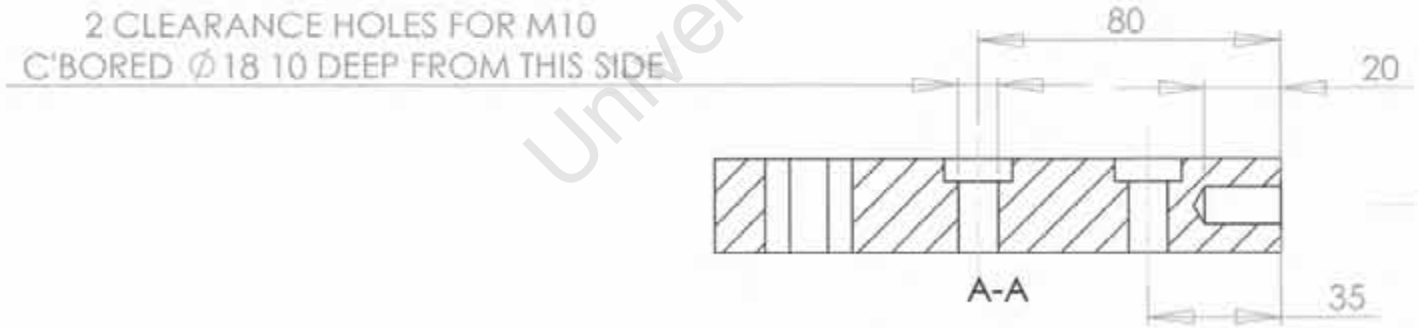

1	2	RIGHT ANGLE PLATE BASE			MILD STEEL	200 x 100 x 25
ITEM	QUANTITY	DESCRIPTION			MATERIAL	SPECIFICATION
UNLESS OTHERWISE SPECIFIED: DIMENSIONS ARE IN MILLIMETERS REMOVE ALL SHARP EDGES TOLERANCES: LINEAR: ± 0.1mm ANGULAR: ± 1°		A4	NAME	DATE	TITLE: RIGHT ANGLE PLATE BASE	
		DRAWN	MARTIN HOOLE	28/09/06		
		CHECKED	MARTIN HOOLE	28/09/06	DWG NO:	FATIGUE - F - 10
		SCALE:1/2			SHEET 1 OF 1	

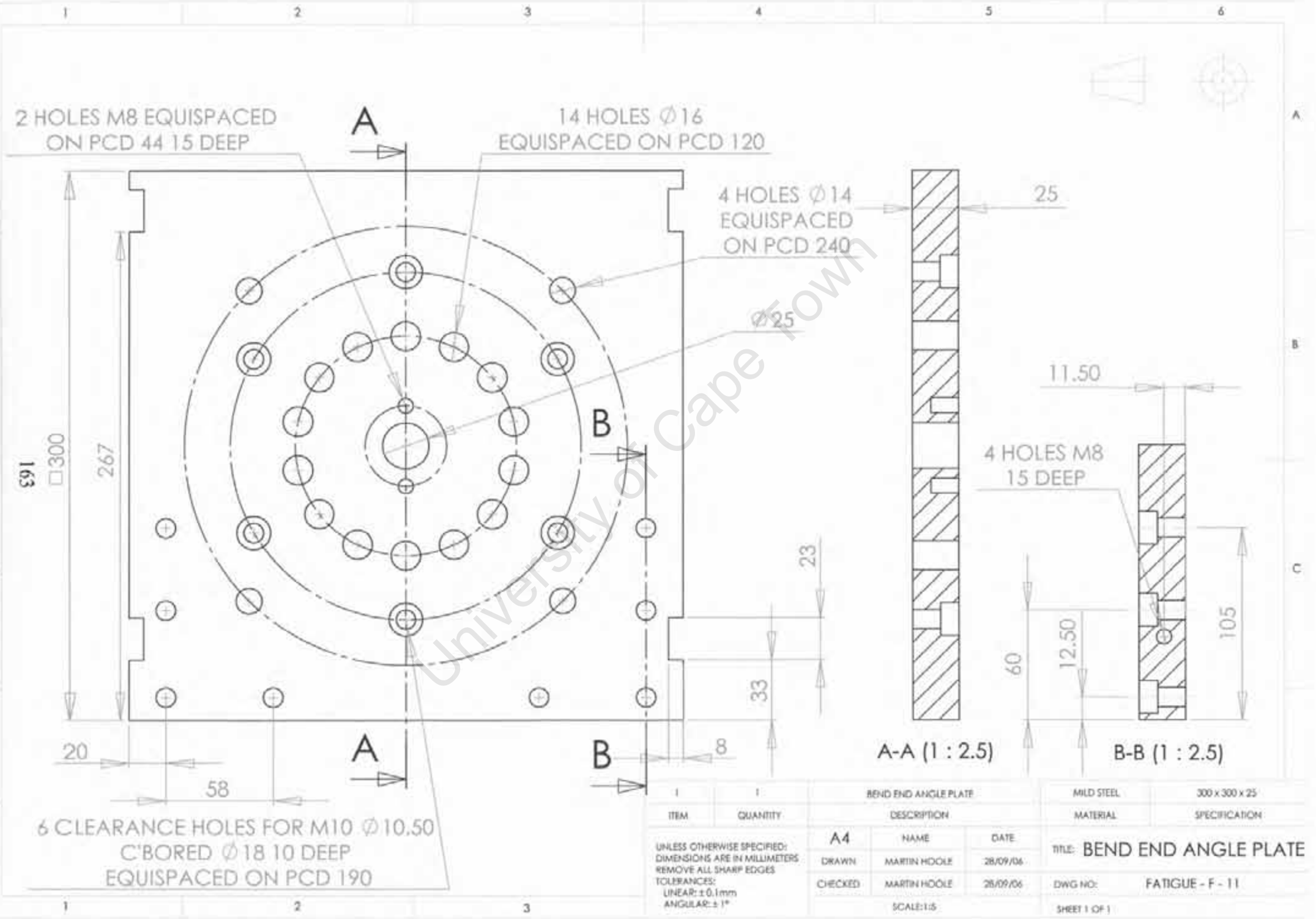

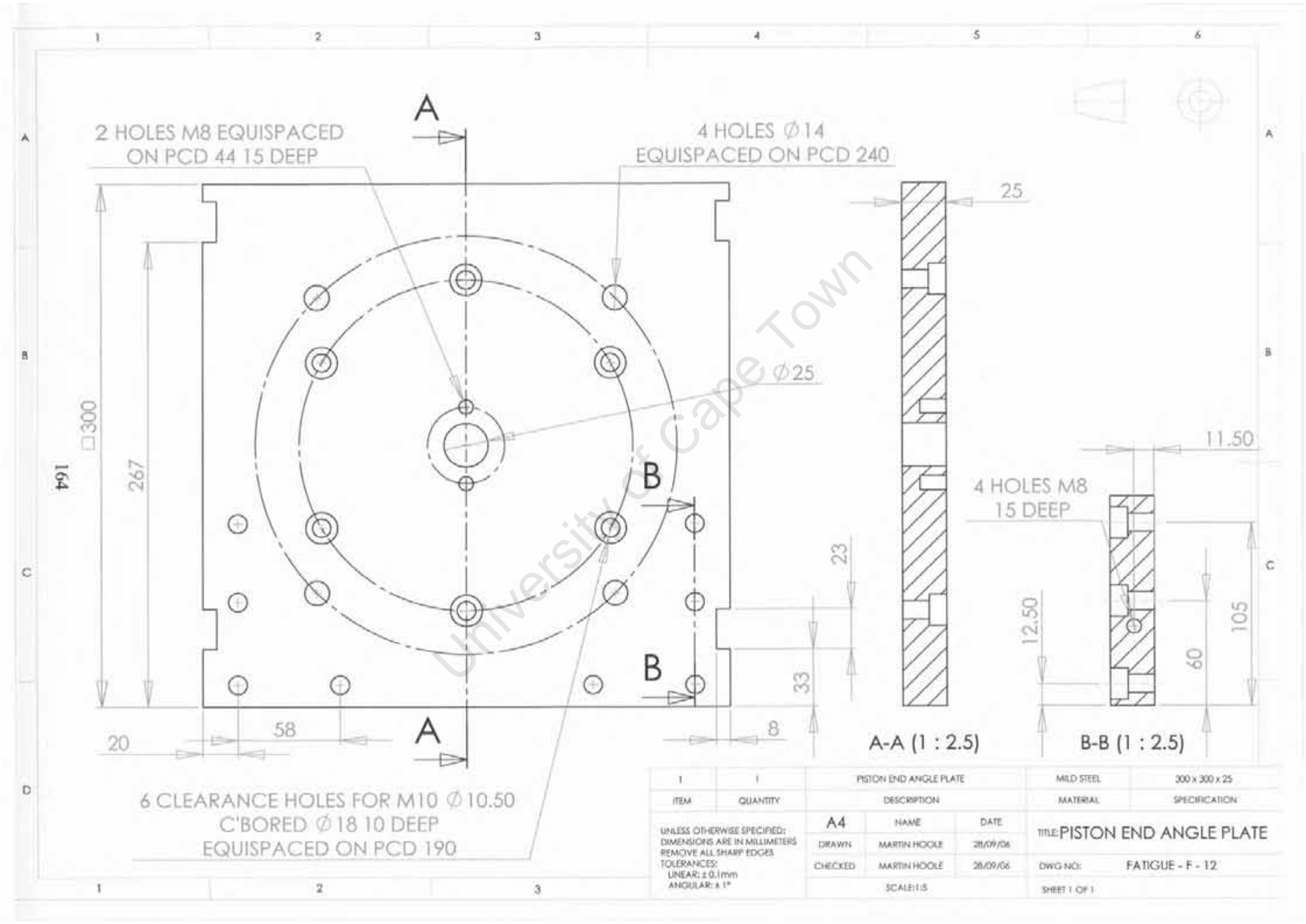

ITEM	QUANTITY	DESCRIPTION	MATERIAL	SPECIFICATION
1	1	PISTON END ANGLE PLATE	MILD STEEL	300 x 300 x 25

UNLESS OTHERWISE SPECIFIED:
DIMENSIONS ARE IN MILLIMETERS
REMOVE ALL SHARP EDGES
TOLERANCES:
LINEAR: ± 0.1mm
ANGULAR: ± 1°

A4	NAME	DATE
DRAWN	MARTIN HOOLE	28/09/06
CHECKED	MARTIN HOOLE	28/09/06

SCALE:1:5

TITLE: PISTON END ANGLE PLATE

DWG NO: FATIGUE - F - 12

SHEET 1 OF 1

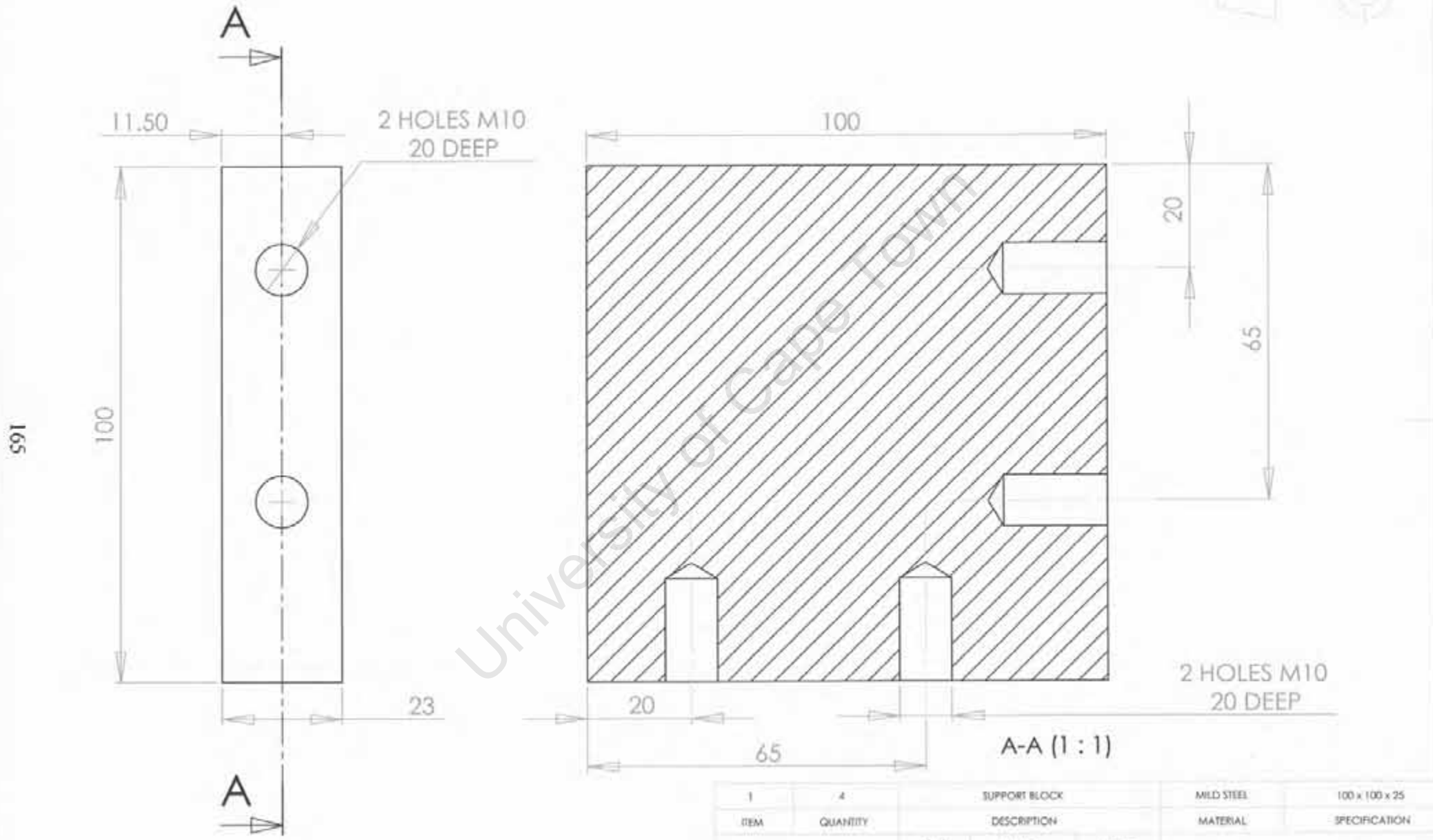

1	4	SUPPORT BLOCK			MILD STEEL	100 x 100 x 25
ITEM	QUANTITY	DESCRIPTION			MATERIAL	SPECIFICATION

UNLESS OTHERWISE SPECIFIED:
DIMENSIONS ARE IN MILLIMETERS
REMOVE ALL SHARP EDGES
TOLERANCES:
LINEAR: ± 0.1mm
ANGULAR: ± 1°

A4	NAME	DATE
DRAWN	MARTIN HOOLE	28/09/06
CHECKED	MARTIN HOOLE	28/09/06
SCALE:1:1		

TITLE: SUPPORT BLOCK

DWG NO: FATIGUE - F - 13

SHEET 1 OF 1

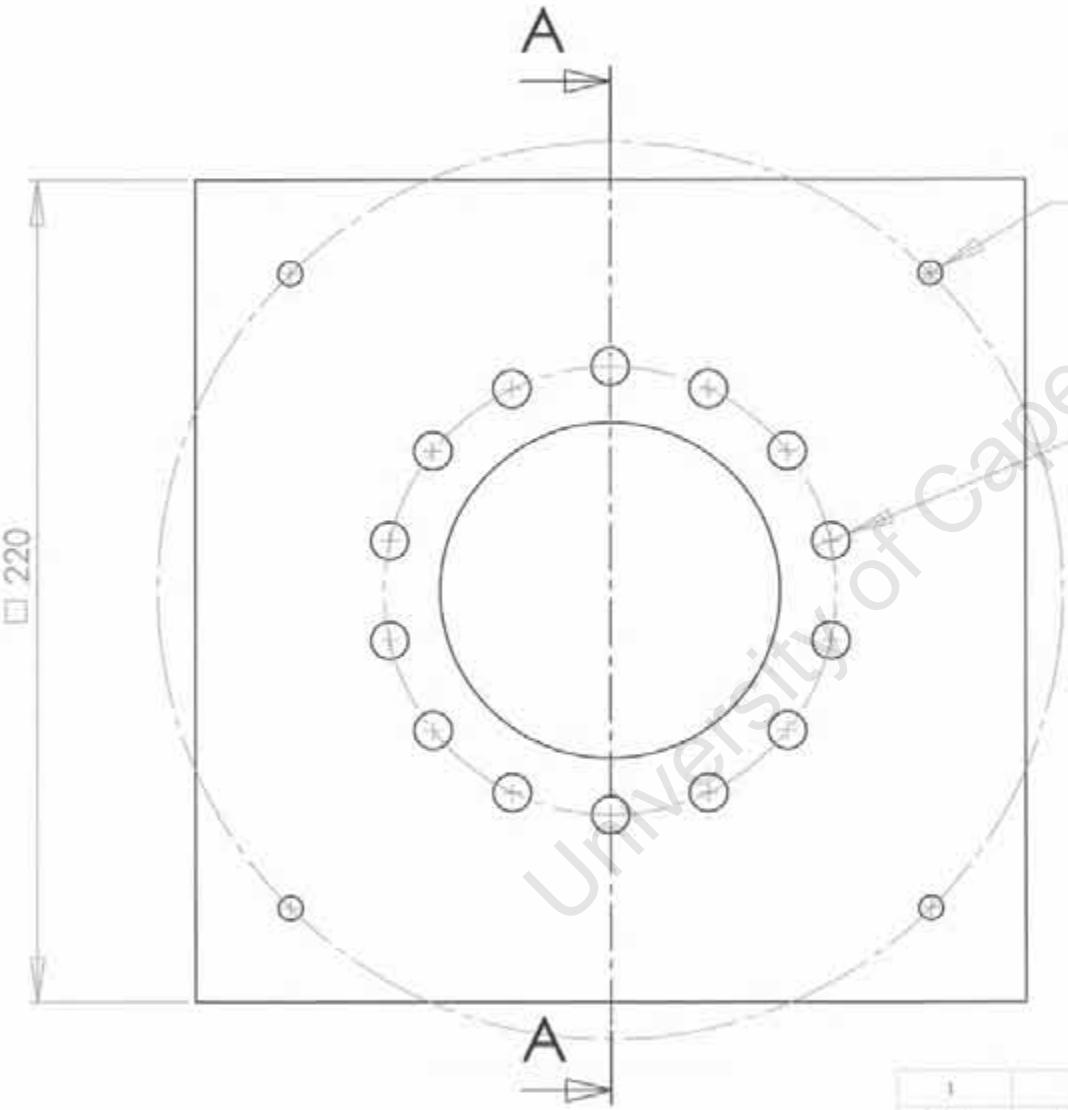

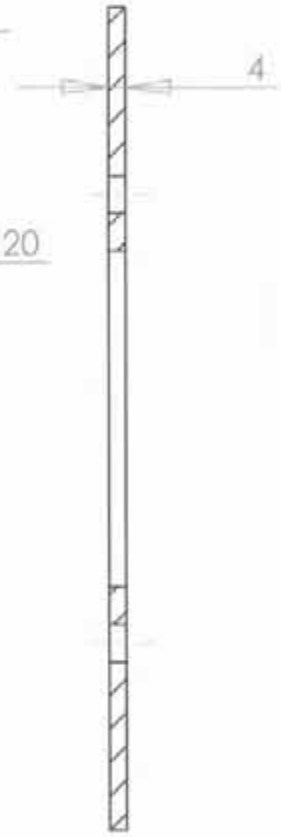

A-A (1 : 2)

1	1	BEND PLATE			ALUMINIUM	220 x 220 x 4
ITEM	QUANTITY	DESCRIPTION			MATERIAL	SPECIFICATION

UNLESS OTHERWISE SPECIFIED:
DIMENSIONS ARE IN MILLIMETERS
REMOVE ALL SHARP EDGES
TOLERANCES:
LINEAR: ± 0.1mm
ANGULAR: ± 1°

A4	NAME	DATE
DRAWN	MARTIN HOOLE	28/09/06
CHECKED	MARTIN HOOLE	28/09/06
SCALE:1:2		

TITLE: BEND PLATE

DWG NO: FATIGUE - F - 14

SHEET 1 OF 1

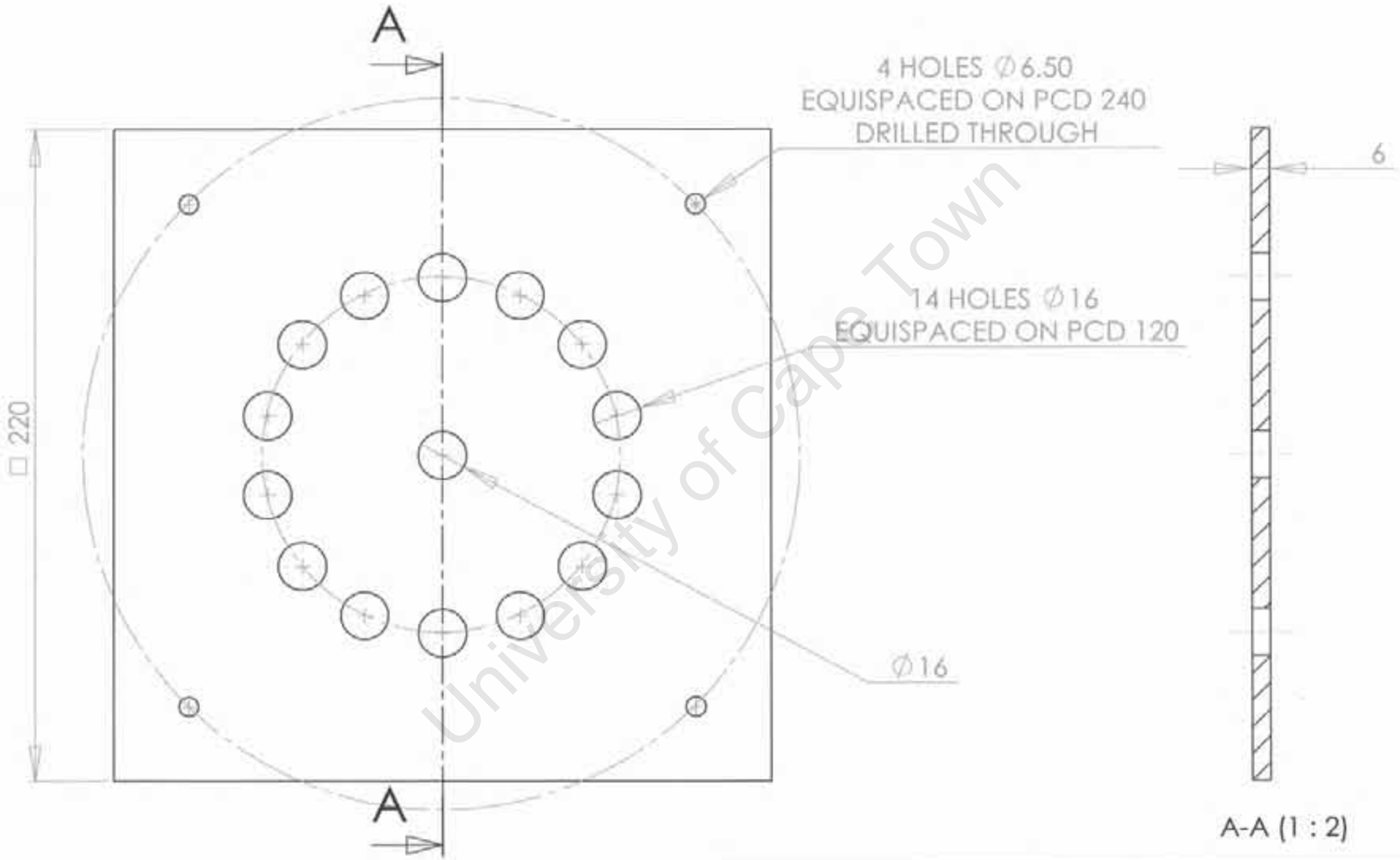

167

1	1	DRIVEN BEND PLATE			ALUMINIUM	220 x 220 x 6
ITEM	QUANTITY	DESCRIPTION			MATERIAL	SPECIFICATION
UNLESS OTHERWISE SPECIFIED: DIMENSIONS ARE IN MILLIMETERS REMOVE ALL SHARP EDGES TOLERANCES: LINEAR: ± 0.1mm ANGULAR: ± 1°		A4	NAME	DATE	TITLE:	DRIVEN BEND PLATE
		DRAWN	MARTIN HOOLE	28/09/06		
		CHECKED	MARTIN HOOLE	28/09/06	DWG NO:	FATIGUE - F - 15
		SCALE:1:2			SHEET 1 OF 1	

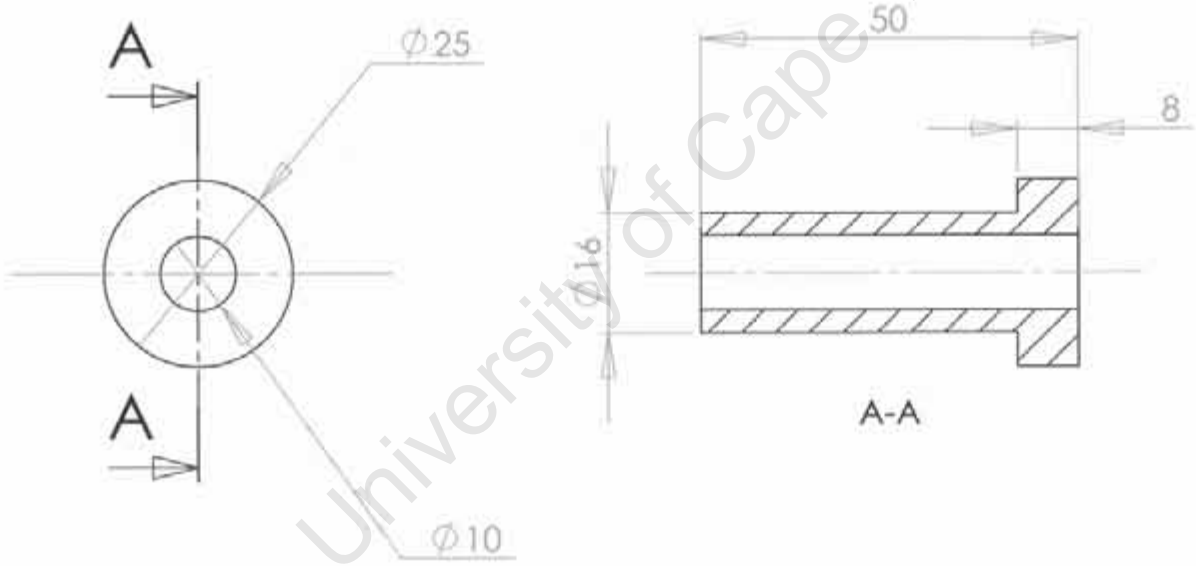

1	4	BEND END BUSH			BRASS BRONZE	Ø 30 x 50
ITEM	QUANTITY	DESCRIPTION			MATERIAL	SPECIFICATION
UNLESS OTHERWISE SPECIFIED: DIMENSIONS ARE IN MILLIMETERS REMOVE ALL SHARP EDGES TOLERANCES: LINEAR: ± 0.1mm ANGULAR: ± 1°		A4	NAME	DATE	TITLE:	BEND END BUSH
		DRAWN	MARTIN HOOLE	28/09/06		
		CHECKED	MARTIN HOOLE	28/09/06	DWG NO:	FATIGUE - F - 16
		SCALE:1:1			SHEET 1 OF 1	

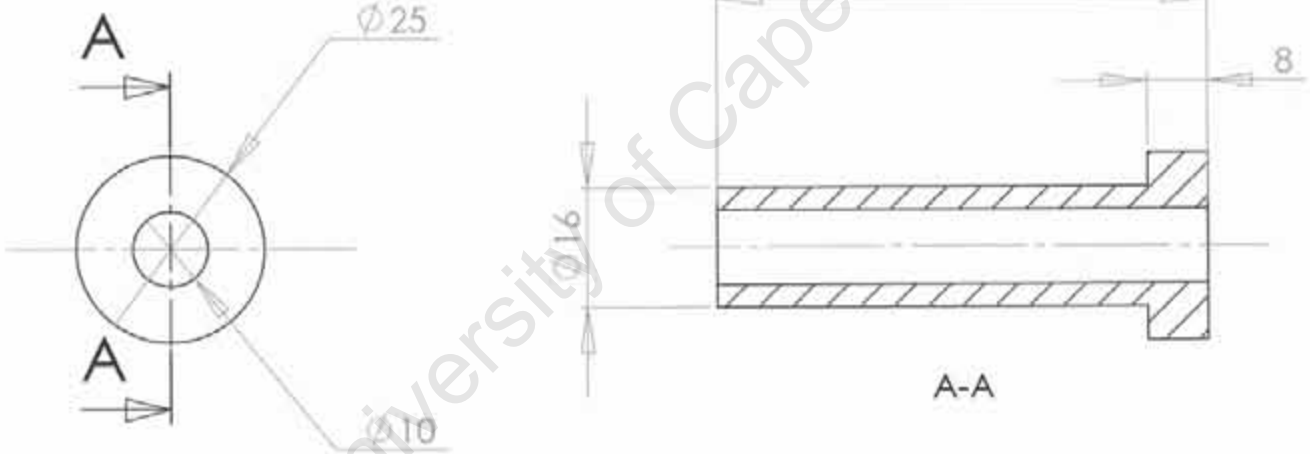

169

1	4	PISTON END BUSH			BRASS BRONZE	Ø 30 x 65
ITEM	QUANTITY	DESCRIPTION			MATERIAL	SPECIFICATION
UNLESS OTHERWISE SPECIFIED: DIMENSIONS ARE IN MILLIMETERS REMOVE ALL SHARP EDGES TOLERANCES: LINEAR: ± 0.1mm ANGULAR: ± 1°		A4	NAME	DATE	TITLE:	PISTON END BUSH
		DRAWN	MARTIN HOOLE	28/09/06		
		CHECKED	MARTIN HOOLE	28/09/06	DWG NO:	FATIGUE - F - 17
		SCALE:1:1			SHEET 1 OF 1	

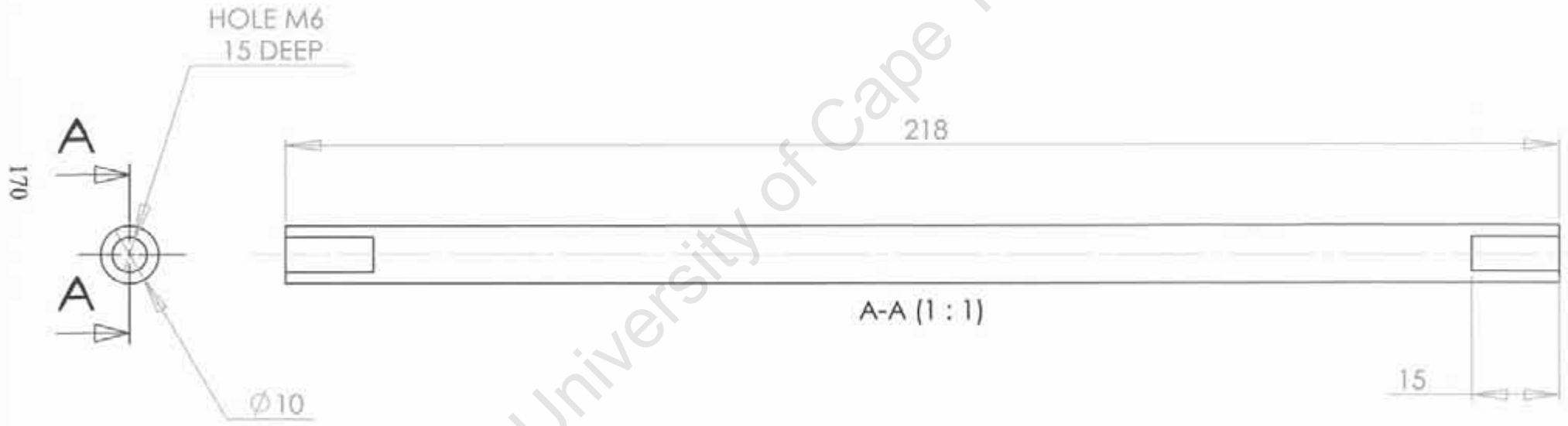

1	4	BEND ROD		SILVER STEEL	Ø 10 x 225
ITEM	QUANTITY	DESCRIPTION		MATERIAL	SPECIFICATION

UNLESS OTHERWISE SPECIFIED: DIMENSIONS ARE IN MILLIMETERS REMOVE ALL SHARP EDGES TOLERANCES: LINEAR: ± 0.1mm ANGULAR: ± 1°	A4	NAME	DATE	TITLE: BEND ROD
	DRAWN	MARTIN HOOLE	28/09/06	
	CHECKED	MARTIN HOOLE	28/09/06	DWG NO: FATIGUE - F - 18
	SCALE:1:1			SHEET 1 OF 1

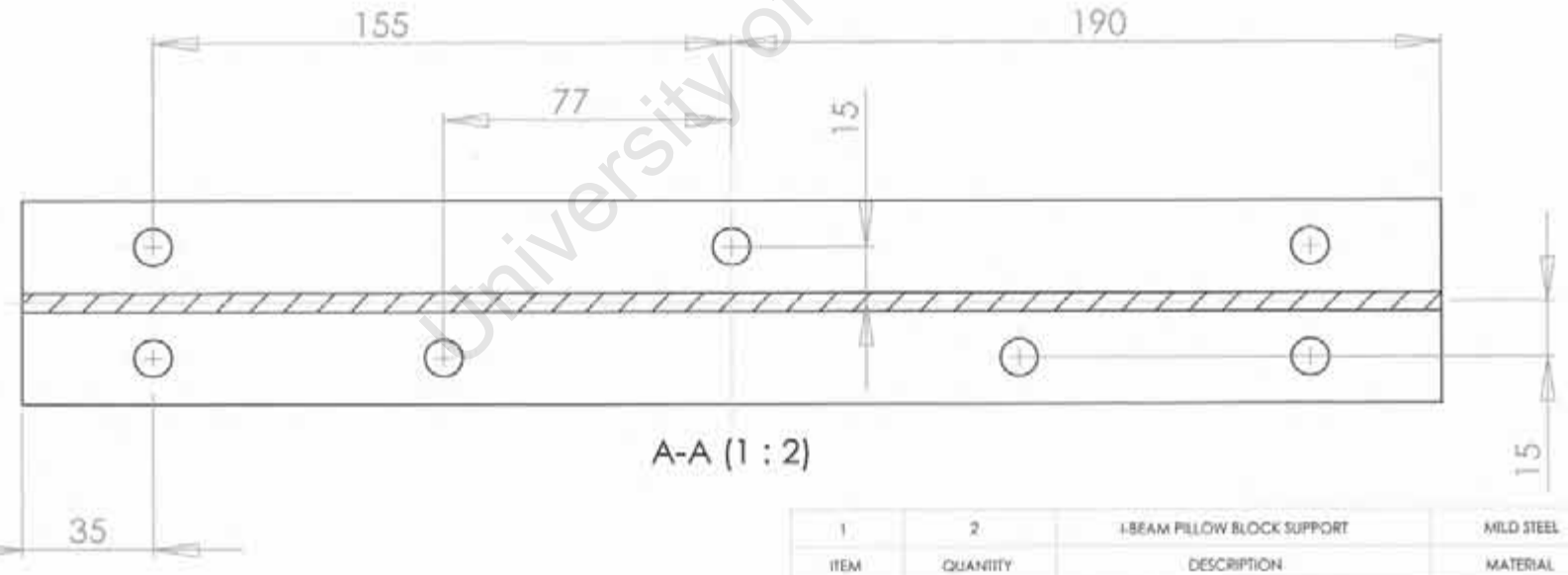

A-A (1 : 2)

1	2	I-BEAM PILLOW BLOCK SUPPORT			MILD STEEL	100 x 55 AA I-BEAM
ITEM	QUANTITY	DESCRIPTION			MATERIAL	SPECIFICATION
UNLESS OTHERWISE SPECIFIED: DIMENSIONS ARE IN MILLIMETERS REMOVE ALL SHARP EDGES TOLERANCES: LINEAR: ± 0.1mm ANGULAR: ± 1°		A4	NAME	DATE	TITLE: I-BEAM PILLOW BLOCK SUPPORT	
		DRAWN	MARTIN HOOLE	28/09/06		
		CHECKED	MARTIN HOOLE	28/09/06	DWG NO:	FATIGUE - F - 19
		SCALE:1:2			SHEET 1 OF 1	

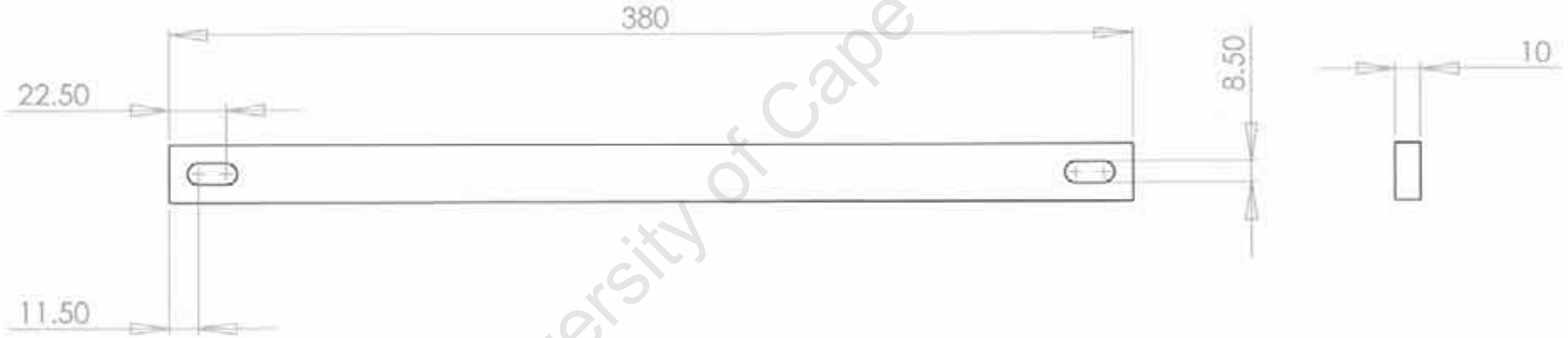

1	4	ANGLE PLATE BRACE			MILD STEEL	390 x 25 x 10
ITEM	QUANTITY	DESCRIPTION			MATERIAL	SPECIFICATION

UNLESS OTHERWISE SPECIFIED:
DIMENSIONS ARE IN MILLIMETERS
REMOVE ALL SHARP EDGES
TOLERANCES:
LINEAR: ± 0.1mm
ANGULAR: ± 1°

A4	NAME	DATE
DRAWN	MARTIN HOOLE	28/09/06
CHECKED	MARTIN HOOLE	28/09/06
SCALE:1:2.5		

TITLE: ANGLE PLATE BRACE

DWG NO: FATIGUE - F - 20

SHEET 1 OF 1

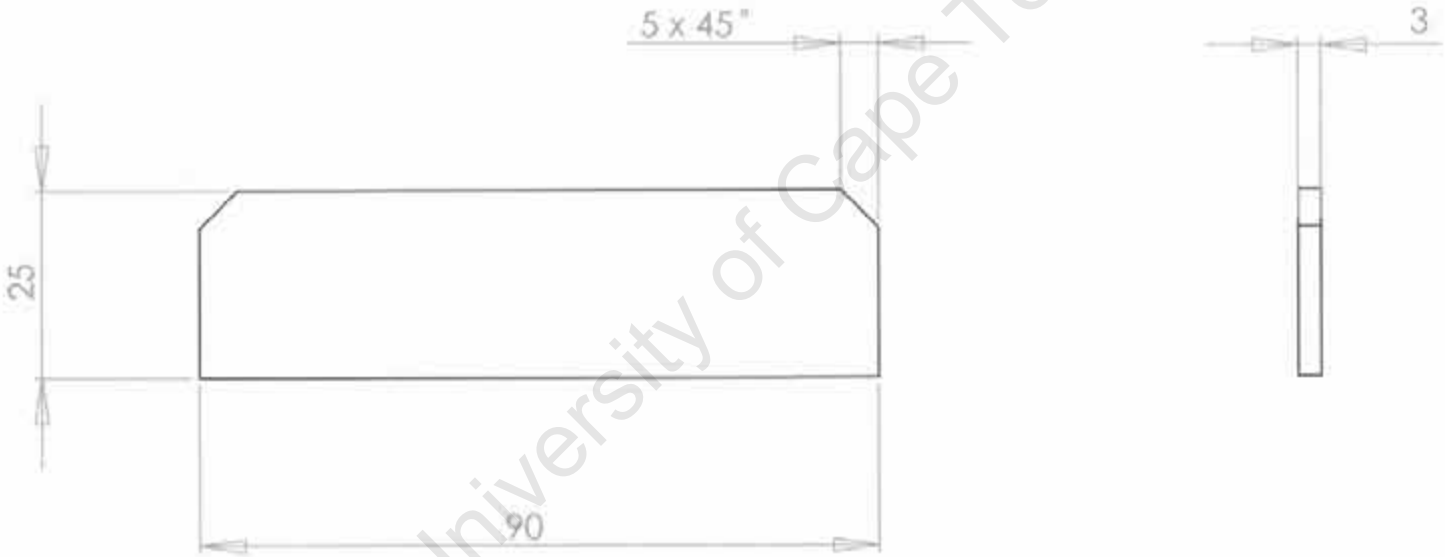

1	14	I-BEAM WEBB			SHEET METAL	90 x 25 x 3
ITEM	QUANTITY	DESCRIPTION			MATERIAL	SPECIFICATION
UNLESS OTHERWISE SPECIFIED: DIMENSIONS ARE IN MILLIMETERS REMOVE ALL SHARP EDGES TOLERANCES: LINEAR: ± 0.1mm ANGULAR: ± 1°		A4	NAME	DATE	TITLE:	I-BEAM WEBB
		DRAWN	MARTIN HOOLE	28/09/06		
		CHECKED	MARTIN HOOLE	28/09/06	DWG NO:	FATIGUE - F - 21
		SCALE:1:1			SHEET 1 OF 1	

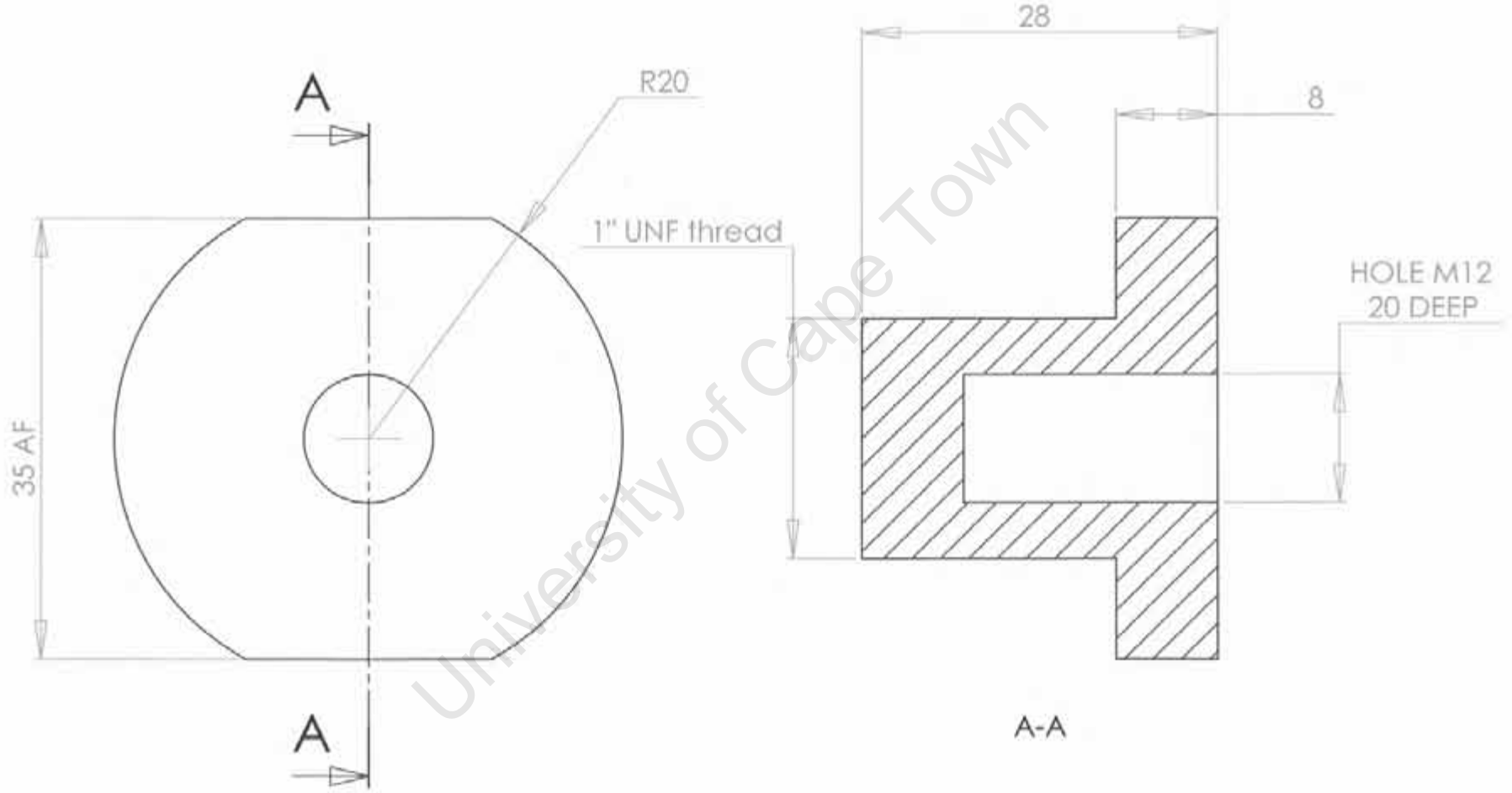

1	2	HANGER BLOCK COUPLING			STEEL	Ø 40 x 28
ITEM	QUANTITY	DESCRIPTION			MATERIAL	SPECIFICATION
UNLESS OTHERWISE SPECIFIED: DIMENSIONS ARE IN MILLIMETERS REMOVE ALL SHARP EDGES TOLERANCES: LINEAR: ± 0.1mm ANGULAR: ± 1°		A4	NAME	DATE	TITLE: HANGER BLOCK COUPLING	
		DRAWN	MARTIN HOOLE	28/09/06		
		CHECKED	MARTIN HOOLE	28/09/06	DWG NO:	FATIGUE - F - 22
		SCALE:2:1			SHEET 1 OF 1	

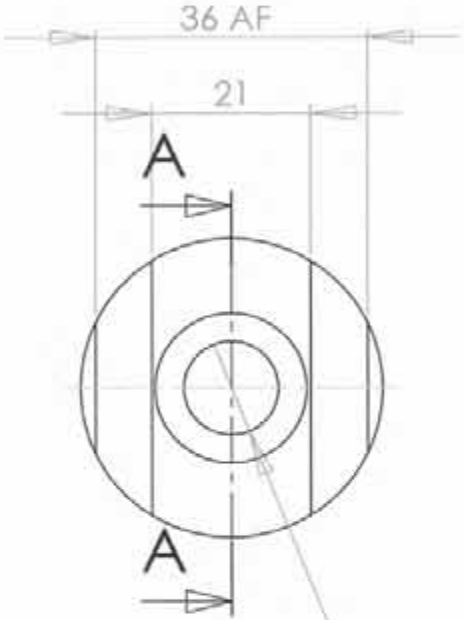

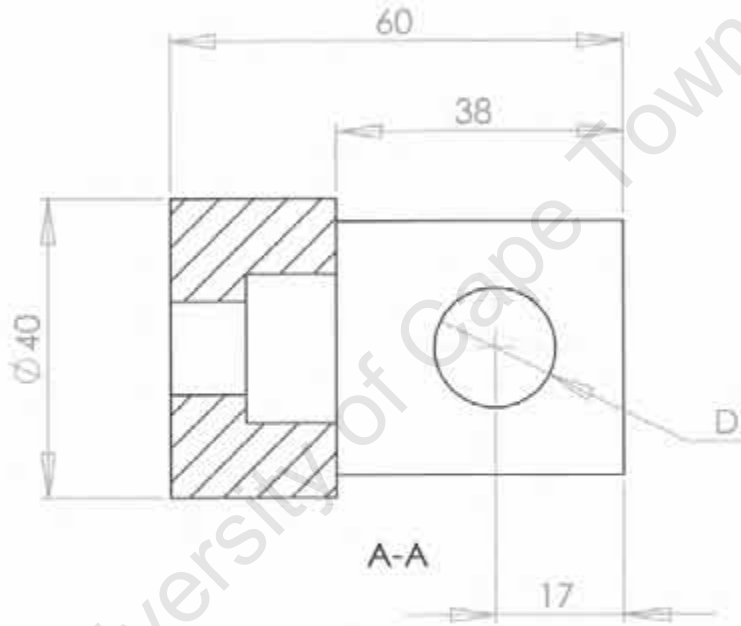

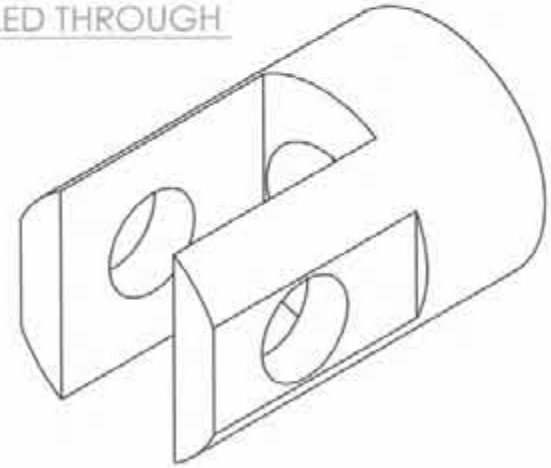

175

1	2	PIN-FRAME			STEEL	Ø40 x 60
ITEM	QUANTITY	DESCRIPTION			MATERIAL	SPECIFICATION
UNLESS OTHERWISE SPECIFIED: DIMENSIONS ARE IN MILLIMETERS REMOVE ALL SHARP EDGES TOLERANCES: LINEAR: ± 0.1mm ANGULAR: ± 1°		A4	NAME	DATE	TITLE:	PIN - FRAME
		DRAWN	MARTIN HOOLE	28/09/06		
		CHECKED	MARTIN HOOLE	28/09/06	DWG NO:	FATIGUE - F - 23
		SCALE:1:1			SHEET 1 OF 1	

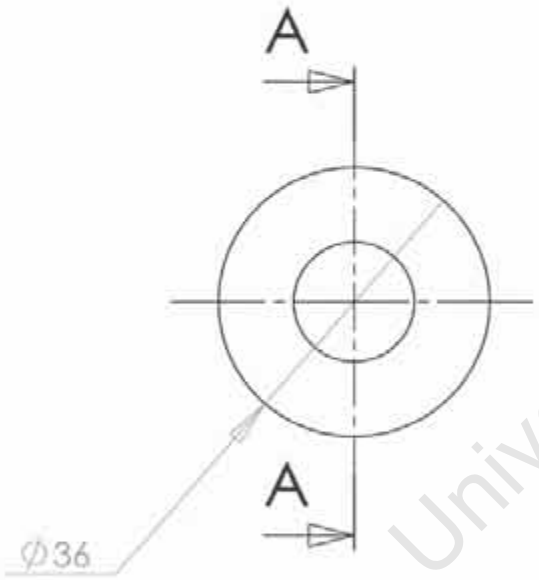

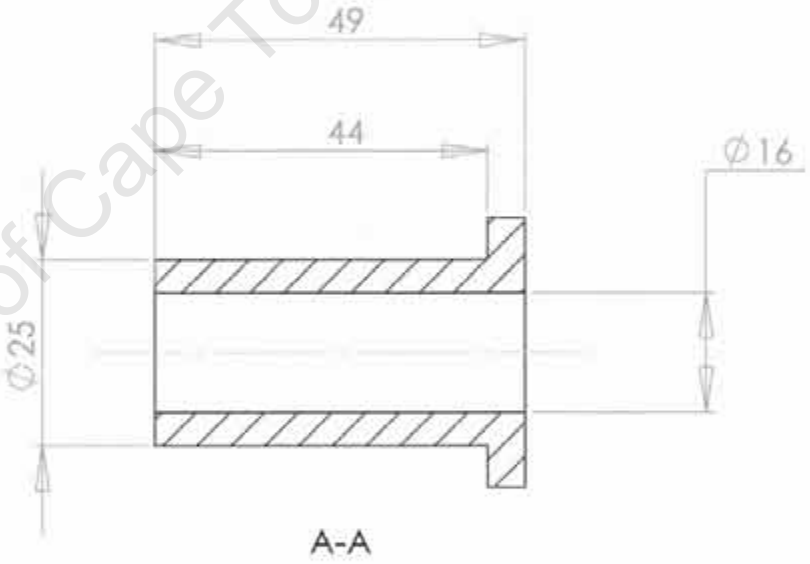

A-A

1	2	16 mm ARM BUSH			VESCONITE	Ø36 x 50
ITEM	QUANTITY	DESCRIPTION			MATERIAL	SPECIFICATION
UNLESS OTHERWISE SPECIFIED: DIMENSIONS ARE IN MILLIMETERS REMOVE ALL SHARP EDGES TOLERANCES: LINEAR: ± 0.1mm ANGULAR: ± 1°		A4	NAME	DATE	TITLE:	16 mm ARM BUSH
		DRAWN	MARTIN HOOLE	28/09/06		
		CHECKED	MARTIN HOOLE	28/09/06	DWG NO:	FATIGUE - F - 24
		SCALE:1:1			SHEET 1 OF 1	

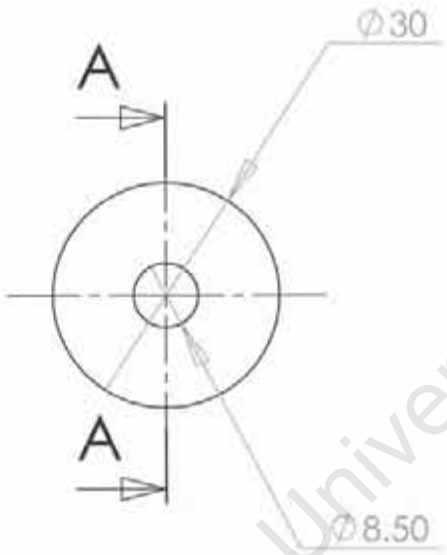

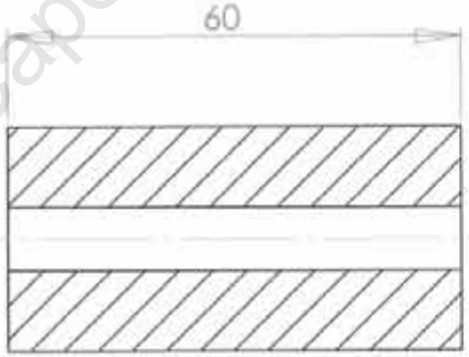

A-A

1	4	MOTOR SPACER			MILD STEEL	Ø30 x 60
ITEM	QUANTITY	DESCRIPTION			MATERIAL	SPECIFICATION
UNLESS OTHERWISE SPECIFIED: DIMENSIONS ARE IN MILLIMETERS REMOVE ALL SHARP EDGES TOLERANCES: LINEAR: ± 0.1mm ANGULAR: ± 1°		A4	NAME	DATE	TITLE:	MOTOR SPACER
		DRAWN	MARTIN HOOLE	28/09/06		
		CHECKED	MARTIN HOOLE	28/09/06	DWG NO:	FATIGUE - F - 25
		SCALE:1:1			SHEET 1 OF 1	

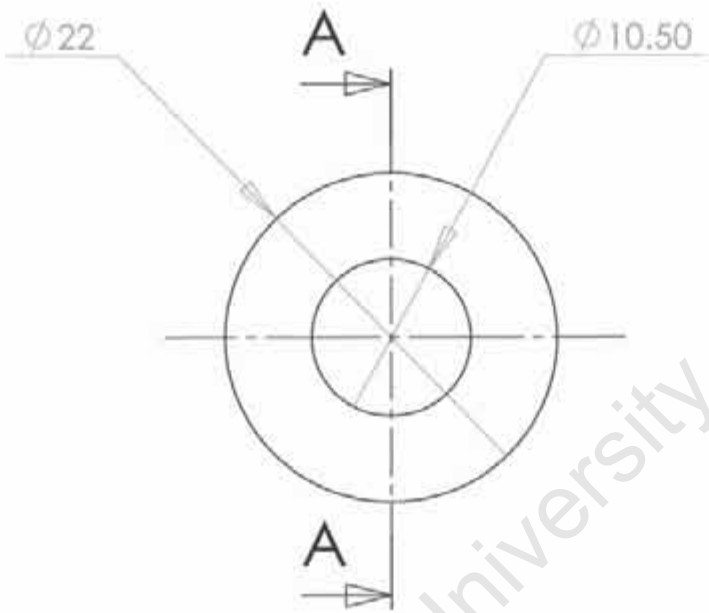

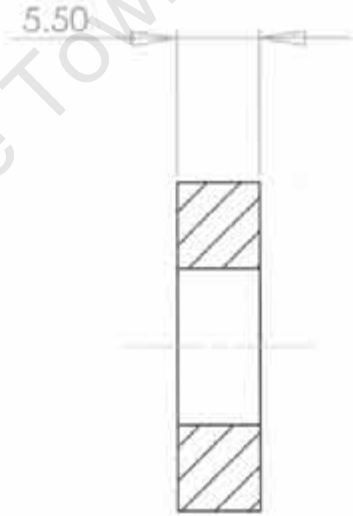

A-A

1	6	OUTER BEND PLATE SPACER			MILD STEEL	Ø22 x 6
ITEM	QUANTITY	DESCRIPTION			MATERIAL	SPECIFICATION
UNLESS OTHERWISE SPECIFIED: DIMENSIONS ARE IN MILLIMETERS REMOVE ALL SHARP EDGES TOLERANCES: LINEAR: ± 0.1mm ANGULAR: ± 1°		A4	NAME	DATE	TITLE:	OUTER BEND PLATE SPACER
		DRAWN	MARTIN HOOLE	28/09/06		
		CHECKED	MARTIN HOOLE	28/09/06	DWG NO:	FATIGUE - F - 26
		SCALE:2:1			SHEET 1 OF 1	

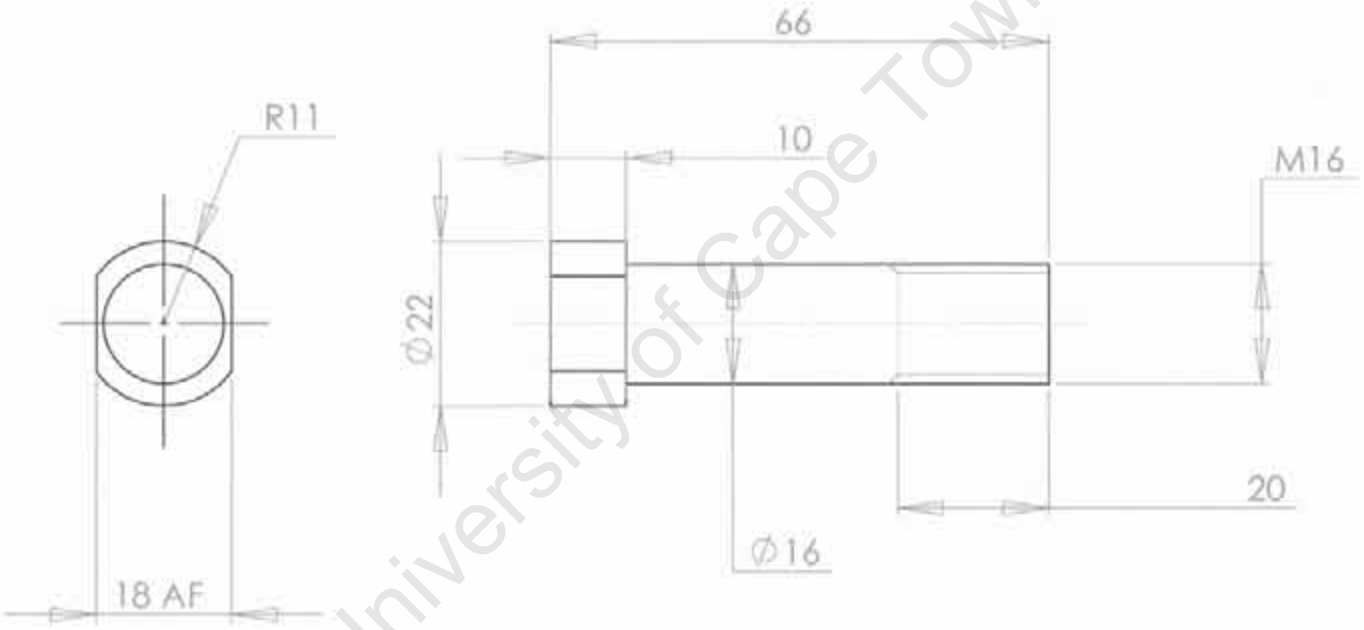

179

1	2	PIN			MILD STEEL	Ø22 x 66
ITEM	QUANTITY	DESCRIPTION			MATERIAL	SPECIFICATION
UNLESS OTHERWISE SPECIFIED: DIMENSIONS ARE IN MILLIMETERS REMOVE ALL SHARP EDGES TOLERANCES: LINEAR: ± 0.1mm ANGULAR: ± 1°		A4	NAME	DATE	TITLE:	PIN
		DRAWN	MARTIN HOOLE	28/09/06		
		CHECKED	MARTIN HOOLE	28/09/06	DWG NO:	FATIGUE - F - 27
		SCALE:1:1			SHEET 1 OF 1	

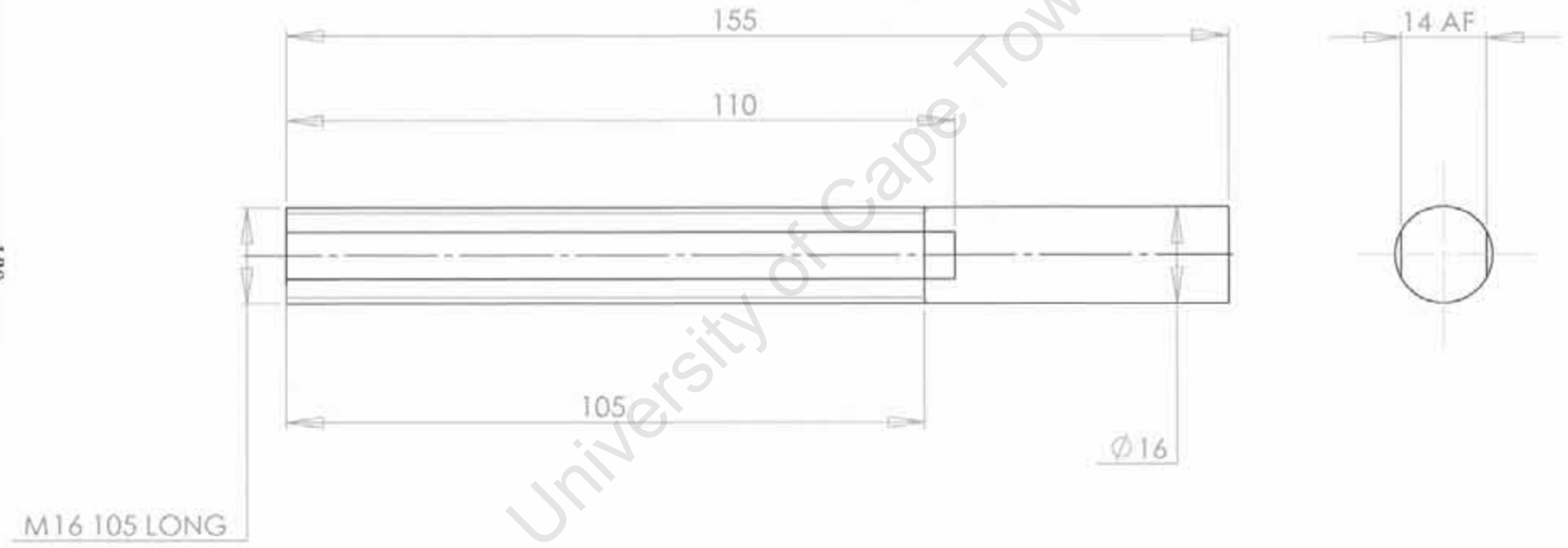

1	1	BEND-SIDE ARM			SILVER STEEL	Ø16 x 150
ITEM	QUANTITY	DESCRIPTION			MATERIAL	SPECIFICATION
UNLESS OTHERWISE SPECIFIED: DIMENSIONS ARE IN MILLIMETERS REMOVE ALL SHARP EDGES TOLERANCES: LINEAR: ± 0.1mm ANGULAR: ± 1°		A4	NAME	DATE	TITLE:	BEND-SIDE ARM
		DRAWN	MARTIN HOOLE	28/09/06		
		CHECKED	MARTIN HOOLE	28/09/06	DWG NO:	FATIGUE - F - 28
		SCALE:1:1			SHEET 1 OF 1	

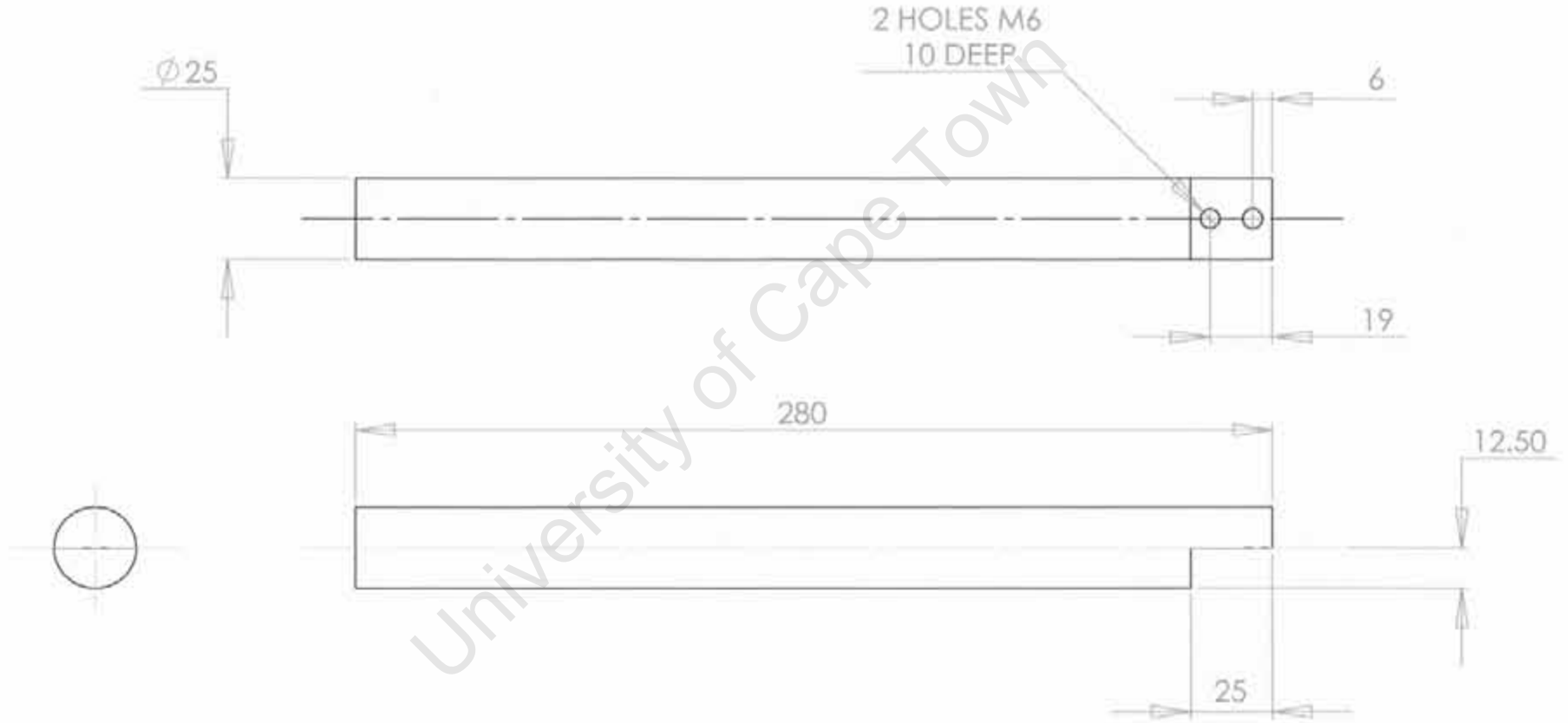

181

1	1	LONG SHAFT			EN8	Ø 25 x 280
ITEM	QUANTITY	DESCRIPTION			MATERIAL	SPECIFICATION
UNLESS OTHERWISE SPECIFIED: DIMENSIONS ARE IN MILLIMETERS REMOVE ALL SHARP EDGES TOLERANCES: LINEAR: ± 0.1mm ANGULAR: ± 1°		A4	NAME	DATE	TITLE:	LONG SHAFT
		DRAWN	MARTIN HOOLE	28/09/06		
		CHECKED	MARTIN HOOLE	28/09/06	DWG NO:	FATIGUE - F - 29
		SCALE:1:2			SHEET 1 OF 1	

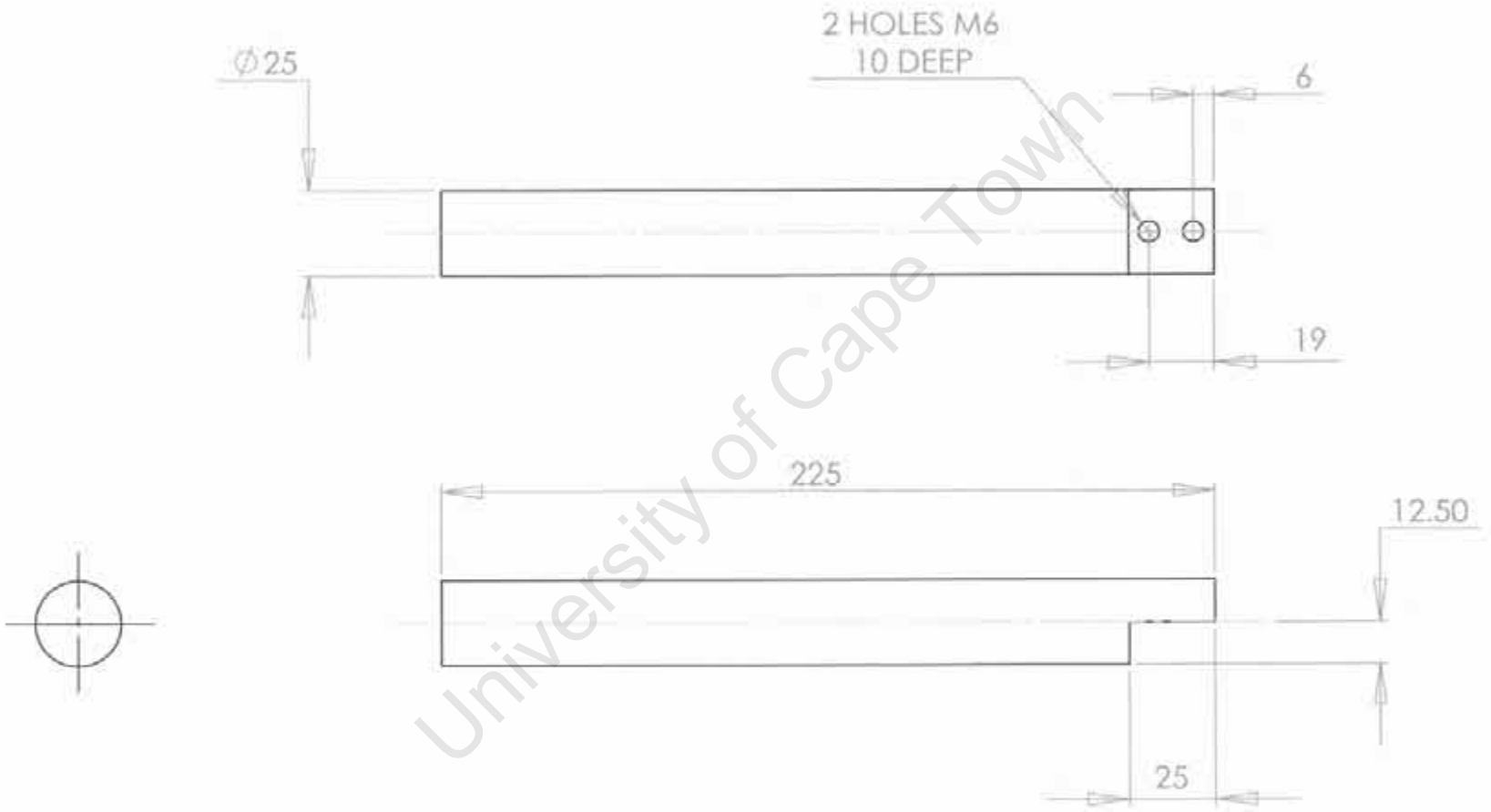

182

1	1	INTERMEDIATE SHAFT			EN8	Ø 25 x 225
ITEM	QUANTITY	DESCRIPTION			MATERIAL	SPECIFICATION
UNLESS OTHERWISE SPECIFIED: DIMENSIONS ARE IN MILLIMETERS REMOVE ALL SHARP EDGES TOLERANCES: LINEAR: ± 0.1mm ANGULAR: ± 1°		A4	NAME	DATE	TITLE:	INTERMEDIATE SHAFT
		DRAWN	MARTIN HOOLE	28/09/06		
		CHECKED	MARTIN HOOLE	28/09/06	DWG NO:	FATIGUE - F - 30
		SCALE:1:2			SHEET 1 OF 1	

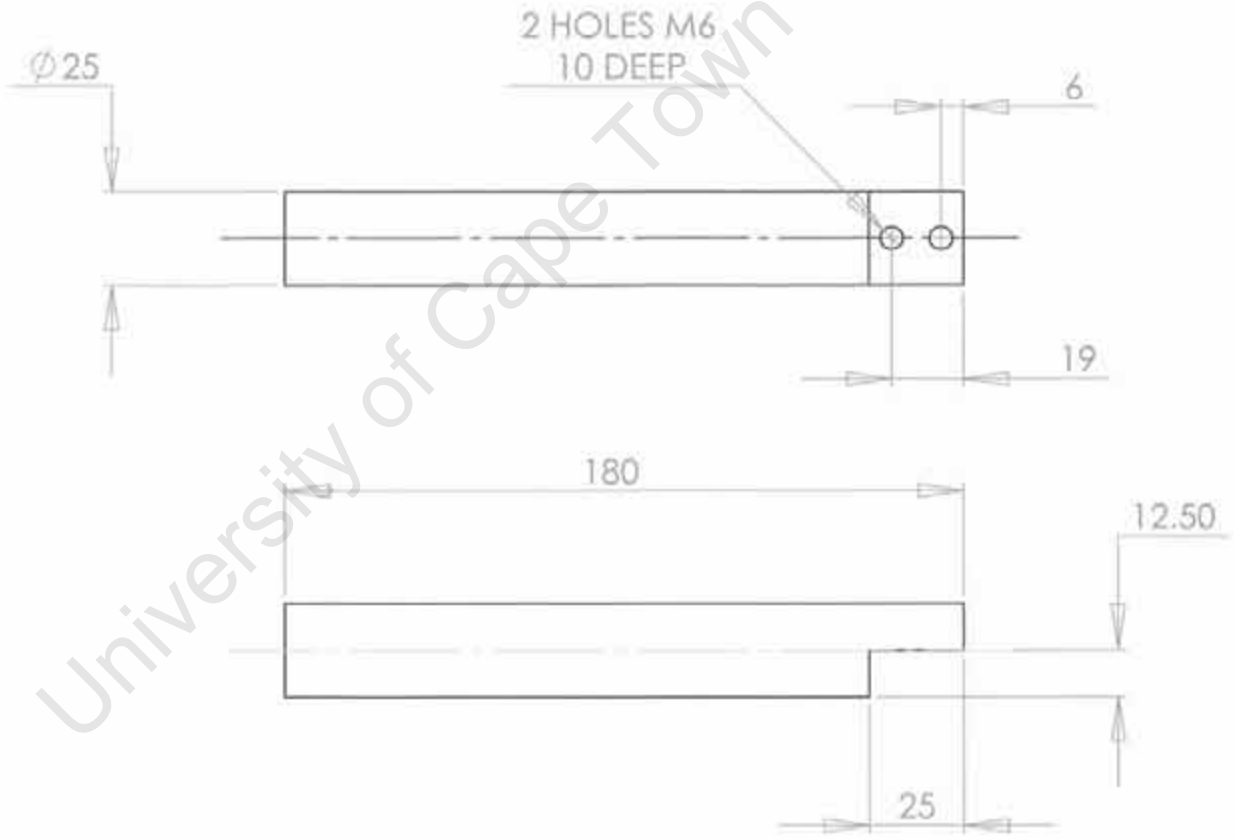

183

1	2	SHORT SHAFT			EN8	Ø 25 x 180
ITEM	QUANTITY	DESCRIPTION			MATERIAL	SPECIFICATION
UNLESS OTHERWISE SPECIFIED: DIMENSIONS ARE IN MILLIMETERS REMOVE ALL SHARP EDGES TOLERANCES: LINEAR: ± 0.1mm ANGULAR: ± 1°		A4	NAME	DATE	TITLE:	SHORT SHAFT
		DRAWN	MARTIN HOOLE	28/09/06		
		CHECKED	MARTIN HOOLE	28/09/06	DWG NO:	FATIGUE - F - 31
		SCALE:1/2			SHEET 1 OF 1	

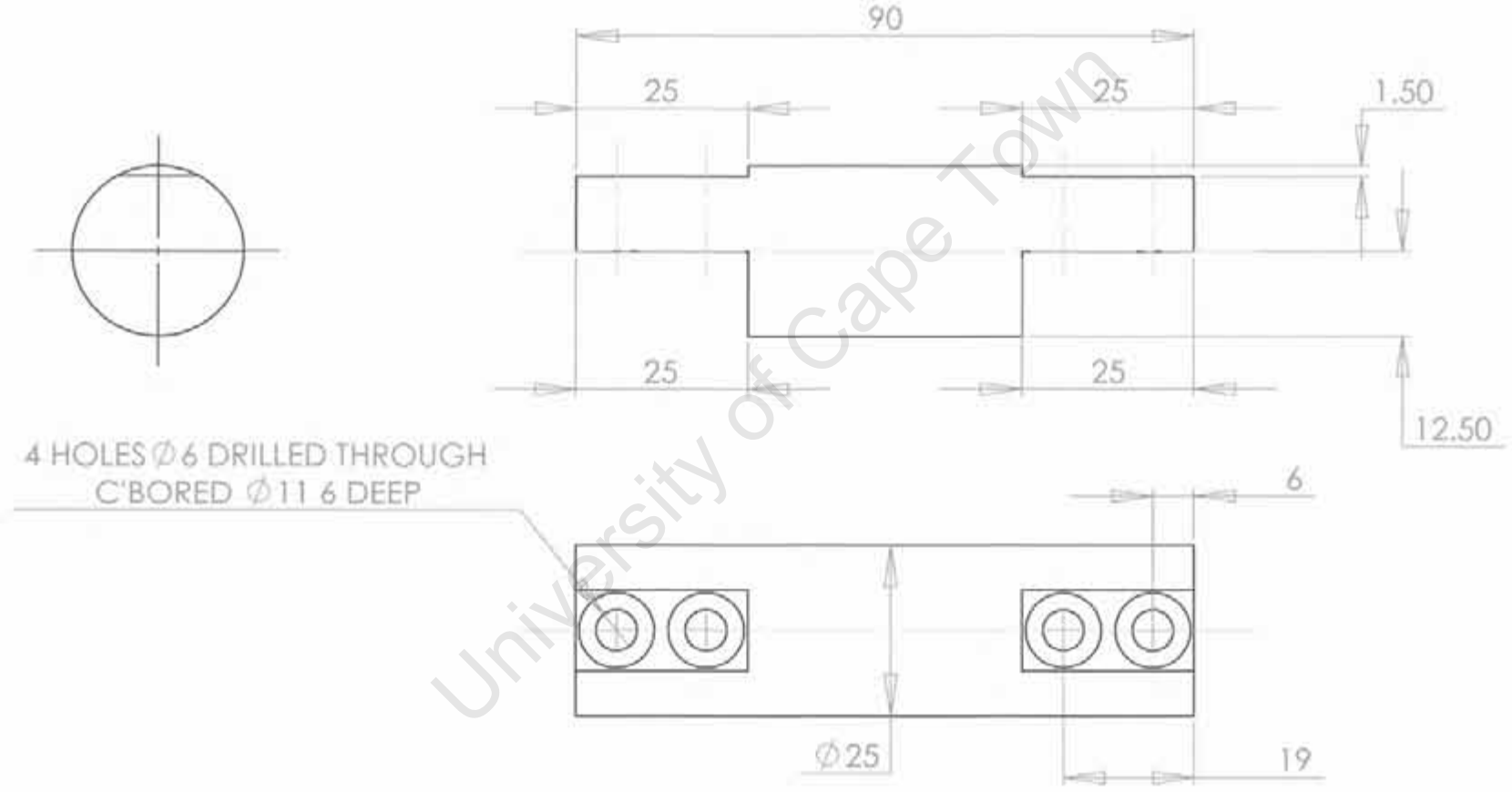

184

1	2	OFFSET SHAFT			ENB	Ø 25 x 90
ITEM	QUANTITY	DESCRIPTION			MATERIAL	SPECIFICATION
UNLESS OTHERWISE SPECIFIED: DIMENSIONS ARE IN MILLIMETERS REMOVE ALL SHARP EDGES TOLERANCES: LINEAR: ± 0.1mm ANGULAR: ± 1°		A4	NAME	DATE	TITLE:	OFFSET SHAFT
		DRAWN	MARTIN HOOLE	28/09/06		
		CHECKED	MARTIN HOOLE	28/09/06	DWG NO:	FATIGUE - F - 32
		SCALE:1:1			SHEET 1 OF 1	

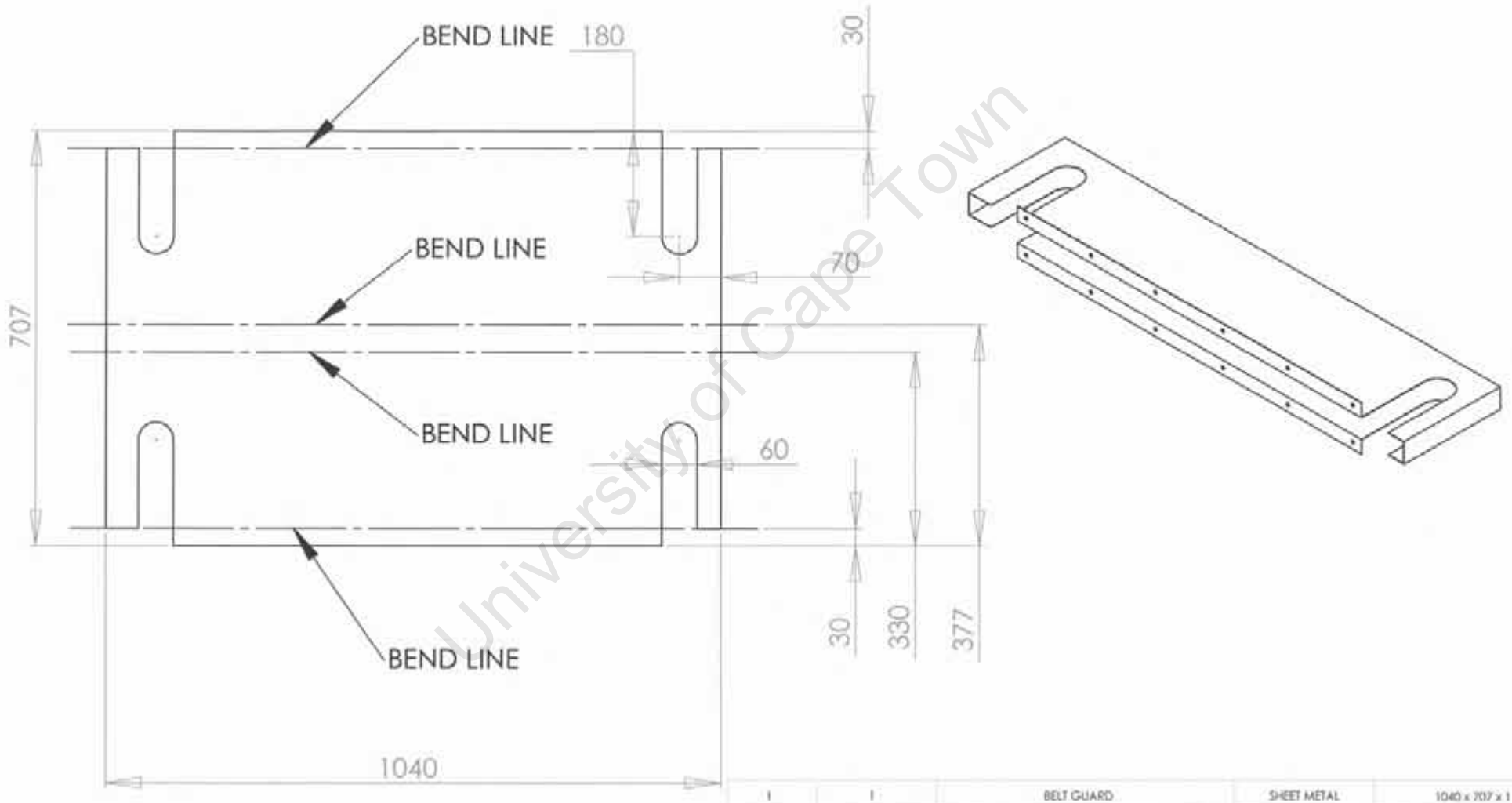

185

ITEM	QUANTITY	DESCRIPTION	MATERIAL	SPECIFICATION
1	1	BELT GUARD	SHEET METAL	1040 x 707 x 1

UNLESS OTHERWISE SPECIFIED:
DIMENSIONS ARE IN MILLIMETERS
REMOVE ALL SHARP EDGES
TOLERANCES:
LINEAR: ± 0.1mm
ANGULAR: ± 1°

A4	NAME	DATE
DRAWN	MARTIN HOOLE	28/09/06
CHECKED	MARTIN HOOLE	28/09/06
SCALE:1:10		

TITLE: BELT GUARD

DWG NO: FATIGUE - F - 33

SHEET 1 OF 1

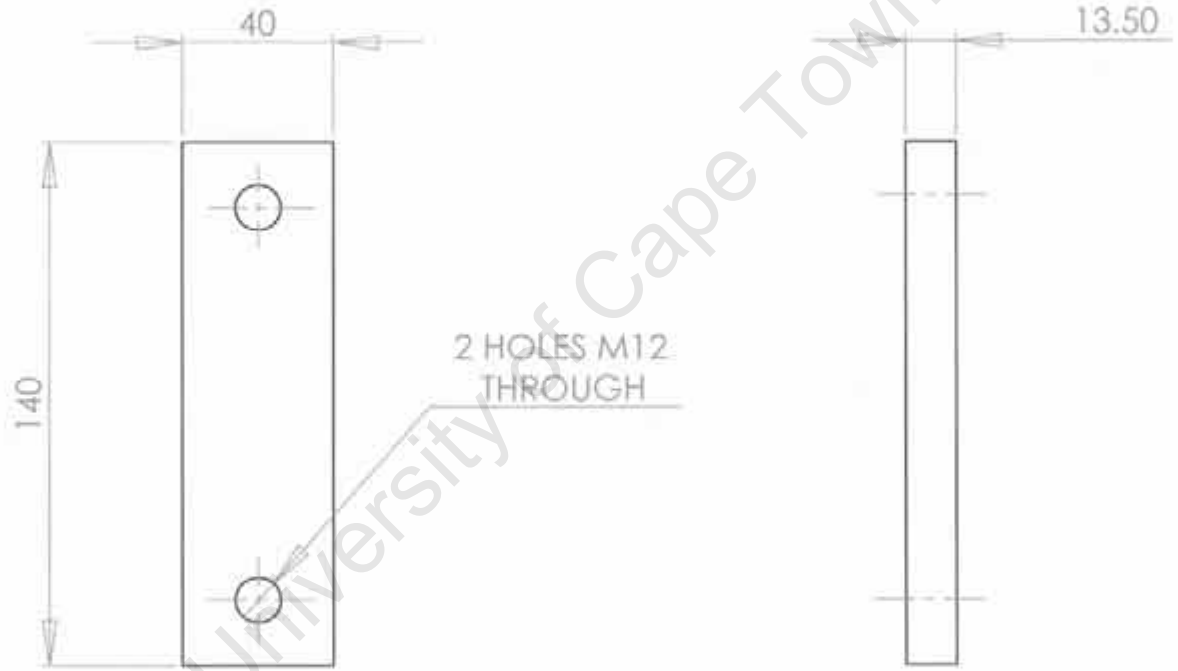

186

1	8	PILLOW BLOCK SPACER			MILD STEEL	140 x 40 x 14
ITEM	QUANTITY	DESCRIPTION			MATERIAL	SPECIFICATION
UNLESS OTHERWISE SPECIFIED: DIMENSIONS ARE IN MILLIMETERS REMOVE ALL SHARP EDGES TOLERANCES: LINEAR: ± 0.1mm ANGULAR: ± 1°		A4	NAME	DATE	TITLE: PILLOW BLOCK SPACER	
		DRAWN	MARTIN HOOLE	28/09/06		
		CHECKED	MARTIN HOOLE	28/09/06	DWG NO:	FATIGUE - F - 34
		SCALE:1:2			SHEET 1 OF 1	

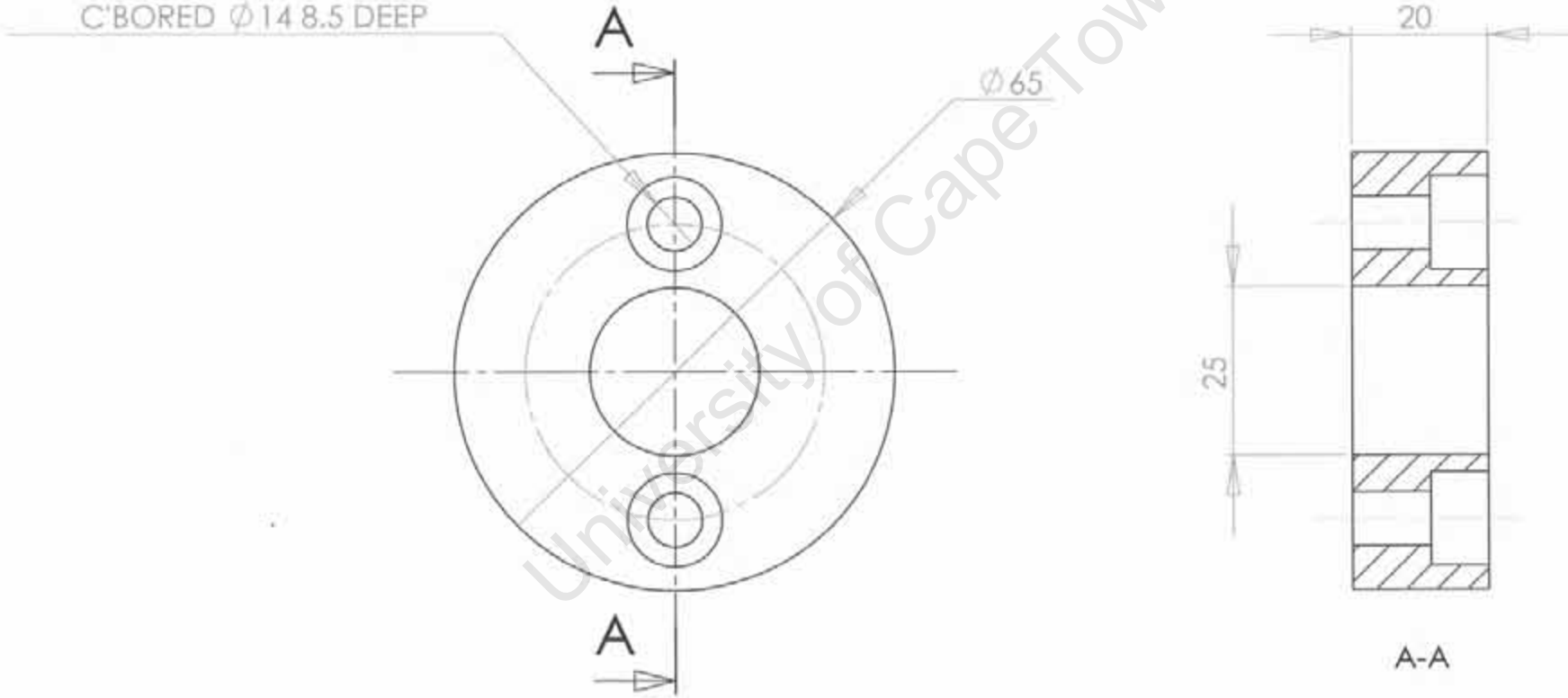

187

1	2	ANGLE PLATE BOSS			MILD STEEL	Ø 65 x 20
ITEM	QUANTITY	DESCRIPTION			MATERIAL	SPECIFICATION
UNLESS OTHERWISE SPECIFIED: DIMENSIONS ARE IN MILLIMETERS REMOVE ALL SHARP EDGES TOLERANCES: LINEAR: ± 0.1mm ANGULAR: ± 1°		A4	NAME	DATE	TITLE:	ANGLE PLATE BOSS
		DRAWN	MARTIN HOOLE	28/09/06		
		CHECKED	MARTIN HOOLE	28/09/06	DWG NO:	FATIGUE - F - 35
		SCALE:1:1			SHEET 1 OF 1	

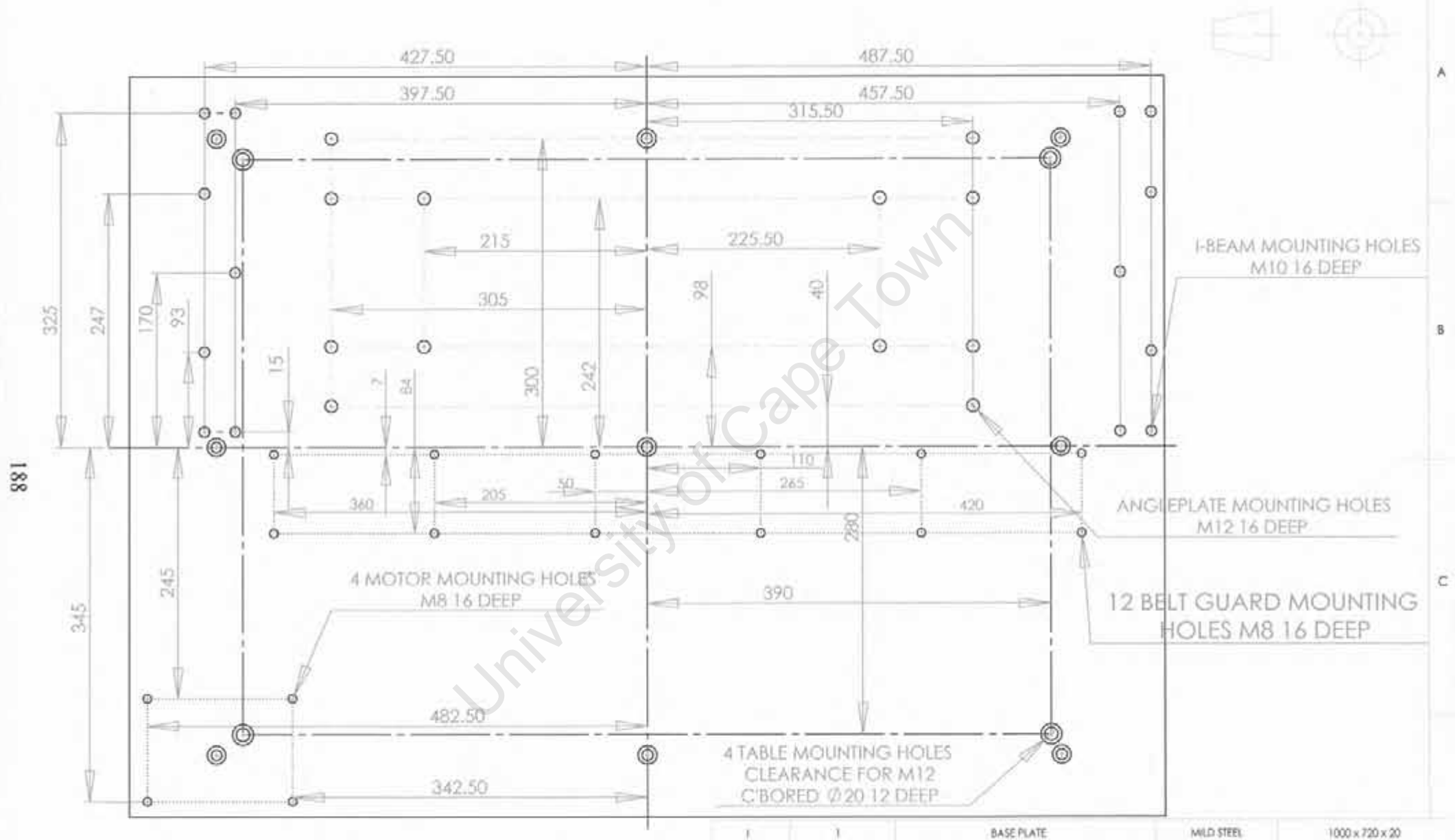

ITEM	QUANTITY	DESCRIPTION	MATERIAL	SPECIFICATION
1	1	BASE PLATE	MILD STEEL	1000 x 720 x 20

UNLESS OTHERWISE SPECIFIED:
DIMENSIONS ARE IN MILLIMETERS
REMOVE ALL SHARP EDGES
TOLERANCES:
LINEAR: ± 0.1mm
ANGULAR: ± 1°

A4	NAME	DATE
DRAWN	MARTIN HOOLE	28/09/06
CHECKED	MARTIN HOOLE	28/09/06
SCALE:1:5		

TITLE: BASE PLATE

DWG NO: FATIGUE - F - 36

SHEET 1 OF 1

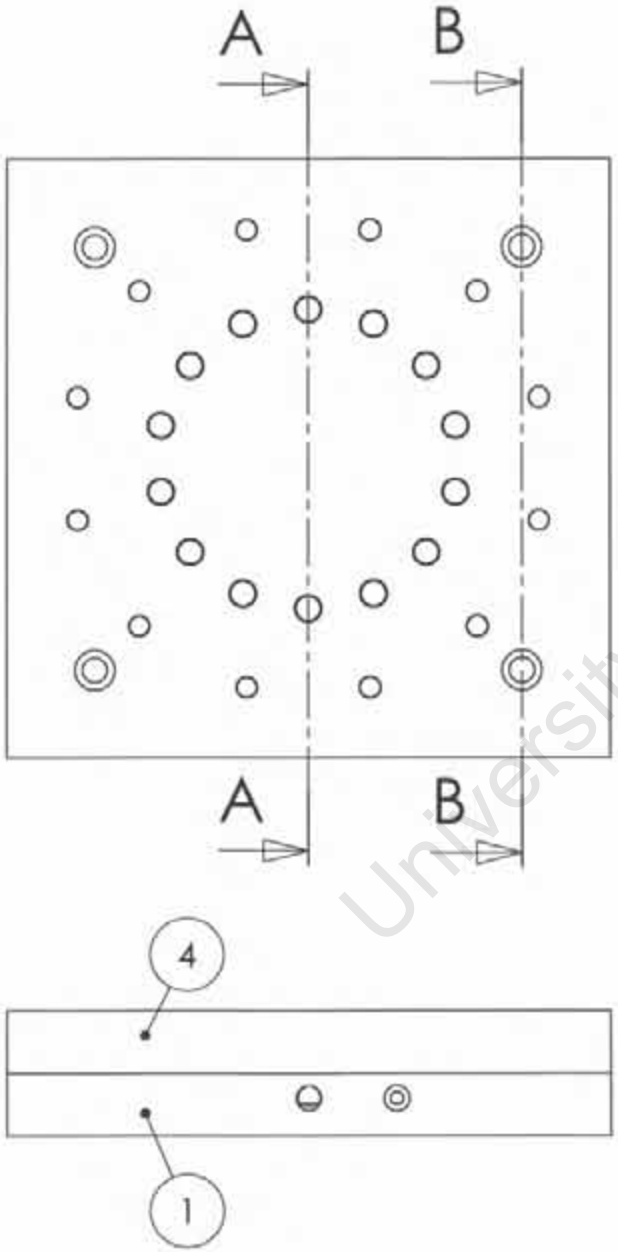

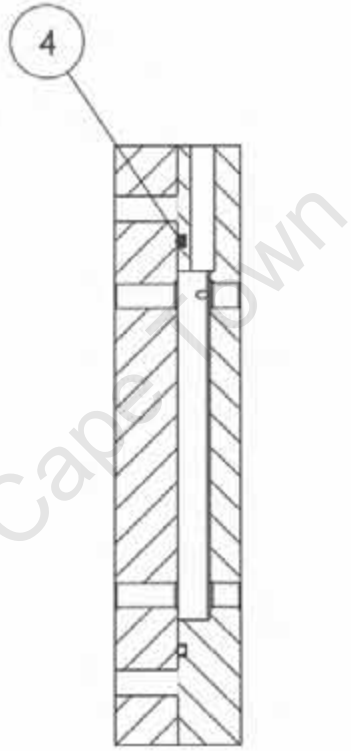

A-A (1 : 3)

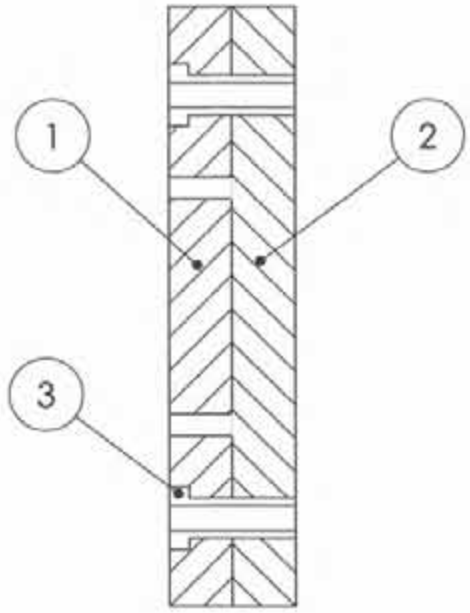

B-B (1 : 3)

ITEM	QUANTITY	DESCRIPTION	MATERIAL	SPECIFICATION
4	1	O-RING	RUBBER	Ø 160 x 4
3	4	BEND END BUSH	BRASS BRONZE	FATIGUE - F - 16
2	1	BEND END INNER PLATE	ALUMINIUM	FATIGUE - F - 02
1	1	BEND END OUTER PLATE	ALUMINIUM	FATIGUE - F - 04

UNLESS OTHERWISE SPECIFIED:
DIMENSIONS ARE IN MILLIMETERS
REMOVE ALL SHARP EDGES
TOLERANCES:
LINEAR: ± 0.1mm
ANGULAR: ± 1°

A4	NAME	DATE
DRAWN	MARTIN HOOLE	28/09/06
CHECKED	MARTIN HOOLE	28/09/06
SCALE:1:3		

TITLE: BEND END FLUID CAVITY ASSEMBL

DWG NO: FATIGUE - F - SUB ASSEM 1

SHEET 1 OF 1

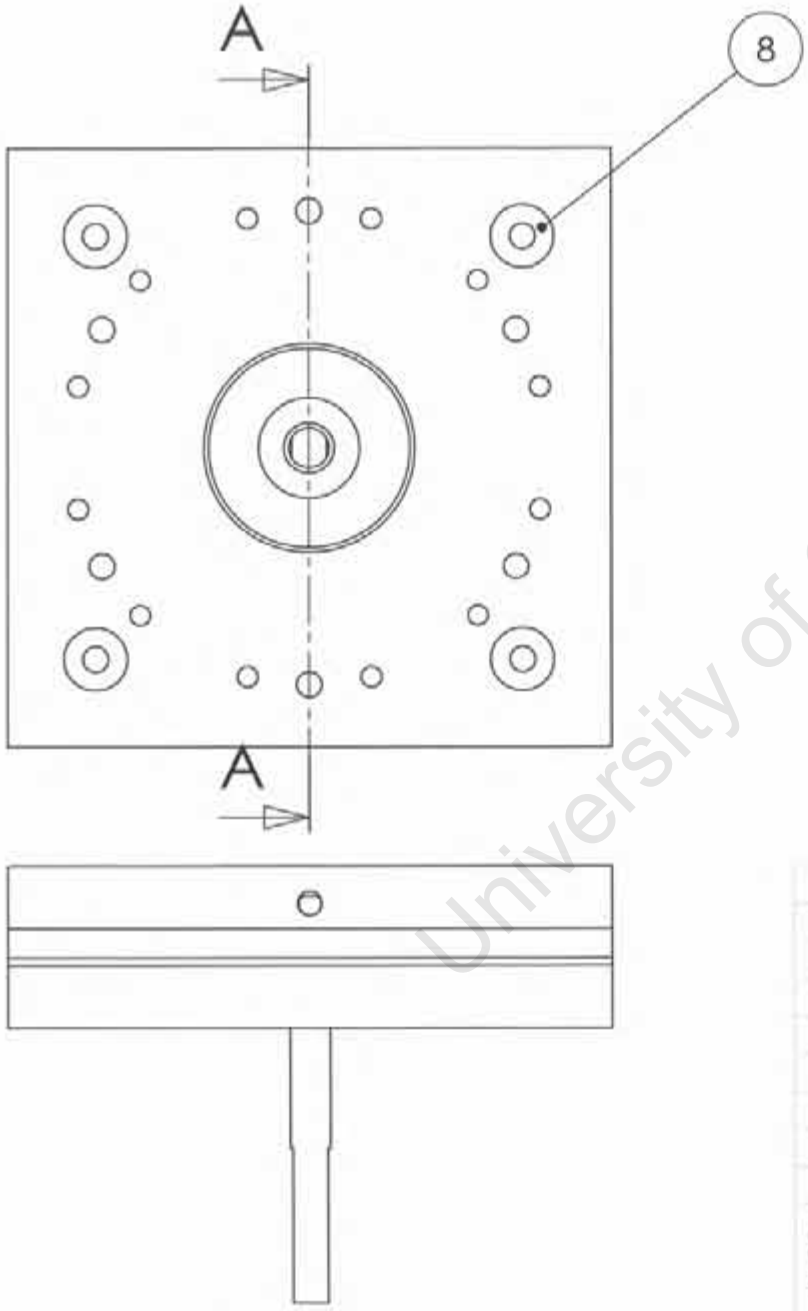

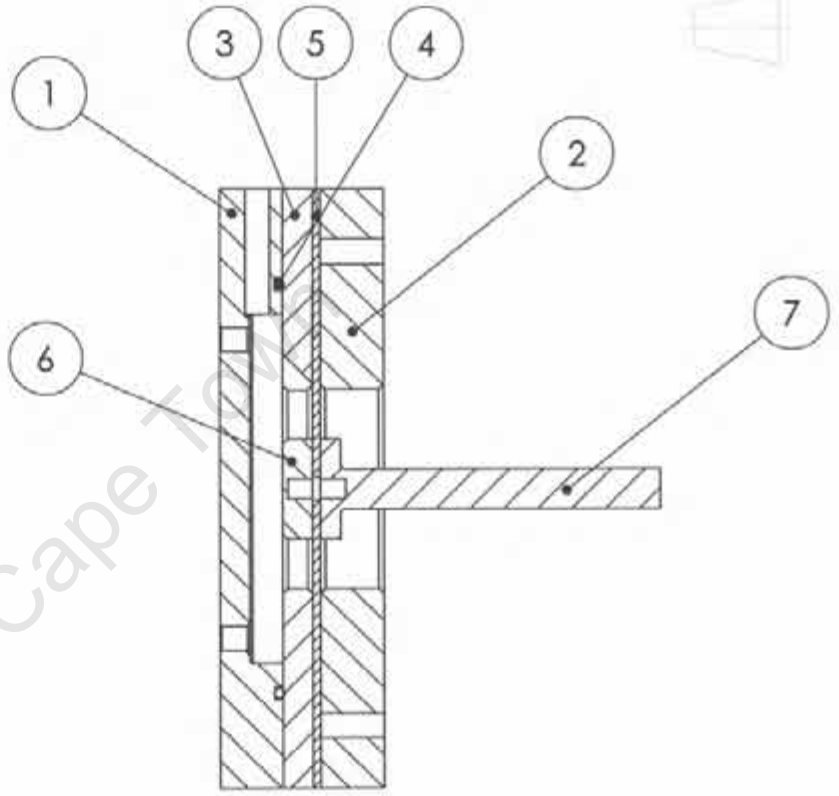

A-A (1 : 3)

ITEM	QUANTITY	DESCRIPTION	MATERIAL	SPECIFICATION
8	4	PISTON END BUSH	BRASS BRONZE	FATIGUE - F - 17
7	1	PISTON END ARM	ALUMINIUM	FATIGUE - F - 07
6	1	GASKET INNER DISC	BRASS BRONZE	FATIGUE - F - 08
5	1	PISTON END GASKET	ALUMINIUM	FATIGUE - F - 05
4	1	O-RING	ALUMINIUM	Ø 160 x 4
3	1	PISTON END SPACER	BRASS BRONZE	FATIGUE - F - 06
2	1	PISTON END INNER PLATE	ALUMINIUM	FATIGUE - F - 03
1	1	PISTON END OUTER PLATE	ALUMINIUM	FATIGUE - F - 01

UNLESS OTHERWISE SPECIFIED:
DIMENSIONS ARE IN MILLIMETERS
REMOVE ALL SHARP EDGES
TOLERANCES:
LINEAR: ± 0.1 mm
ANGULAR: ± 1°

A4	NAME	DATE
DRAWN	MARTIN HOOLE	28/09/06
CHECKED	MARTIN HOOLE	28/09/06
SCALE: 1:3		

TITLE: END END FLUID CAVITY ASSEMBL

DWG NO: FATIGUE - F - SUB ASSEM 2

SHEET 1 OF 1

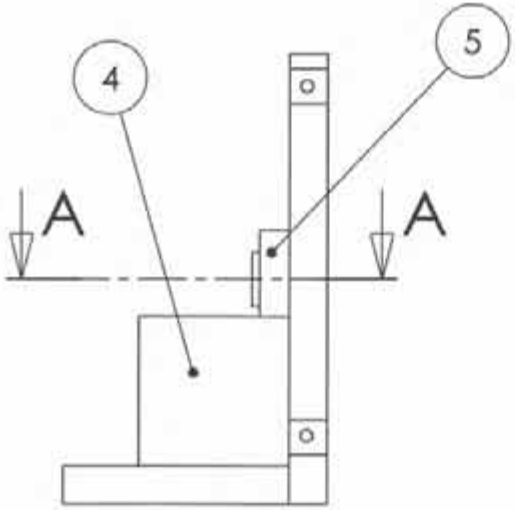

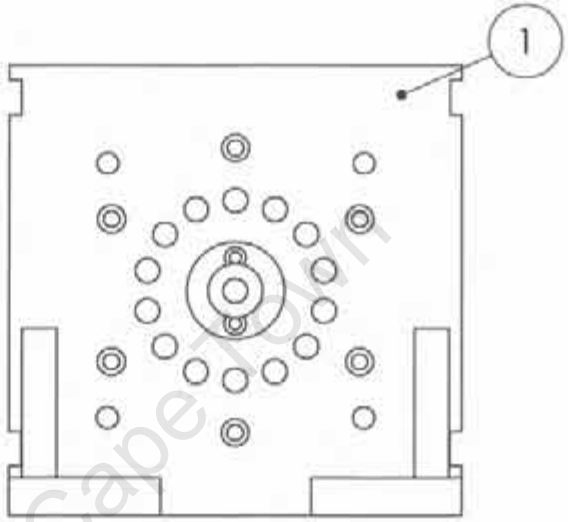

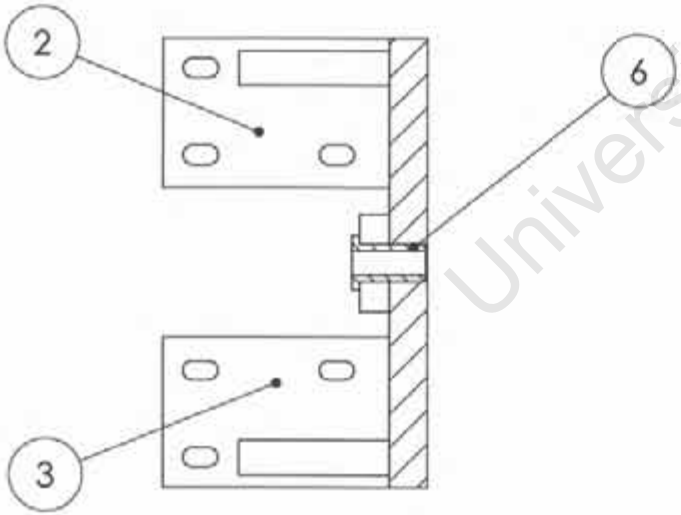

A-A

191

ITEM	QUANTITY	DESCRIPTION	MATERIAL	SPECIFICATION
6	1	16 mm ARM BUSH	VESCONITE	FATIGUE - F - 24
5	1	ANGLE PLATE BOSS	MILD STEEL	FATIGUE - F - 35
4	2	SUPPORT BLOCK	MILD STEEL	FATIGUE - F - 13
3	1	RIGHT ANGLE PLATE BASE	MILD STEEL	FATIGUE - F - 10
2	1	LEFT ANGLE PLATE BASE	MILD STEEL	FATIGUE - F - 09
1	1	BEND END ANGLE PLATE	MILD STEEL	FATIGUE - F - 11

UNLESS OTHERWISE SPECIFIED:
DIMENSIONS ARE IN MILLIMETERS
REMOVE ALL SHARP EDGES
TOLERANCES:
LINEAR: ± 0.1 mm
ANGULAR: ± 1°

A4	NAME	DATE
DRAWN	MARTIN HOOLE	28/09/06
CHECKED	MARTIN HOOLE	28/09/06
SCALE:1:5		

TITLE: BEND END ANGLE PLATE ASSEMBLY

DWG NO: FATIGUE - F - SUB ASSEM 3

SHEET 1 OF 1

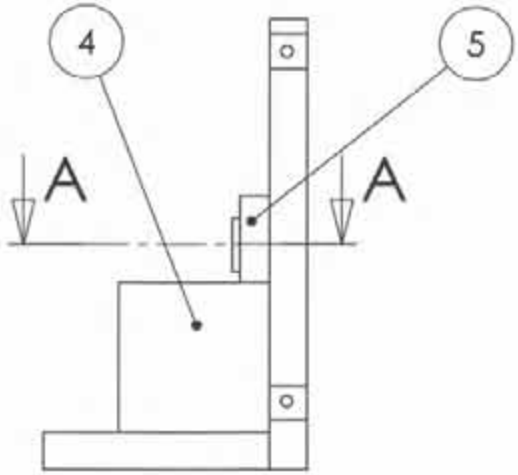

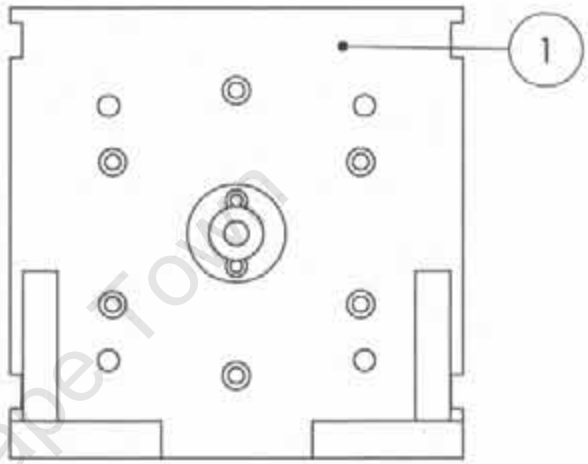

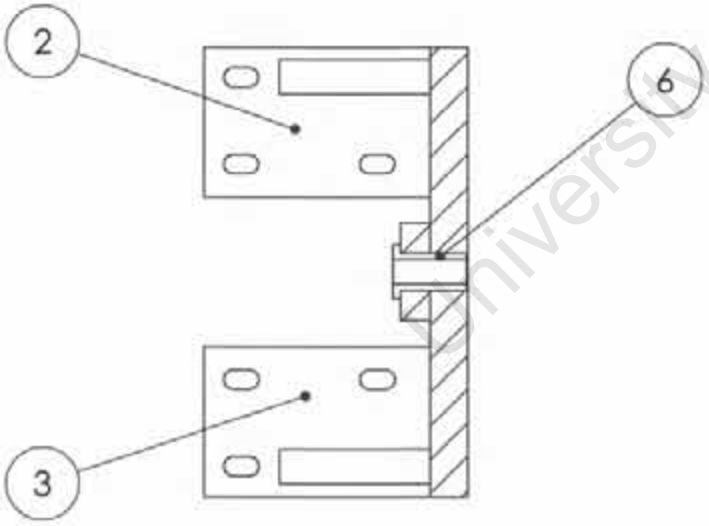

A-A

192

ITEM	QUANTITY	DESCRIPTION	MATERIAL	SPECIFICATION
6	1	16 mm ARM BUSH	VESCONITE	FATIGUE - F - 24
5	1	ANGLE PLATE BOSS	MILD STEEL	FATIGUE - F - 35
4	2	SUPPORT BLOCK	MILD STEEL	FATIGUE - F - 13
3	1	RIGHT ANGLE PLATE BASE	MILD STEEL	FATIGUE - F - 10
2	1	LEFT ANGLE PLATE BASE	MILD STEEL	FATIGUE - F - 09
1	1	PISTON END ANGLE PLATE	MILD STEEL	FATIGUE - F - 12

UNLESS OTHERWISE SPECIFIED:
DIMENSIONS ARE IN MILLIMETERS
REMOVE ALL SHARP EDGES
TOLERANCES:
LINEAR: ± 0.1mm
ANGULAR: ± 1°

A4	NAME	DATE
DRAWN	MARTIN HOOLE	28/09/06
CHECKED	MARTIN HOOLE	28/09/06
SCALE:1:5		

TITLE: PISTON END ANGLE PLATE ASSEMBLY

DWG NO: FATIGUE - F - SUB ASSEM 4

SHEET 1 OF 1

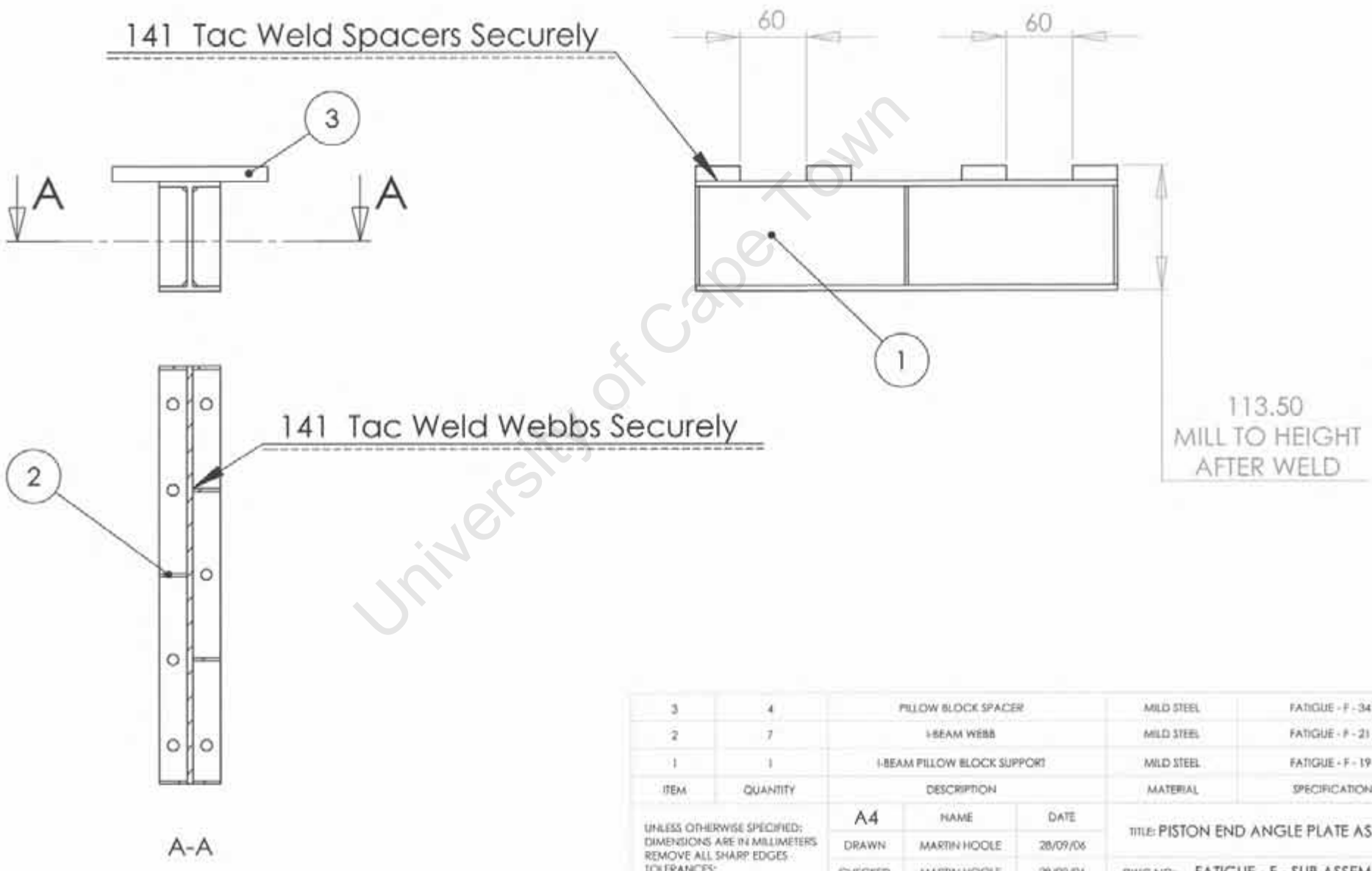

193

ITEM	QUANTITY	DESCRIPTION	MATERIAL	SPECIFICATION
3	4	PILLOW BLOCK SPACER	MILD STEEL	FATIGUE - F - 34
2	7	I-BEAM WEBB	MILD STEEL	FATIGUE - F - 21
1	1	I-BEAM PILLOW BLOCK SUPPORT	MILD STEEL	FATIGUE - F - 19

UNLESS OTHERWISE SPECIFIED:
DIMENSIONS ARE IN MILLIMETERS
REMOVE ALL SHARP EDGES
TOLERANCES:
LINEAR: ± 0.1mm
ANGULAR: ± 1°

A4	NAME	DATE
DRAWN	MARTIN HOOLE	28/09/06
CHECKED	MARTIN HOOLE	28/09/06
SCALE:1:5		

TITLE: PISTON END ANGLE PLATE ASSEMBLY

DWG NO: FATIGUE - F - SUB ASSEM 5

SHEET 1 OF 1

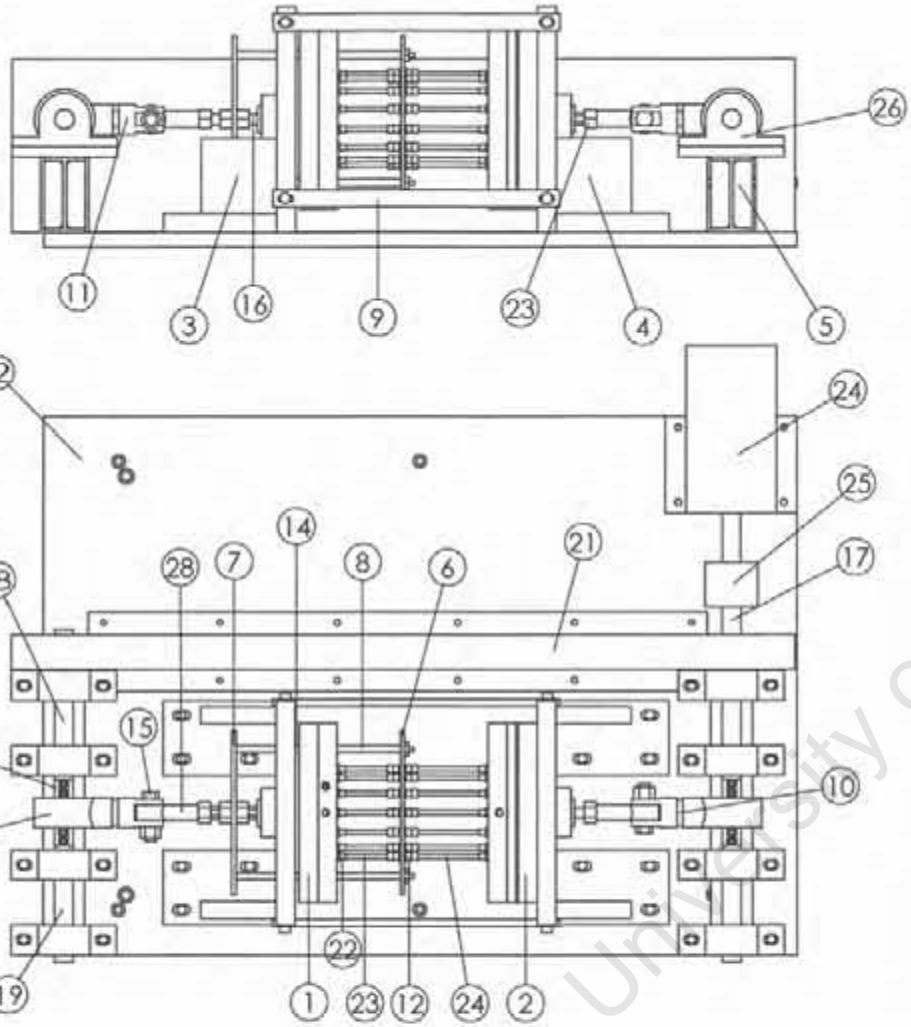

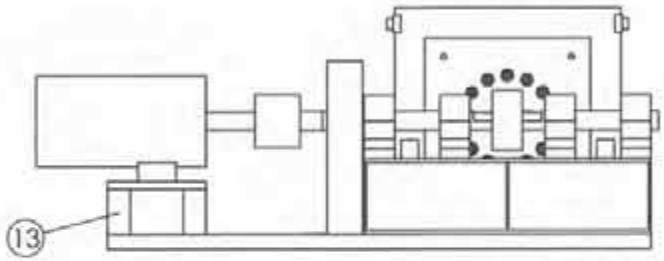

ITEM	QUANTITY	DESCRIPTION	MATERIAL	SPECIFICATION
31	2	ROD END		PHS 18 EC
30	2	HANGER BLOCK		UCECH 205
29	8	PILLOW BLOCK		25mm
28	1	DOG CLUTCH		FENNER 25mm
27	1	MOTOR		1.5 kW FENNER MOTOR
26	6	LOCKNUT		16mm
25	1	BASE PLATE	MILD STEEL	FATIGUE - F - 36
24	14	POLYETHYLENE TUBE	POLYETHYLENE	6 x 4 x 120
23	14	SILICON TUBE	SILICON	6 x 3 x 32.8
22	28	LUER CONNECTOR	ALUMINIUM	4 mm LUER
21	1	BELT GUARD	SHEET METAL	FATIGUE - F - 33
20	2	OFFSET SHAFT	EN8	FATIGUE - F - 32
19	2	SHORT SHAFT	EN8	FATIGUE - F - 31
18	1	INTERMEDIATE SHAFT	EN8	FATIGUE - F - 30
17	1	LONG SHAFT	EN8	FATIGUE - F - 29
16	1	BEND SIDE ARM	SILVER STEEL	FATIGUE - F - 28
15	2	PIN	MILD STEEL	FATIGUE - F - 27
14	6	OUTER BEND PLATE SPACER	MILD STEEL	FATIGUE - F - 26
13	4	MOTOR SPACER	MILD STEEL	FATIGUE - F - 25
12	14	BULKHEAD FITTING	ALUMINIUM	FESTO 4 mm BULKHEAD
11	2	PIN FRAME	STEEL	FATIGUE - F - 23
10	2	HANGER BLOCK COUPLING	STEEL	FATIGUE - F - 22
9	4	ANGLE PLATE BRACE	MILD STEEL	FATIGUE - F - 20
8	4	BEND ROD	SILVER STEEL	FATIGUE - F - 18
7	1	DRIVEN BEND PLATE	ALUMINIUM	FATIGUE - F - 15
6	1	BEND PLATE	ALUMINIUM	FATIGUE - F - 14
5	1	PILLOW BLOCK SUPPORT ASSEMBLY		FATIGUE - F - ASSEM 5
4	1	PISTON END ANGLE PLATE ASSEMBLY		FATIGUE - F - ASSEM 4
3	1	BEND END ANGLE PLATE ASSEMBLY		FATIGUE - F - ASSEM 3
2	1	PISTON END FLUID CAVITY ASSEMBLY		FATIGUE - F - ASSEM 2
1	1	BEND END FLUID CAVITY ASSEMBLY		FATIGUE - F - ASSEM 1
ITEM	QUANTITY	DESCRIPTION	MATERIAL	SPECIFICATION

UNLESS OTHERWISE SPECIFIED:
DIMENSIONS ARE IN MILLIMETERS
REMOVE ALL SHARP EDGES
TOLERANCES:
LINEAR: ± 0.1mm
ANGULAR: ± 1°

A4	NAME	DATE
DRAWN	MARTIN HOOLE	28/09/06
CHECKED	MARTIN HOOLE	28/09/06

SCALE:1:10

TITLE: F - ASSEMBLY

DWG NO: FATIGUE - F - ASSEMBLY

SHEET 1 OF 1

References

Bradshaw D, Groenewald P, Laubscher R, Nannan N, Nojilana B, Norman R, Pieterse D and Schneider M. Initial Burden of Disease Estimates for South Africa, 2000. Cape Town: South African Medical Research Council, 2003.

Callister WD Jr. *Materials Science and Engineering — an Introduction,* Fifth edition. John Wiley & Sons, Inc, 2000.

Canby CA. *Problem based anatomy*. Elsevier Inc, 2006.

Conti JC, Strope ER. Radial Compliance of Natural and Mock Arteries: How This Property Defines the Cyclic Loading of Deployed Vascular Stents. *Biomedical Sciences Instrumentation* 2002; 38:163-171.

Ding Z, Friedman MH. Quantification of 3-D coronary arterial motion using clinical biplane cineangiograms: *The International Journal of Cardiac Imaging* 2000; 16: 331-346.

Ding Z, Zhu H, Friedman MH. Coronary artery dynamics *in vivo. Annals of Biomedical Engineering* 2002; 30:419-429.

Dodge JT Jr, Brown BG, Bolson EL, Dodge HT. Lumen diameter of normal human coronary arteries. Influence of age, sex, anatomic variation, and left ventricular hypertrophy or dilation. *Circulation* 1992; 86:232-246.

Endoh R, Homma T, Furihata Y, Sasaki Y, Fukushima T. A morphometric study of the distribution of early coronary atherosclerosis using arteriography. *Artery* 1988; 15:192-202.

Fayad ZA, Fuster V, Fallon JT, Jayasundera T, Worthley SG, Helft G, Aguinaldo JG, Badimon JJ, Sharma SK. Noninvasive in vivo human coronary artery lumen and wall imaging using black-blood magnetic resonance imaging. *Circulation,* 2000; 102:506-510.

Fisher M, Fieman S. Geometric factors of the bifurcation in carotid atherogenesis. *Stroke* 1990; 21:267-271.

Forman RG, Shivakumar V, Cardinal JW, Williams LC, McKeighan PC. Fatigue Crack Growth Database for Damage Tolerance Analysis. U.S. Department of Transportation, 2005.

Friedman MH, Baker PB, Ding Z, Kuban BD. Relationship between the geometry and quantative morphology of the left anterior descending coronary artery. *Atherosclerosis* 1996; 125:183-192.

Friedman MH, Brinkman AM, Qin JJ, Seed WA. Relation between coronary artery geometry and the distribution of early sudanophilic lesions. *Atherosclerosis* 1993; 98:193-199.

Friedman MH, Ding Z. Relation between the structural asymmetry of coronary branch vessels and the angle at their origin. *Journal of Biomechanics* 1998; 31:273-278.

Friedman MH, Ding Z. Eaton GM, Seed WA. Relationship between the dynamics of coronary arteries and coronary atherosclerosis: Proceedings of 1999 Summer Bioengineering Conference; Big Sky, MT.

Gazetopoulos N, Ioannis PJ, Karydis C, Lolas C, Kiriakou K, Tountas C. Short left coronary artery trunk as a risk factor in the development of coronary atherosclerosis. *Brit Heart J. 1976;* 38:1160-1165.

Gazetopoulos N, Ioannis PJ, Marselos A, Kelekis D, Lolas C, Avgoustakis D, Tountas C. Length of main left coronary artery in relation to atherosclerosis of its branches. *Brit Heart J.* 1976; 38:180-185.

Gray H. *Gray's Anatomy*. Gramercy Books, 1977.

Gross MF, Friedman MH. Dynamics of coronary artery curvature obtained from biplane cineangiograms. Journal of Biomechanics 1998; 31:479-484.

Hatchett R and Thompson D. *Cardiac Nursing - A Comprehensive Guide.* Harcourt, 2002.

Heart Disease and Stroke Statistics - 2006 Update: *Circulation* 2006; 113:85-151.

Hennemuth A, Boskamp T, Fritz D, Kühnel C, Bock S, Rinck D, Scheuering M, Peitgen H-0. One-click coronary tree segmentation in CT angiographic images. *International Congress Series* 2005; 128] :3 1 7— 321.

Hofman MBM, Wickline SA, Lorenz CH. Quantification of in-plane motion of the coronary arteries during the cardiac cycle: Implications for acquisition window duration for MR flow quantification. *J. Magn. Reson. Imaging* 1998; 8:568-576.

Ikeda U, Kuroki M, Ejiri T, Hosoda S, Yaginuma T. Stenotic lesions and the bifurcation angle of coronary arteries in the young. *Jpn Heart J.* 1991; 32:627-633.

Johnston BM, Johnston PR, Corney S, Kilpatrick D. Non-Newtonian blood flow in human right coronary arteries: Transient simulations. *Journal of Biomechanics* 2006; 39:1116-1128.

Johnson, KR, Patel SJ, Whigham A, Hakim A, Pettigrew RI, Oshinski JN. Three-Dimensional, Time-Resolved Motion of the Coronary Arteries. *Journal of Cardiovascular Magnetic Resonance* 2004; 6:663-673.

Kucher N, Lipp E, Schwerzmann M, Zimmerli M, Allemann Y, Seiler C. Gender differences in coronary artery size per 100g of left ventricular mass in a population without cardiac disease. *Swiss Med Wkly* 2001; 131:610-615.

Marieb. *Human anatomy and physiology,* fourth edition. Benjamin/Cummings Science Publising, 1998.

Nguyen ND, Hague AK. Effect of hemodynamic factors on atherosclerosis in the abdominal aorta. *Atherosclerosis* 1990; 84:33-39.

Pao YC, Lu JT, Ritman EL. Bending and twisting of an In Vivo coronary artery at a bifurcation. Journal of Biomechanics 1992; 25: 287-295.

Pedley TJ. The Fluid Mechanics of Large Blood Vessels. Cambridge University Press; Cambridge, 1980.

Prosi M, Perktold K, Ding Z, Friedman MH. Influence of curvature dynamics on pulsatile coronary artery flow in a realistic bifurcation model. Journal of Biomechanics 2004; 37: 1767-1775.

Ramesh R. Strope ER, Price KS, Conti JC. Frequency dependant hysteresis of silicon and latex mock arteries used in stent testing. *Biomedical Sciences Instrumentation* 2005; 41: 163-168.

Sakata N, Joshita T. Ooneda J. Topographical study on arteriosclerotic lesions at the bifurcations of human cerebral arteries. *Heart and Vessels* 1985; 1:70-73.

Sakata N, Takebayashi S. Localization of atherosclerotic lesions in the curving sites of human internal carotid arteries. *Biorheology* 1988; 25:567-578.

Saltissi S, Webb-Peploe MM, Coltart DJ. Effect of variation in coronary artery anatomy on distribution of stenotic lesions. *Brit Heart J.* 1979; 42:186-19].

Sharp WV, Donovan DL, Teague PC, Mosteller RD. Arterial occlusive disease: A function of vessel bifurcation angle. *Surgery* 1982; 91:680-685.

Shechter G, Resar JR, McVeigh ER. Displacement and Velocity of the Coronary Arteries: Cardiac and Respiratory Motion. *IEEE Transactions on Medical Imaging* 2006; 25:369-375.

Sherwood. *Human physiology — from cells to systems,* fifth edition. Thomson Brooks/Cole, 2004.

Shimamoto R, Suzuki J-I, Yamazaki T, Tsuji T, Ohmoto Y, Morita T, Yamashita H, Honye J, Nagai R, Akahane M, Ohtomo K. A new method for measuring coronary artery diameters with CT spatial profile curves. *Radiography* 2007; 13: 44 — 50.

Sinha A-M, Mahnken AH, Borghans A, Krü er S, Koos R, Dedden K, Wildberger JE, Hoffmann R. Multidetector-row computed tomography vs. angiography and intravascular ultrasound for the evaluation of the diameter of proximal coronary arteries. *International Journal of Cardiology* 2006; 110: 40 — 45.

Smedby 0, Hogman N, Nilsson S, Erikson U, Olsson AG, Walldius G. Two-dimensional tortuosity of the superficial femoral artery in early atherosclerosis. *J. Vasc. Res.* 1993; 30:181-191.

Stary HC, Blankenhorn DH, Chandler AB, Glagov S, Insull W JR, Richardson M, Rosenfeld ME, Schaffer SA, Schwartz CJ, Wagner WD, Wissler RW. A definition of the intima of human arteries and of its atherosclerosis-prone regions. *Atherosclerosis Thrombosis* 1992; 12:120-134.

Ullman. *The mechanical design process,* second edition. McGraw-Hill, 1997.

Van De Graaf. *Human Anatomy,* sixth edition. McGraw-Hill, 2002.

van Geuns R-JM, Wielopolski PA, de Bruin HG, Rensing BJ, van Ooijen PMA, Hulshoff M, Oudkerk M, de Feyter PJ. Magnetic Resonance Imaging of the Coronary Arteries: Techniques and Results. *Progress in Cardiovascular Diseases* 1999; 42:157-166.